AD-A092 632 NAVAL POSTGRADUATE SCHOOL MONTEREY CA F/G 8/10
SUBSURFACE DYNAMICAL PROPERTIES OF VARIABLE FEATURES SEEN IN SA--ETC(U)
JUN 80 J E JOHNSON

UNCLASSIFIED NL

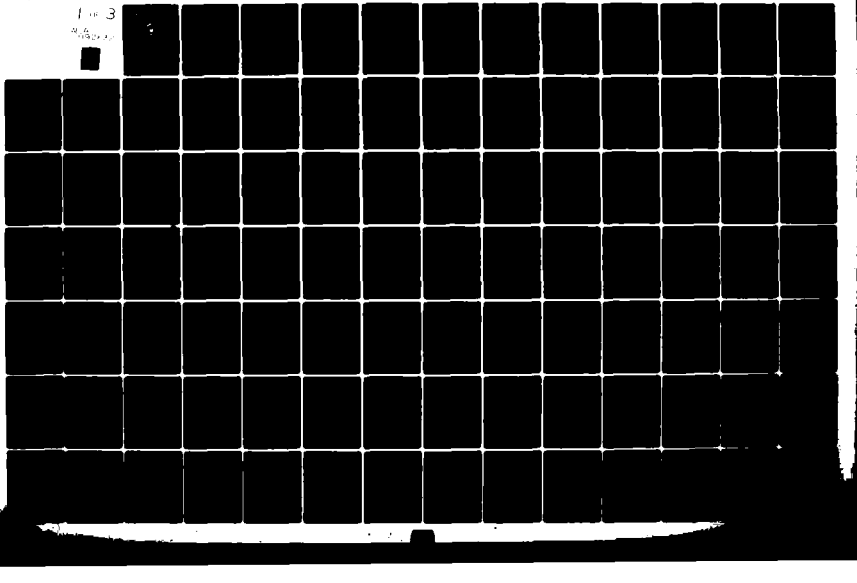

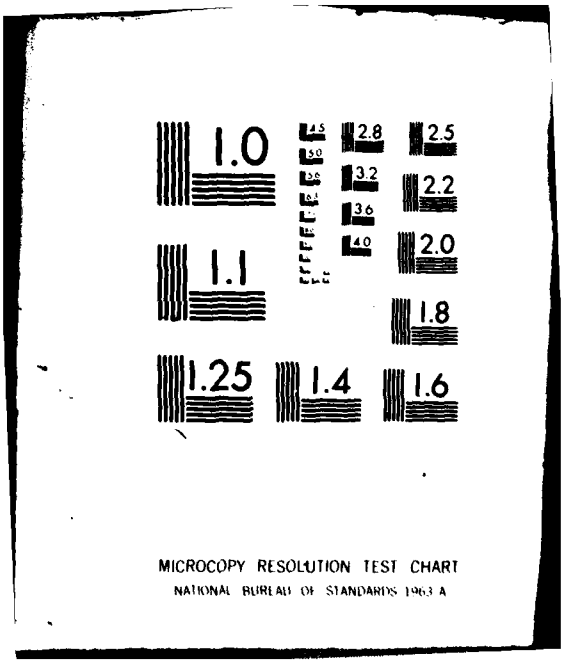
1.0
1.1
1.25
1.4
1.6
1.8
2.0
2.2
2.5
2.8
3.2
3.6
4.0
4.5
5.0
5.6
6.3
7.1
MICROCOPY RESOLUTION TEST CHART
NATIONAL BUREAU OF STANDARDS 1963 A

NAVAL POSTGRADUATE SCHOOL

Monterey, California

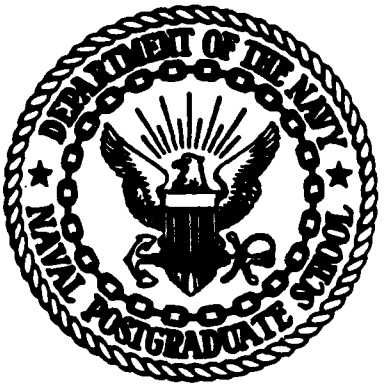

THESIS

SUBSURFACE DYNAMICAL PROPERTIES OF VARIABLE FEATURES SEEN IN SATELLITE IR IMAGERY OFF POINT SUR AND THEIR ACOUSTIC SIGNIFICANCE

by

John Edward Johnson, Jr.

June 1980

Thesis Advisor: C. N. K. Mooers

Approved for public release; distribution unlimited.

UNCLASSIFIED

SECURITY CLASSIFICATION OF THIS PAGE (When Data Entered)

REPORT DOCUMENTATION PAGE	READ INSTRUCTIONS BEFORE COMPLETING FORM
1. REPORT NUMBER	2. GOVT ACCESSION NO. AD-A092 632 / 3. RECIPIENT'S CATALOG NUMBER
4. TITLE (and Subtitle) (6) Subsurface Dynamical Properties of Variable Features Seen in Satellite IR Imagery off Point Sur and Their Acoustic Significance.	5. TYPE OF REPORT & PERIOD COVERED (9) Master's Thesis; June 1980
	6. PERFORMING ORG. REPORT NUMBER
7. AUTHOR(s) (10) John Edward Johnson, Jr.	8. CONTRACT OR GRANT NUMBER(s)
9. PERFORMING ORGANIZATION NAME AND ADDRESS Naval Postgraduate School Monterey, California 93940	10. PROGRAM ELEMENT, PROJECT, TASK AREA & WORK UNIT NUMBERS 61153N
11. CONTROLLING OFFICE NAME AND ADDRESS Naval Postgraduate School Monterey, California 93940 (11)	12. REPORT DATE June 1980
	13. NUMBER OF PAGES 239
14. MONITORING AGENCY NAME & ADDRESS(if different from Controlling Office)	15. SECURITY CLASS. (of this report) Unclassified
	15a. DECLASSIFICATION/DOWNGRADING SCHEDULE

16. DISTRIBUTION STATEMENT (of this Report)

Approved for public release; distribution unlimited.

17. DISTRIBUTION STATEMENT (of the abstract entered in Block 20, if different from Report)

18. SUPPLEMENTARY NOTES

19. KEY WORDS (Continue on reverse side if necessary and identify by block number)

Satellite IR Imagery, TIROS-N, Coastal Upwelling, Bottom Topography Effects, Acoustics

20. ABSTRACT (Continue on reverse side if necessary and identify by block number)

This study is a continuation of chemical mesoscale research of cold water anomalies detected by satellite IR imagery off the Point Sur area with emphasis upon description of the thermal structure. Analysis of dynamic forcing is restricted to the relationship between equatorward alongshore wind stress and coastal upwelling. The preferred location of the features was on the south side of Point Sur near the axis of a mesoscale canyon (consistent with —over

DD FORM 1 JAN 73 1473A (Page 1) EDITION OF 1 NOV 65 IS OBSOLETE S/N 0102-014-6601

UNCLASSIFIED

SECURITY CLASSIFICATION OF THIS PAGE (When Data Entered)

#20 - ABSTRACT - (CONTINUED)

background theory). In all cases, a surface (upper 100 m) 'lens' type feature with horizontal dimensions of 20 km at 50 m was observed below the surface cold spot expression. Typical temperature changes across the feature were of the order of 3°C/10 km with temperature changes across frontal zones of the order of 1°C/km. The surface density field pattern of November 1979 was similar to the surface temperature pattern. As determined by Parabolic Equation (PE) Acoustic Model runs, the presence of the wedge decreased propagation loss particularly in the cross shelf directions.

Approved for public release; distribution unlimited.

Subsurface Dynamical Properties of Variable Features Seen in Satellite IR Imagery off Point Sur and Their Acoustic Significance

by

John Edward Johnson, Jr.
Lieutenant, United States Navy
B.S., United States Naval Academy, 1973

Submitted in partial fulfillment of the requirements for the degree of

MASTER OF SCIENCE IN METEOROLOGY AND OCEANOGRAPHY

from the

NAVAL POSTGRADUATE SCHOOL

June 1980

Author John Edward Johnson, Jr.

Approved by: Christopher N. K. Mooers
Thesis Advisor

Eugene J. Fiaganza
Second Reader

Christopher N. K. Mooers
Chairman, Department of Oceanography

William M. Tolles
Dean of Science and Engineering

ABSTRACT

This study is a continuation of chemical mesoscale research of cold water anomalies detected by satellite IR imagery off the Point Sur area with emphasis upon description of the thermal structure. Analysis of dynamic forcing is restricted to the relationship between equatorward alongshore wind stress and coastal upwelling. The preferred location of the features was on the south side of Point Sur near the axis of a mesoscale canyon (consistent with background theory). In all cases, a surface (upper 100 m) "lens" type feature with horizontal dimensions of 20 km at 50 m was observed below the surface cold spot expression. Typical temperature changes across the feature were of the order of 3°C/10 km with temperature changes across frontal zones of the order of 1°C/km. The surface density field pattern of November 1979 was similar to the surface temperature pattern. As determined by Parabolic Equation (PE) Acoustic Model runs, the presence of the wedge decreased propagation loss particularly in the cross shelf directions.

TABLE OF CONTENTS

LIST OF TABLES

LIST OF ILLUSTRATIONS

Figure

Figure

Figure

ACKNOWLEDGMENTS

I would like to express my sincere thanks to Dr. Chris Mooers, my thesis advisor, whose unique skill in tempering unbridled academic freedom with appropriate criticism and guidance made this an enjoyable thesis; to Dr. Eugene Traganza, my first reader, whose motivation and patience were most appreciated; and to Mr. Larry Breaker and Miss Bonnie Hunter, whose help and enthusiasm carried a great deal of the load. Finally, my thanks to my wife, Cheryl, for that all crucial support and understanding only she could provide. This research was conducted with the support of the Office of Naval Research, Chemical Oceanography, Code 482.

I. INTRODUCTION AND BACKGROUND

A. INTRODUCTION

The use of satellite imagery enhances the observation of the complex circulation patterns and surface temperature patterns prevalent particularly in eastern boundary currents. Such patterns are intricately related to coastal upwelling events, defined as "an interval longer than an inertial period during which local winds initiate and maintain coastal upwelling" [Thompson, 1974].

The purpose of this research is to investigate the various dynamical properties manifest in the area off Point Sur by upwelling related sea surface temperature anomalies detected initially by the Tiros-N Advanced Very High Resolution Radiometer (AVHRR) and confirmed by synoptic ship observations of temperature, salinity and nutrient fields taken during chemical mesoscale research cruises on R/V ACANIA in 1979. The Point Sur area is indicative of a large portion of the west coast north of Point Conception and south of Cape Mendocino, and processes occurring there are characteristic of those occurring within the region (Fig. 1).

Much of the recent literature on the oceanography of the area involves climatology and averaging techniques on spatial and time scales which mask the mesoscale anomalies which exist off Point Sur. These have time scales of approximately two weeks and spatial dimensions of 40 to 60 km

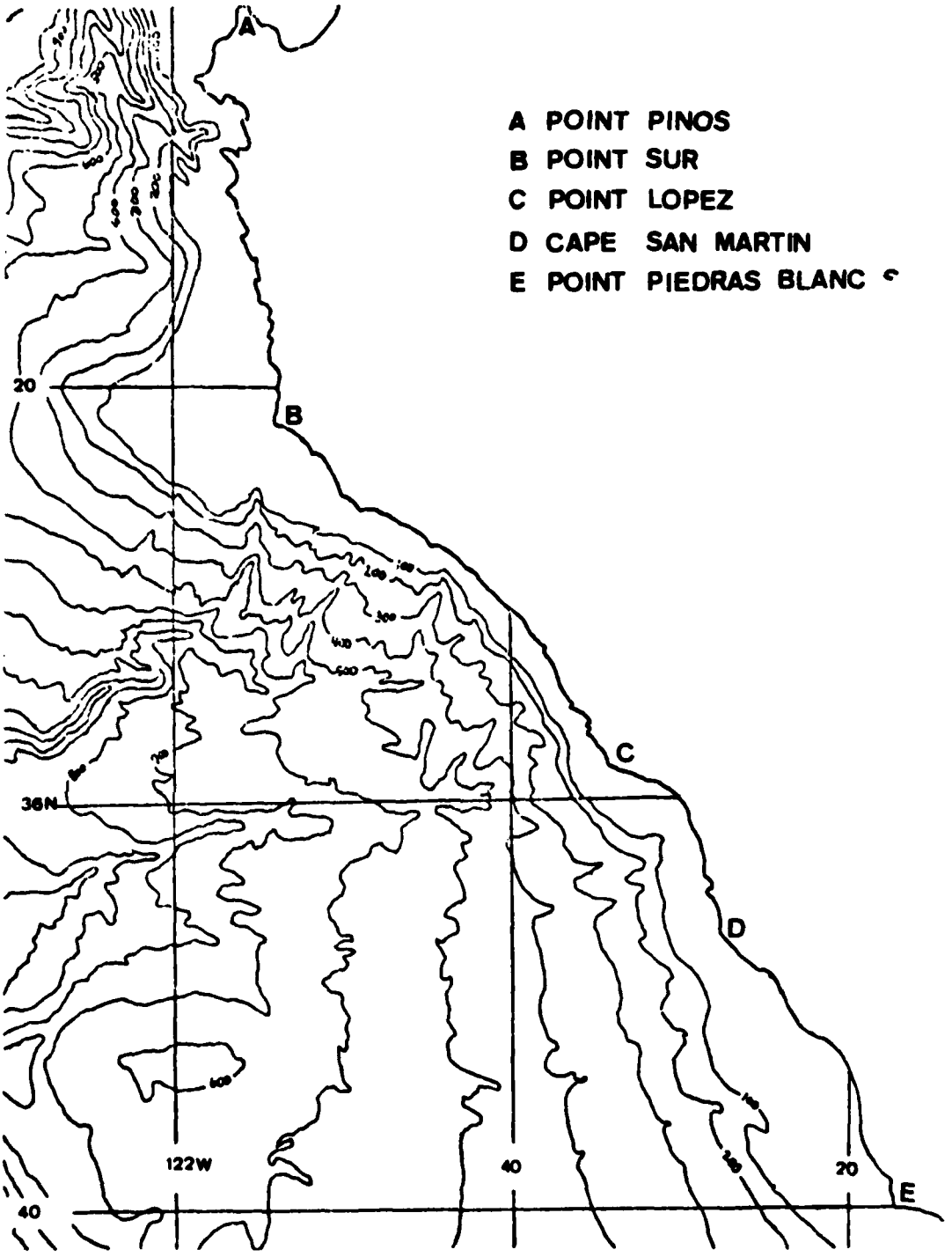

Fig. 1. The area of interest and the location of wind stations at Point Pinos, Point Sur and Point Piedras Blancas

with significant frontal bands which are of the order of one to two km wide. The availability of synoptic satellite imagery with one km and 0.5°C resolution in the 10 to 12.5 μm infrared band leads to the observation that anomalous cold sea surface temperatures (SST) normally associated with upwelling processes are present year round. In addition, Expendable Bathythermograph (XBT) data acquired in conjunction with nutrient and SST measurements of anomalous areas indicate complex thermal structure extending to 400 m.

Interactions of particular interest are local wind driven upwelling and offshore surface Ekman transport within 25 to 50 km of Point Sur, though certainly this is not the only dynamical forcing present. Specific objectives are to identify appropriate spatial and temporal scales, to make observations on the subsurface structure of features observed by satellite imagery, to investigate the diurnal variation of the sea breeze and of the SST as detected by Expendable Bathythermograph (XBT) probes, SST' thermistors at 2 m, bucket thermometers, and satellites, and to compare acoustic propagation in an upwelling (cold wedge) situation to a non-upwelling situation.

The importance to the Navy of this research is the increase in understanding of the effects on underwater sound transmission due to varying water masses in eastern boundary current regions. The satellite detection of upwelling-type features and the associated knowledge of the typical

sub-surface structure of these features can provide real time information crucial to mission planning.

B. BACKGROUND

1. Typical Upwelling Features and Effects

Upwelling is a phenomenon which has well noted impact upon many physical and biological processes:

Temperature: Upwelling through vertical advection and accompanying horizontal advection results in surface water temperatures much below normal for the latitude and season. Vertical cross sections of temperature in an upwelling region show the shallow isotherms ascending steeply.

Salinity: In the upwelling region of the California coast, salinity increases with depth such that upwelling increases the surface salinity.

Density: The density structure follows the temperature structure with isopycnals rising in upwelling regions. A very strong pycnocline may intersect the sea surface to form a front.

Nutrients: Nutrients present in the upwelling water may be characterized as "biochemically" new on the basis of nitrate to phosphate ratios which approach 15:1. Nutrients present in the open ocean surface water approach 5:1 [Nestor, 1979].

Climate: There is a marked effect upon the climate which generally makes the West Coast at these latitudes cooler. As the air cools, the relative humidity increases. Thus, low stratus and fog are common in a shallow layer with warm air aloft. Cool sea water contributes to diurnal sea breeze by increasing the pressure gradient. Onshore winds bring cool, moist air as far as 50 mi inland [Smith, 1968].

2. Mean Flow

a. Introduction

The California Current System is comprised of four currents: the California Current, the California

Undercurrent, the Davidson Current, and the Southern California Current [Hickey, 1979]; the first three of these currents directly influence the Point Sur area.

b. California Current

The California Current is part of the North Pacific Subtropical (anticyclonic) Gyre centered near Hawaii. It is a continuation of the West Wind Drift in the North Pacific and it turns westward between 20N and 30N where it becomes part of the North Equatorial Current [Sverdrup et al, 1942]. The Current is a strong wind-driven equatorward current which exhibits significant seasonal variations proportional to the changes in the wind field [Brown, 1974]. Off Point Conception the mean annual location is 270 km offshore, and the Current is of the order of 700 km wide and flows south at 10 to 30 cm sec^{-1}.

c. California Undercurrent

Northward subsurface flow over the continental slope comprises the California Undercurrent, also called the counter current. Flow is maximum at 200 to 250 m in summer and fall [Pavlova, 1966 and Hickey, 1979]. Coddington (1979) calculated geostrophic flow alongshore near the shelf break in the area of interest to be 15 cm sec^{-1}. In studying the Undercurrent near Point Sur, Wickham, et al., (1974) observed the expected intensification in fall and weakening in spring and movement of the maximum velocity core to the surface in December. In addition, a seasonal onshore-offshore migration

of the principle flow was noted. At 36° 20' N in August 1972, Wickham (1975) noted two branches of the Undercurrent with characteristic speeds of 20 cm sec^{-1} separated by an intense equatorward flow with maximum speed of 80 cm sec^{-1} located 25 km from the shelf break. Event scale fluctuations in the flow appear to be correlated with fluctuations in the alongshore component of the local wind stress [Hickey, 1979].

d. *Davidson Current*

A seasonal flow known as the Davidson Current is the surface expression of the high speed core which rises from 200 m to the surface during the late fall and winter north of Point Conception. This flow appears to have a jet-like structure vertically and horizontally and it extends to the bottom over the continental slope. The current is near the coast, usually within 100 km, well inshore of the California Current and is confined roughly to the continental shelf and slope. In the area of interest, Blumberg (1975) observed the Davidson current within 30 km of the coast in winter 1974. The flow is generally related to the weakening of northerly (upwelling favorable) winds and the occurrence of southeasterly (downwelling favorable) winds.

e. Variability

A great deal of variability in the properties of the currents affecting the Point Sur area has been observed. There is a permanent cyclonic eddy off the area which produces northward flow during all months except April [Hickey, 1979].

The U.S. Coast Guard continental shelf temperature survey for October 1970 indicates a warm tongue or eddy off Point Sur which suggests the existence of an anticyclonic feature [Soluri, 1971]. An anti-cyclonic eddy was observed there in August 1970 and January 1972, and a cyclonic eddy in February 1971 [Brown, 1974]. According to Brown, currents at 200 m are similar to those at the surface in general near the Central California Coast. An exception is off Point Sur where an anticylonic surface eddy was superimposed on a cyclonic eddy at 200 m.

3. Water Masses

Reid, Roden, and Wyllie (1958) describe water masses that contribute to the California Current System. The Subartic Water mass and the Central Water mass are advected from the west and northwest. The Davidson Current is composed of a mixture of Equatorial Water advected from the south and the water upwelled along the coast [Brown, 1974]. This classification is simplified by the descriptive use of two extreme water masses, "northern", made up of Subartic North Pacific Water and "southern", made up of Equatorial Pacific Water [Sverdrup et al, 1942]. The percent composition of the water can be defined by use of Fig. 2. Below 800 m off Monterey, the water is greater than 60% southern water. This proportion increases with depth and towards shore [Brown, 1974]. The Undercurrent is characteristically warmer and more saline than the California Current, and it has a salinity maximum on the $\sigma_t = 26.54$ surface.

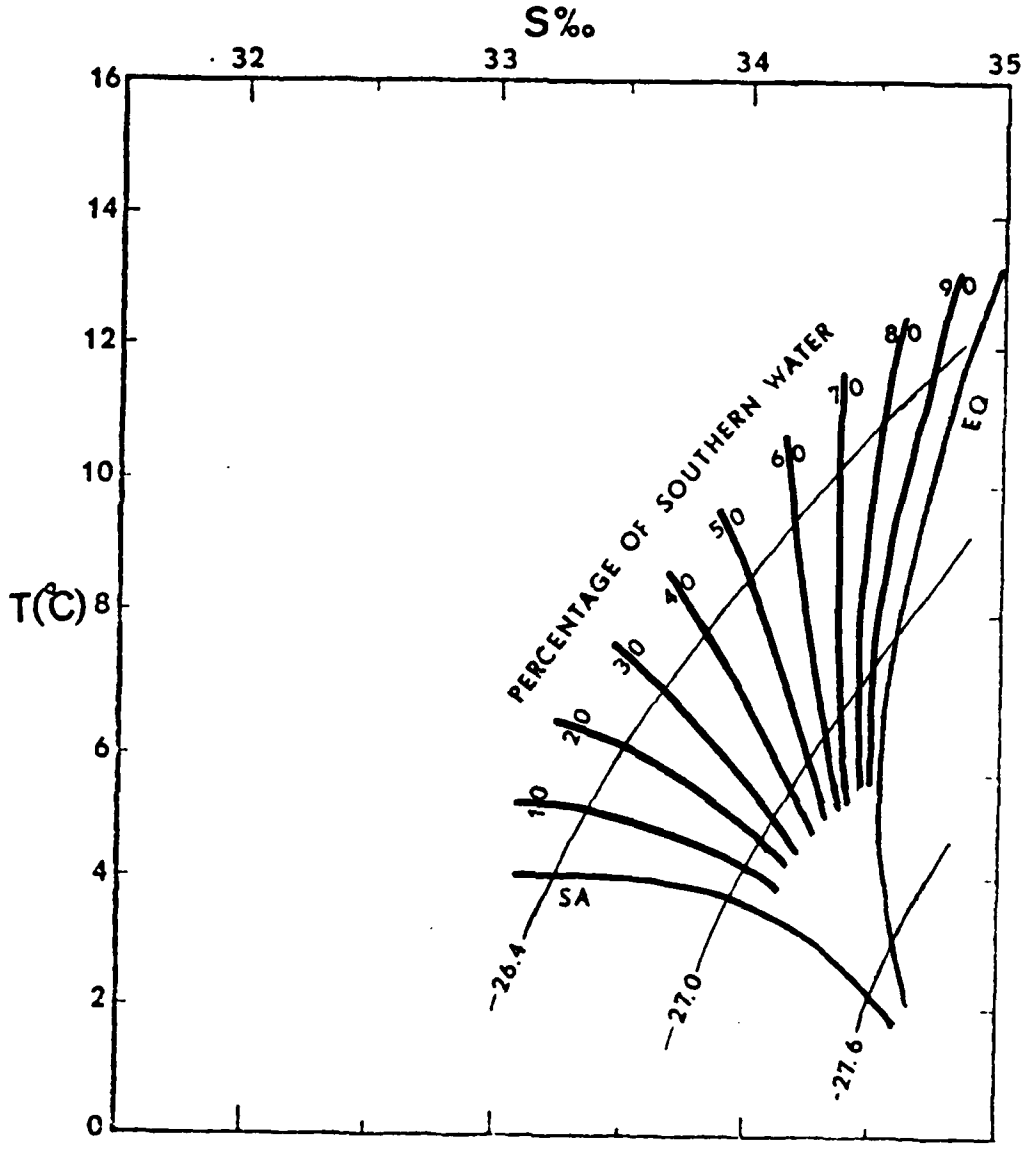

Fig. 2. Graph showing T-S curves defining Subarctic Water and Equatorial Pacific Water, and curves for various percentages of Equatorial Pacific Water assuming mixing along surfaces of equal σ_t [Brown, 1974].

4. Oceanic Climatology

Skogsberg (1936) described the waters of the Monterey Bay area in terms of three major phases, "cold water", "warm water", and the "low thermal gradient" phases. Bolin later described these phases and labeled them as the "upwelling", "oceanic", and the "Davidson Current" periods, respectively [Soluri, 1971].

The upwelling period is the most persistent of the three. It is usually initiated with the onset of persistent northerly winds. The subsequent transport of surface water away from the coast results in replacement by colder subsurface layers from depths which depend upon a number of factors but which generally appears not to exceed 200 m. The sea surface temperatures are the lowest of the annual cylce and surface salinity is the highest. Upwelling is characterized by a shoaling of isotherms towards the coast where the temperature is of the order of 10°C less than offshore. Below the level of the upwelling source water, the slope of the isotherms typically reverses sign, which is indicative of a change in sign of the "thermal wind" at the core of a jet, such as, the Undercurrent.

In the areas of intense upwelling, tongues of low temperature water extend away from the coast in the surface layer and in between are higher temperature tongues extending towards the coast. The flow within the warm tongues is directed towards the north, and the flow within the cold

tongues is directed towards the south [Blumberg, 1975]. According to Pirie (1973), such features are approximately 50 km in width off Point Sur. Based on Shepard (1970), upwelling flows follow preferred routes along the bottom in Monterey Bay, in particular along the axis of the Monterey Submarine Canyon.

In September, there is a transition during which the calm of the oceanic period prevails. Upwelling becomes intermittent as the northerly winds weaken. The surface features break into irregular eddies with complex offshore transport. Cold dense surface water sinks and is replaced by the convergence of warm water from offshore areas. Characteristic of the period is a shallow, sharp thermocline and sea surface temperatures greater than 13°C, the highest of the year [Soluri, 1971].

In November, the upwelling ceases with the onset of southerly winds. In the surface layers, the Davidson Current dominates and lasts until late January. Sea surface temperatures decrease slightly during this period which is characterized by a thick homogeneous upper layer and by a weak thermocline depressed to 50 to 100 m [Blumberg, 1975].

5. Theory

a. Model Review

(1) Highlights of Models. The models reviewed are summarized:

NAME	DATE	RESULTS OF INTEREST
Hidaka	1954	Upwelling is confined to a viscous boundary layer of dimensions $(A/f)^{1/2}$ where A is the horizontal eddy viscosity and f is the coriolis parameter. Typical values are ca. 1 to 10 km.
Yoshida	1955	Width scale is the baroclinic radius of deformation (ca. 10 km); with equatorward wind stress, an equatorward surface jet and poleward undercurrent also exist.
Charney	1955	Spinup of a wind driven coastal jet is related to conservation of potential vorticity.
Yoshida and Mao	1957	Upwelling is accounted for mainly by surface wind stress curl. Intense upwelling occurs only during summer and fall in northern upwelling areas.
Arthur	1965	Due to conservation of potential vorticity preferred location for upwelling is on the equatorward side of a cape on the west coast of a continent.
Garvine	1971	Alongshore pressure gradients may be important elements in coastal upwelling dynamics; they can provide mass compensation through onshore geostrophic flows.
OBrien and Hurlburt	1972	Transverse motion may be generated in two ways, directly by wind stress and indirectly by reacting to the thermal wind imbalance.
McNider and OBrien	1973	With a four layered model, Ekman drift took place in the surface layer and onshore flow through the lower layers. Structure tilted away from the coast with depth. A one cell pattern was formed. Propagating internal waves were manifested in the transverse circulation.
Allen	1973	The interior onshore flow may be completely confined to the bottom Ekman layer.

Hurlburt and Thompson	1973	Equatorward wind stress resulted in a surface equatorward jet, a poleward geostrophic undercurrent, and reduced Ekman drift in the surface layer due to N-S slope of the sea surface. Kelvin wave and continental shelf wave dynamics were important.
Gill and Clarke	1974	Non-local winds influence local upwelling intensity. Long baroclinic Kelvin waves induce upwelling only near coastal or topographic irregularities or at the shelf break. Upwelling can be inferred from sea level changes.
Pedlosky	1974	Onshore and upwelling flow is sensitive to all scales of forcing. For intermediate scales of order 10^2 km, upwelling is confined to shallow layers.
Hurlburt	1974	A topographic beta (vorticity) effect (β_t) was described from the mesoscale alongshore variations due to topgraphy with a scale $0(10^2)$ km which may excite Kelvin waves. A wedge shaped slope where $\beta_t > 0$ resulted in a poleward undercurrent while $\beta_t < 0$ did not.
Thompson	1974	With radiative heat fluxes and turbulence included, two "cyclonic" cells, as reported by Mooers (1973), occurred in a vertical plane normal to the coast within 10 to 50 km. Consistent with potential vorticity conservation, there was secondary upwelling region over the shelf break. Flow split at the shelf into two segments, one fed the primary upwelling region while the other fed the secondary upwelling region. Solar heating appeared to strengthen zonal sea surface temperature contrast and enhance frontal intensification. Upwelling once initiated continued for a significant period, i.e., several days, after the wind forcing was removed due to the effects of alongshore currents and shears. Maintenance in the upper 20 m required continuous wind forcing.

Suginohara	1974	Upwelled portion of the pycnocline propagated poleward with the speed of an internal Kelvin wave after the wind ceased.
Anderson and Gill	1975	Upwelling relaxation involves radiation of offshore propagating planetary long waves.
Peffley	1976	Bottom topographic variations were more influential than coastline irregularities in determining the longshore distribution of upwelling. With the inclusion of topography, the northward propagation of the upwelling zone was apparent.
Killworth	1978	The zone of upwelling started south of a ridge and as time progressed, due to Kelvin waves, it moved north to center over the ridge. A complicated cyclonic over anticyclonic circulation pattern formed above the ridge.
Pedlosky	1978	The effect of non-linearity was to sharpen the zone of upwelling into a frontal discontinuity. With a uniform stress field, upwelling circulation entered the mixed layer in a narrow region in comparison with the radius of deformation.
Endoh, et al.,	1980	With a two dimensional rigid lid model, double cell circulation was possible with a low Richardson number in the thermocline. The change of sign of the cross shelf velocity occurred in the middle of the thermocline as opposed to the base.

Highlights of these theories and models with particular items of interest in the Point Sur area within the scope of this paper are listed below.

(2) Preferred Location. Upwelling is expected to occur within a baroclinic radius of deformation from the coast [Yoshida, 1955]. The presence of a cape is expected

to modify the alongshore flow such that upwelling should be stronger on the south side of the cape. Enhanced upwelling should occur near the shelf break [Hurlburt and Thompson, 1973].

(3) Topographic and Coastline Effects. Upwelling is more intense near a cape, slightly greater to the south than the north. The effect of a mesoscale canyon is to decrease the intensity of upwelling north of its axis, increase it south of its axis and increase it on its axis nearshore. The circulation pattern attributed to effects of the canyon consists of two asymmetric cells, one to the north and one to the south. The southern cell is cyclonic in the surface layer and anticyclonic below [Hurlburt, 1974].

(4) Thermal Structure. Strong sea surface temperature gradients exist within 10 to 50 km of the coast and the region of maximum sea surface temperature gradient moves offshore with time during continuous favorable wind stress [Thompson, 1974]. The response of the surface temperature field is not instantaneous. A lag of about one day typically occurs off NW Africa between the onset of strong winds and a significant drop in temperature [Barton, et al., 1977]. Also, the effects of upwelling do not disappear over a period of several days when the wind is unfavorable to upwelling [Huyer, et al., 1974].

(5) Jets. The poleward jet does not extend past the continental slope [Hurlburt, 1975], and the lowest interface is downwarped after the poleward jet is established

[McNider and O'Brien, 1973]. The equatorward jet tilts offshore with depth [Thompson, 1974]. Large amplitude fluctuations in alongshelf flow are associated with one-to-ten day wind events. There are few persistent features observed in cross shelf and vertical velocity components [Curtin, 79].

(6) Remarks. Upwelling can only attain a maximum seaward extent of about 30 km even with an infinite wind stress. However, the interaction between planetary long waves and coastal upwelling causes the width to increase with time [Anderson and Gill, 1975]. Wind stress with an alongshore scale $0(10^3)$ km is the most important forcing mechanism driving alongshore currents [Pedlosky, 1974]. When the wind is "turned off", the upwelled water propagates poleward with the speed of an internal Kelvin wave [Suginohara, 1974].

In reality, upwelling is a three dimensional phenomenon complicated by irregular and unsteady winds, by irregular bottom topography and by thermohaline effects. Also, the models and theories have deficiencies. Most important of these is an inadequate description and parameterization of mixing [Yoshida and Mao, 1957; Pedlosky, 1978]. Yet the mixing zone ensures that fluid flowing seaward in the upper layer is not heavier than the fluid in the layers below [Pedlosky, 1978]. Other obvious deficiencies are: short run times which result in effectively linear models; e.g., Peffley (1976) or which result in only a barotropic dynamic response; e.g., Hurlburt (1974) and Thompson (1974); the neglect of longshore

variations and derivatives; e.g., Hurlburt and O'Brien (1972); unrealistic topography, an almost universal problem in numerical models prior to 1974; and, the use of averaging techniques which mask upwelling on smaller temporal and spatial scales; e.g., Yoshida and Mao (1957), Pedlosky (1974).

b. Forcing

(1) Continental Shelf or Coastally Trapped Waves

In some areas, notably in the Gulf of Guinea, classical upwelling theory does not apply, i.e., there is little or no correlation between upwelling and local wind stress. Instead, coastally trapped waves forced by wind events located on the order of 100 km to the east are important [Clarke, 1979].

The term continental shelf wave includes such phenomena as coastally trapped topographic waves of varying wavelengths from $0(10^1)$ km to $0(10^3)$ km and edgewaves with wavelengths $0(10^2)$ km [Sturr, 1969]. Such waves are confined to the effective wave guide imposed by the continental slope, continental shelf, and "coastal wall" (shoreface) and exhibit the following properties: an offshore decay of wave amplitude with an e-folding on the order of a wavelength, one-way propagation, and very low frequencies, i.e., less than the inertial frequency [Mysak, 1967].

In general, the coastal water response to forcing such as Ekman pumping from non-uniform wind stress with significance to upwelling includes baroclinic and barotropic Kelvin and topographic Rossby waves. The hydrodynamics

of the system, i.e., shelf geometry and density stratification, and the wind structure, i.e., temporal and spatial scales, determine the relative importance of the various trapped waves.

The two layered, variable depth model of Wang (1976) supports the conjecture that the baroclinic Kelvin and topographic Rossby waves are eigenmodes of the coastal hydrodynamical system. In the limit of a vanishing coastal wall, the topographic Rossby wave is the only trapped wave of sub-inertial frequency. With little stratification, the result is a barotropic shelf wave and with larger stratification, a bottom trapped wave. In the more general case with coastal wall and bottom slope effects, both the baroclinic Kelvin wave and topographic Rossby wave are eigenmodes of the system, raising the possibility of resonance. For example, in a continuously stratified model, mode one behaves as a topographic Rossby wave for small wave numbers and as a baroclinic Kelvin wave for larger wave numbers [Wang and Mooers, 1976]. Scattering into other modes by topographic features could be an important source of anomalies [Wang, 1976; Allen, 1976]. Such scattering perturbs flow adjacent to alongshore variations in topography, and the subsequent disturbances propagate as free continental shelf waves [Allen, 1976].

Topographic Rossby waves are basically quasi-geostrophic and governed by the potential vorticity conservation of a perturbation flow in a homogeneous water

column [Wang, 1976]. A wavelength of $o(10^3)$ km and phase speed of 1 ms^{-1} are typical [Brink and Van Leer, 1980]. The baroclinic Kelvin wave is a non-dispersive, non-geostrophic internal gravity wave governed by coastal boundary conditions and confined within a baroclinic radius of deformation of the coast. Phase propagation is poleward and parallel to the coast in the eastern boundary current regime in the Northern Hemisphere [Wang, 1976]. A wavelength of $0(10^3)$ km and phase speed 0.1 to 1 ms^{-1} are typical [Brink and Van Leer, 1980].

(2) Baroclinic Instability. Mysak (1977) suggested that the California Undercurrent is baroclinically unstable with respect to poleward traveling quasi-geostrophic waves. In a channel 75 km wide, the first mode was most unstable with a wavelength of 65 to 94 km, period of 5 to 10 days, and an e-folding time of 4 to 13 days. Topography and stratification had a stabilizing effect whereas the vertical shear had a de-stabilizing effect. When second order ageostrophic effects are included, formation of a cold eddy is predicted in the offshore region. Hence, a baroclinic instability process may induce the prevalent temperature perturbations observed in satellite IR images of the eastern boundaries of mid-latitude basins.

(3) Atmospheric Forcing. Near surface sea temperature anomalies are caused by a variety of mechanisms. Among these are horizontal advection by surface geostrophic

and Ekman flows, horizontal divergence of the surface layer produced by wind stress curl, anomalous heat flux at the surface and anomalous entrainment of heat at the base of the mixed layer generated by wind stirring and convective overturning [Elsberry and Gallacher, 1979].

Wind stress is calculated from:

$$\vec{\tau} = \rho_a C_D |\vec{V}| \vec{V} \qquad (1)$$

where:

- $\vec{\tau}$ denotes the stress vector,
- ρ_a is the density of air (typically 0.00122g/m^3),
- $\vec{V}$ is the observed wind velocity,
- $|\vec{V}|$ is the observed wind speed,
- C_D is an empirical drag coefficient.

The value of C_D depends upon the height of the wind measurement and the averaging techniques employed. It varies with the atmospheric stability and the spectral properties of ocean waves [Davidson, 1974]. Commonly used values are 0.0016 [Bakun, 1973] and 0.0013 [Nelson, 1976].

Estimates of the transport in the surface layer of the ocean due to the stress of the wind are based upon Ekman's (1905) theory which leads to the following equation for the total integrated mass transport of pure drift currents:

$$\vec{V}_E = 1/f \; \vec{\tau} \times \vec{k} \qquad (2)$$

where:

$\vec{V}_E$ is the total mass transport resulting from an applied local wind stress,

f is the coriolis parameter, and

$\vec{k}$ is a unit vector directed vertically upward.

Effects of density stratification, lateral mixing and the variation of the coriolis parameter with latitude are neglected. The minimum favorable wind stress required is of the order of 0.5 dyne cm^{-2} [Curtin, 1979].

Upwelling indices are proportional to the square of the equatorward component of the wind; positive values denote equatorward wind and offshore Ekman transport. They are based on nearsurface geostrophic winds and a simplified frictional boundary layer approximation. The surface wind is assumed to be 0.7 times the nearsurface geostrophic wind and shifted 15° counterclockwise. The program uses the Fleet Numerical Oceanography Command six-hourly sea level pressure analysis. This analysis is performed on a 63 x 63 grid over the Northern Hemisphere and therefore resolution is approximately 380 km [Bakun, 1973]. The indices suffer from an inability to resolve mesoscale features of EKman transport.

Long term monthly mean onshore-offshore wind stresses in 1-degree squares immediately adjacent to the

coast at 36 N are directed offshore except for the month of July and are maximum offshore in November with a value of 0.07 dynes cm^{-2}. Alongshore stresses are equatorward year round with a maximum in June of 1.22 dynes cm^{-2}. Wind stress was more variable in magnitude than direction implying that upwelling is possible year round south of Cape Mendocino. This contrasts with the area off Oregon and Washington. Also, the area of maximum stress shifts northward through the spring and summer. In April, it is from Point Conception to San Francisco [Nelson, 1976].

The surface wind stress curl is the forcing function for the vertically integrated mass transport of the meridional component of the wind driven ocean circulation. The meridional transport is directly proportional to the vertical component of the curl of the wind stress, $\vec{k} \cdot (\nabla \times \vec{\tau})$. Positive wind stress curl is associated with northward meridional Sverdrup transport and surface Ekman divergence. Wind induced upwelling will occur whenever divergence in the surface wind drift is not balanced by other horizontal flow (Fig. 3).

Along the central California coast, the existence of an offshore maximum in the alongshore wind stress results in a line of zero wind stress curl somewhat parallel to the coast approximately 200 to 300 km offshore during the spring and summer upwelling. Using a coarse grid of 5-degree squares, Yoshida and Mao (1957) estimated this boundary to be approximately 500 km from the coast.

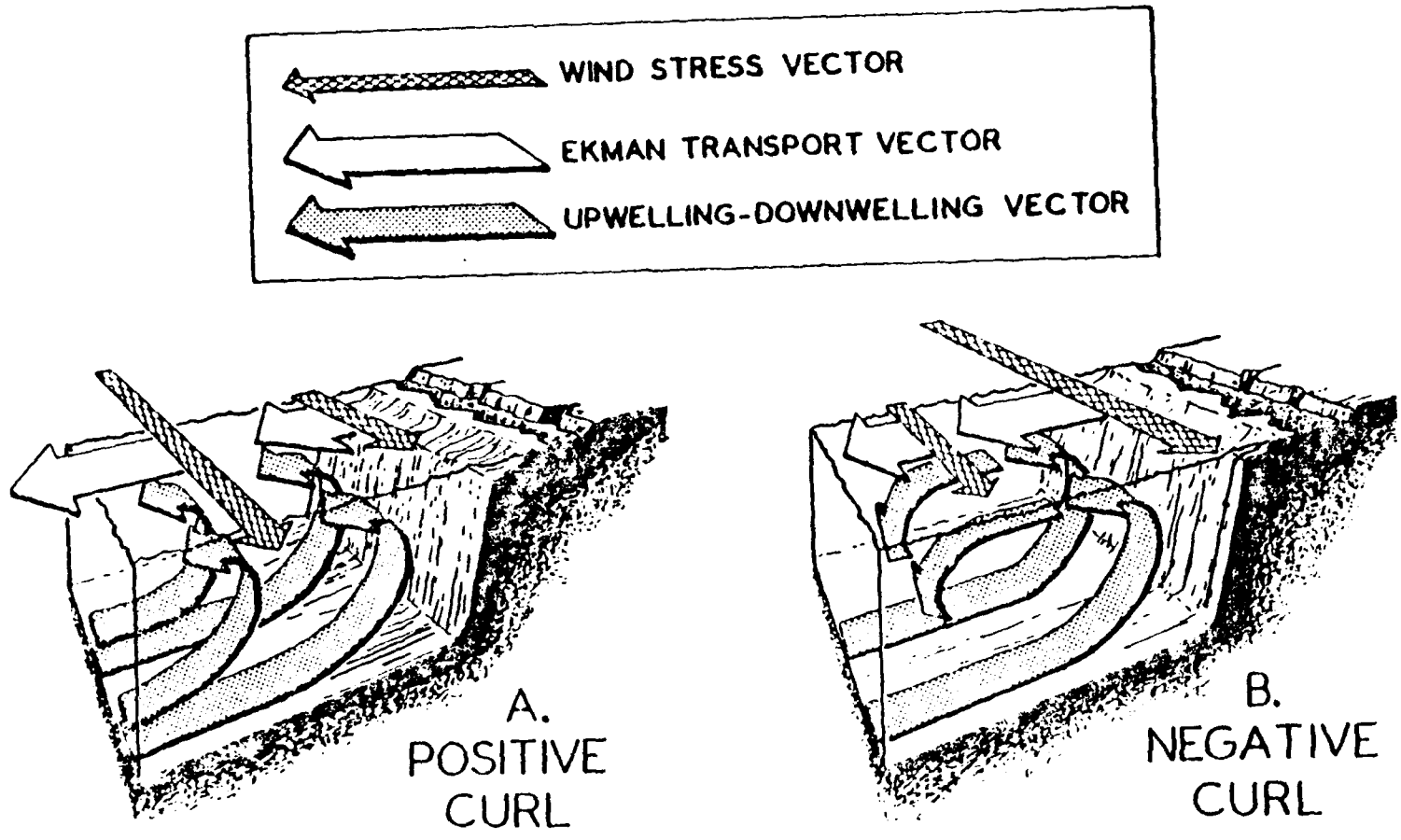

Fig. 3. A conceptual diagram of the relationship of wind stress curl to divergence and convergence of surface Ekman transport offshore of the primary coastal upwelling zone [Nelson, 1976].

Negative curl in the offshore region is due to the atmospheric circulation associated with the high pressure system over the interior ocean, while positive curl inshore is due to the frictional influence of the local topography on the local wind field. Large areas of Ekman divergence extend several hundred kilometers off shore [Nelson, 1976]. At 36 N, the long term monthly wind stress curl is positive except in February and May and maximum in July with a value of 0.46 dynes cm^{-2} per 100 km [Nelson, 1976].

Changes in the general atmospheric circulation over the North Pacific account for the major seasonal variations in the surface wind stress. Monthly mean surface pressure charts typically show two well developed pressure cells. A high pressure system over the ocean shifts northwest and intensifies from spring to summer. A semi-permanent thermal low pressure system is centered over the southwestern United States throughout the year. A trough is fully developed over the Central Valley in California during the summer. Geostrophic circulation associated with these cells leads to equatorward surface wind stress along the coast. During the winter, both of these pressure cells weaken and the high pressure system is displaced southward by the intensifying Aleutian low.

Seasonal variations in the gradient between the two systems control the location and magnitude of the wind stress maximum. During the winter, this gradient is

weak. Strong summer heating of the continent deepens the low and increases the pressure gradient normal to the coast. As a result of this and the northwest motion of the high cell, the region of maximum wind stress moves from south of Point Conception to Cape Mendocino from spring to summer.

Wind funnelling due to orography influences some upwelling areas, such as the Gulf of Lyons, by imposing local areas of positive wind stress curl. Another local factor which is not well known is the sea breeze phenomenon which reinforces the pressure gradient normal to the coast during the day and relieves it at night. This sea breeze circulation has surface effects at least as far as 20 km offshore [Halpern, 1974].

(4) Heat Fluxes and Mixing. Other processes affecting ocean thermal structure are solar radiation, back radiation, evaporation and condensation and sensible heat fluxes. The first of these, solar radiation, is a function of the altitude of the sun and cloudiness. In the first meter of water, 50% of the incident solar radiation is absorbed. The rest is absorbed exponentially with depth. Reflection of incident radiation averages 10%. Off Peru, upwelling indices and solar radiation do not correlate, providing evidence that fog caused by coastal upwelling paradoxically does not significantly reduce daily net radiation [Mickelson, 1978]. Measurements off Southern California indicate a loss of 37 Ly

day^{-1} in solar radiation due to upwelling related clouds. Consequently SST is 1°C colder when upwelling occurs [Tont, 1975].

The second of these processes is effective back radiation which is a function of sea surface temperature, air temperature, and the moisture content of the air. Leipper (1947) asserted that back radiation is unimportant in altering the pattern of sea surface temperature since net radiation in cloudy regions is not significantly different from that of clear areas.

Third is evaporation and condensation which depend upon the difference between the vapor pressure at the sea surface and in the air, and the wind velocity. Both tend to diminish the SST gradient by differential warming and cooling [Leipper, 1947].

Finally, there is the sensible heat flux between the ocean and air. This depends upon the air mass above the water which determines the vertical temperature structure of the air and its stability. A cold air mass, which may be unstable, will lower the sea surface temperature while a warm air mass which may be stable and therefore an inefficient conductor of energy may slightly warm the sea surface. Anomalous sea surface temperatures can also be caused by anomalous redistribution of heat in the upper oceanic layers [Elsberry, 1978].

Unusually large periodic variations in sea temperature in shallow stratified water can be the result of tidal stirring over an irregular bottom. The maximum velocity of the tidal flow is inversely proportional to depth. Any locality where bottom topography varies will have widely differing tidal velocities with associated shears.

If the water mass is homogeneous; such as, in the wintertime shallow shelf waters of the temperate zone, there will be no effect. Vertical stirring in stratified water may markedly reduce the sea surface temperature creating a cold spot with a diameter generally not greater than 5 km. The region affected is limited by: (1) the dimension of the area with variable bottom topography, (2) the area of stratified water; and (3) the distance over which tidal water migrates. The effects are greatest in shallow water, but if the cold anomaly does not reach the surface a shallow, more intense thermocline results [Leipper, 1947; Simpson and Pingress, 1977].

(5) Feedback Mechanisms. Sea surface temperature anomalies affect the atmosphere in different manners. In a simple feedback model, wind stress parallel to the coast brings cold water to the surface and cools adjacent air the order of 1°C for 2°C change in sea surface temperature [Tont, 1980]. The resulting temperature contrast between the continent and the ocean increases the local pressure gradient. The alongshore surface winds are increased and upwelling is

enhanced. This mechanism is reduced by atmospheric stability which decouples the momentum transfer from atmosphere to ocean.

Gerst (1965) correlated cloud observations with sea surface temperature anomalies (Table I).

Table I

Correlation of cloud observations with sea surface temperature anomalies [Gerst, 1969]

Cloud Type	Location	Remarks
Stratus	Over California Current	Warm air mass over upwelling area
Clear	Over California Current	Cold air mass over upwelling region
Stratus	Coast	Upwelling
Frontal Clouds	Coast	Warm tongues of surface water
Vortices	Coast	Cold tongues of surface water

Off the coast of Oregon, the horizontal gradient of ambient air temperature reflected the sign of sea surface temperature only to a height of approximately 150 m [Elliott, 1977]. Temperature and moisture fields were very uniform over an area 45 km offshore by 90 km alongshore particularly when there was an inversion. A strong isotach maximum existed approximately 30 km offshore. It was associated with the seaward edge of the seabreeze circulation and helped to maintain a positive wind stress curl.

6. Satellite Usage

a. General

Satellites employed recently as remote sensor platforms for the ocean environment include the Earth Resources Technology Satellite (ERTS) the NOAA 4 and 5 satellites, each equipped with a Very High Resolution Radiometer (VHRR), and the TIROS-N satellite. In addition, the Defense Meteorological Satellite Program (DMSP) offers limited distribution for satellite images of excellent resolution for oceanographic studies [Fett, 1979], even though it was described as "incapable of defining sea surface phenomena" by Platz (1975). A concise review of satellite systems and capabilities is in Traganza (1979).

Advantages of using such information is apparent; e.g., synopticity and broad coverage. However, there are numerous sources of error and misinterpretation due to sensor electronics, geometric distortion, calibration, and atmospheric attenuation. Variations in the signal to noise ratio due to random noise and system noise, which increases as the radiometer ages, introduce spatial and temporal errors. Geometric errors are caused by distortion of the image due to the curvature and rotation of the earth and relative motion of the satellite along its roll, pitch, and yaw axes. This problem is most apparent with polar orbiting satellites because successive views of the same area are made at different angles [Legeckis, 1978].

When comparing satellite derived temperatures to ground truth data, it must be kept in mind that satellite measurements are the average sea surface temperatures of an area approximately 1 km^2 while ground truth data is usually a point measurement. Also, the satellite senses skin temperature only while typical ship measurements are taken below the sea surface.

The greatest errors are induced by atmospheric attenuation of thermal energy along the path between the sea surface and the sensor due to absorption and scattering. These effects are minimized as much as possible by system design and operation in the 10.5 to 12.5 μm band.

The effects of absorption of energy by moisture in the atmosphere present the most severe problems due to the magnitude of the absorption and the variability of the moisture field. Over the ocean, this attenuation at mid-latitudes results in sensor temperature readings that are typically 2 to 6°C lower than the actual sea surface temperature [Maul and Sidran, 1973]. Characteristic profiles of temperature and moisture can be constructed parametrically from SST and integrated water vapor content. Through a cloud free atmosphere, the difference in the 10.5 to 12.5 μm band is estimated to be +/- 0.5°C [Logan and Willard, 1974]. However, these methods fail for very dry and hazy atmospheres, in the presence of thin cirrus, or for atmospheres which deviate from typical profiles of temperature and humidity.

Nadir angle, cloud amount, and cloud height all must be considered for their effects upon transmission through the atmosphere. Maul and Sidran (1973) found that 8°K temperature differences at the sea surface registered less than 3°K at the satellite when viewed at zero nadir angle, and 1°K when viewed at 60° nadir angle. A 10% cloud cover can introduce errors ranging from 0.5°K to 4°K depending on the cumuliform cloud height. Thus, the analysis must be cloud free; or somehow adjustments must be made for the clouds.

To make quantitative, absolute SST measurements then, the profile of temperature and moisture along the transmission path must be known. Depending upon conditions, SST can be 1° to 10°K higher than sensed due to water vapor absorption, 0.1° to 1°K higher due to aerosol absorption, and 0.1°K higher due to CO_2 and O_3 absorption [Legeckis, 1978]. However, Legeckis also states, "Although atmospheric absorption reduces the absolute value of SST as recorded by the satellite, the relative distribution of ocean temperature can be measured within the limitation of noise and spatial variation of the atmosphere."

Finally, when viewing images, the image enhancement techniques used must be taken into consideration. The infrared temperature response is from -90°C to 60°C. Gray shades can be assigned to different temperature bands in order to highlight different sea surface thermal features. Improper enhancement will prevent detection of these features.

A review of satellite imagery alone is subjective due to the gray shading techniques employed and by the lack of temperature scales. Temperatures and temperature gradients are relative to others within the same image. These can best be described as apparent temperatures due to the attenuation effects of the atmosphere upon skin temperature.

Of interest in the case studies to be discussed here is the existence of a plume-like or eddy-like feature, its seaward extent and size, curvature, location of maximum relative gradients and the width of the coastal upwelling band along the coast. No moisture correction is considered. Satellite images were selected from APR 79 to DEC 79 on the basis of atmospheric clarity near Point Sur.

b. TIROS-N

The TIROS-N polar orbiting satellite was launched 13 OCT 78 into a nearly circular orbit approximately 854 km above the earth with a period of 102.0 minutes. It is ascending (northward) about 1500 local time. The sensor of interest on board TIROS-N is the Advanced Very High Resolution Radiometer (AVHRR). The AVHRR has 1.1 km spatial resolution and 0.5°C temperature resolution from 10.5 to 12.5 μm, i.e., infrared. (The spectral response curve is available in Kiddwell (1979).) TIROS-N is the prototype for the new series of NOAA satellites which will carry the same instruments as those on board TIROS-N. Presently, NOAA-6 is also operational.

II. PROCEDURES AND OBSERVATIONS

A. DATA ACQUISITION AND ANALYSIS

Data acquisition was done in support of chemical mesoscale research operations conducted by Traganza, et al., (1979), aboard R/V ACANIA. Preliminary satellite image interpretation was done at the National Environmental Satellite Service (NESS) office at Redwood City. Pertinent information about features off Point Sur was communicated by telephone to the R/V ACANIA prior to each cruise. Images were enhanced and mailed at a later date.

The study area extends 100 km south of and 50 km west of Point Sur. Three cruises of interest into the area are reviewed; 29 APR to 1 MAY 1979, 26 to 28 SEP 1979, and 28 to 29 NOV 1979. Each cruise made several transits through the upwelling-type features identified by satellite. The R/V ACANIA maintained a speed of 10 Kts on each transit. Position was determined by Loran C; coverage is good in the Central California Coastal region. A running plot of thermal and nutrient (nitrate and phosphate) information was maintained and used to ensure adequate coverage of areas of interest.

Information collected increased as the series of cruises progressed. Essentially, keel depth (2m) sea temperature was monitored and recorded continuously. Expendable Bathythermograph (XBT) drops were made at an average spacing of 5 km with increased spatial sampling at frontal or transition

areas. Bucket temperatures were taken with each XBT drop. Cloud cover, wind, swell and barometric observations were taken hourly. Additional data acquired will be specified in individual cases. Data obtained during a fourth cruise from 7 to 9 AUG 1979 are presented in Appendix C. Nutrient samples were also acquired [Nestor, 1979 and Conrad, 1980].

The thermal data were used to construct vertical cross sections of temperature along the cruise track, horizontal plan views of the temperature structure at various depths, plots of thickness between isotherms, isotherm depth contours, and mixed layer depth (MLD) plots. Means and standard deviations were calculated for temperatures at various depths to determine the validity of a particular XBT and the presence of anomaous features. Internal wave analysis did not influence the cruise planning, but where possible, i.e., at cruise track intersections, vertical thermal cross section versus time plots were constructed to try to detect the influence of internal waves. Finally, the differences between bucket temperatures and SST (injection) were plotted to recognize diurnal effects upon the near surface temperature structure.

Information from other sources was later compiled. The 500 mb height analysis and the sea level (SL) analysis from the National Meteorological Center (NMC) were reviewed to determine synoptic scale atmospheric forcing which may have influenced the ocean structure in the area of interest. Wind

observations from Point Pinos, Point Sur and Point Piedras Blancas were reviewed for comparison with ship observations and geostrophic winds. Upwelling Indices, Ekman transports and SL pressures were obtained through NOAA [Bakun, 1973]. A California surface temperature field from Fleet Numerical Oceanography Command was reviewed for each cruise. Satellite IR images from Redwood City were summarized to determine the time scales, spatial scales, growth rates, advection, and the average width of the coastal upwelling region and of other features observed.

B. GENERAL OBSERVATIONS

1. Orography

The terrain in the Point Sur area is rugged and precipitous with two breaks in the coastal mountain range which rises steeply to 1 km within 2 km of the coast. The Little Sur River Valley is located 4 km north of Point Sur. It is oriented E-W and runs 20 km inland. The Big Sur River Valley is 5 km south of Point Sur. It is oriented NW-SE and runs 28 km inland. Numerous small creeks are located normal to the coast both north and south of Point Sur.

2. Bottom Topography

Bottom topography in the domain of interest includes mesoscale canyons and ridges, capes, rises, and the Davidson Seamount. The width of the continental shelf decreases from 12 km at its widest off Point Sur at the northern boundary to 3 km at its narrowest off Point Piedras Blancas

in the middle of the area, 90 km south of Point Sur, and increases to 8 km off Point Conception at the southern boundary, 180 km south of Point Sur.

The northern area is dominated by a shallow cape extending west from Point Sur with a slope of 0.04 to the 2000 m isobath. The center is dominated by the Sur Canyon and Lucia Canyon, both oriented E-W. The former has a maximum axial slope of 0.07 and the latter, 0.05. Both canyons can be distinguished in isobaths as shallow as 100 m. The southern area has a more gradual, wedge-shaped bottom with its axis oriented WSW, 80 km south of the cape off Point Sur. There are three small (of the order of 10 km width, 100 m above the sea floor) rises in the general area.

To the east, the coastline and isobaths less than 200 m are oriented approximately 330°T. To the west, the depth drops off uniformly to 4000 m within 70 km of the coast with the exception of the Davidson Seamount located at 35° 50' N, 122° 35' W which rises from 4000 m to less than 1400 m within 10 km. The bathymetric chart is presented in Fig. 4, the alongshore bottom profile measured 15 km offshore is presented in Fig. 5, and the bottom profiles normal to the coast are presented in Fig. 6.

The topographic Beta effect at 36 N 122 W is calculated from:

$$\beta_t = f/h \, \partial h/\partial y$$

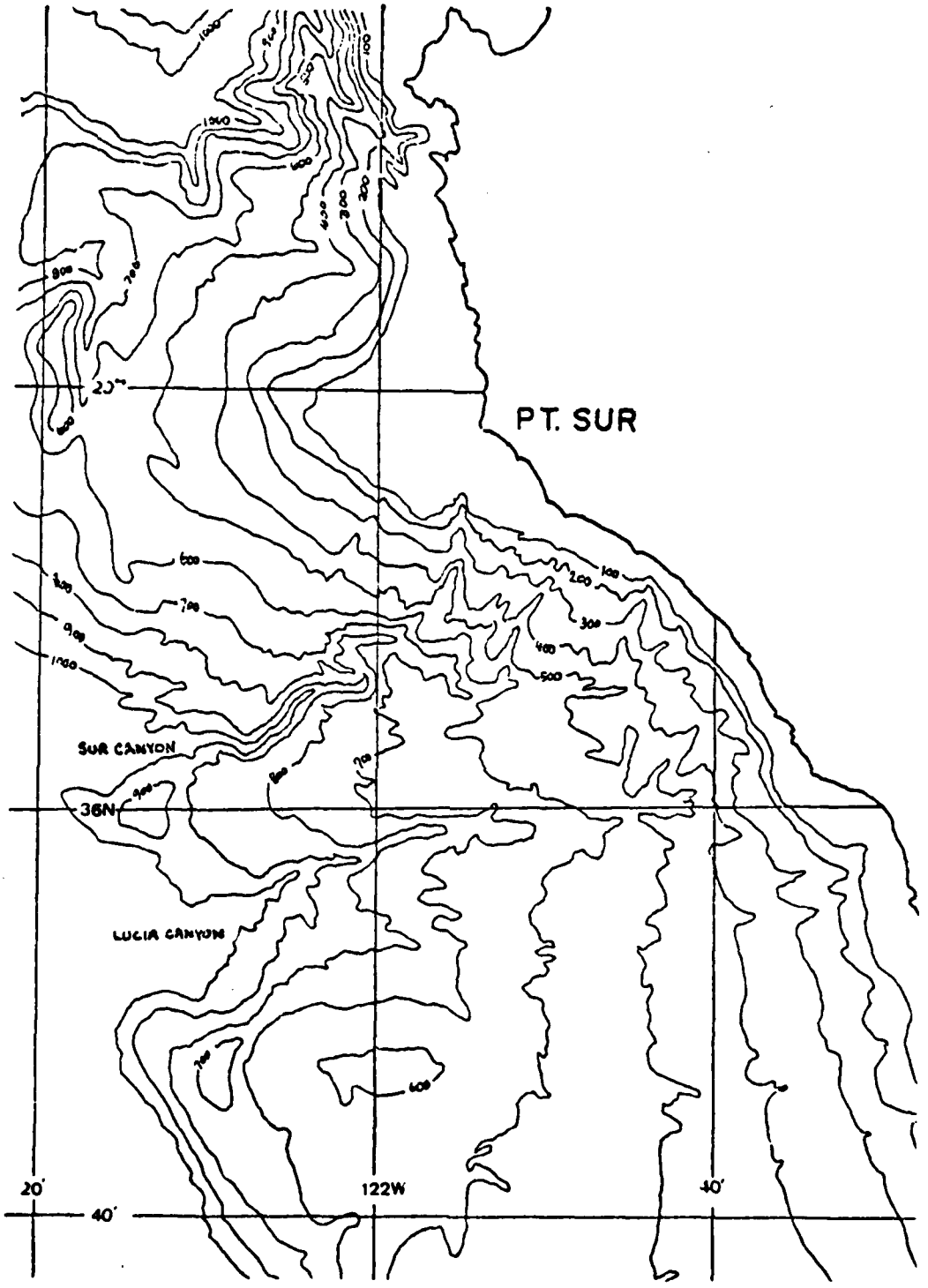

Fig. 4. Bottom topography (in fathoms) off Point Sur

Fig. 5. Alongshore bottom profile (in fathoms) measured 15 km offshore

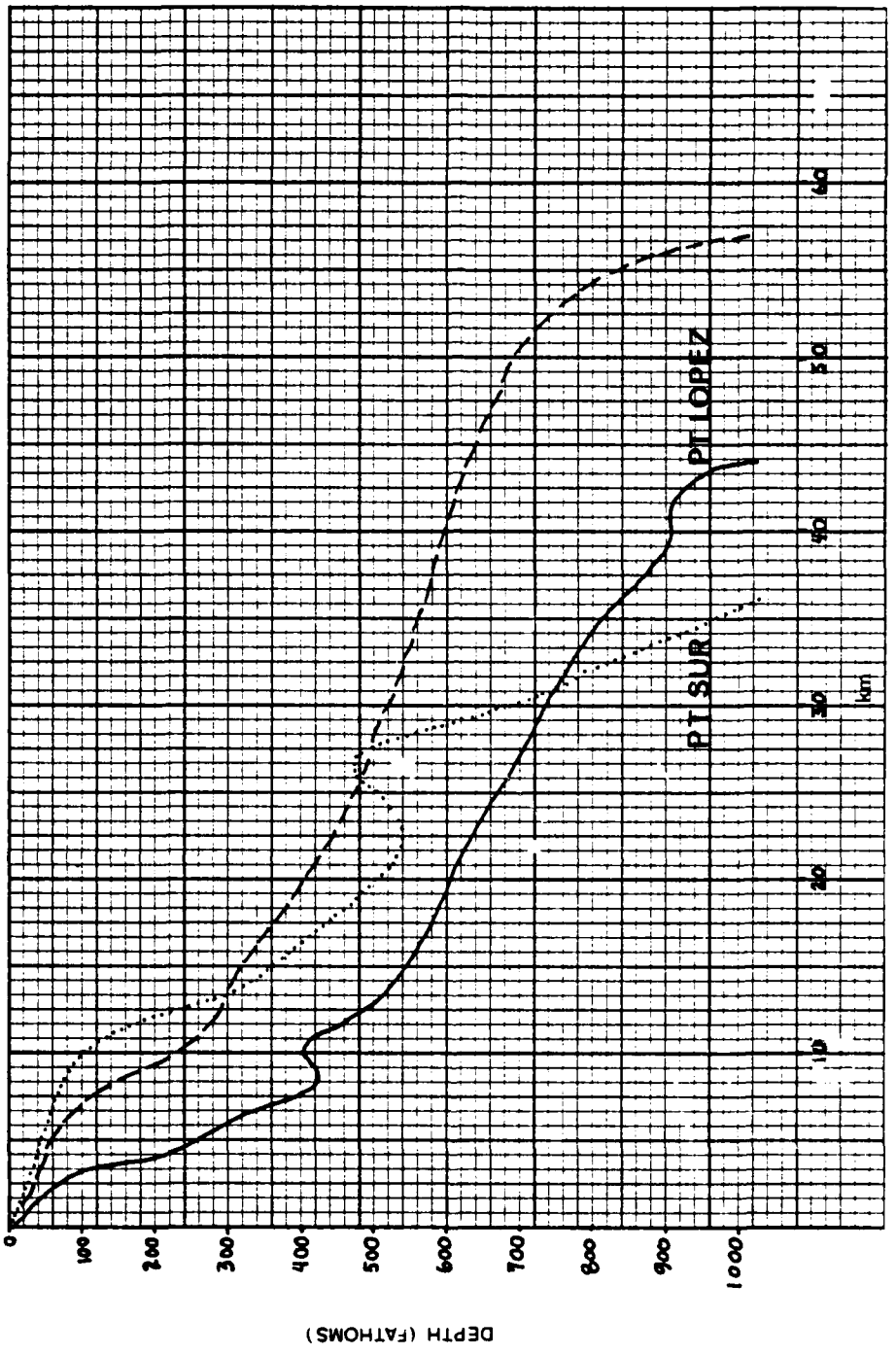

Fig. 6. Offshore bottom profile (in fathoms) taken 270° T from shore to the 1000 fathom isobath.

where f is the coriolis parameter, h is the total depth and $\partial h/\partial y$ is the change in depth along the north-south axis [Thompson, 1974]. At 36 N 122 W, these values are: $f \simeq 8.5 \times 10^{-5}$ sec^{-1}; h ≃ 1.3 km; $\partial h/\partial y \simeq 0.04$ ($\Delta h \simeq 1.3$ km, $\Delta y \simeq 30$ km). β_t is of the order of 10^{-10} cm^{-1} sec^{-1}.

C. SPECIFIC OBSERVATIONS

1. Case I (29 APR to 1 MAY 79)

a. Summary of Oceanic Surface Conditions

The cruise from 29 APR to 1 MAY 79 investigated and verified the existence of a cold plume-like feature extending 80 km southwest from Point Sur. A good estimate of the position of the center of the feature at 35 45 N 122 W was obtained through preliminary analysis of satellite imagery, and a cruise track was planned with three 120 km transits intersecting at the center. The goal of the cruise was to obtain two dimensional sampling of both the feature and the surrounding oceanic water (Fig. 7). Approximately 70 XBT's were used with an average spacing of 5 km.

From 10 APR to 6 MAY 1979, six TIROS-N orbits were reviewed. The IR images were taken at approximately 1430 to 1445 local time, and in all images, the area of interest was relatively free of cloud contamination. Satellite analysis is summarized in Fig. 8.

On 10 APR, there was no evidence of any upwelling related feature present. A uniform band of relatively cold

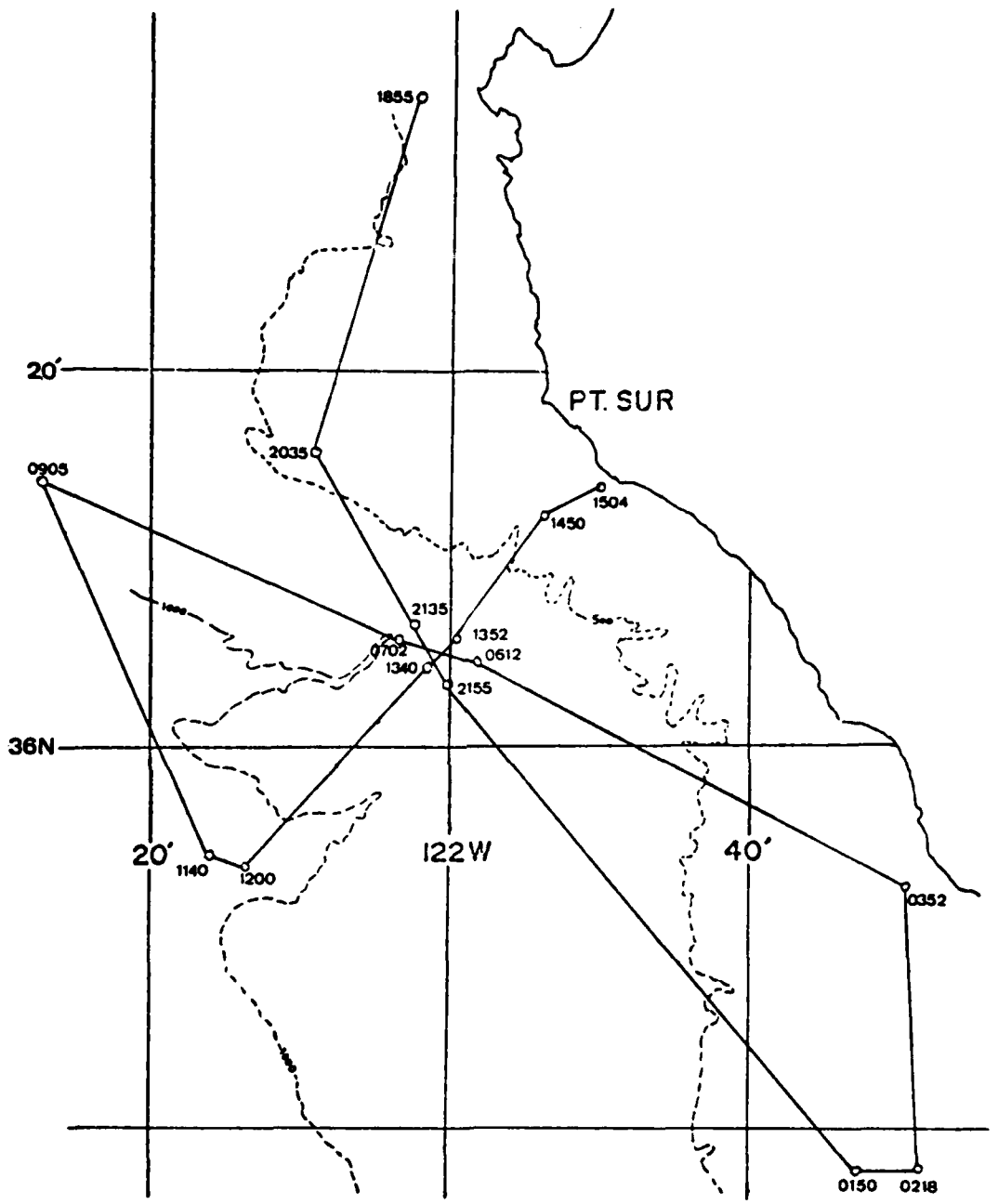

Fig. 7. Cruise track from 30 APR to 1 MAY 79. Times are GMT.

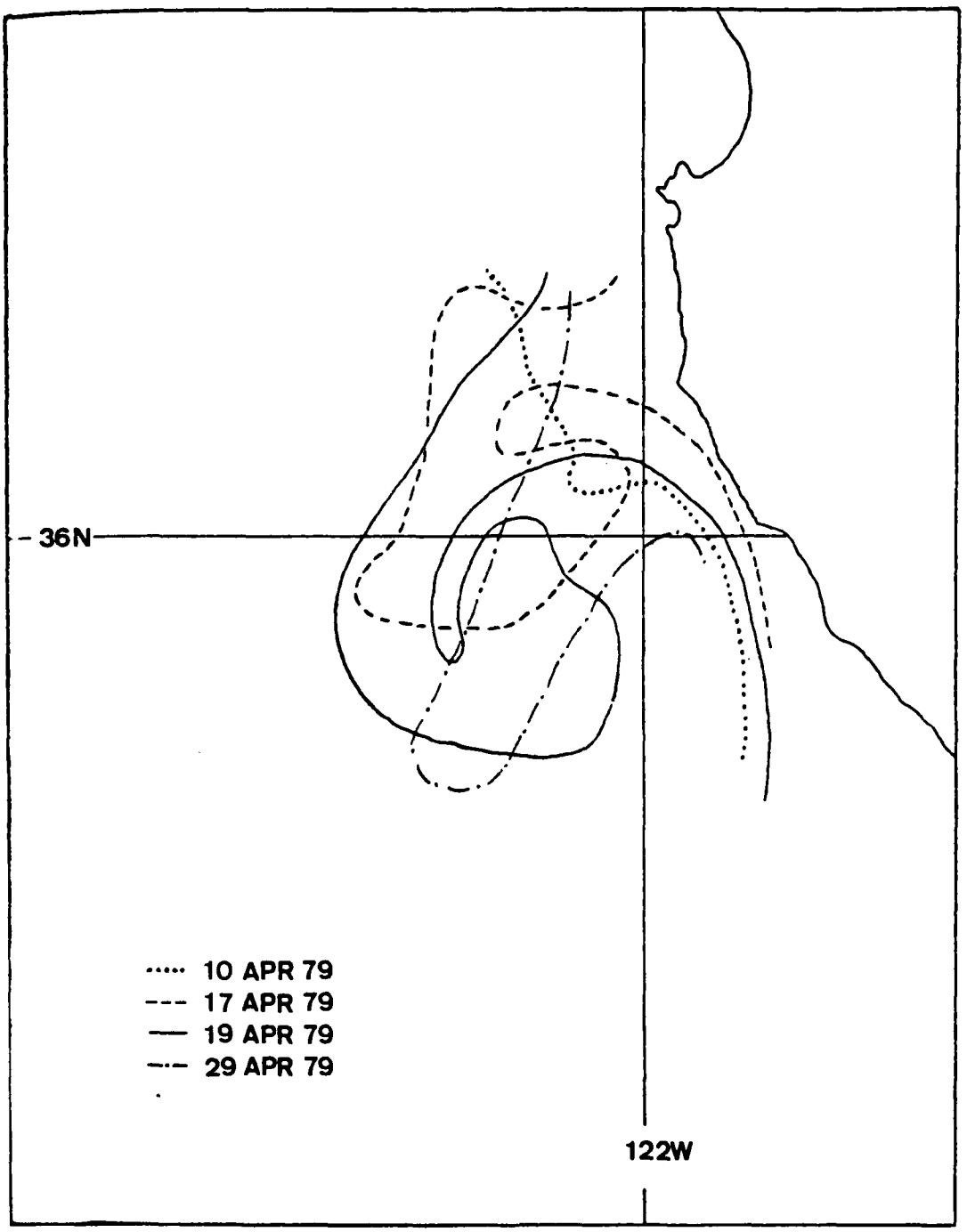

Fig. 8. Satellite features observed from 10 APR to 6 MAY 1979.

water along the coast was approximately 15 km wide from Point Piedras Blancas to Point Sur, and 30 km wide from Point Sur to Monterey Bay, with sharp discontinuity at Point Sur. There was no evidence of eddies.

Seven days later, on 17 APR, there was an obvious but diffuse cold cyclonic feature extending seaward 50 km from Point Sur along 240°T. This was a well formed elliptic feature with strong gradients to the north and southeast, and weak gradients to the west and southwest. The feature was approximately 50 km wide. The coastal band of colder water remained uniform in size, but it was narrower than observed previously. From Point Piedras Blancas north it was approximately 5 km wide. Some cumulus cloud cover contaminated the picture to the west.

On 18 APR, the main axis of the same feature had shifted slightly south to bear 230°T from Point Sur, and the feature had elongated seaward to 80 km. Increased cyclonic curvature was evident, and the surface area of cold water had increased significantly. Again, the coastal band of cold water was a uniform 15 km wide from Point Piedras Blancas to Point Sur. There were some individual cumulus clouds to the west.

On 19 APR, the cyclonic curvature had increased and the identified feature was almost circular in shape. A distinct cold pocket was observed within the feature and there was a plume of colder water running from Point Sur along 225°T around the northern boundary of the cold pocket.

The feature had apparently decreased in diameter to 72 km. The coastal band of cold water remained 15 km wide. The area of interest was cloud free.

Ten days later, on 29 APR, the first day of the cruise, there was evidence of a cold plume-like feature only. There was no cyclonic development. The plume extended from Point Sur along 220°T for 80 km. It was 30 km wide nearshore and 10 km wide at its seaward end. Within the plume, colder water was closer to shore. Throughout the area of interest, there were low level stratus clouds.

The plume persisted and was observable seven days later on 6 May although it had significantly decreased in size to a narrow feature extending along 250°T from Point Sur for 20 km, then bending south for an additional 15 km. It was uniformly 5 km wide. The coastal band from Point Piedras Blancas north to Point Sur was uniformly 15 km wide.

Two distinct features were observed during this period of time. The first, an obviously cyclonic eddy-type feature developed and dissipated over a maximum of 19 days. The center was generally located west-southwest, 50 km from Point Sur. It averaged 25 km in radius. The second was a plume-like feature extending WSW, 80 km from Point Sur. This feature was probably s stage of development of the eddy-type feature previously described because it was distinguishable in all images except that of 10 APR. In all images, the band of cold coastal water was uniformly 15 km

wide and parallel to the coast. No alongshore advection of the feature of interest or of any other features along the coast was observed.

In FNOC's SST analysis for 29 APR 1979 (Fig. 9), a cold (12°C) pocket was analyzed from approximately Point Conception to south of San Francisco Bay extending seaward approximately 70 km. The 12° isotherm was distorted seaward off Point Sur, but the general shape north of Point Sur was not the same as observed in satellite imagery. The analyzed SST off Point Sur in the area of the cruise was approximately 12°C (in situ SST measurements ranged from 9 to 13°C).

b. Summary of Atmospheric Conditions

NMC 500 mb and SL analyses were reviewed from 10 APR to 6 MAY 1979. The predominant large scale feature at 500 mb during this period was a relatively stationary cold core low in the Gulf of Alaska, generally located between 45 and 50 N and 140 and 150 W. Numerous short wave features were superimposed upon the basic zonal flow over the Central California coast. Short waves passed through every 6 to 8 days. Winds at Oakland were generally westerly at 35 to 40 knots increasing to 75 to 80 knots at the end of the period.

In particular, on the days of the cruise, 29 APR to 1 MAY, the Alaskan low regressed to the northwest as a short wave trough and an enclosed low over Central California replaced a weak ridge in the area and a weak high pressure system over Eastern Oregon.

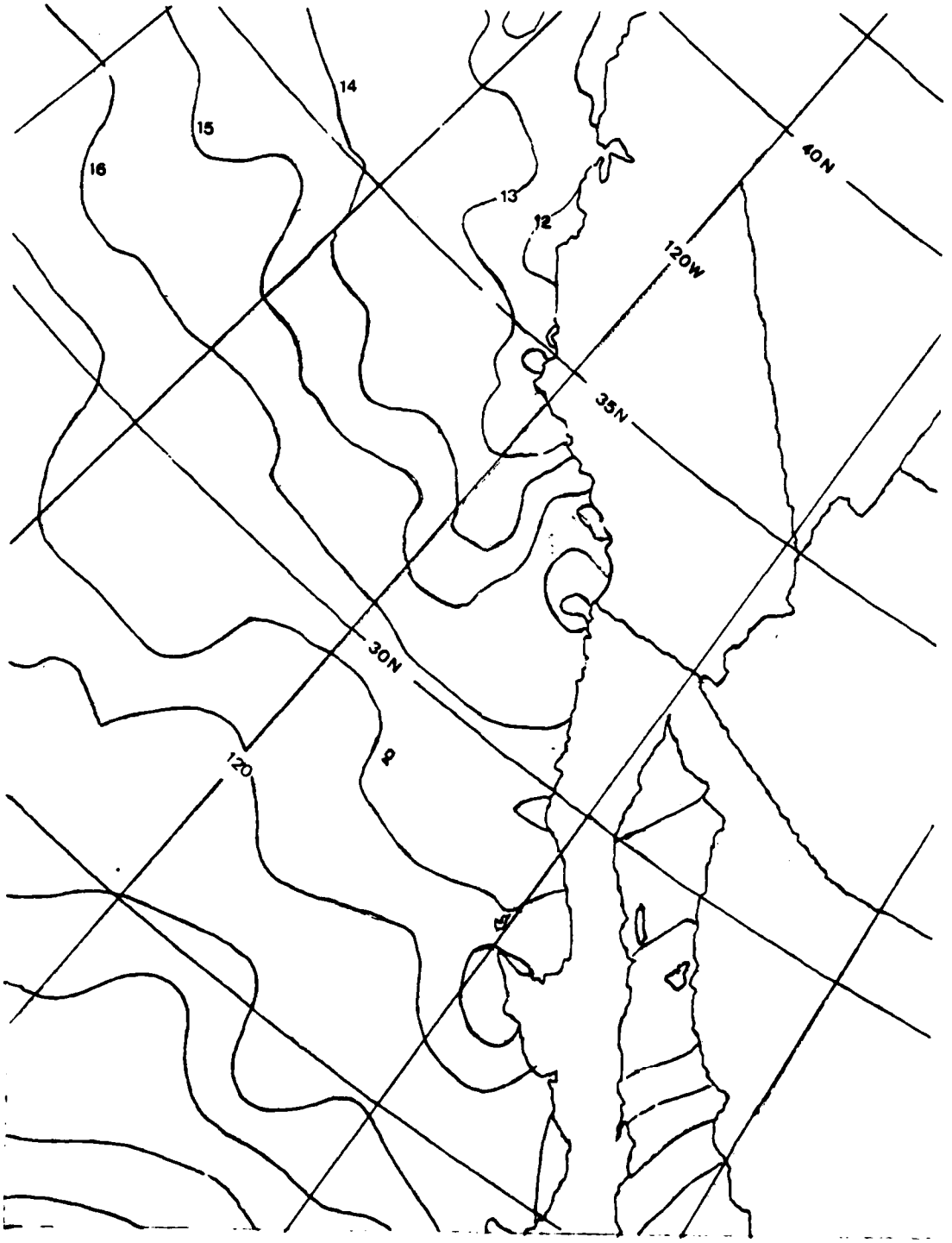

Fig. 9. FNOC SST analysis for 29 APR 79.

The SL chart during this time was dominated by a thermal low located over Southern Nevada with a trough extending northwest parallel to the coast, and by a broad high pressure system 500 km off the coast. Geostrophic winds were northerly. Frontal passages occurred on numerous occasions including one on 26 APR and one on 6 MAY. All fronts propagated from the NW except for the front which passed through on 26 APR which propagated from the SW due to a strong high pressure system off Baja California. In particular, on the days of the cruise, the SL charts were very consistent with a low over Southeast Nevada and a weak high well offshore. 00Z 30 APR charts are presented in Fig. 10.

The SL pressure analysis at 36 N 122 W from FNOC varied between 1013 and 1021 mb over the period from 10 APR to 6 MAY. Daily fluctuations of 2 to 3 mb are evident. The SL pressure fluctuations had a time scale of 6 days. During the cruise, SL pressure decreased from 1016 to 1013 mb.

The analyzed wind stress magnitude at 36 N 122 W was large and on the order of 3 to 4 dynes cm^{-2} from 28 APR to 4 MAY. Ekman transport had large offshore values within this period, i.e., 3 to 4 m^3 sec^{-1} m^{-1} on 01 MAY, and the associated upwelling index was large. Open ocean vertical velocity was variable with a negligible value on 28 and 29 APR, downwelling (0.5×10^{-3} cm sec^{-1}) on 30 APR, upwelling of the same magnitude on 01 and 02 MAY followed by a long period of downwelling (Fig. 11).

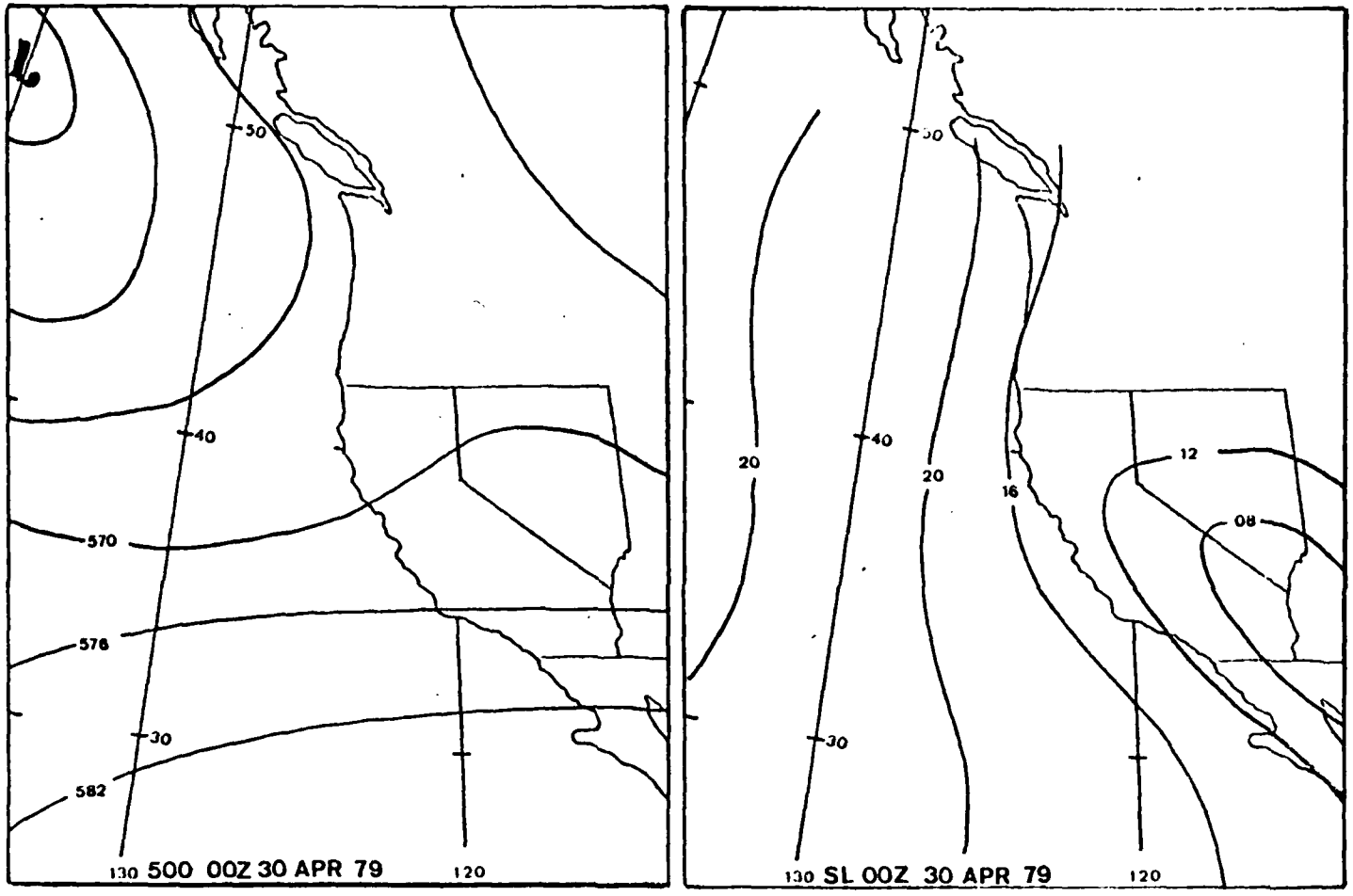

Fig. 10. 500 mb and SL analysis for 30 APR 79.

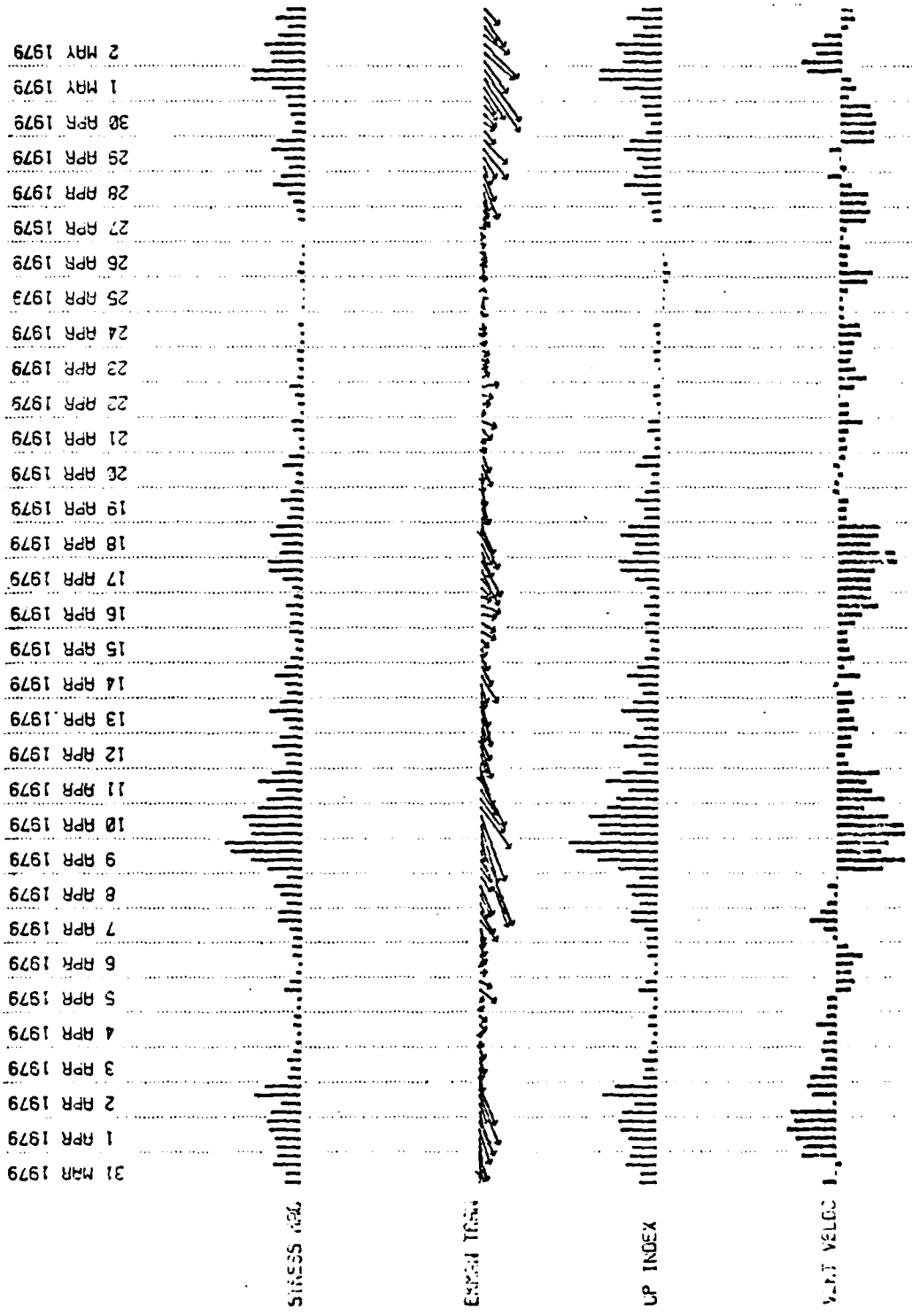

Fig. 11. Stress magnitude, Ekman transport, Upwelling Indices and Vertical Velocity for APR and MAY 79.

Fig. 11. (Continued)

Early morning haze changed to scattered stratus which persisted through the afternoon of 28 APR until noon 29 APR when conditions cleared. Partly cloudy conditions set in during the evening and lasted until the end of the cruise. Visibility was good, i.e., 15 km, except for early morning haze. Winds were generally north northwest at 5 m sec^{-1}. However, from 1300 to 1600 on 30 APR, they shifted to SE at 2 m sec^{-1}. Swells were consistently from the northwest, one meter. The barometer was steady at 1018.6 mb until the afternoon of 30 APR when it dropped to 1015.9 mb in 6 hours.

The coastal station at Point Piedras Blancas (80 km south of Point Sur) was the only station recorded during this period. Light winds from the NE and northwest were reported until 1230 Z 28 APR when the wind steadied at west northwest 7.5 m sec^{-1}. No percipitation was recorded.

During the cruise, the ship was between 10 and 50 km from the station with a closest point of approach (CPA) of 14.5 km at 0430. Ship winds at the time were NW, 2.5 m sec^{-1}; observed winds at Point Piedras Blancas were stronger than the shipboard winds and from the SW as compared to NW for shipboard winds. No sea breeze is evident in either.

c. Thermal Structure

The vertical cross sections (Figs. 12-14) showed distinctive thermal structure. A general feature observed in all three legs is a gradual rise in the isotherms below

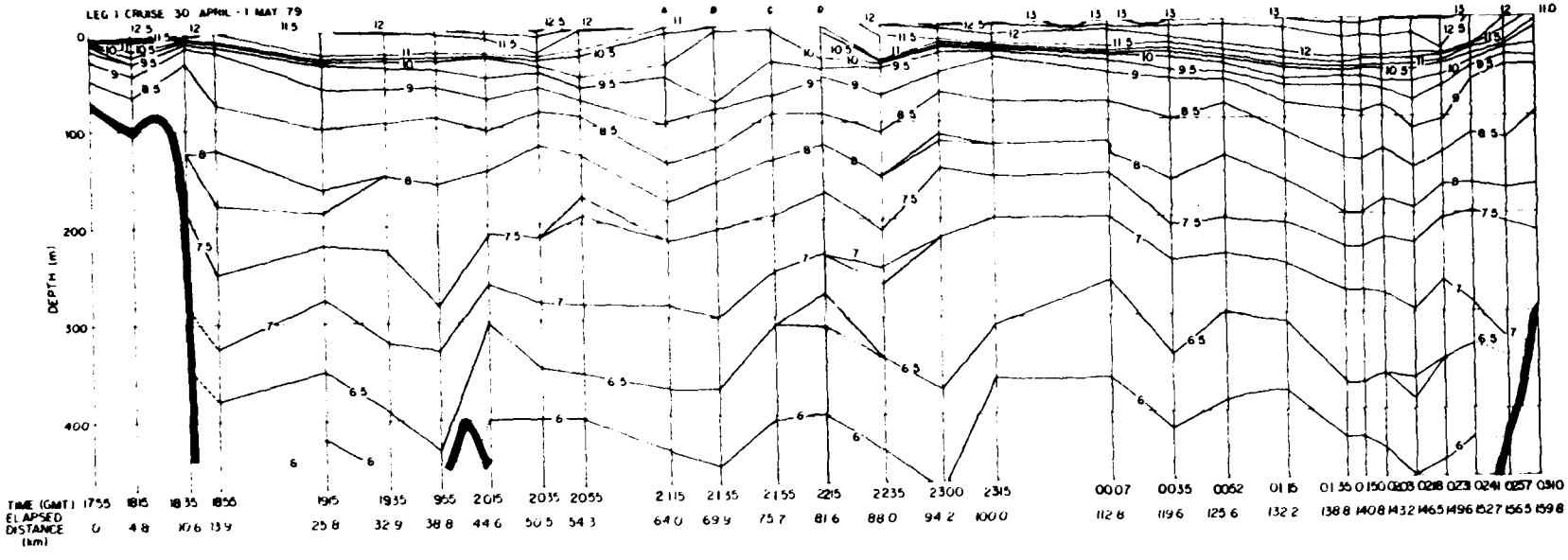

Fig. 12. Leg 1 1755 30 APR to 0310 1 MAY 79.

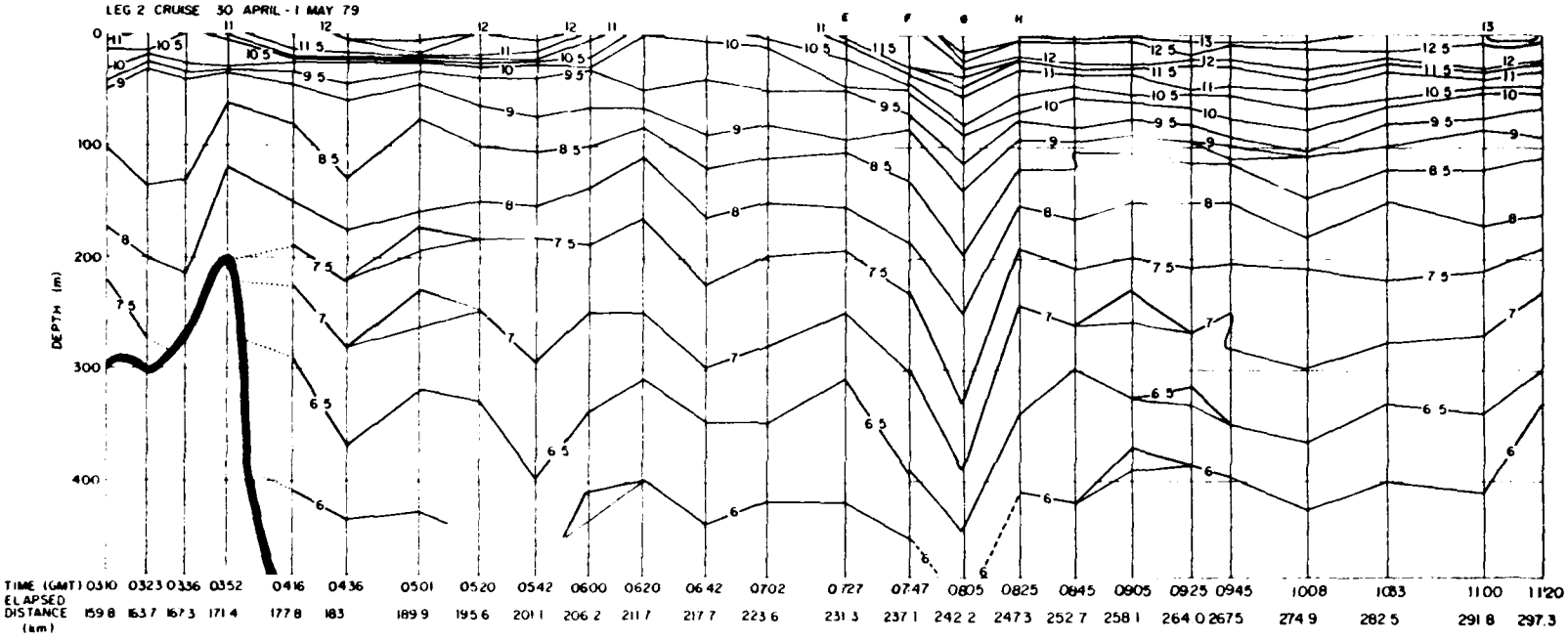

Fig. 13. Leg 2 0310 to 1120 1 MAY 72.

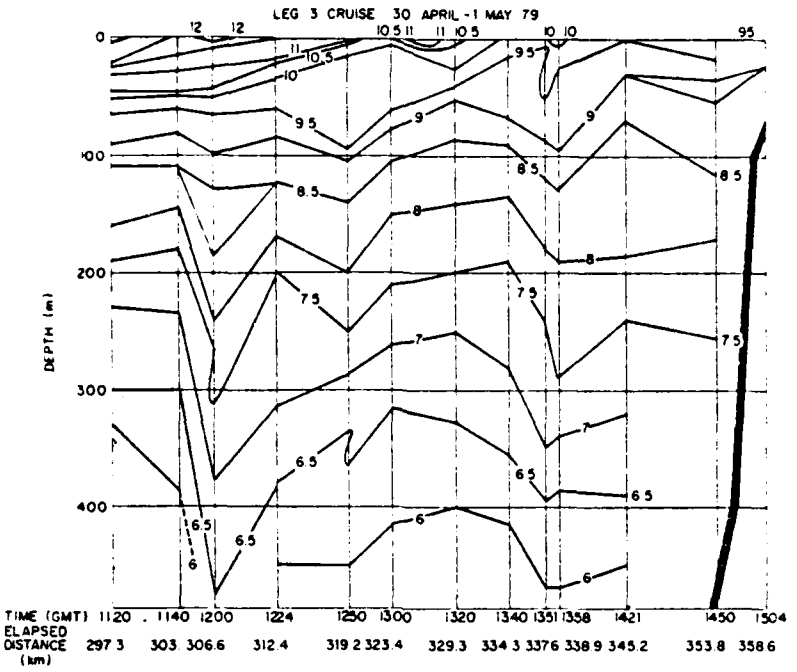

Fig. 14. Leg 3 1120 to 1504 1 MAY 72

the mixed layer which peaks at or near the observed cold surface feature. Also evident were numerous small scale fluctuations, perhaps the manifestion of XBT errors or other processes such as internal waves, etc.

Leg 1 (Fig. 12) was generally a SE transit which passed through the cold surface feature from 2035 to 2300, and entered cold shelf water at 0231. The slope of the isotherms in the mixed layer on the northwest side of the feature (from 2035 to 2115) was approximately 2.5 m/km while on the SE side (from 2215 to 2235) the slope was approximately 5 m/km.

The vertical transect through the feature indicated a structure with a diameter of 31 km at the surface and of 44 km at 40 m. Below this, the isotherms, e.g., 9.5°C, increased about 40 m in depth. A strong thermocline was also evident from 20 to 50 m except within the cold feature and coastal water. The slope of the isotherms entering cold coastal water was approximately 3.8 m/km (0231 to 0310).

The general slope of the isotherms was of the order of 1.3 m/km, with the peak occurring around 2315, some 25 km SE of the surface feature. XBT traces of interest through the surface feature (Fig. 15) show the decrease in surface temperature.

Leg 2 was generally a west northwest transit which left the colder coastal water at 0352 and passed through the cold surface feature from 0542 to 0747. The deep isotherms

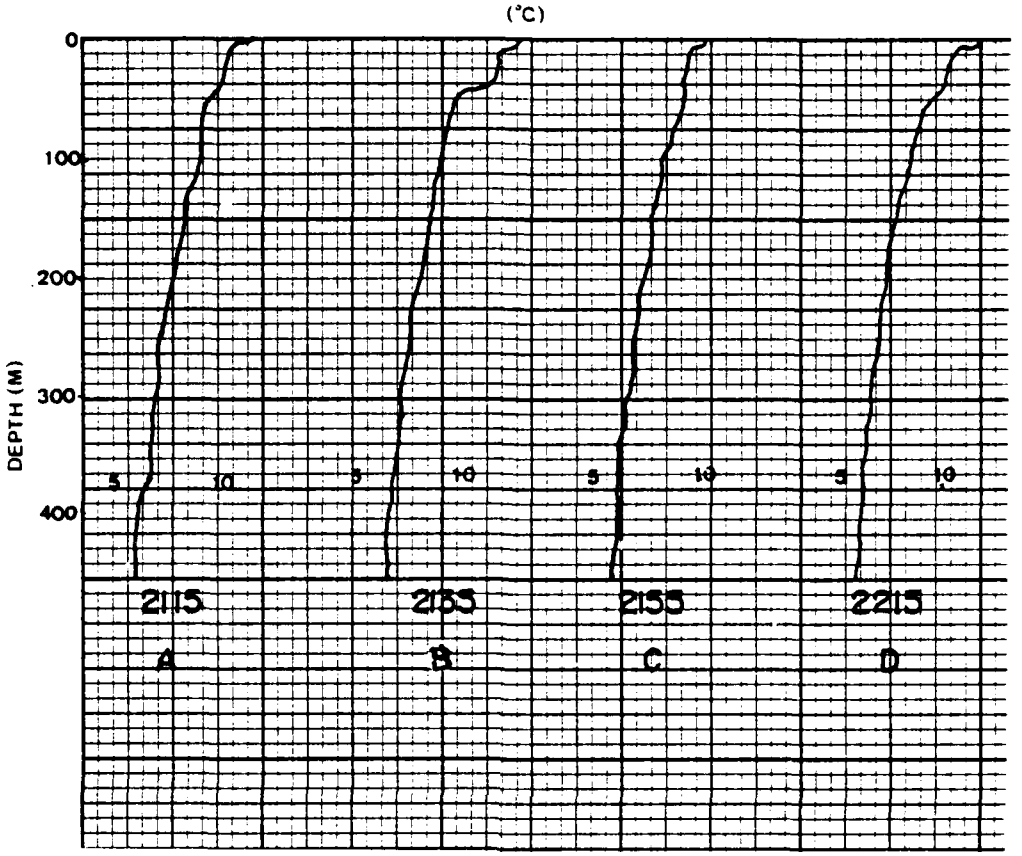

Fig. 15. Selected XBT traces from leg 1.

showed the same general rise with a similar slope as shown in leg 1. On this axis, however, the peak in the rise was almost directly below the surface feature. A similar decrease in depth of isotherms below the cold surface feature was evident as was the structure, with length scales of 25 km on the surface and 40 km at 40 m. A strong thermocline was evident except within the cold surface feature and to the west. Also of interest was the rapid deepening of isotherms from 0727 to 0825 25 km west northwest of the surface feature. (The XBT traces of interest are in Fig. 16.)

Leg 3 was generally a NE transit which went along the axis of the cold feature, normal to the coast. Penetration through the cold surface feature occurred between 1320 and 1421. Generally, all the isotherms rose towards the coast. The slope of the isotherms was 2.3 m/km. No strong thermocline was observed. A sharp deepening of isotherms similar to that observed on leg 2 was evident at depth at 1200, 18 km southwest of the cold surface feature and at 1358, 14 km northeast. However, these were not supported by adjacent XBT's.

Plan views derived from the XBT traces and SST thermistors are presented in Figs. 17-26. The SST plot distinctly showed the plume-type feature observed in satellite imagery. The plume extended 55 km southwest of Point Sur along the axis of the rise between the Sur Canyon and Lucia Canyon. The cold spot was near the head of the Sur Canyon.

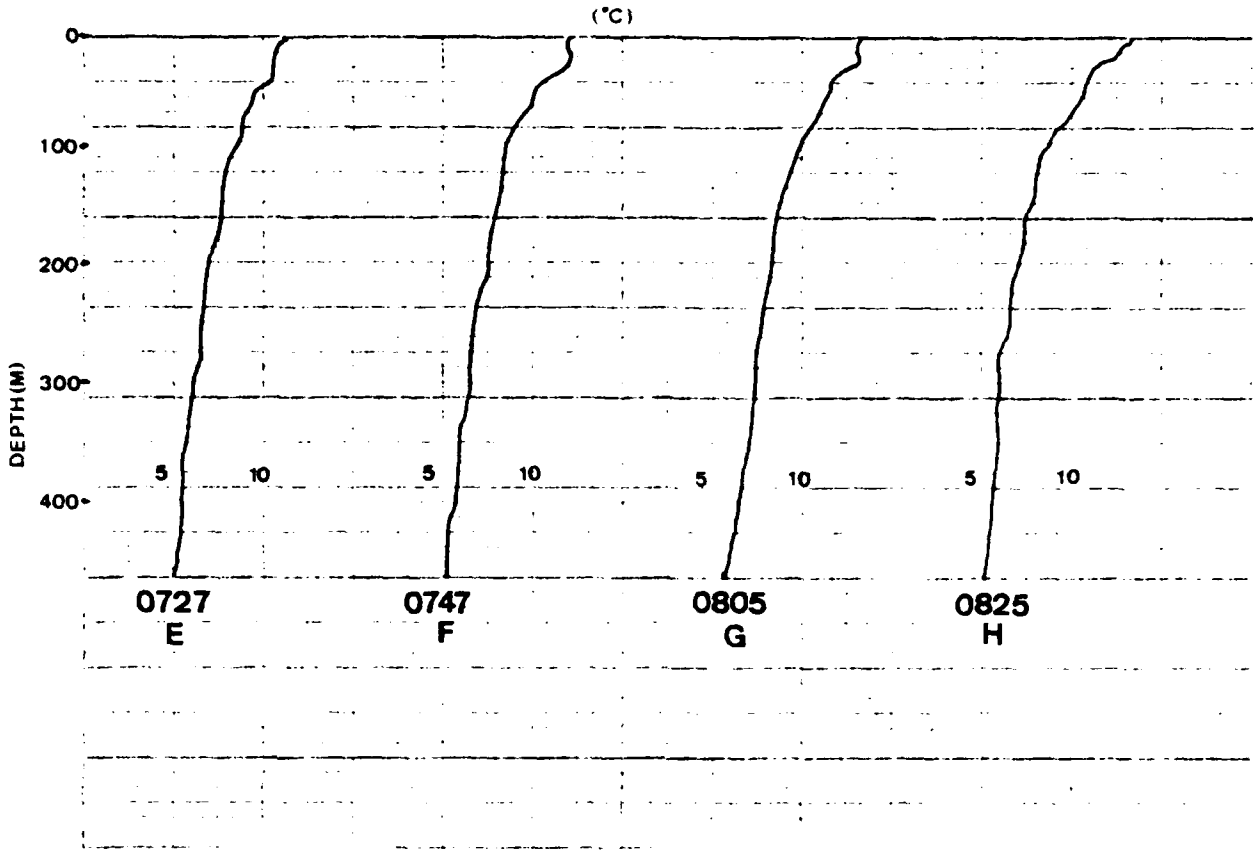

Fig. 16. Selected XBT traces from leg 2.

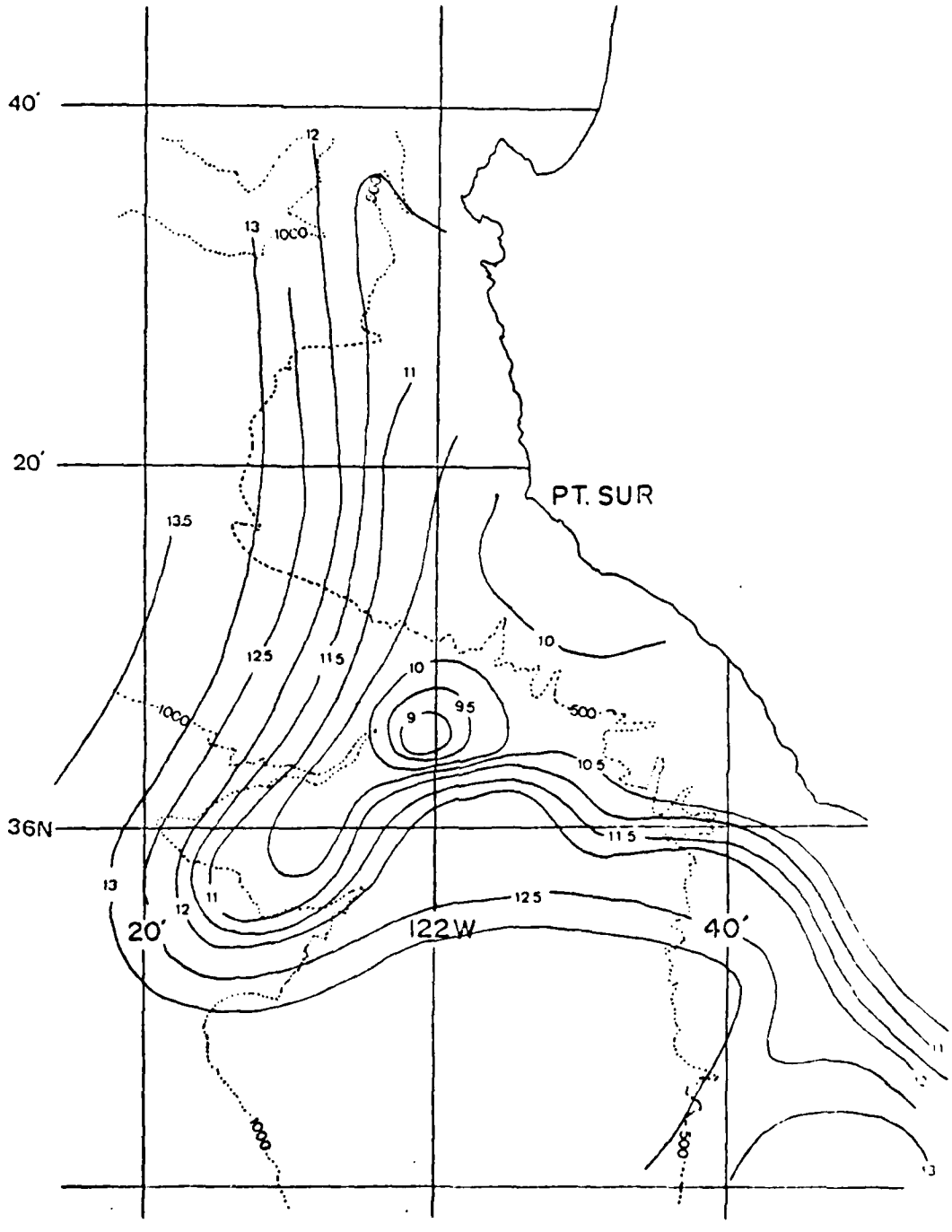

Fig. 17. SST (°C), 30 APR to 1 MAY 79.

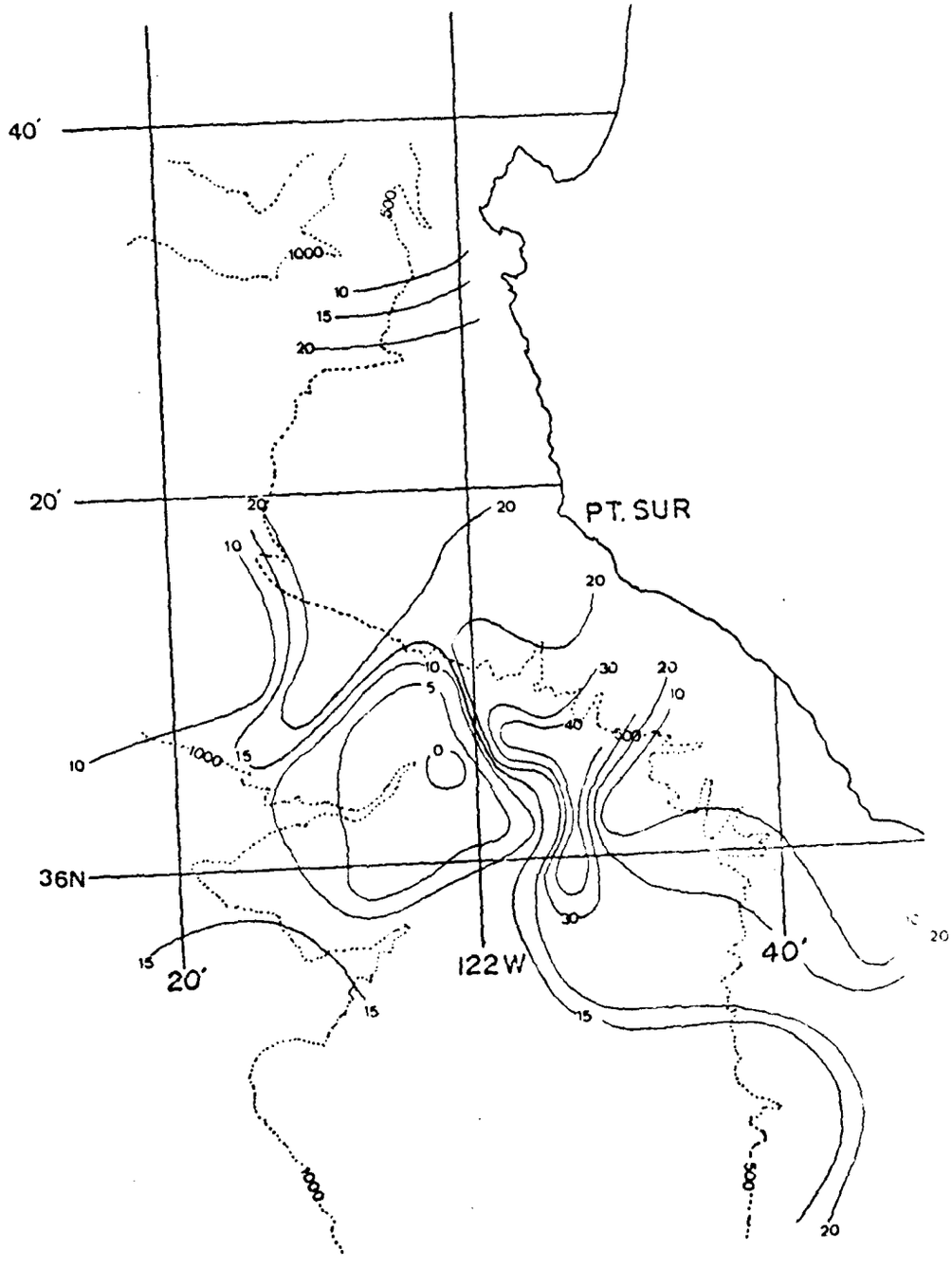

Fig. 18. MLD (m), 30 APR to 1 MAY 79.

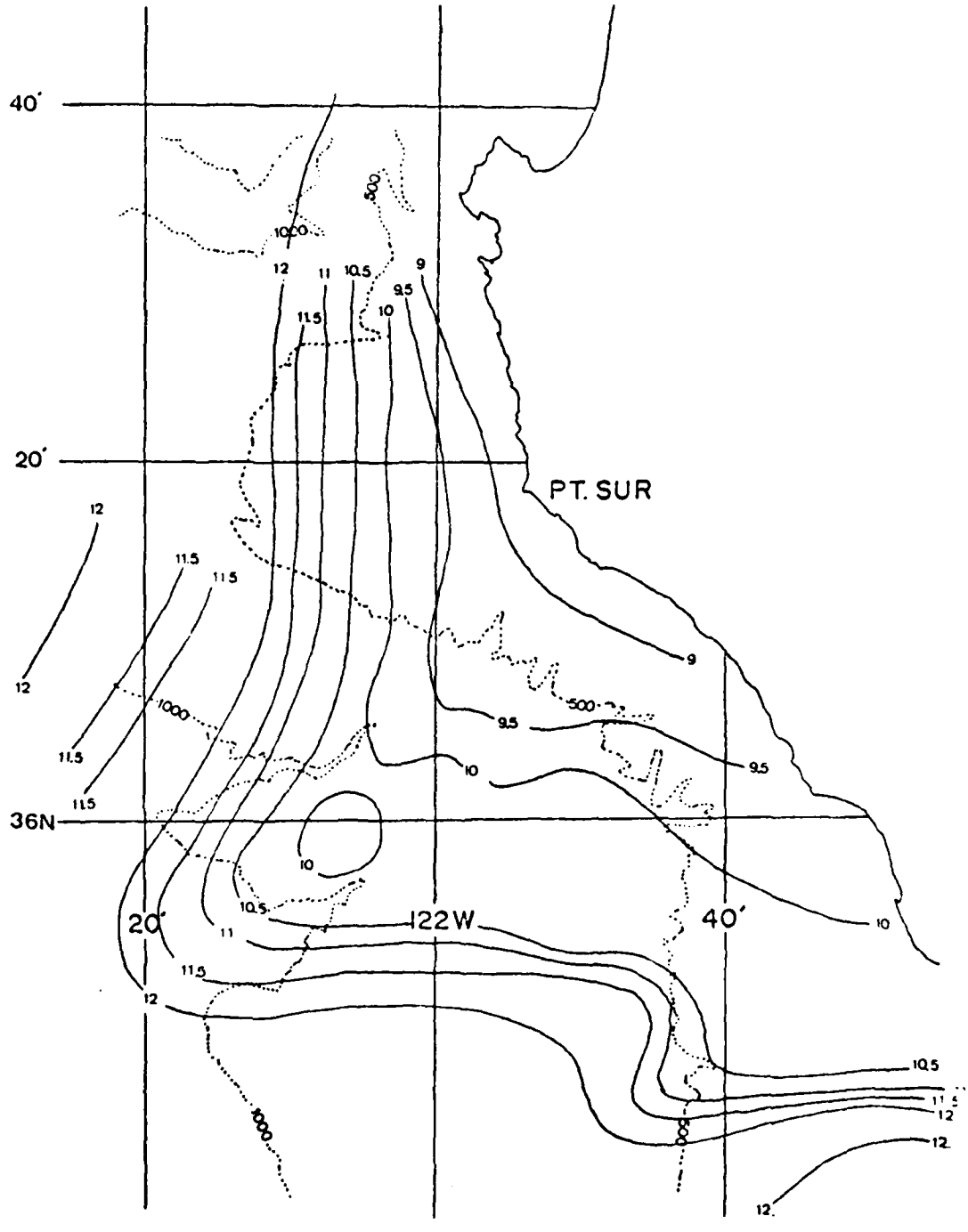

Fig. 19. 25 m temperature field (°C), 30 APR to 1 MAY 79.

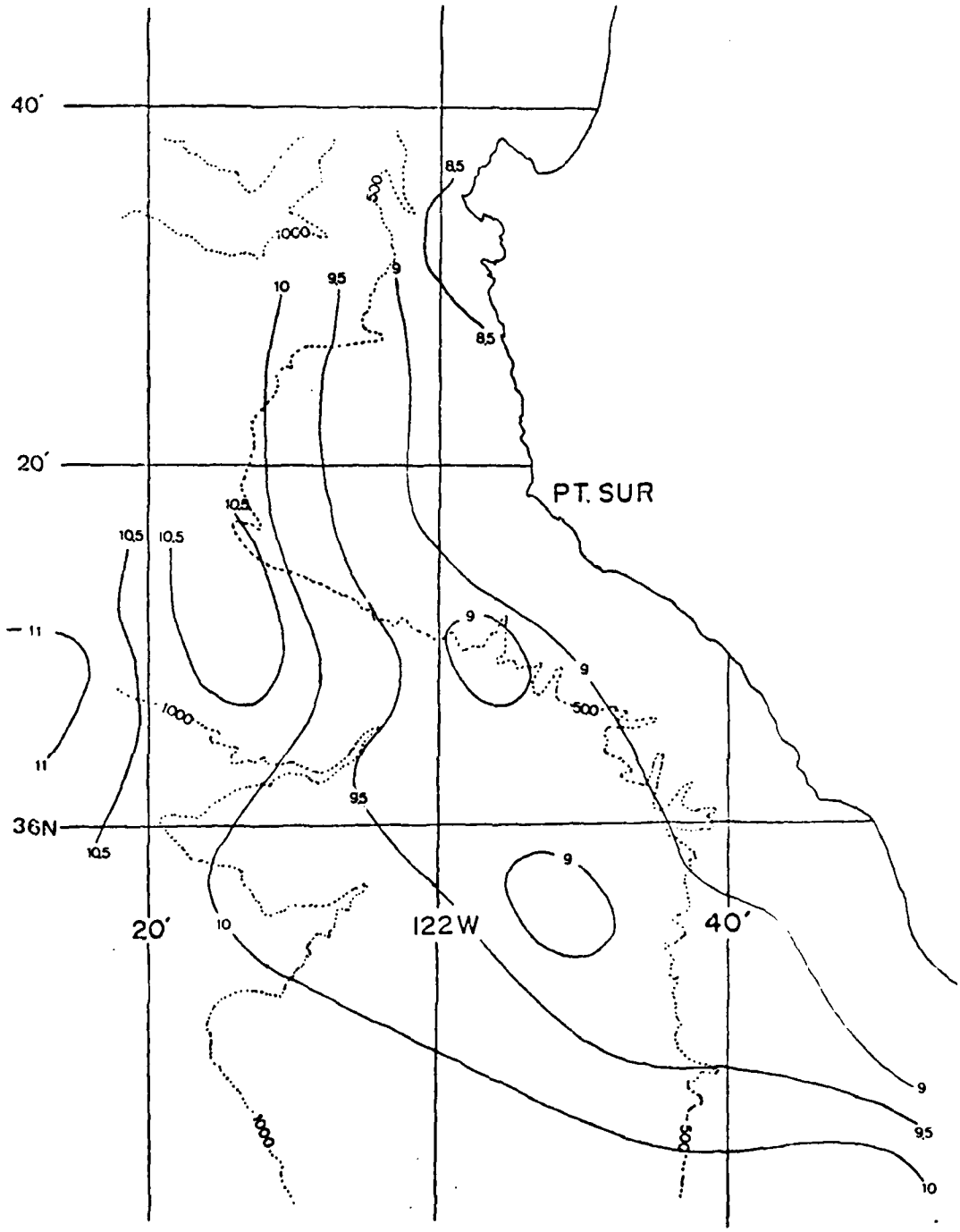

Fig. 20. 50 m temperature field (°C), 30 APR to 1 MAY 79.

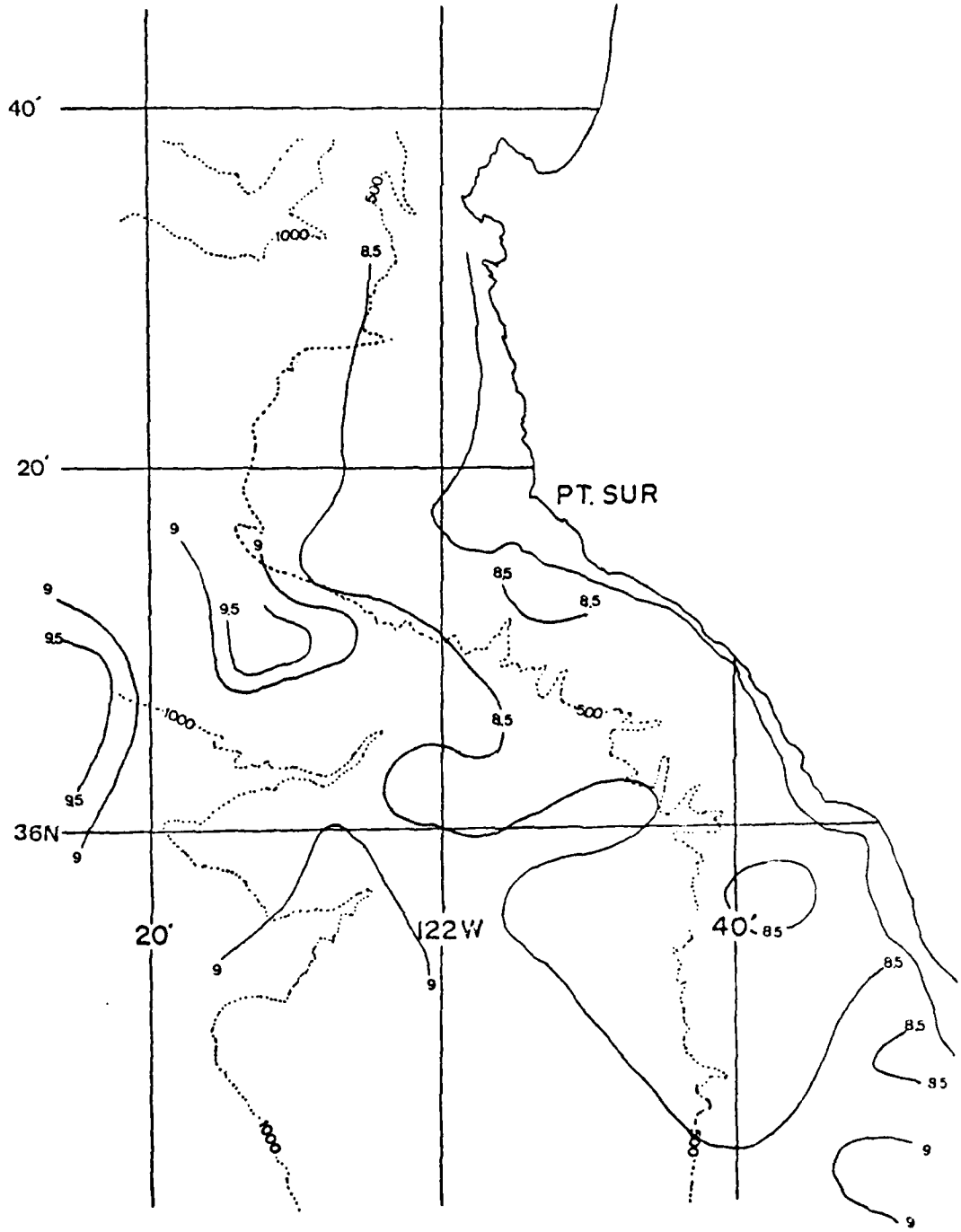

Fig. 21. 100 m temperature field (°C), 30 APR to 1 MAY 79.

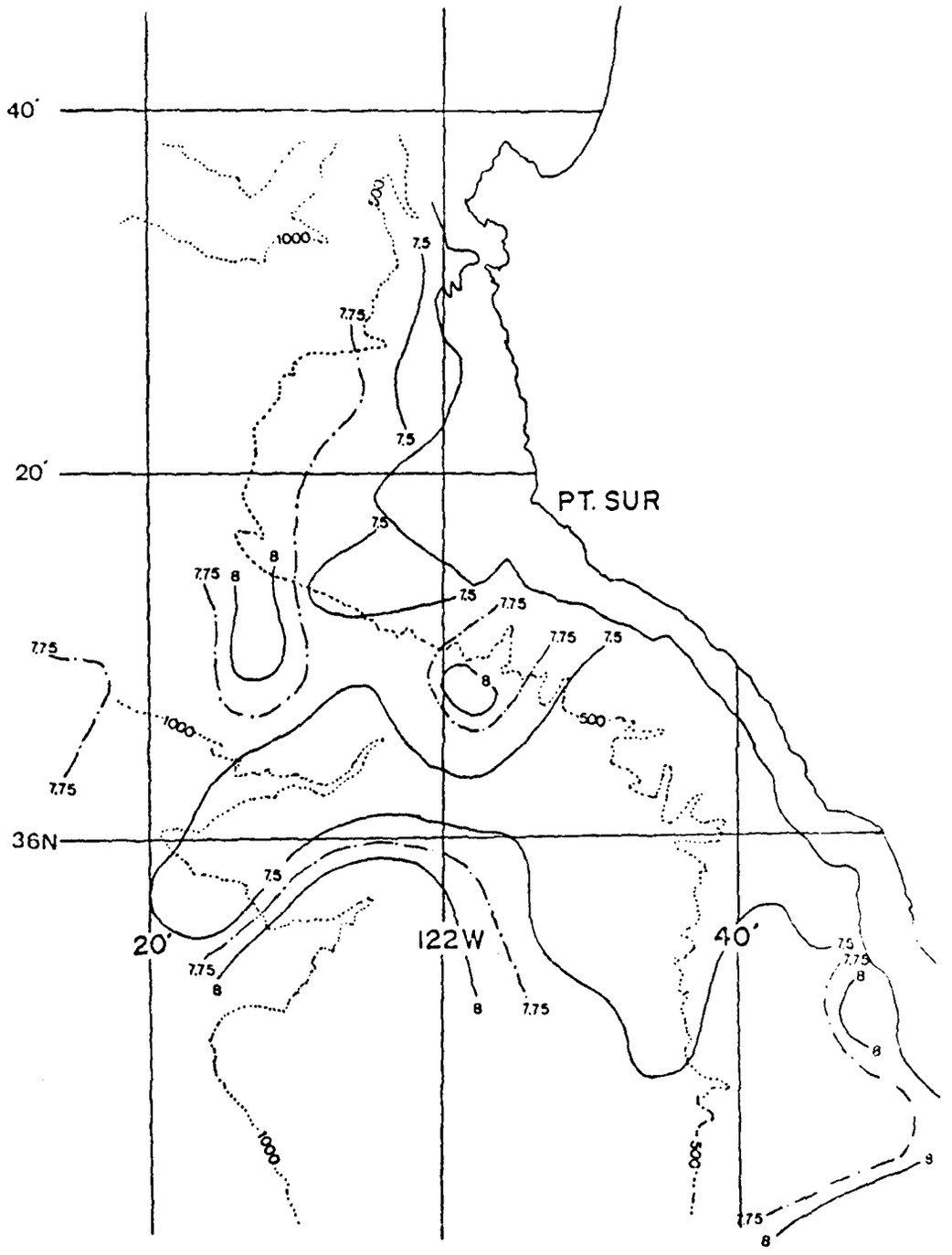

Fig. 22. 200 m temperature field (°C), 30 APR to 1 MAY 79.

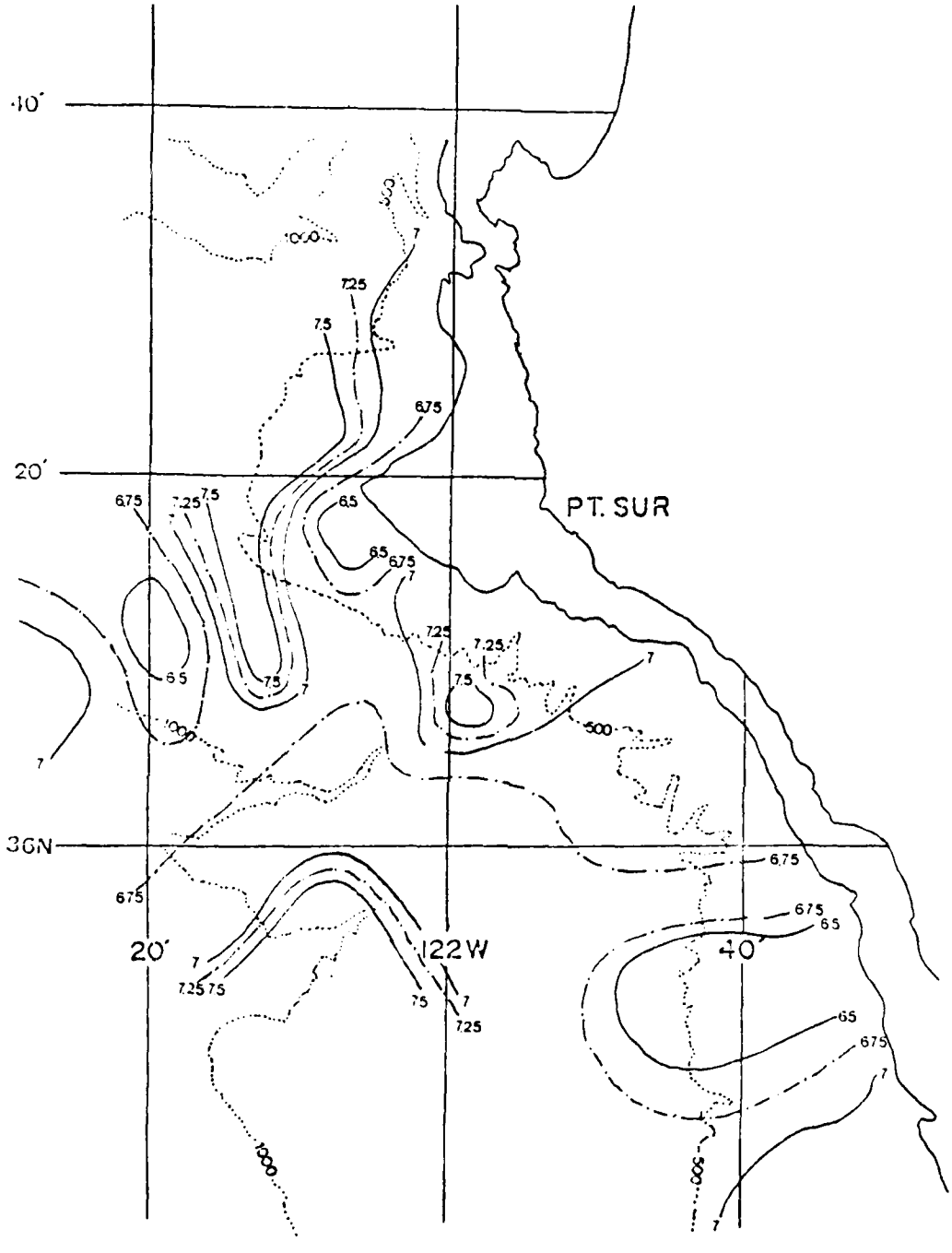

Fig. 23. 300 m temperature field (°C), 30 APR to 1 MAY 79.

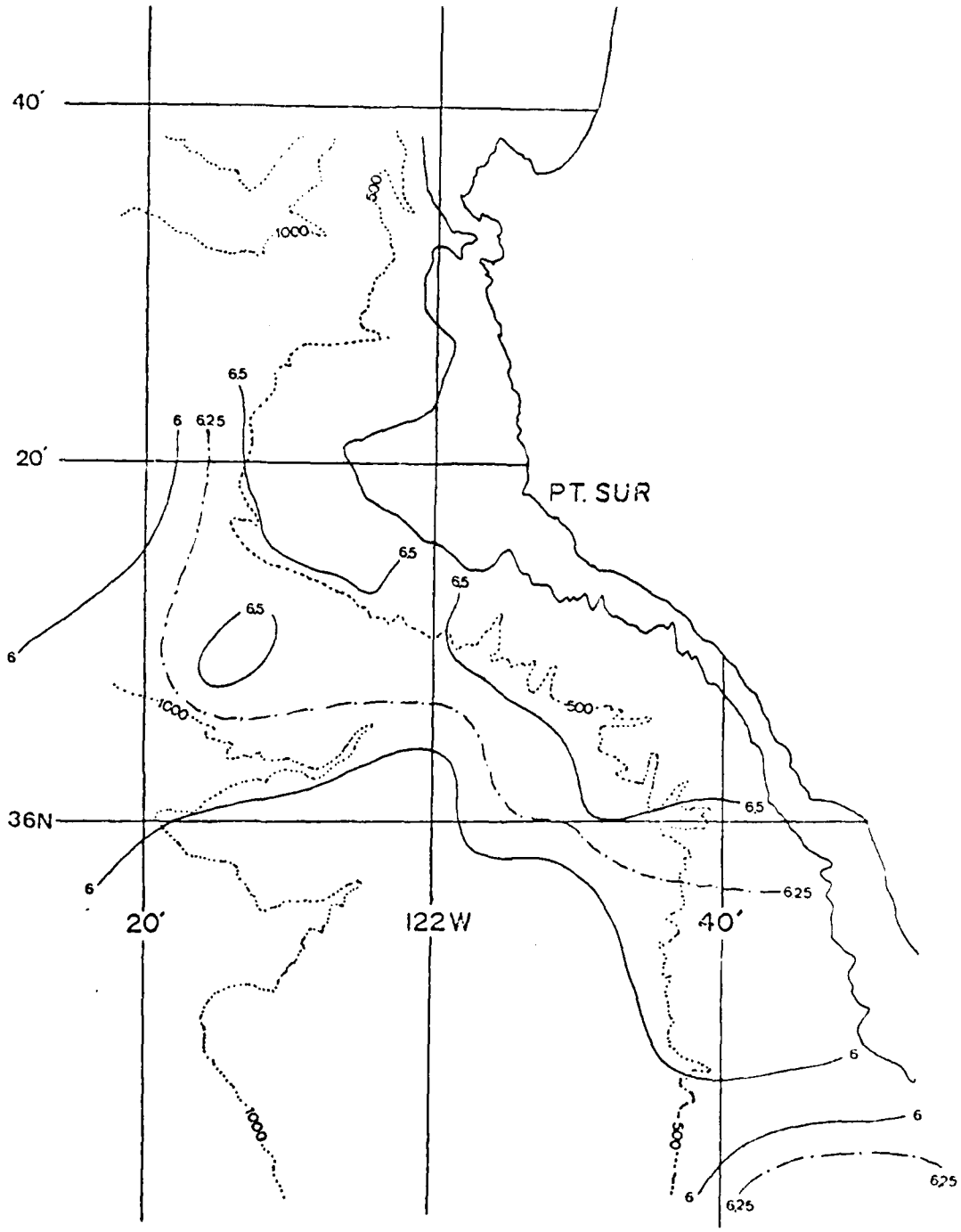

Fig. 24. 400 m temperature field (°C), 30 APR to 1 MAY 79.

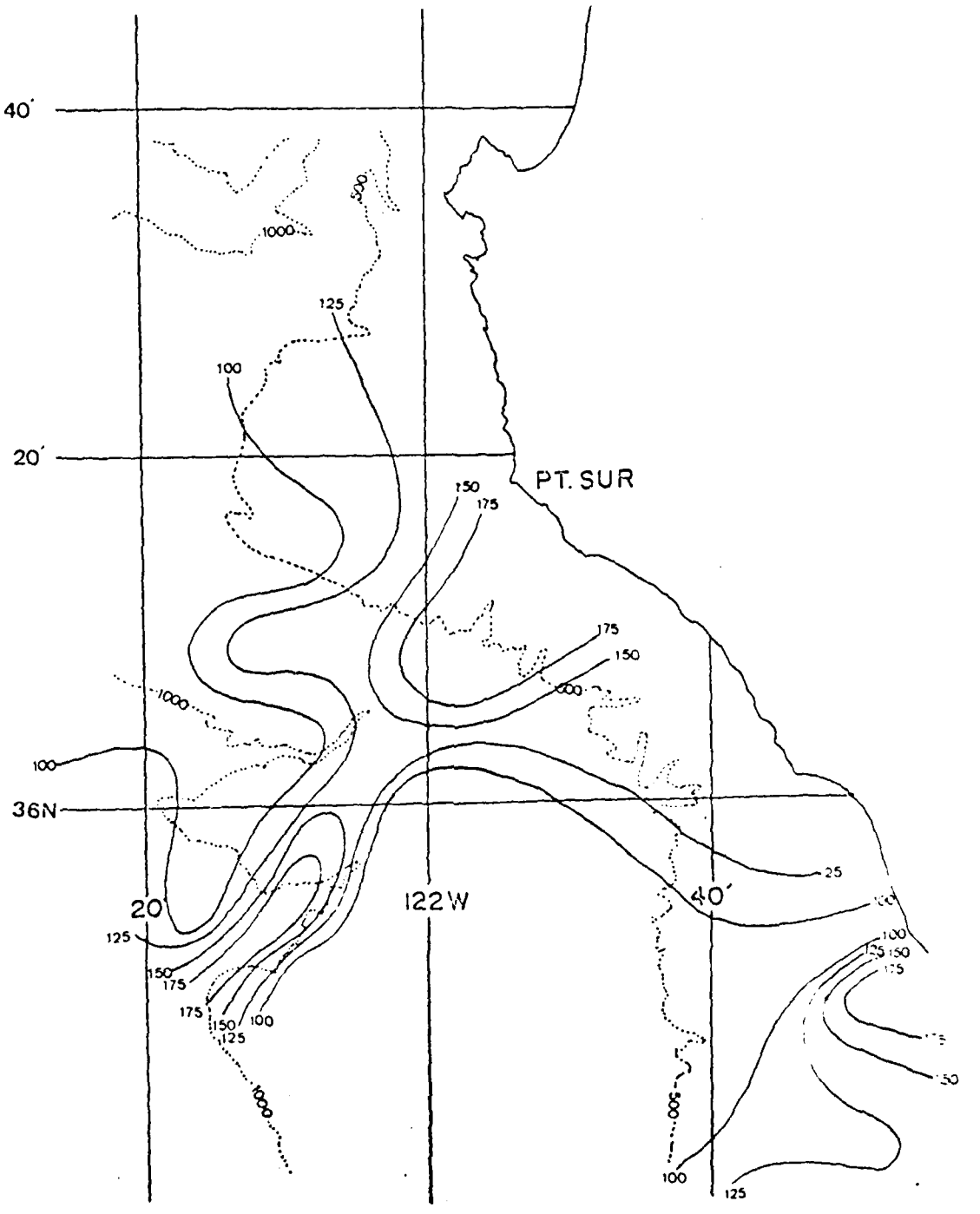

Fig. 25. Thickness (m) between 10°C and 8°C isothermal surfaces, 30 APR to 1 MAY 79.

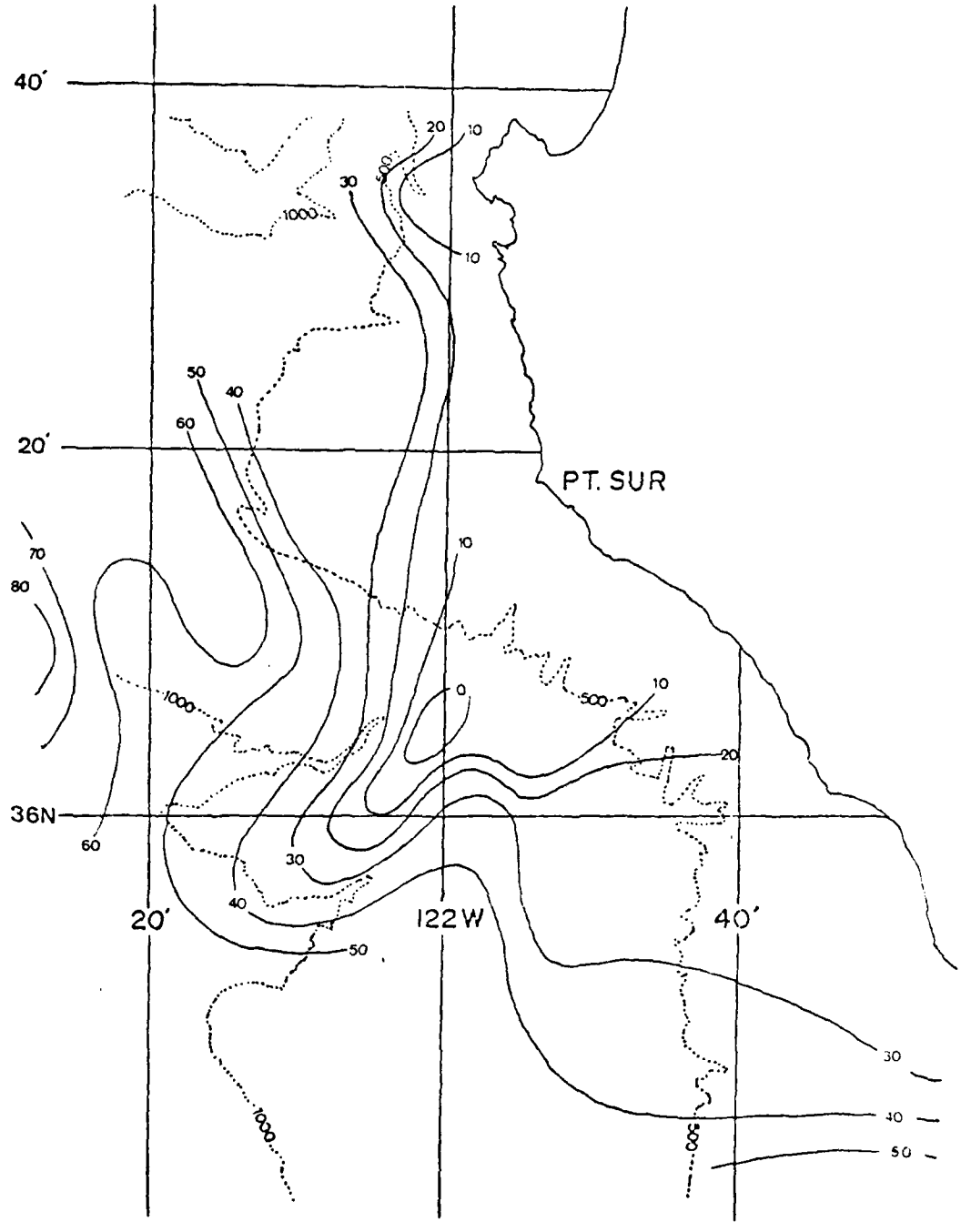

Fig. 26. Depth (m) of the 10°C isothermal surface, 30 APR to 1 MAY 79.

The sharpest temperature gradient was alongshore to the SE, 1°C/km. Alongshore to the NW, it was 4°C/10 km and offshore to the SW, 2°C/10 km.

The MLD plot (Fig. 18) showed a pattern somewhat similar to the SST plot with a minimum (1m) in the center of the cold spot and a maximum (40 m) NE of it towards Point Sur.

The 25 m plot indicated the same general pattern as the SST plot. However, there was no distinct cold spot. Instead, there was a cold protrusion extending offshore. The areas of high temperature gradients were shifted away from the center identified at the surface. This more clearly demonstrates the structure indicated in the vertical cross sections, i.e., the feature was larger at depth than at the surface. These gradients were: alongshore to the SE, 0.1°C/km. alongshore to the NW, 0.1°C/km, and offshore to the SW, 0.05°C/km. With an offshore cold protrusion present, the 50 m plot was vaguely similar to the SST plot. Temperatures ranged from 8.4 to 11.1°C with isotherms generally parallel to topography. The strongest temperature gradients, 0.2°C/km, at this level were associated with a warm tongue 20 km NW of the cold surface feature (Fig. 20).

The temperature patterns at 100 to 400 m were not similar to those of the SST. However, at all of these levels, the strongest temperature gradients (0.5°C/km at 100 m, 0.5°C/km at 200 m, 0.2°C/km at 300 m, and 0.2°C/km

at 400 m) were associated with the warm intrusion identified at 50 m. All plots showed distinctive structure which was not parallel to topography, with warmest temperatures offshore and occasional warmer pockets near the coast.

The thickness of the layer between the 10 and 8°C isotherms was calculated from XBT data. The 10°C isotherm was chosen because of its general location in the upper 50 m and the 8°C isotherm because of its location around 200 m. The 10°C isotherm displayed evidence of being upwelled, and the 8°C isotherm was one of the deep isotherms which "rose" as discussed earlier. An axis of thickness maxima was evident along the same axis as the cold feature indicated in the SST.

The isothermal surface, 10°C (Fig. 26), closely resembled SST. The 10°C isotherm intersected the surface within the "cold spot".

The final information extracted is a time series of profiles from two sets of XBT's dropped within a kilometer of each other. This information of "opportunity" was not planned. The 2135, 0702, and 1340 XBT's were dropped near 35° 45' N 122° 02' W, and the 0642 and 1352 XBT's were dropped near 35° 45' N 121° 59' W. Temporal changes in the isotherm depths greatly exceeded the previously discussed spatial slopes. Using the r.m.s. values of depth changes and the time between drops, vertical velocities calculated averaged 6×10^{-2} cm sec^{-1}.

Few bucket temperatures were taken. However, they were greater than the 2m temperatures by 0.1 to 0.7°C, as recorded between 0000 and 0357.

2. Case II (26 to 28 SEPT 79)

a. Summary of Oceanic Surface Conditions

The cruise from 26 to 28 SEP 79 investigated and verified the existence of a cold plume-like feature extending 100 km SW from Point Sur. A good estimate of the position of the center of the feature at 35 45 N 122 15 W was obtained through preliminary satellite analysis and a cruise track was planned with seven 80 km transits in a modified star pattern (Fig. 27). The goals of the cruise were to obtain two-dimensional sampling of both the feature and the surrounding oceanic water, to sample both during day and night in order to minimize diurnal effects, and to maximize revisit time at the center. 140 XBT's were used with an average spacing of 4 km. Data sets acquired were the same as described in previous sections.

From 9 SEP to 16 OCT 79, seventeen IR images from both TIROS-N and NOAA-6 satellites were reviewed. The area of interest was obscured by clouds associated with a frontal system on 20, 24, 28, and 29 SEP. A satellite summary is presented in Fig. 28.

On 9 SEP, a warm, anticyclonic eddy-like feature existed to the southeast of Point Sur. This dominated the surface pattern from Point Piedras Blancas to Point Sur. A

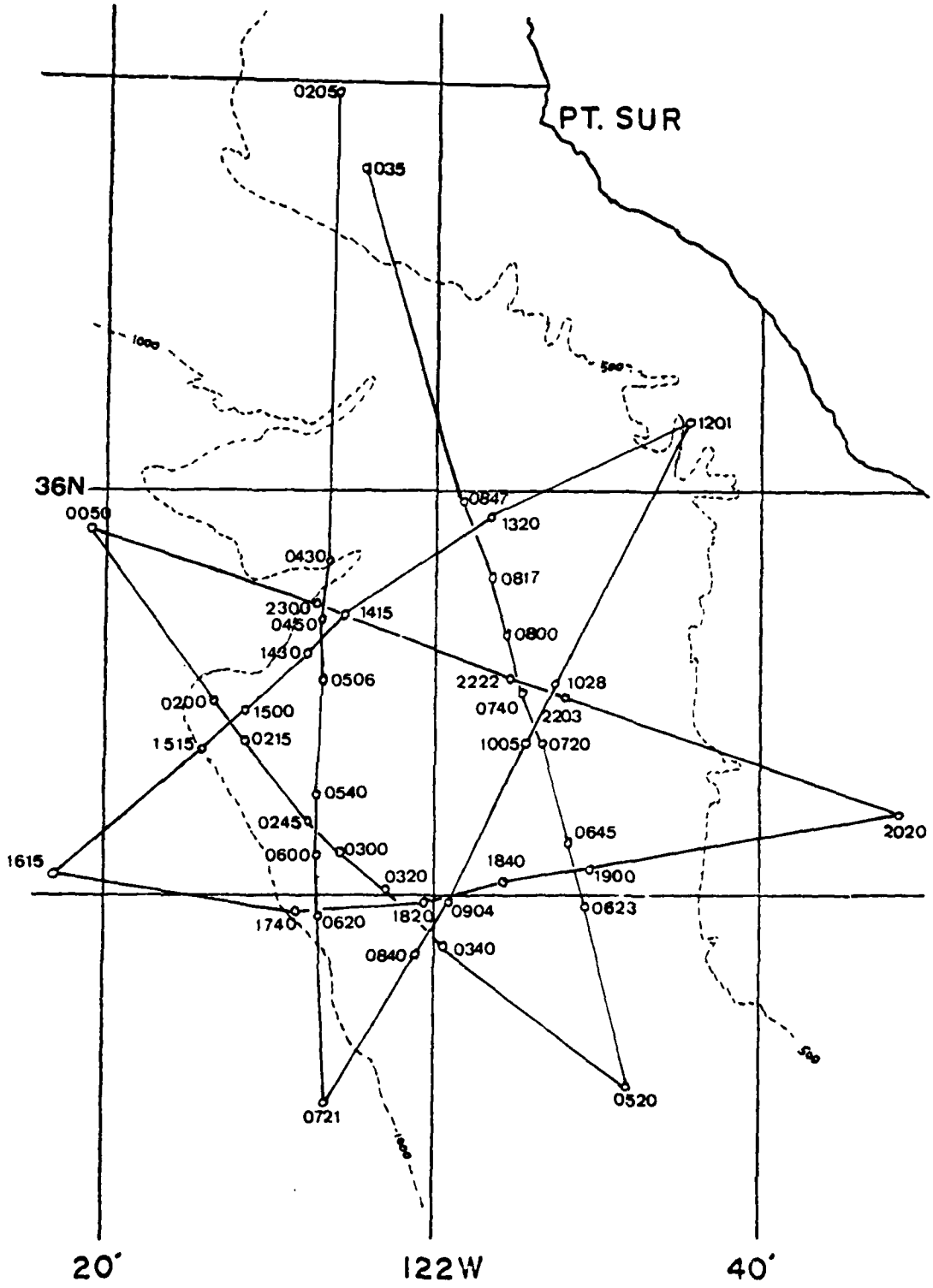

Fig. 27. Cruise track from 26 to 28 SEP 79. Times are GMT.

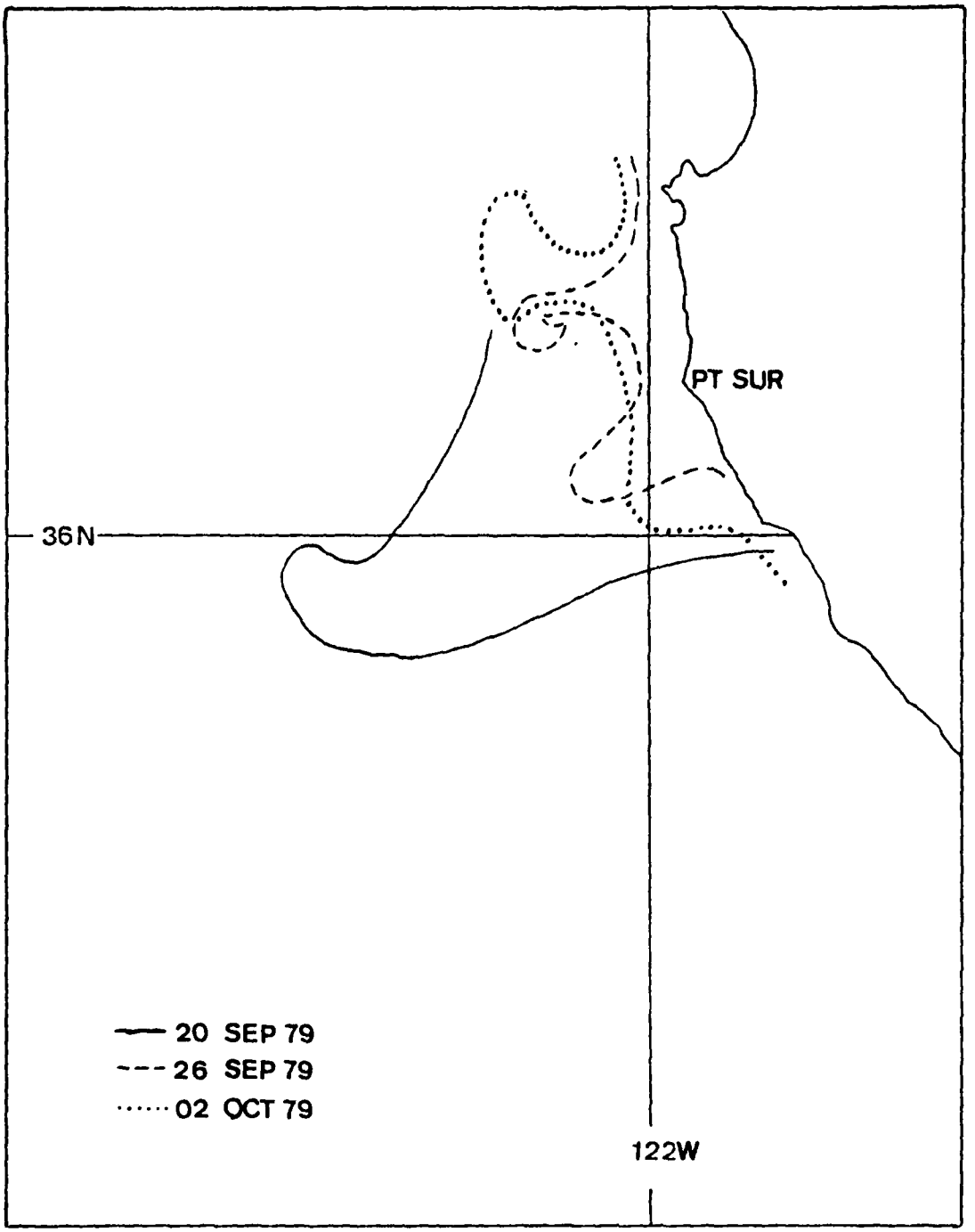

Fig. 28. Satellite features observed from 20 SEP to 02 OCT 79.

cold plume-like feature extended from Point Sur along 250°T for 120 km, and it was 25 km wide. Relatively strong gradients to the south of the plume separated it from the eddy. Coastal cold water was uniformly 15 km wide. The plume persisted through 15 SEP with the axis gradually shifting to a bearing of 235°T. Intensely cold water extended 6 km seaward from the coast. Also, the eddy had become diffuse and indistinguishable . On 16 SEP the plume curved anticyclonically to the north. Again, the water was relatively cold where the plume was rooted nearshore off Point Sur. This was the predominant feature through 20 SEP. The coastal band of cold water was not uniform in width due to numerous small eddies and plumes.

The 25 SEP image showed a more diffuse feature of the same general shape and size as observed earlier. However, a relatively cool plume had begun to form at Point Sur, and it was superimposed upon the previously existing feature. Based on the 26 SEP image, this plume developed cyclonic curvature which persisted through 2 OCT, though the feature was diffuse. However, cold water was again observed at the coastline extending along the old plume axis for 30 km. On 14 and 17 OCT no distinct feature was observed off Point Sur, but cold coastal water extended uniformly to 60 km offshore.

Generally, it appears that a large, plume-like feature was formed off Point Sur about 18 SEP. By 20 SEP, it had acquired a northward, anticyclonic curvature.

Between 20 and 26 SEP, this plume became diffuse and a new intense coastal upwelling event commenced. Evident in these images was a superpositioning of one feature upon a pre-existing feature, and in particular, coastal upwelling events on 25 SEP and 2 OCT made discrete inputs of cold water into a plume-like feature. Numerous similar features were observed elsewhere along the coast. No alongshore advection was noted.

Based on the SST analysis from FNOC for 26 SEP 79 (Fig. 29), isotherms were uniformly distorted near the coast, with no indication of the upwelling feature. As analyzed, the SST near Point Sur is approximately 15.5°C.

b. Summary of Atmospheric Conditions

NMC 500 mb and SL charts were reviewed from 19 SEP to 4 OCT 79. Flow at 500 mb was predominantly zonal in nature at the beginning of the period. A large wave trough influenced the Central California coast until 25 SEP when a low pressure system and associated trough strengthened offshore. On 1 OCT, the low became cutoff over Southern California with a ridge to the North. This low propagated to the north, and it was over Monterey Bay by 4 OCT. There were few short wave systems. Oakland winds were consistently westerly at an average speed of 20 knots with backing and veering to the NW and SW appropriately as systems passed through. In particular, during the days of the cruise, from 26 to 28 SEP 79, the central coast was under the influence of a weak trough which strengthened

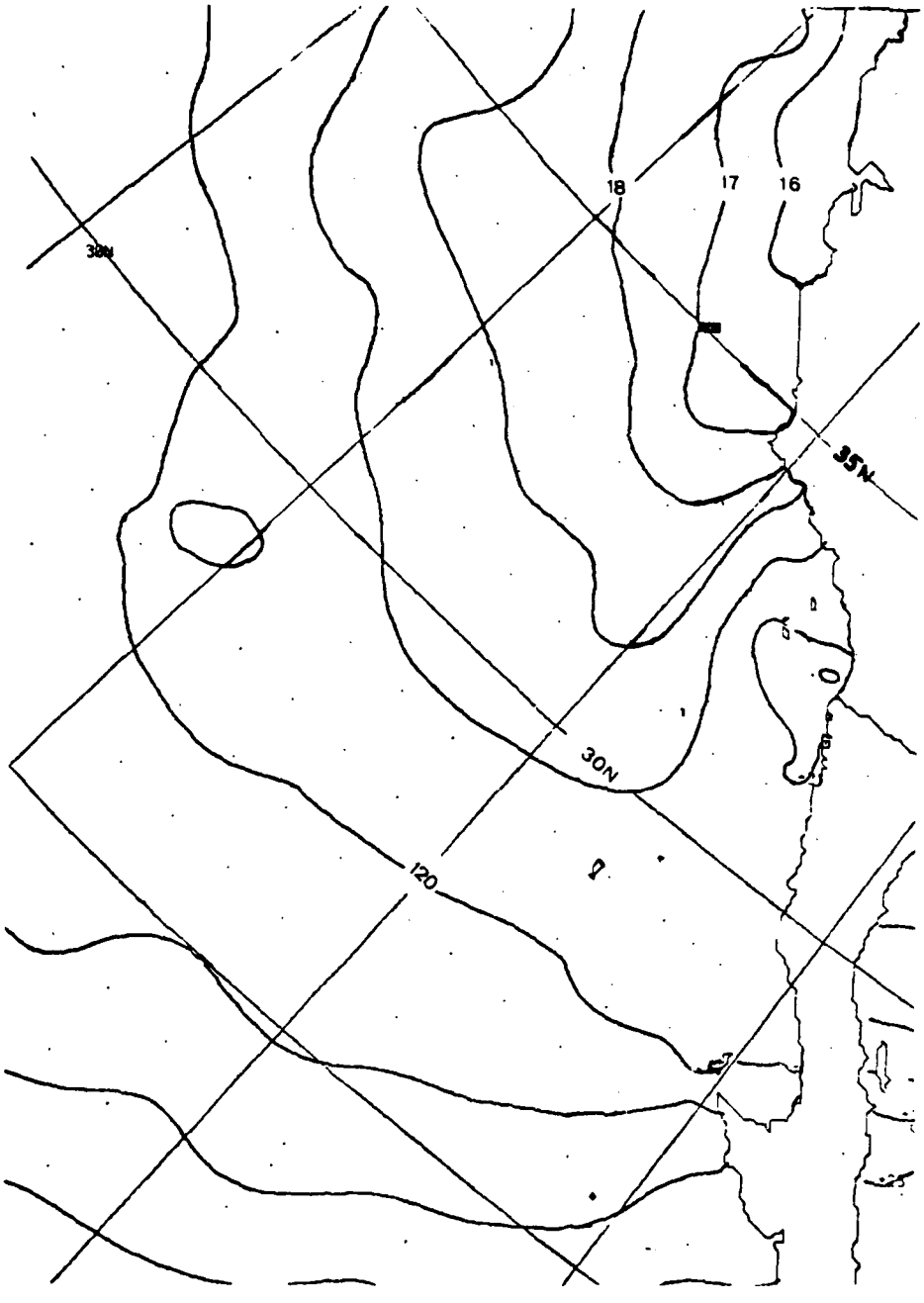

Fig. 29. FNOC SST analysis for 26 SEP 79.

and formed a cutoff low over Southern California by 12Z 29 SEP.

The SL chart was dominated by a thermal low over Baja California with an associated thermal trough extending to the NW parallel to the coast, and by a weak high pressure system located approximately at 40 N 130 W, offshore of the Northern California and Oregon area. Geostrophic winds along the coast were northerly. This flow did not dramatically change. A high pressure system which moved eastward from a position offshore of Oregon on 26 SEP produced minor perturbations in the northern limit of the trough. This system retrogressed the following day (Fig. 30). A cold front system observed in Northern California on 2 OCT became stationary and parallel to the coast at Eureka, California on 3 OCT. In particular, during the days of the cruise, the offshore high intensified as the thermal trough extended from Southern California to the NW and formed an enclosed low pressure system over Northern California. This developed weak and variable geostrophic winds over the Central California coast.

The SL pressure analysis at 36 N 122 W from FNOC varied between 1010 and 1020 mb with daily fluctuations of 1 to 2 mb from 19 SEP to 4 OCT. The SL pressure fluctuations had a time scale of 5 days. During the cruise, SL pressure increased from 1014 to 1018 mb.

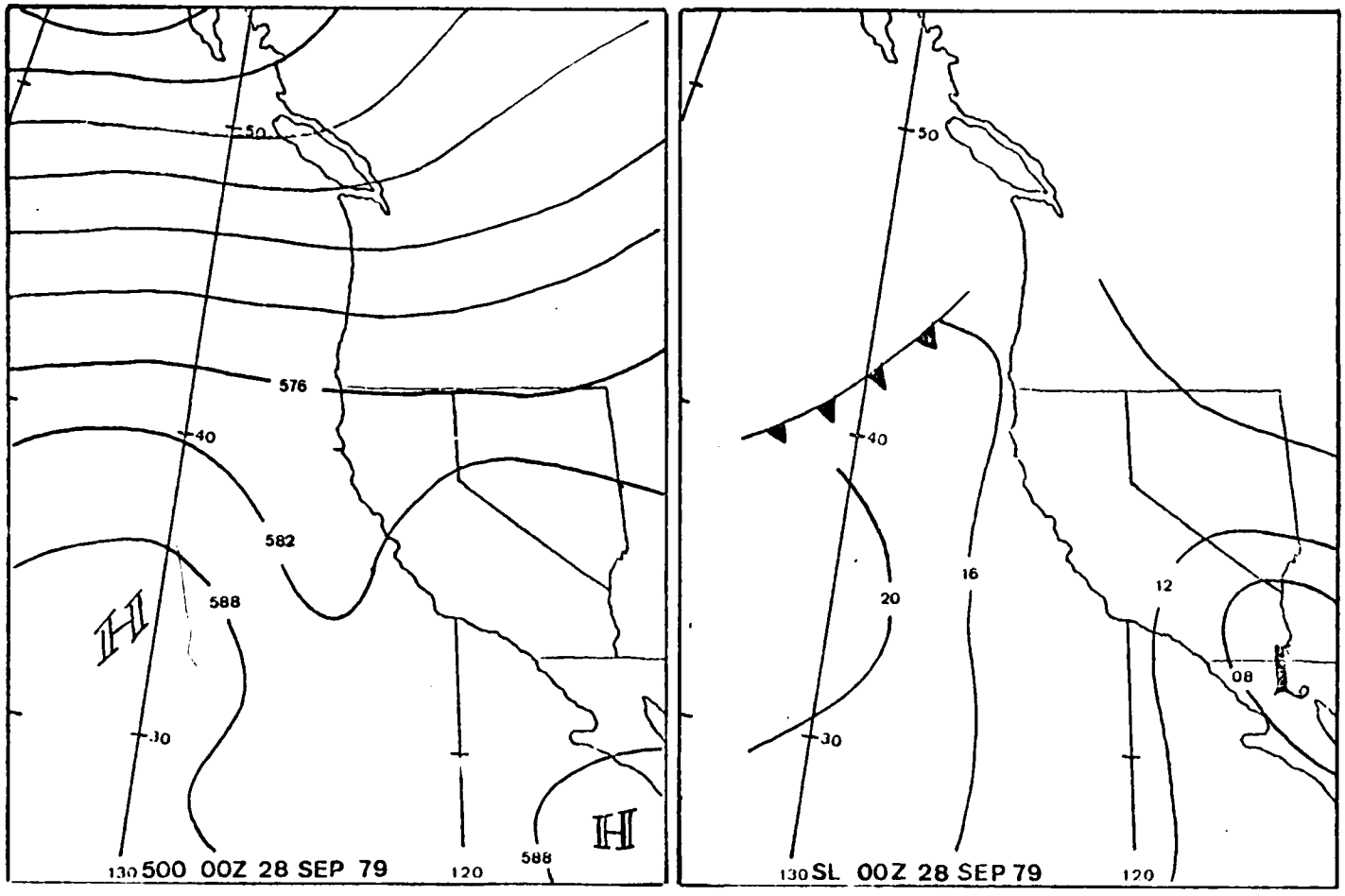

Fig. 30. 500 mb and SL analysis for 28 SEP 79.

The analyzed wind stress magnitude at 36 N 122 W was small and relatively constant, of the order of 0.5 to 0.75 dynes cm^{-2} from 21 SEP to 5 OCT. The Ekman transport was light and variable as was the associated upwelling index. The vertical velocity was variable with offshore upwelling on 21 and 30 SEP (1×10^{-3} cm sec^{-1}), downwelling on 22 SEP of the same order of magnitude, and negligible values at other times (Fig. 31).

Partly cloudy conditions persisted on 26 SEP 79 changing to overcast conditions which lasted throughout the cruise until clearing around 2000 27 SEP. Visibility was good, i.e., 15 km, except for early morning fog or haze (5 km). Winds were calm until 1200 26 SEP when they steadily increased to 9 m s^{-1} (0700 27 SEP). The winds decreased to 4 ms^{-1} (1700 27 SEP) then increased back to 8 m s^{-1} and remained strong through the rest of the day. The winds were consistently from the NNW. Swells were northwesterly 1 to 2 m throughout. The barometer dropped slightly from 1016.2 to 1014.6 mb.

Land station observations were examined from Point Pinos, Point Sur, and Point Piedras Blancas from 2300 26 SEP to 1400 28 SEP 79. Generally, all stations and the ship had a strong alongshore (NW) component between 3 and 5 m sec^{-1}. The ship winds were consistently so during the entire cruise while the stations at Point Pinos and Point Piedras Blancas had an occasional SE component. Point Sur had a NW component until 1200 28 SEP when it shifted to the SE.

Fig. 31. Stress magnitude, Ekman transport, Upwelling Indices and Vertical Velocity for SEP and OCT 79.

Fig. 31. (Continued)

AD-A092 632 NAVAL POSTGRADUATE SCHOOL MONTEREY CA F/G 8/10
SUBSURFACE DYNAMICAL PROPERTIES OF VARIABLE FEATURES SEEN IN SA--ETC(U)
JUN 80 J E JOHNSON

UNCLASSIFIED NL

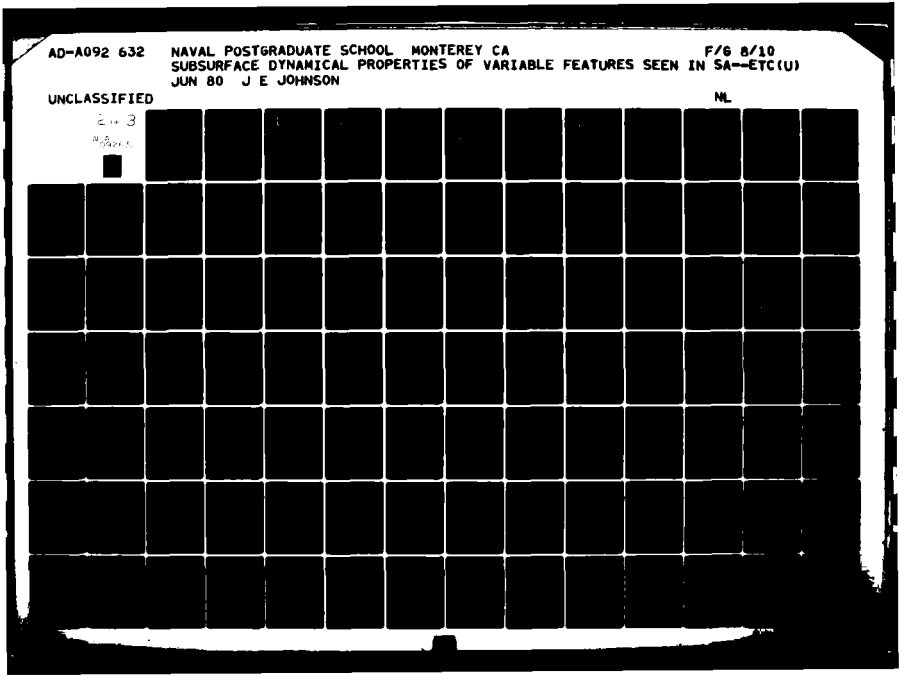

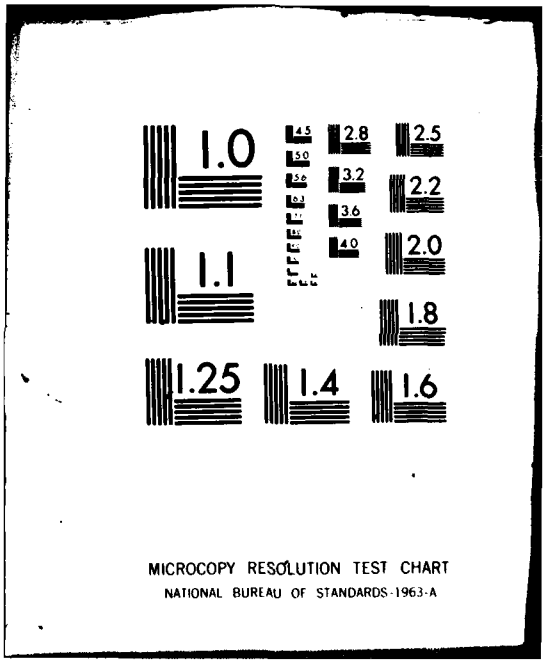
1.0
1.1
1.25
1.4
1.6
1.8
2.0
2.2
2.5
2.8
3.2
3.6
4.0
4.5
5.0
5.6
MICROCOPY RESOLUTION TEST CHART
NATIONAL BUREAU OF STANDARDS-1963-A

The onshore-offshore component is more variable than the alongshore component at all stations. The R/V ACANIA an onshore component between 1 and 3 m sec^{-1} until 0500 28 SEP when it shifted to an offshore direction between 1 and 2 m sec^{-1}. Point Pinos and Point Sur varied both in direction and magnitude with Point Pinos generally recording a wind with an onshore component. Point Piedras Blancas is the only station which seemed to have a diurnal variation. Offshore winds dominated at 1 to 2 m sec^{-1} until about 1500 (0800 local) when they shifted to onshore at 1 to 3 m sec^{-1} until about 0200 (1900 local). At the same time, the alongshore component was southerly.

During most of the cruise, the R/V ACANIA was not near Point Pinos. It was within 15 km of Point Sur at 0205 27 SEP on the transit south to the area and 1020 28 SEP on the transit north. During the first period, R/V ACANIA and Point Sur winds had the same direction but different speeds, with Point Sur being stronger. During the second period, the R/V ACANIA and Point Sur winds were nearly 180° out of phase and had the same speed. The ship was within 20 km of Point Piedras Blancas, at 2020 27 SEP. The R/V ACANIA alongshore wind was 3 m sec^{-1} in close agreement with the Piedras Blancas speed (4 m sec^{-1}), but the onshore components were out of phase with the R/V ACANIA reporting offshore winds at 1 m sec^{-1}, Piedras Blancas onshore winds at 3 m sec^{-1}.

c. Thermal Structure

A general feature of the thermal structure (Figs. 32-38) is a strong thermocline between 20 and 40 m except under the cold surface feature. The gradual rise in isotherms below the mixed layer near the cold feature was only observed on the first leg. As in Case I, numerous small scale fluctuations are evident.

Leg 1 (Fig. 32) was a southerly transit made from 0420 to 0601 along the eastern side of the cold surface feature. The slope of the isotherms within the mixed layer on the northern side of the feature (from 0420 to 0430) was approximately 3 m/km while on the southern side (from 0601 to 0620) the slope was approximately 2.6 m/km. The vertical transect of the feature indicates a structure with a diameter of 15 km at the surface and of 25 km at 45 m. Below this, the isotherms; e.g., 11.5°C, slightly increase in depth but not as dramatically as observed in Case I. The strong thermocline is evident from 20 to 30 m, particularly to the south of the feature. No such structure exists within the feature.

The general rise of the isotherms is of the order of 5 m/km with the peak occurring 15 km north of the surface feature. The rise is not perceptible on the south side.

Leg 2 (Fig. 32) was a northeast transit well to the east of the feature. AT 1143, the ship entered cold coastal water 15 km from the shore. The 16°C isotherm sloped at 4 m/km, the thermocline was evident from 15 to 45 m.

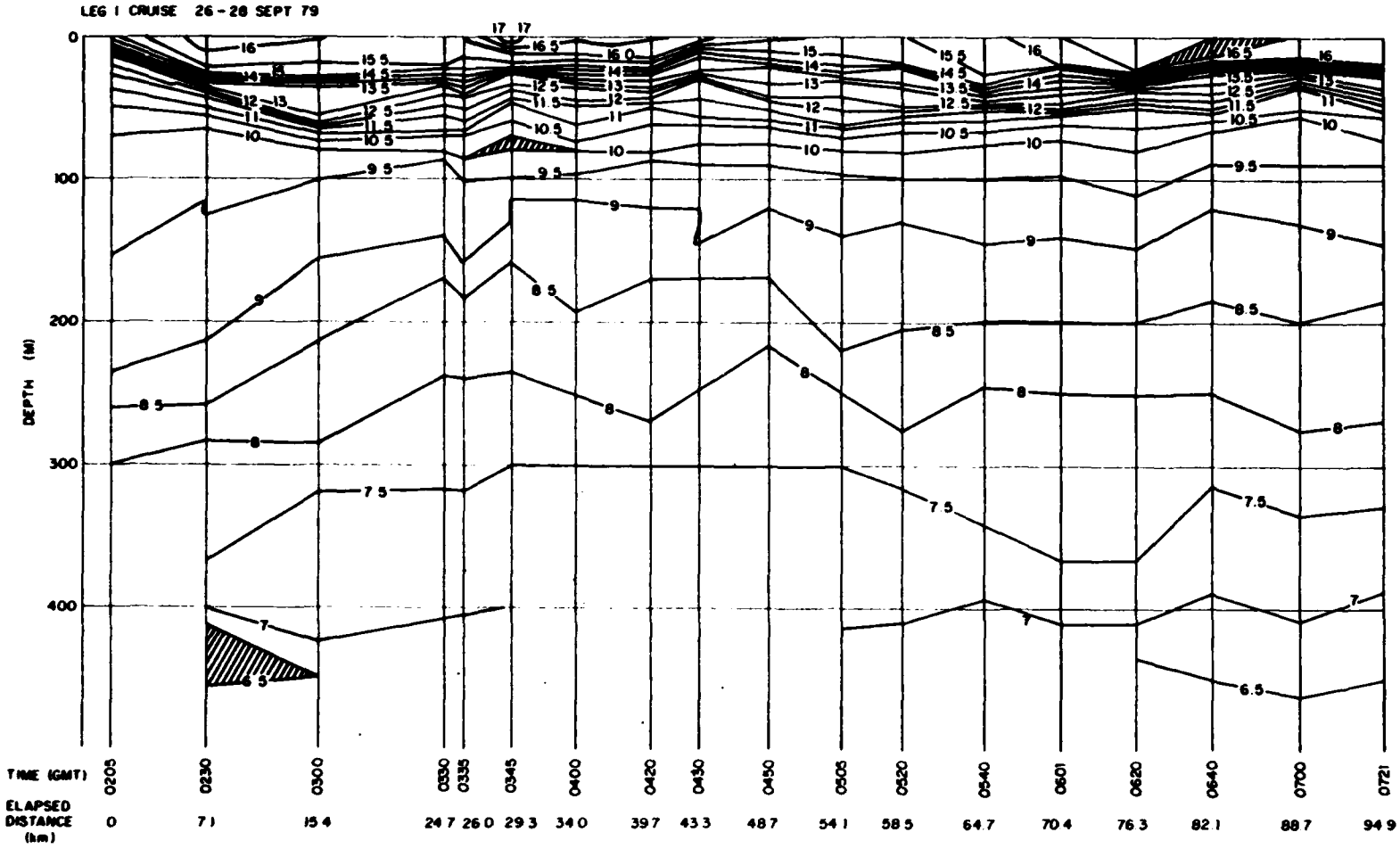

Fig. 32. Leg 1 0205 to 0721 27 SEP 79.

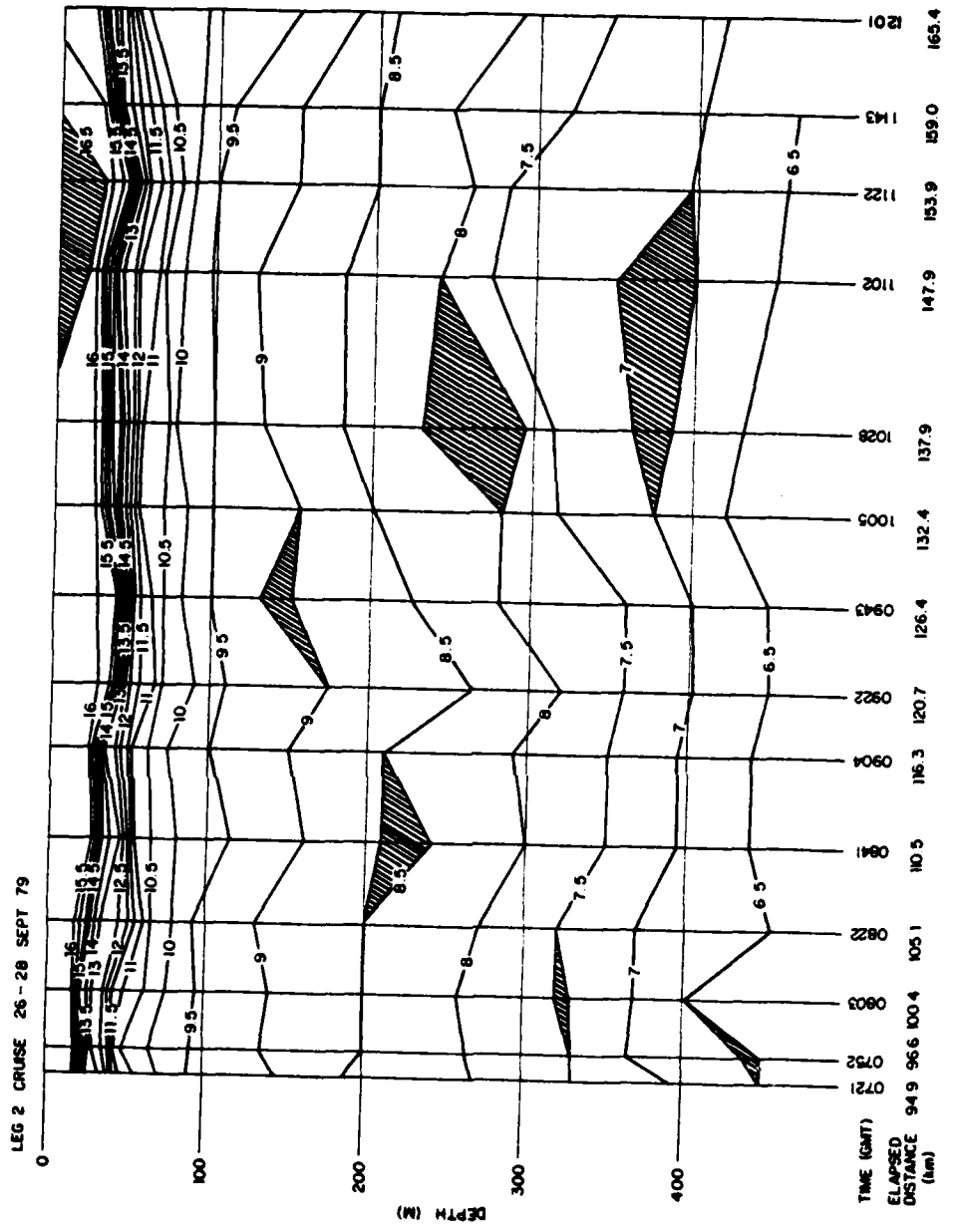

Fig. 33. Leg 2 0721 to 1201 27 SEP 79.

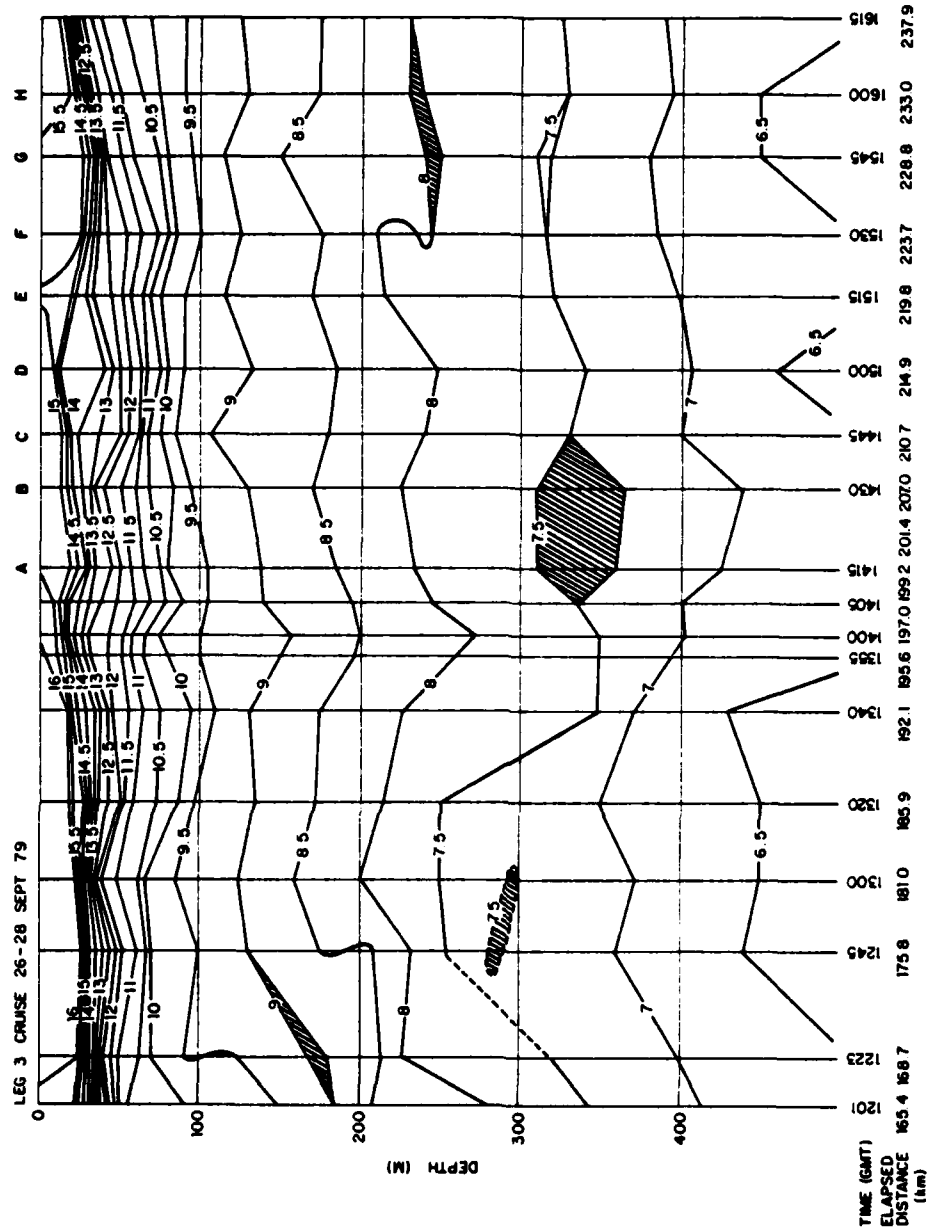

Fig. 34. Leg 3 1201 to 1615 27 SEP 79.

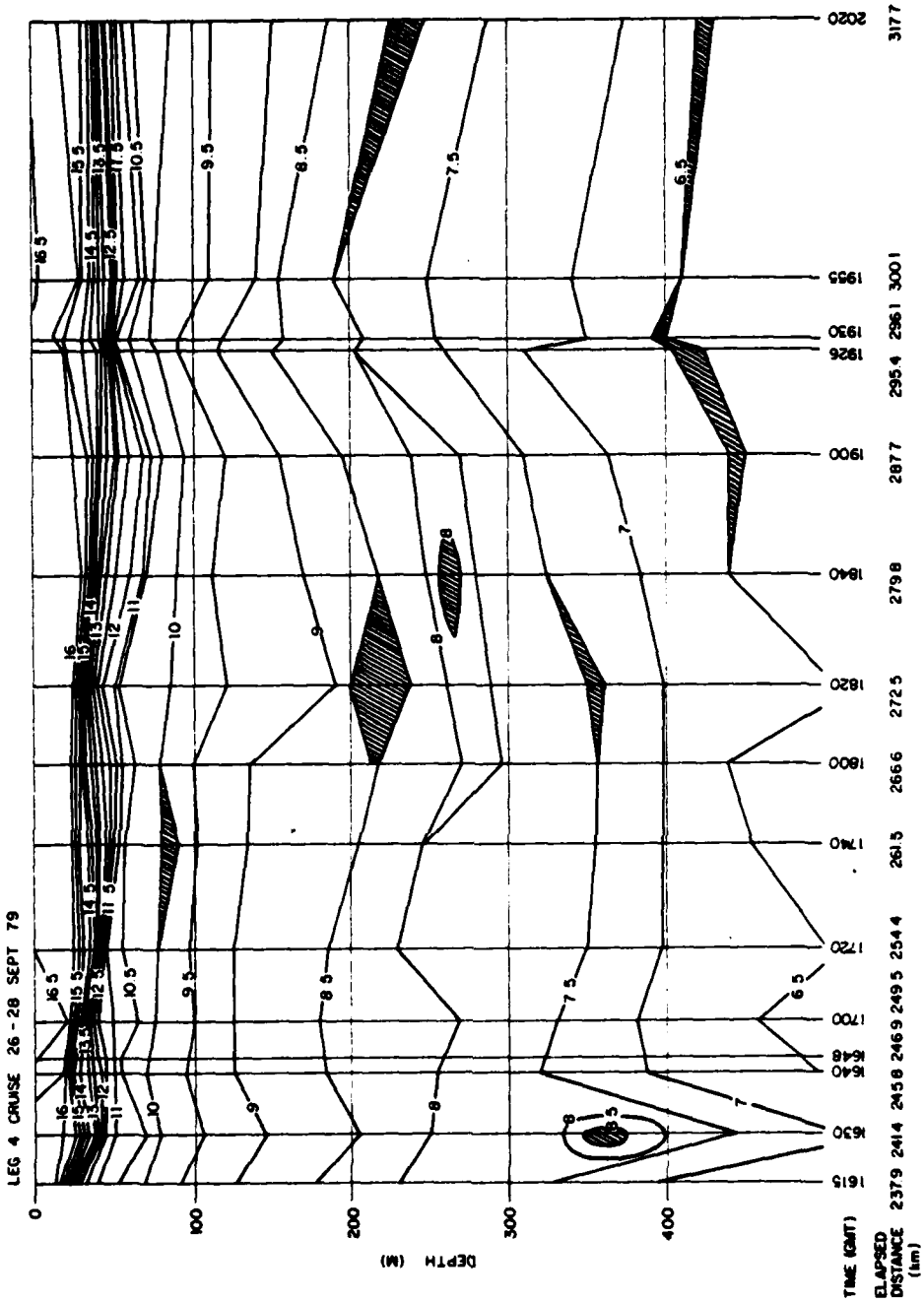

Fig. 35. Leg 4 1615 to 2020 27 SEP 79.

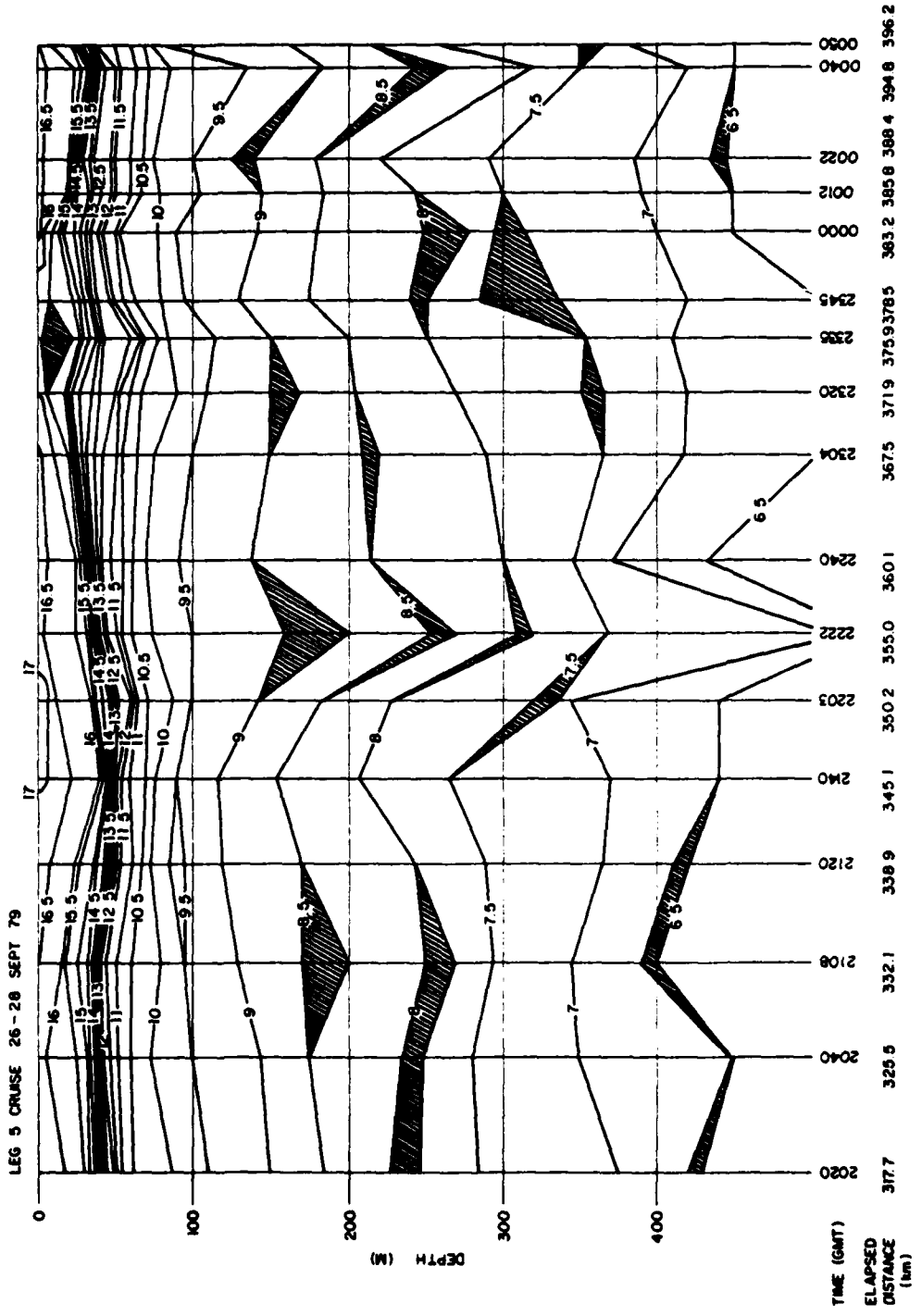

Fig. 36. Leg 5 2020 27 SEP to 0050 28 SEP 79.

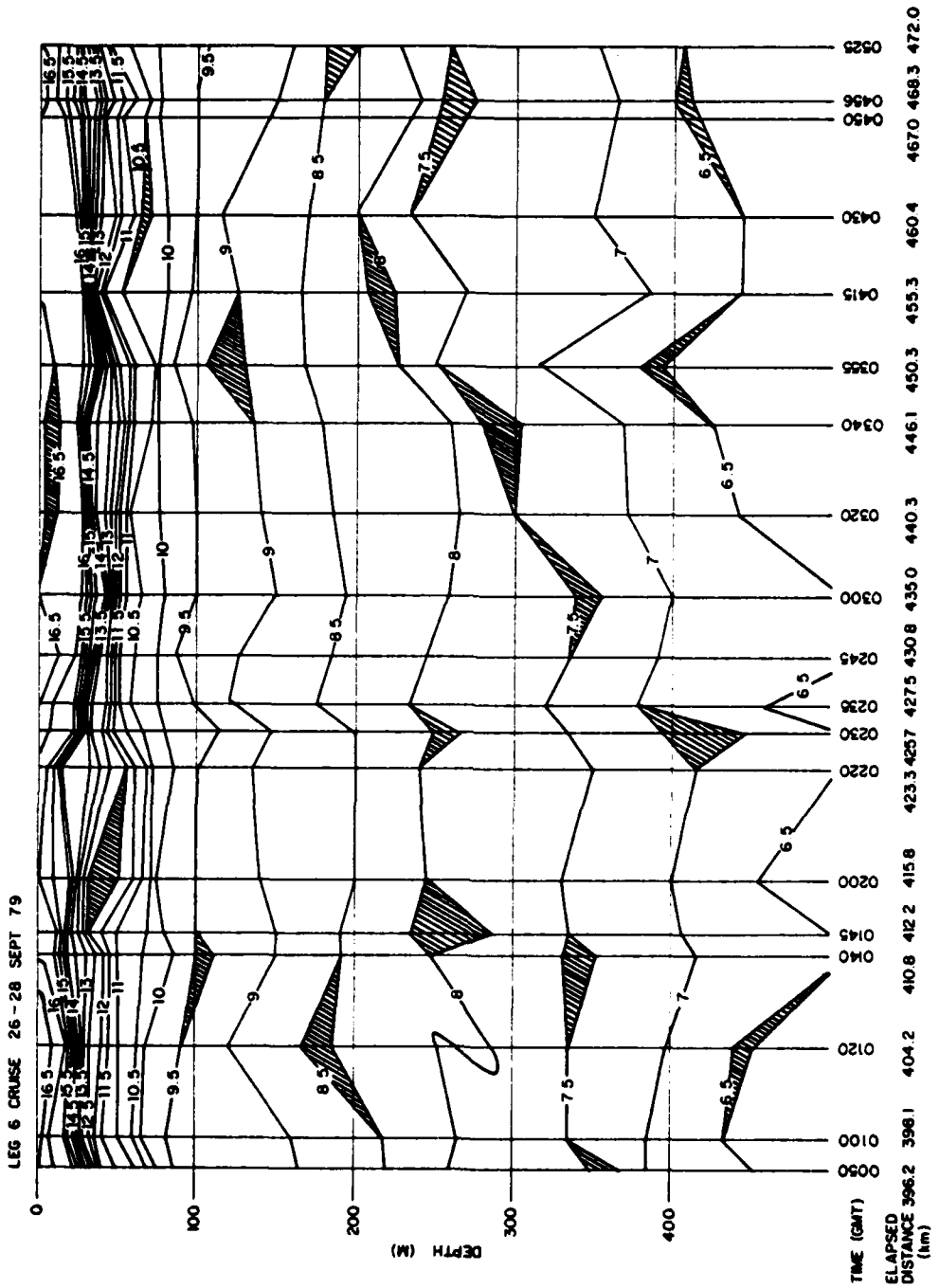

Fig. 37. Leg 6 0050 to 0525 28 SEP 79.

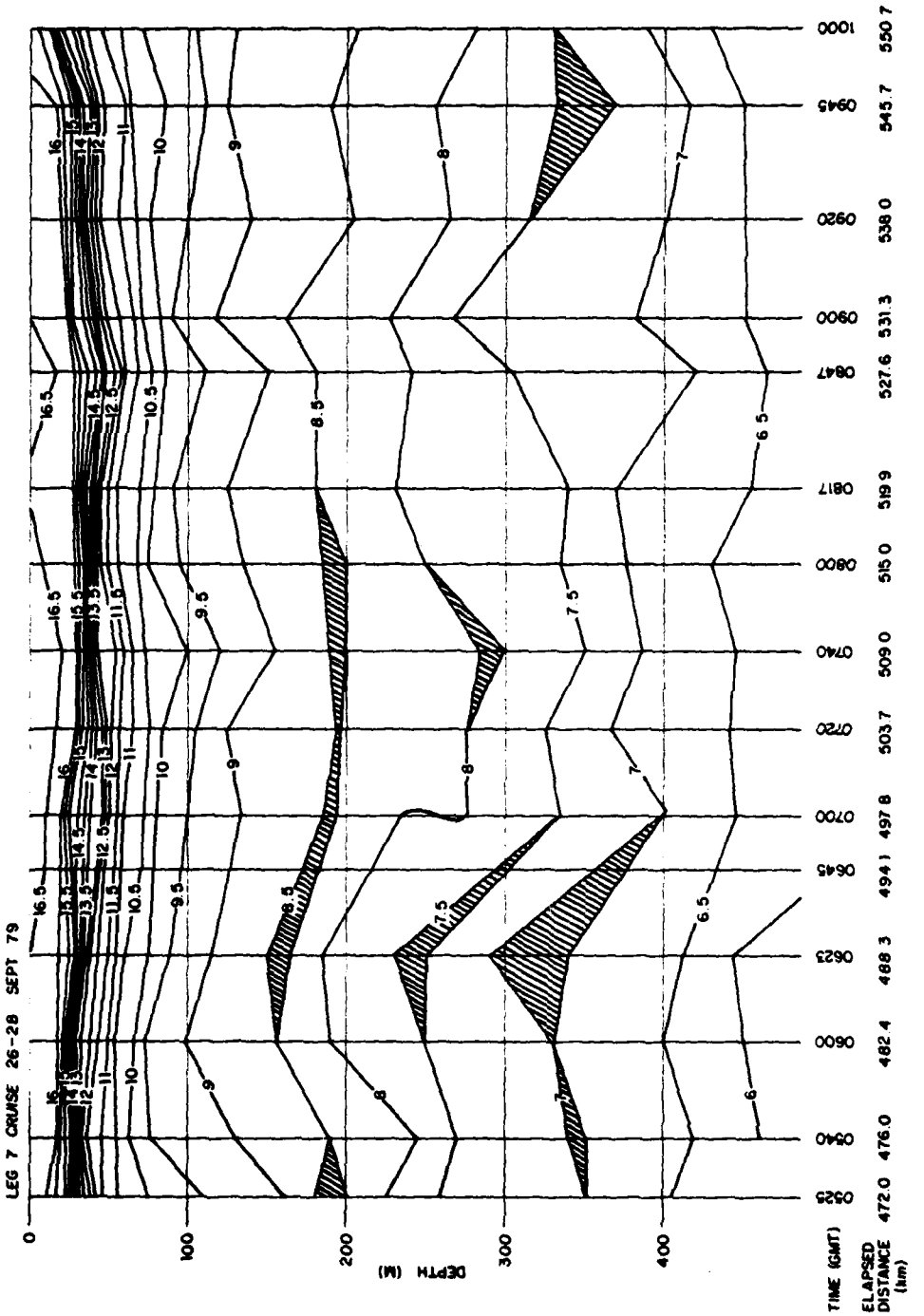

Fig. 38. Leg 7 0525 to 1000 28 SEP 79.

Leg 3 (Fig. 34) was a southwest transit which exited the coastal water at 1223, 12 km from shore and travelled along the axis of the feature from 1340 to 1600. The slope of the isotherms within the mixed layer on the NE side of the feature (from 1340 to 1415) was approximately 2.6 m/km while on the south side (from 1500 to 1545) the slope was approximately 2 m/km.

The vertical transect was not as distinctive as previously observed. The diameter at the surface was 30 km while at 30 m it was 42 km. Below the center of the feature, i.e., at 1445 and 1500, isotherms such as the 13°C increase depth only about 15 m.

There was a general rise of about 50 m of the 8, 8.5 and 9°C isotherms (between 100 and 300 m) from the start to the end of the transit. Again, no strong thermocline existed within the cold feature (Fig. 39).

Leg 4 (Fig. 35) was an east transit made well to the south of the feature. Of interest is the 1630 XBT which showed a steep deepening of isotherms 15 km SW of the feature, as in Case I. However, this was not supported by adjacent XBT's.

Leg 5 (Fig. 36) was a west-northwest transit which passed through the feature between 2304 and 0012. Features similar to those observed before were again noted, i.e. ; east-southeast slope of 1.6 m/km, west-northwest slope of 5 m/km, surface diameter of 10 km, subsurface (25 m) diameter

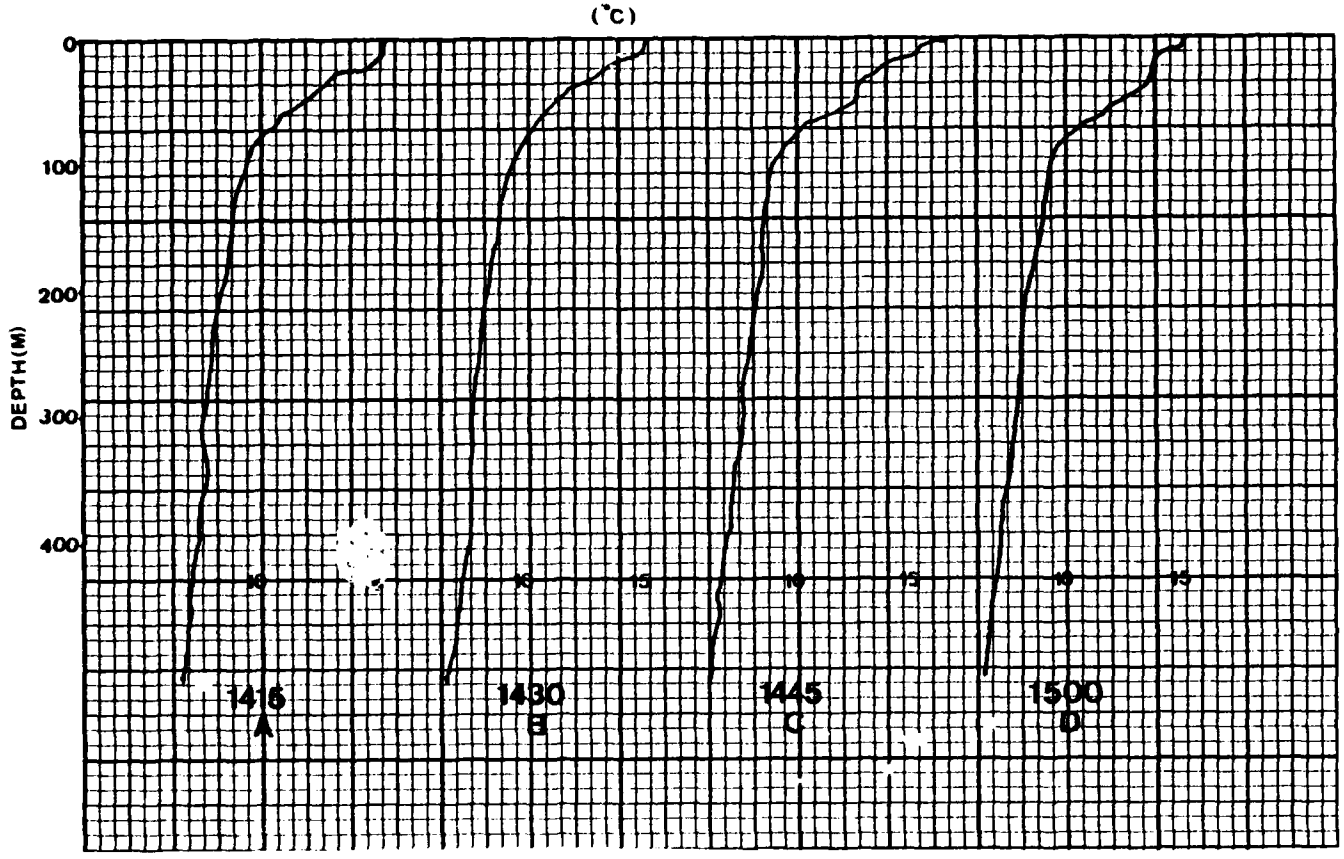

90T

Fig. 39. Selected XBT traces from leg 3.

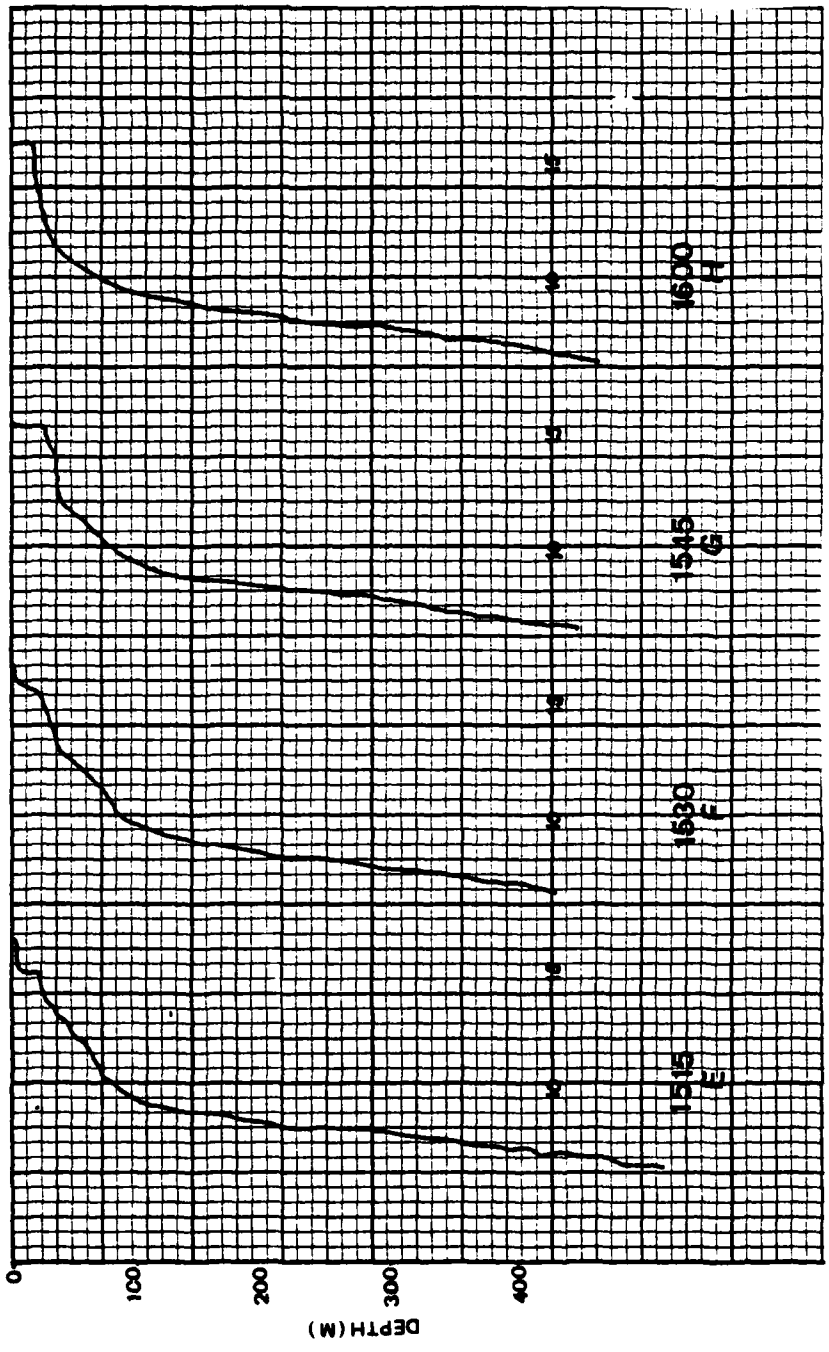

Fig. 39 (Continued)

of 18 km, isotherms below (12°) deepening (15 m), and no strong thermocline within the feature. There was a steep deepening of isotherms at 2222, about 20 km southeast of the feature. The slope of the isotherms, i.e., 7 to 9°C, between 2140 and 2222 does support this deepening.

Leg 6 (Fig. 37) was a southeast transit through the center of the cold surface feature, orthogonal to leg 3. Upwelling related features were observed between 0120 and 0245. As noted before, these are: northwest slope of 2.5 m/km, southeast slope of 8 m/km, surface diameter of 17 km, subsurface (25 m) diameter of 22 km, isotherms (13.5°C) below deepening (15 m), and no strong thermocline within the feature.

Leg 7 (Fig. 38) was a northerly transit which passed well to the east of the feature. The SST (Fig. 40) has a distinct cold core as observed in satellite IR imagery (Appendix B). The feature is centered at 65 km SSW of Point Sur, and it is of roughly elliptical shape with its major axis aligned along the Lucia Canyon axis. The area within the 15°C isotherm was 3 km^2. The sharpest temperature gradient, 1.5°C/10 km, was alongshore to the southeast. Offshore gradients were weaker. Stronger gradients, 2.5°C/10 km, exist in a front oriented E-W off Point Sur in a narrow plume. This front was not as sharp as the feature in the satellite IR imagery; however, there was a cold spot oriented in the same manner in the imagery (Appendix B).

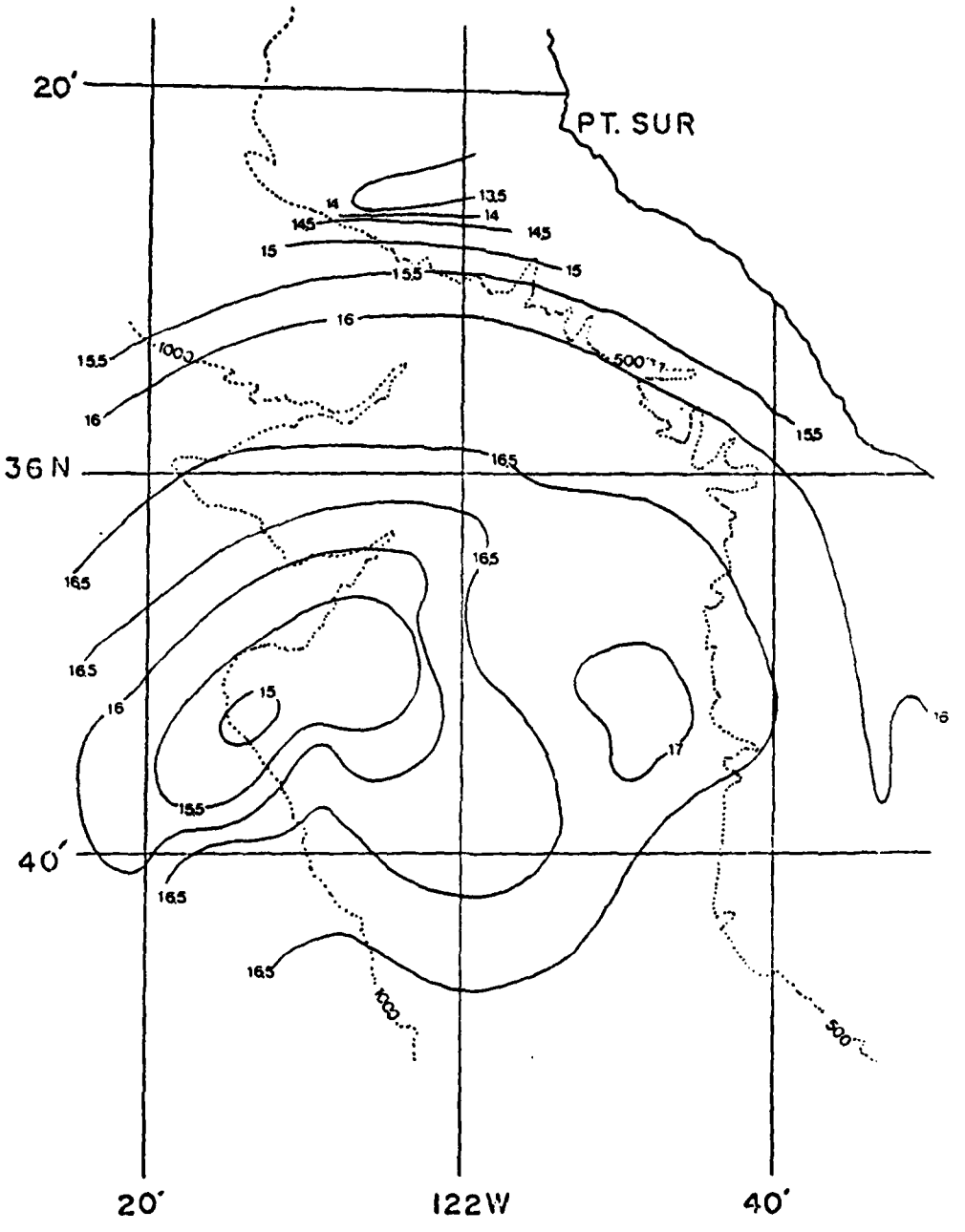

Fig. 40. SST (°C), 26 to 28 SEP 79.

The MLD (Fig. 41) had a pattern somewhat similar to the SST. Minimum values of less than 5 m were within the cold feature. Maximum values, 30 and 40 m, were 32 km to the east (towards shore) along the Lucia Canyon axis.

The 25 m temperature resembles the SST, with the cold spot shifted 2 to 3 km northeast and numerous warm sports, including one slightly south of the surface cold spot. The density of XBT casts precluded sampling the E-W front off Point Sur, but the 15°C isotherm appeared to be oriented E-W there. Maximum gradients were no longer associated with the cold spot. Frontal areas to the south and north had gradients of the order of 2.0°C/10 km.

The 50 m temperature does not resemble the SST. Below the cold surface feature, there was a warm area except for what could be a continuation of the cold surface feature as manifested in a closed 12°C isotherm located at 16 km to the northeast. Temperatures ranged from 10.5°C near shore to 13.0°C within the warm anomalies. Maximum gradients were approximately 1°C/km in many areas, generally around the anomaly.

The temperature fields on the 100 to 400 m surfaces manifested the warm anomaly present at 50 m. The strongest gradients at these depths were generally associated with a cold tongue protruding to the northwest adjacent to the warm anomaly. These values were: 0.3°C/km at 100 m, 0.1°C/km at 200 m, 0.1°C/km at 300 m, and .05°C/km at 400 m. There were

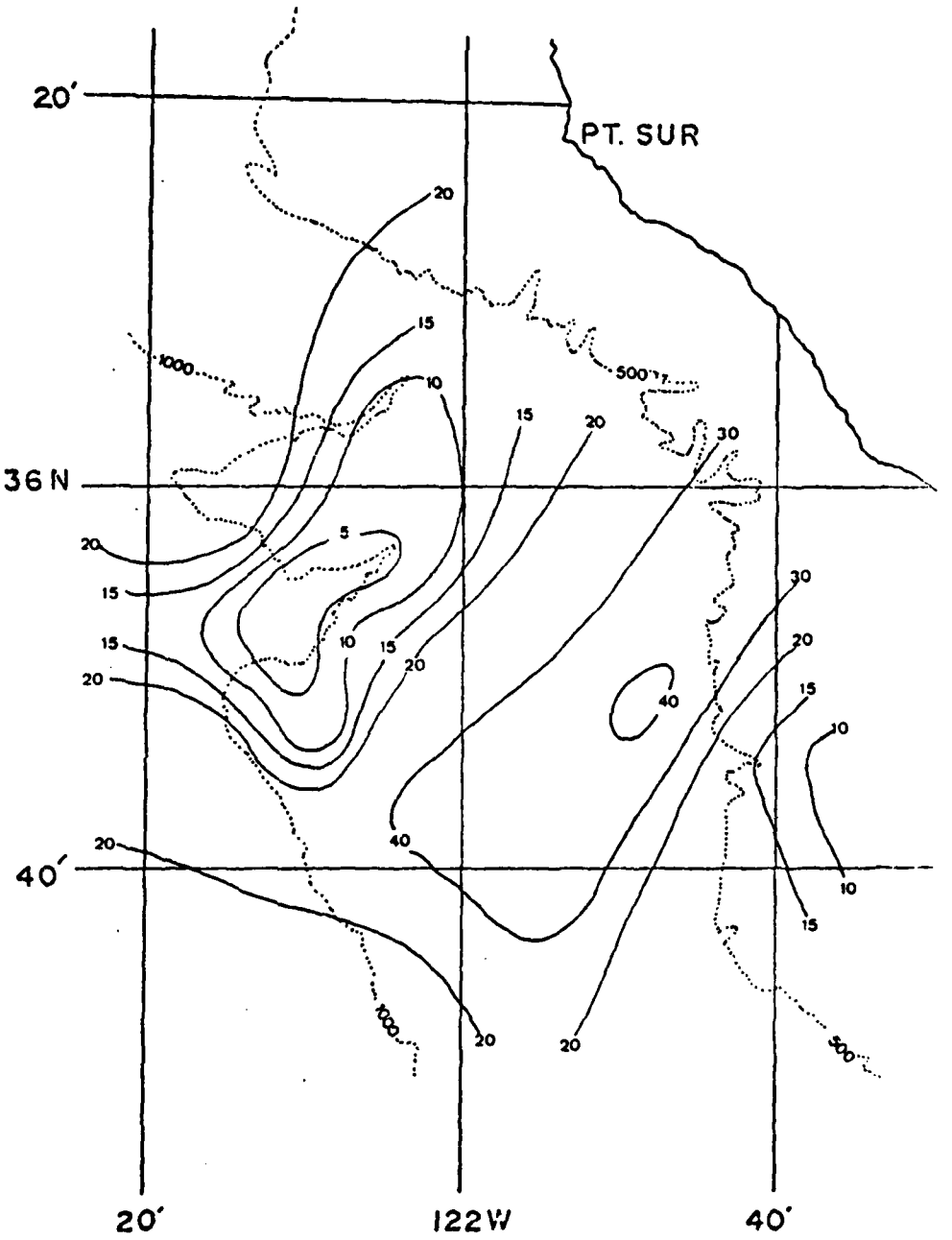

Fig. 41. MLD (m), 26 to 28 SEP 79.

distinctive structures on all surfaces which were not parallel to topography.

The thickness between the 15 and 9°C isotherms (Fig. 48) had maxima in many areas, including under the "cold spot" and along the axis of the Lucia Canyon. Other general areas of maxima are to the northwest and southeast of the feature.

The pattern of the depth of the 15°C isothermal surface (Fig. 49) closely resembles that of the SST. Minimum depths were within the "cold spot" and at the E-W front near Point Sur.

The final information extracted is a time series of temperature profiles from XBT's dropped within a kilometer. One such case was observed at the intersection of legs 1, 3 and 5. As in Case I, temporal changes in the depth of isotherms greatly exceeded the spatial slopes previously discussed. Using r.m.s. depth changes and the time between XBT drops, vertical velocities calculated were about 5×10^{-2} cm sec^{-1}.

Sufficient bucket temperatures were taken to analyze the difference between bucket and thermistor (2 m) temperatures. The data were smoothed with a five point running mean. There was a mean difference of -0.12°C and a standard deviation with the thermistor temperatures higher than the bucket temperatures. Large negative differences were observed at night from 0400 to 1500. Bucket temperatures were slightly higher than thermistor temperatures during daylight hours.

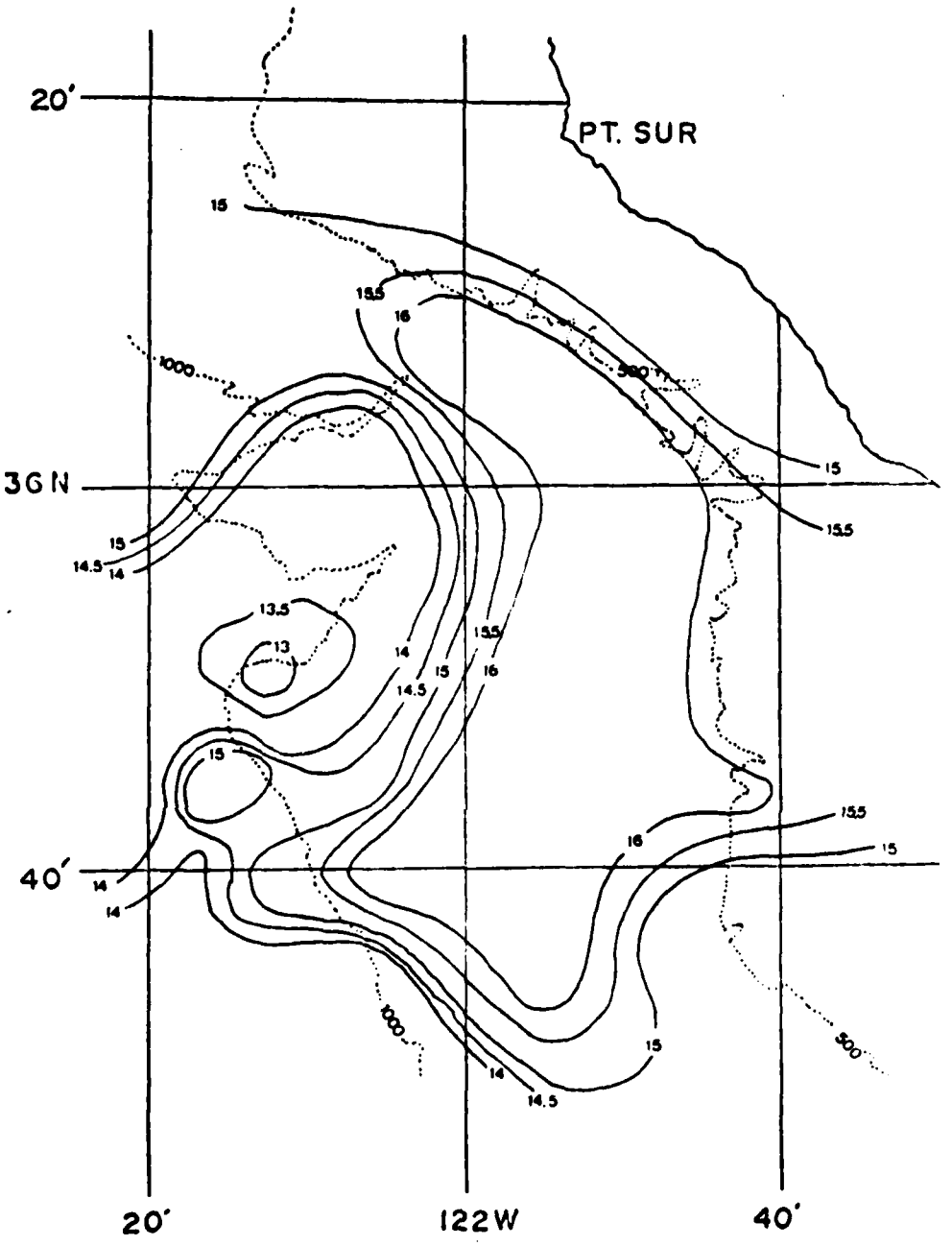

Fig. 42. 25 m temperature field (°C), 26 to 28 SEP 79.

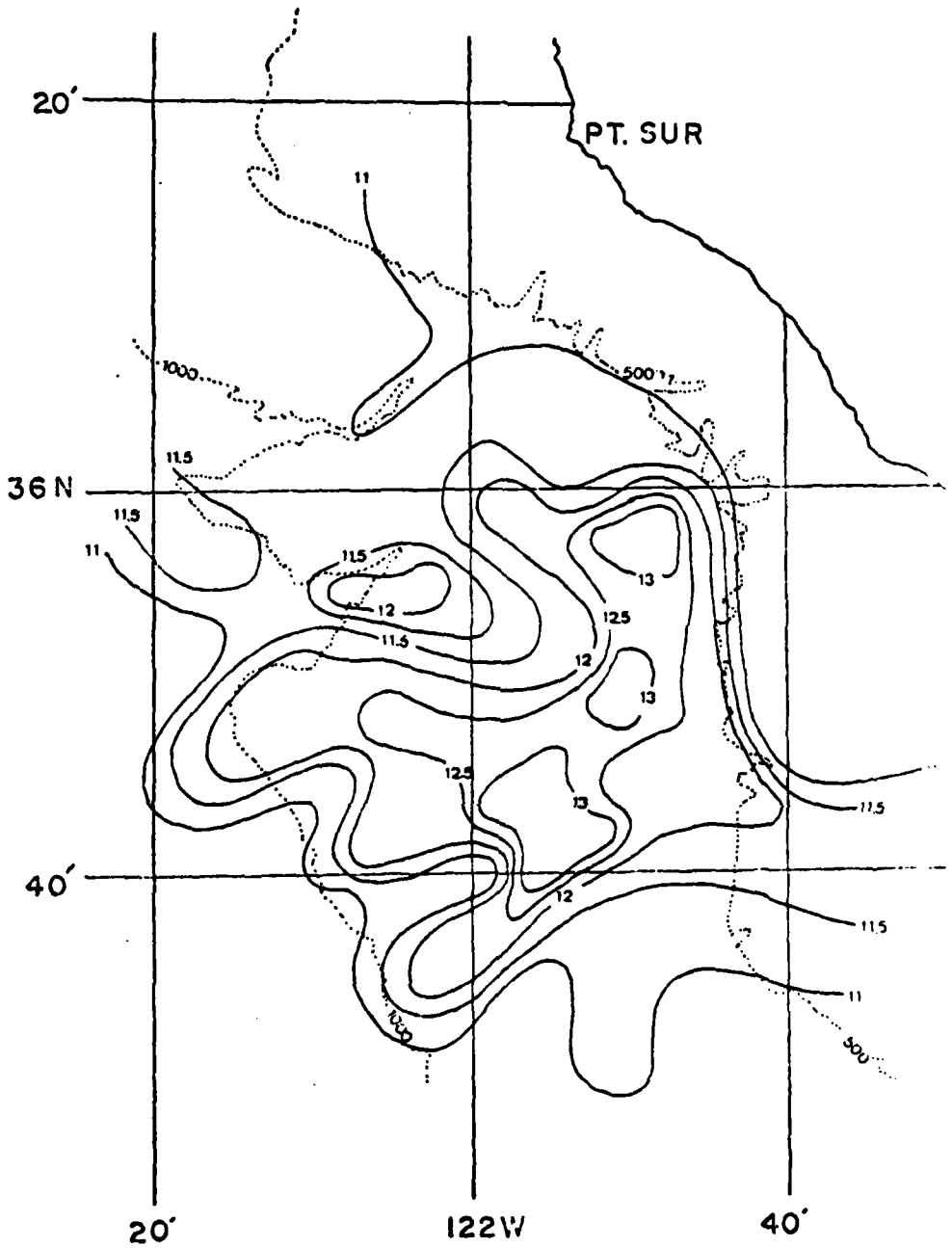

Fig. 43. 50 m temperature field (°C), 26 to 28 SEP 79.

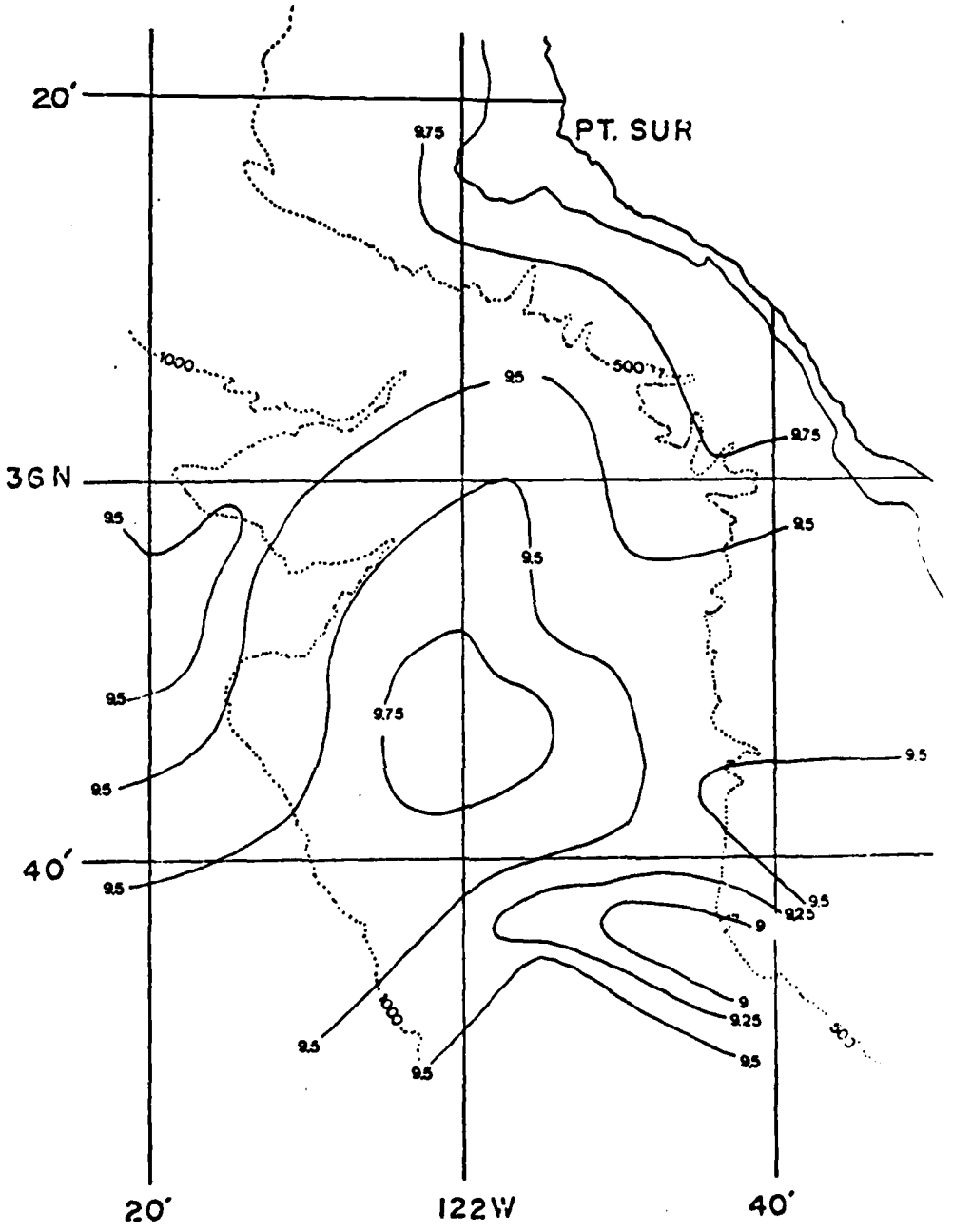

Fig. 44. 100 m temperature field (°C), 26 to 28 SEP 79.

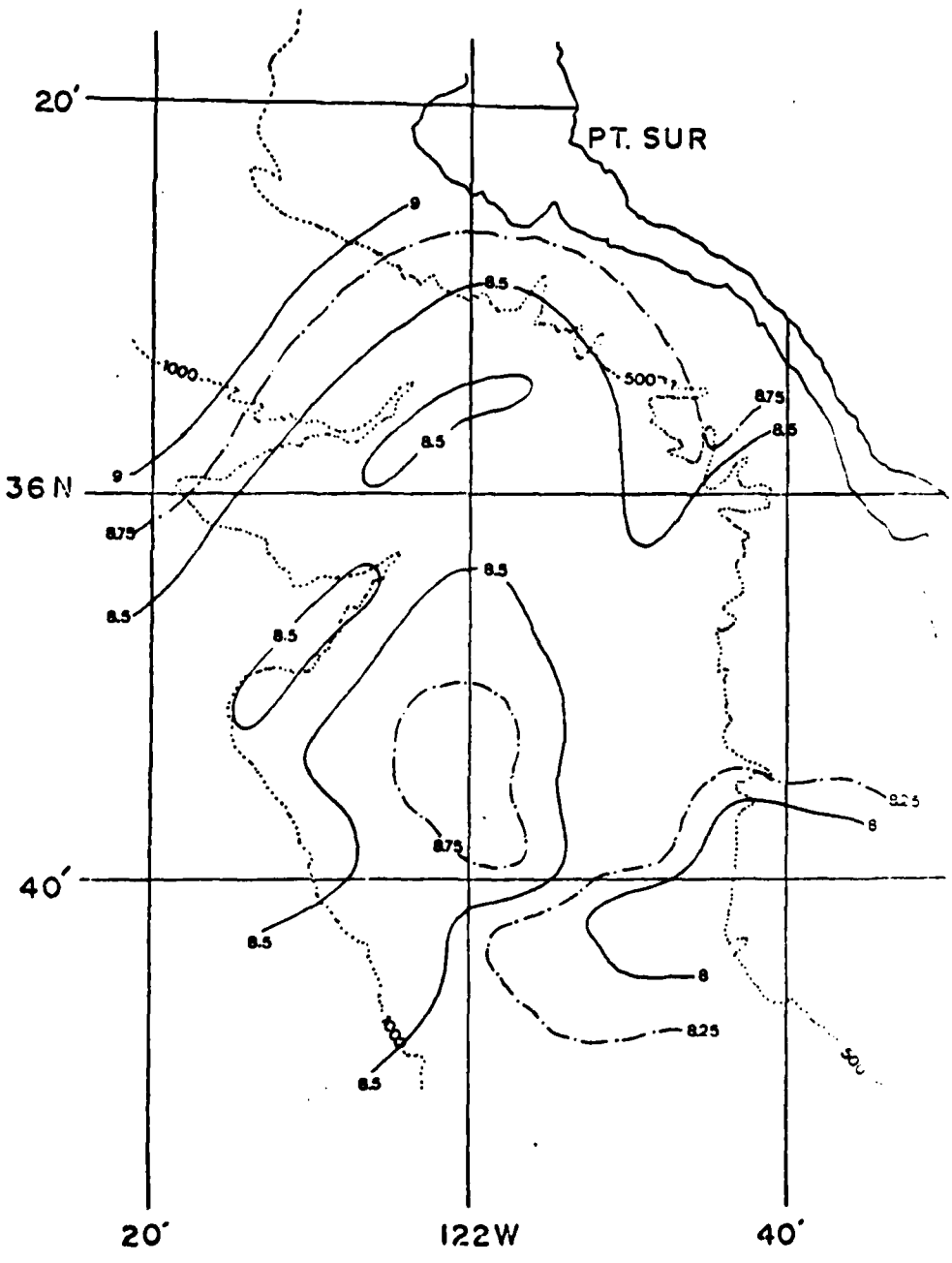

Fig. 45. 200 m temperature field (°C), 26 to 28 SEP 79.

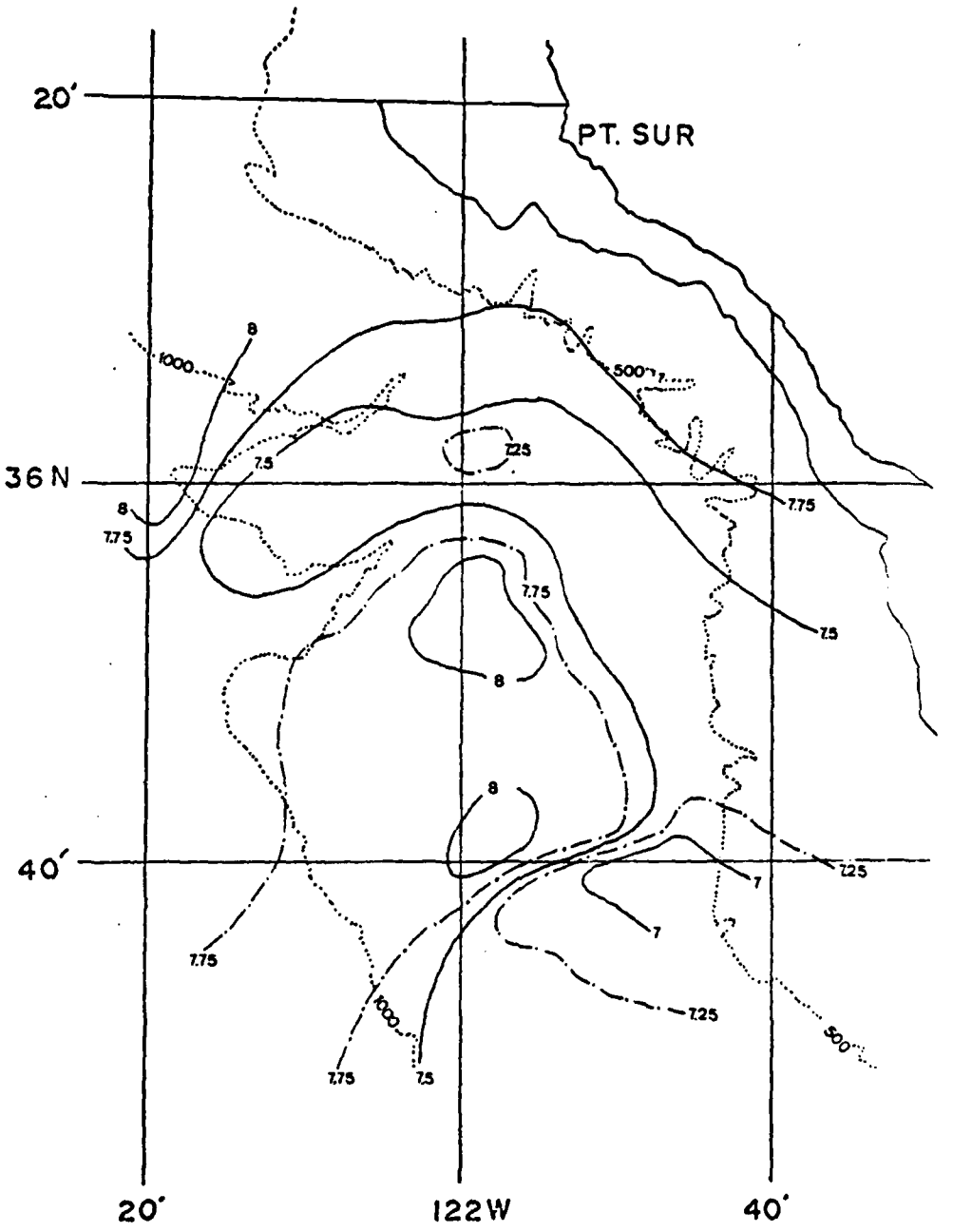

Fig. 46. 300 m temperature field (°C), 26 to 28 SEP 79.

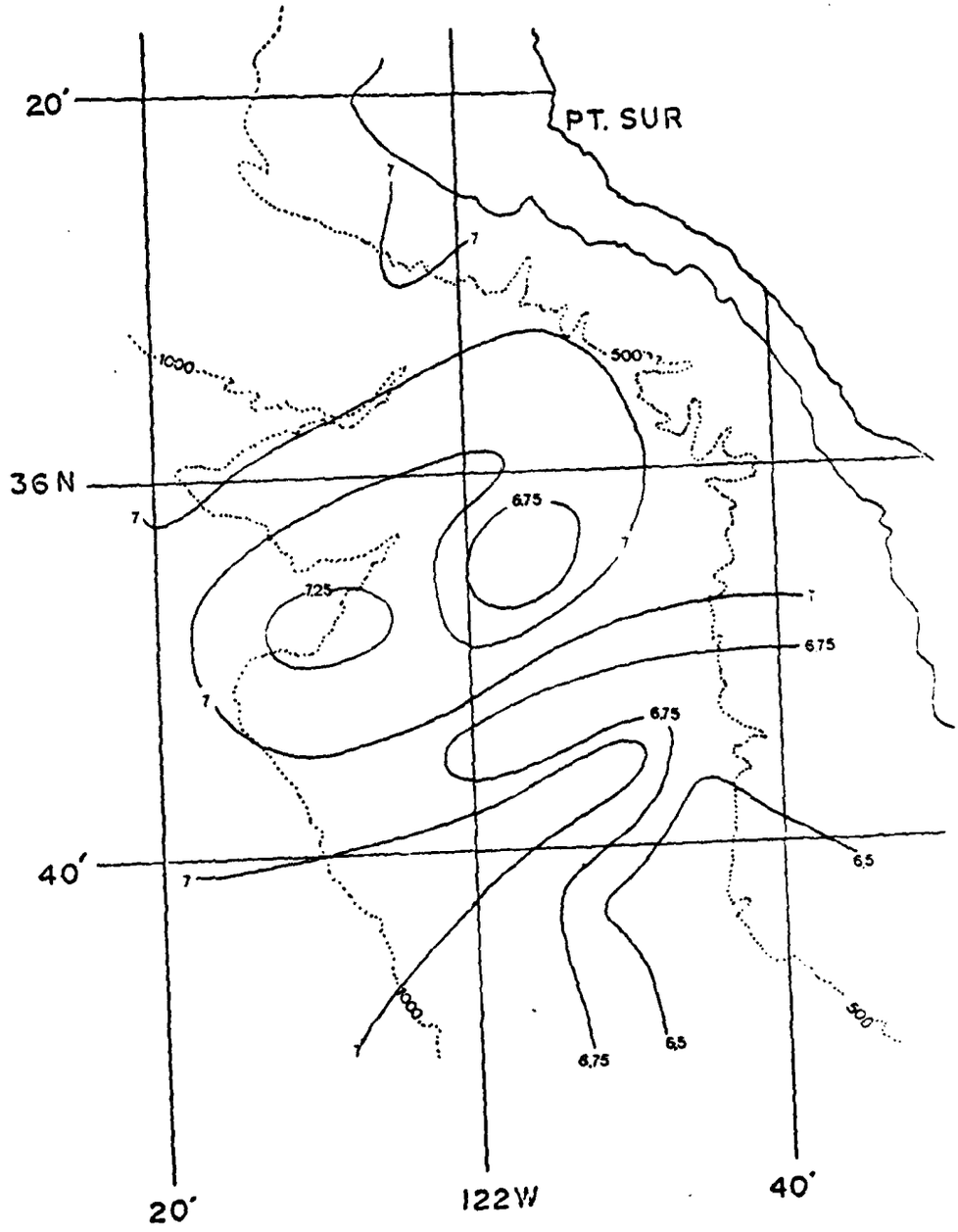

Fig. 47. 400 m temperature field (°C), 26 to 28 SEP 79.

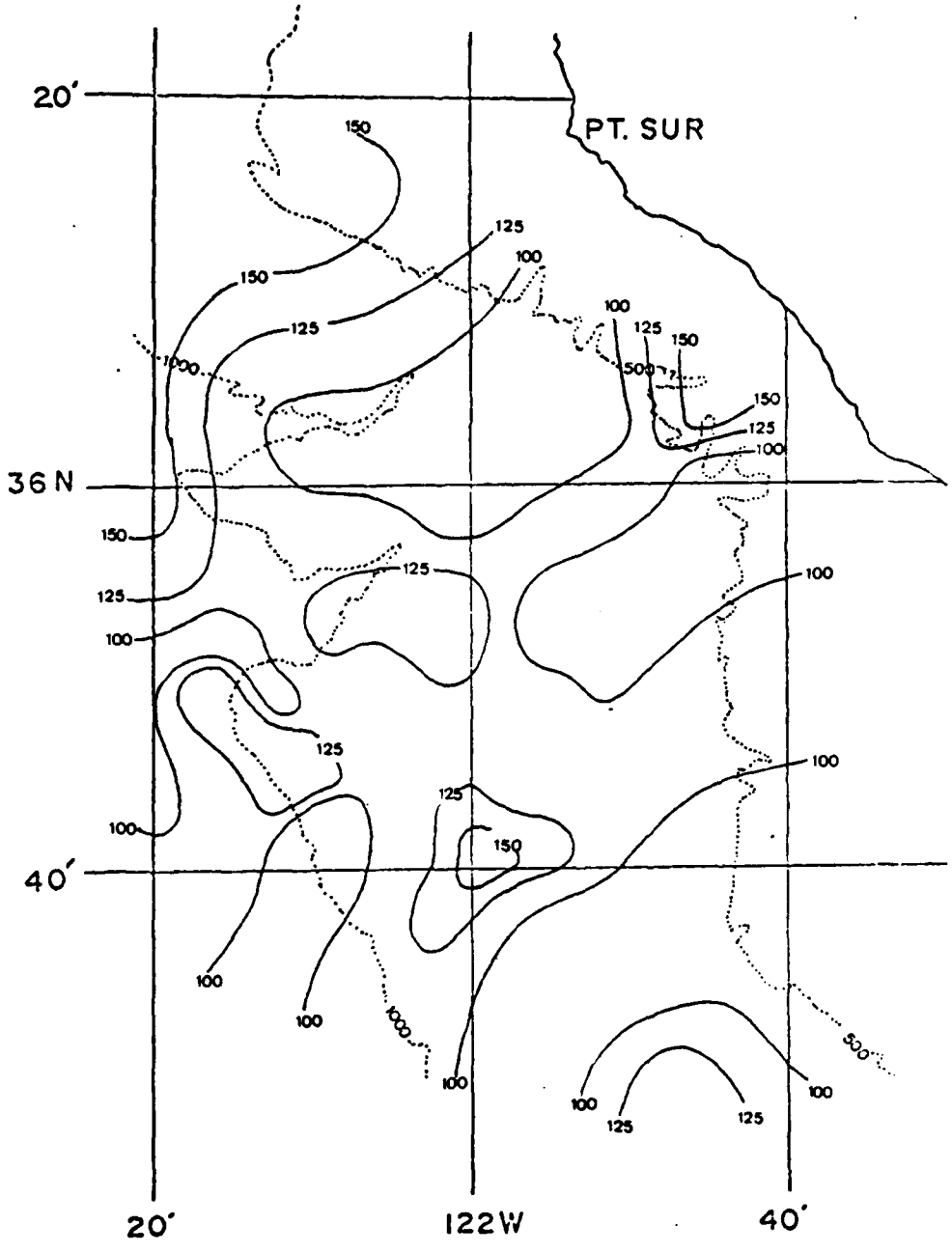

Fig. 48. Thickness (m) between 15° and 9°C isothermal surfaces, 26 to 28 SEP 79.

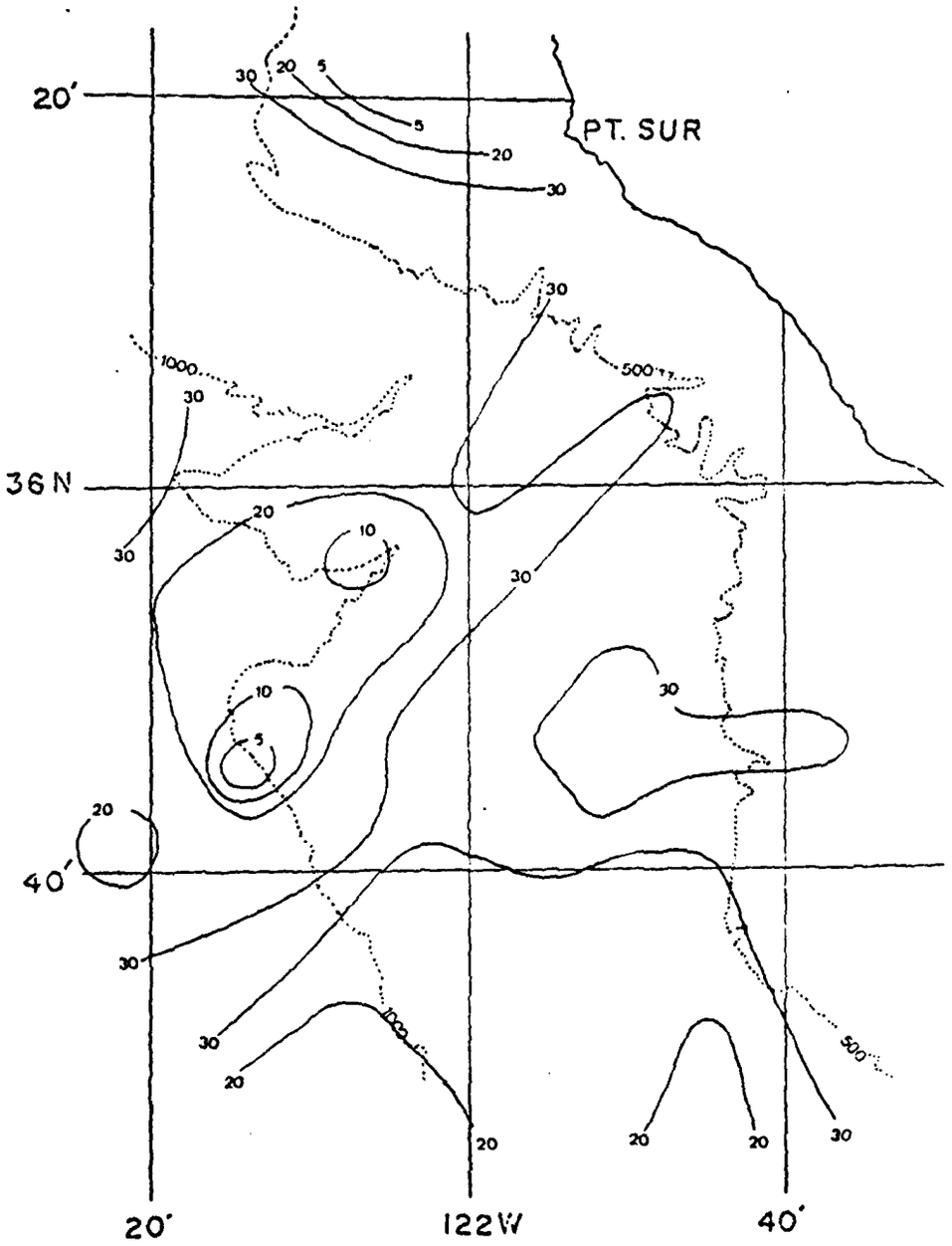

Fig. 49. Depth (m) of the 15°C isothermal surface, 26 to 28 SEP 79.

3. Case III (28 to 29 Nov 79)

a. Summary of Oceanic Surface Conditions

The cruise from 28 to 29 NOV 79 investigated and verified the existence of a cold plume-like feature extending 25 km southwest from Point Sur. Due to intermittent cloud cover obscuring the area, no position information was obtained from the satellite imagery prior to the cruise. Enough imagery was observed to suggest a small feature close to Point Sur, and a prior cruise had detected a frontal type feature in the immediate vicinity on 26 and 27 NOV.

The cruise plan included a transit south parallel to the coast in order to penetrate the front, followed by a square search and then a ladder search to delineate the band of coastal upwelled water found within 10 km of the coast and to find the plume off Point Sur [Fig. 50).

XBT usage was restricted to 40 XBT's at an average spacing of 9 km. In addition, seven STD casts were made (Fig. 50), salinity samples were taken from the keel injection (2 m), and wind observations were recorded simultaneously with XBT casts.

From 9 NOV to 14 DEC 79, nineteen TIROS-N and NOAA 6 IR images were reviewed. Cloud contamination due to low stratus and high cirrus clouds was severe from 23 to 29 NOV, and on 9 DEC. A satellite summary is presented in Fig. 51.

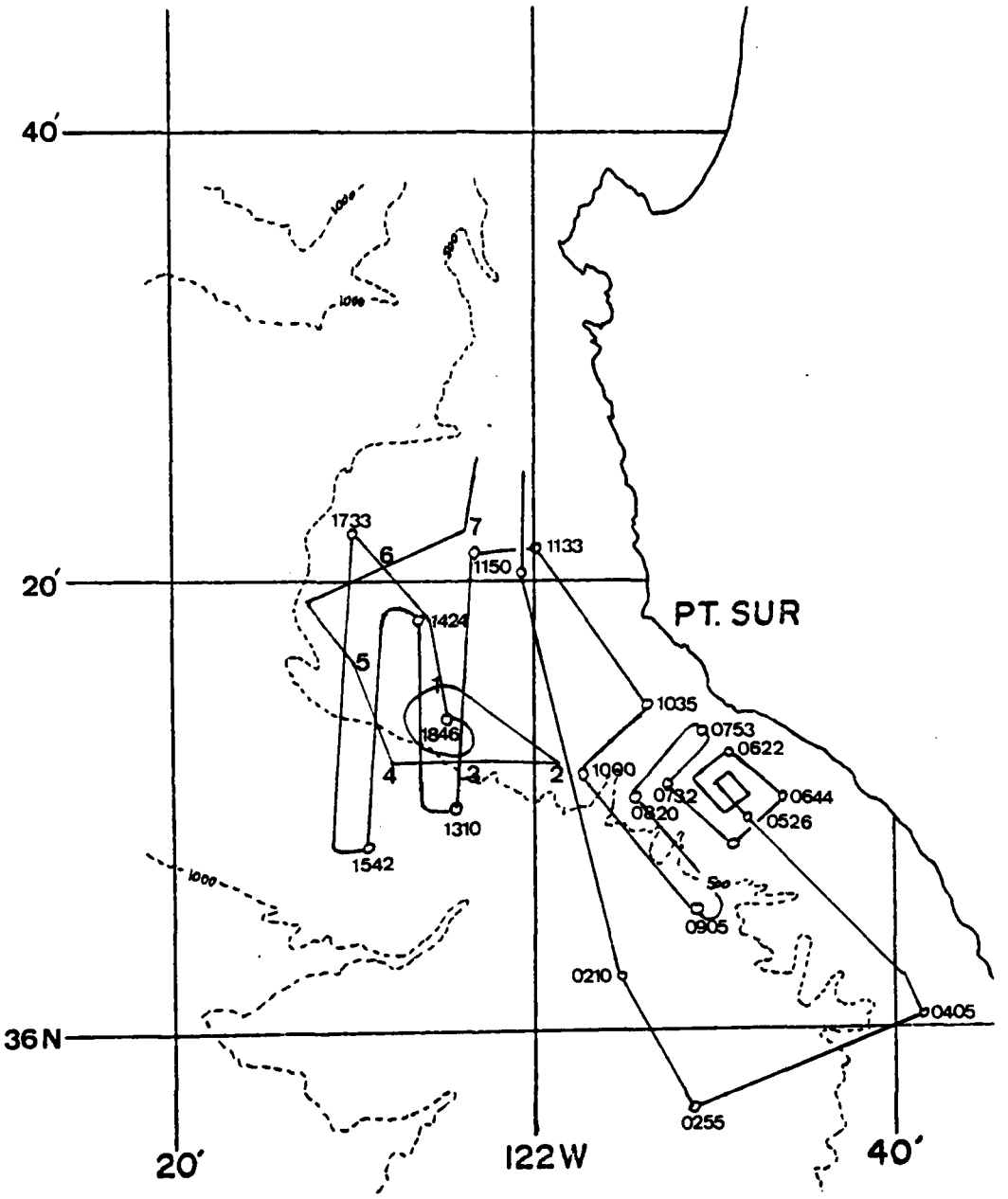

Fig. 50. Cruise track from 28 to 29 NOV 1979. STD cast positions numbered 1 through 7. Times are GMT.

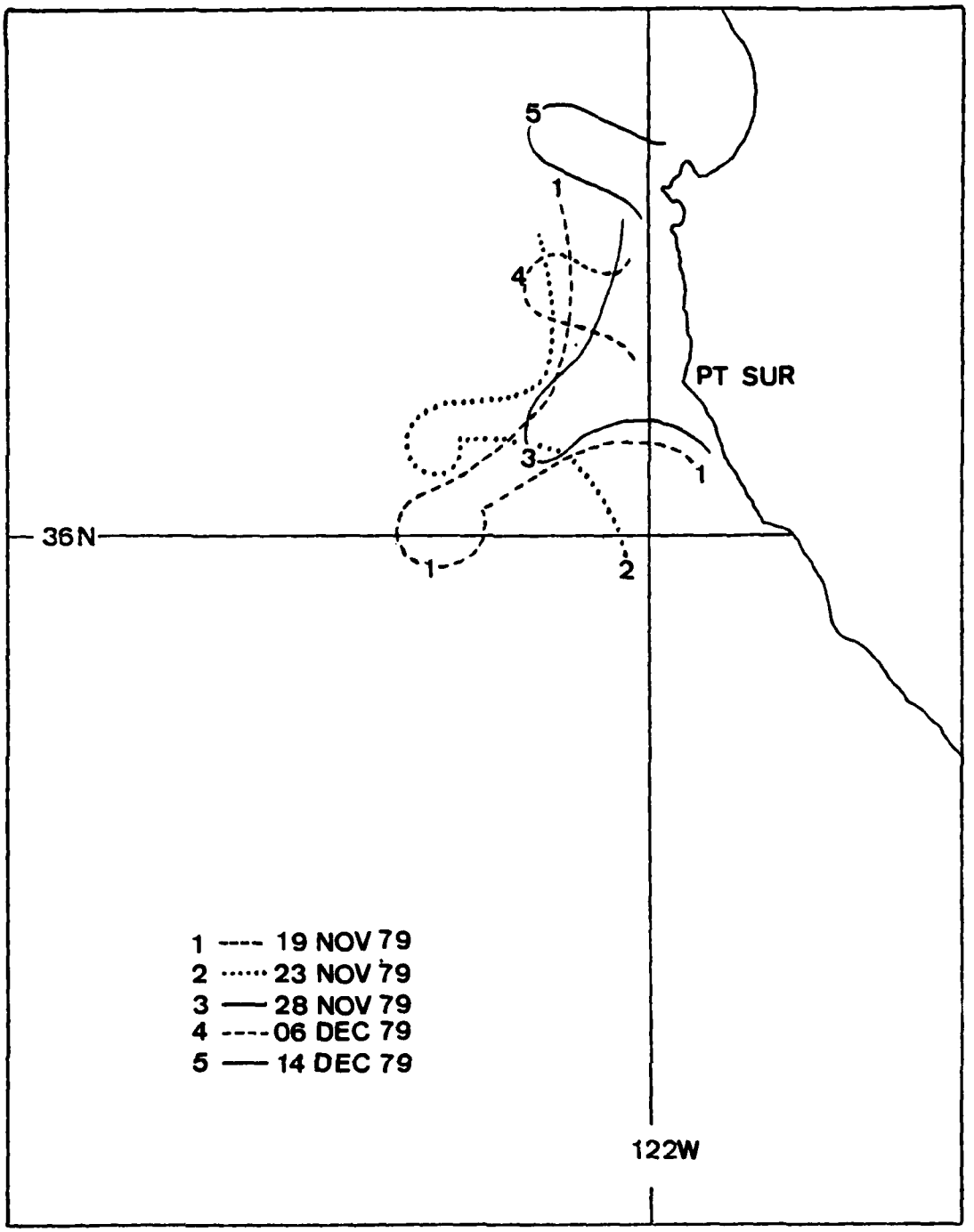

Fig. 51. Satellite features observed from 19 NOV to 14 DEC 79.

On 9 NOV, there were many diffuse, indistinct features off Point Sur. Cold coastal water generally extended 15 km offshore. On 11 NOV, there were several parallel plumes along the coast. A discernable, but weak plume had formed off Point Sur bearing 245°T, 35 km seaward. It had a central core of cold water 15 km wide. The coastal band of cold water had narrowed to a 3 km width.

By 19 NOV, the same plume had developed further and curved to the south in a cyclonic fashion, extending seaward 50 km. A uniform band of cold coastal water extended from Point Piedras Blancas to Monterey Bay, and it was 25 km wide.

On 20 NOV, the same cyclonic plume was visible, bearing 220°T from Point Sur and extending 60 km offshore. There was no significant band of cold coastal water from Point Piedras Blancas to Point Sur. However, it was 30 km wide from Point Sur to Monterey Bay. This feature persisted until 23 NOV when it appeared to have shifted north bearing 235°T from Point Sur. There was cloud contamination near the seaward end of the feature.

On 27 NOV, intermittent cloud cover partially obscured the area off Point Sur. However, the plume described earlier appeared to be more diffuse. Cold coastal water was uniformly 15 km wide from Point Piedras Blancas to Point Sur. Although fog or low stratus obscured much of the 28 NOV image, no feature could be distinguished. A small

plume-like feature developing off Point Sur was evident. The width off the coastal band of cold water remained uniform. These conditions persisted on 29 NOV.

An apparent cold plume-like feature, 8 km in width, was distinguishable on 6 DEC, bearing 240°T from Point Sur and extending 30 km seaward. There was a "cold spot" adjacent to the coast at the base of the plume. The coastal band of cold water was 5 km wide. This feature persisted through the 14 DEC image. However, during this time period, it had rotated from a bearing of 240°T from Point Sur to a bearing of 310°T and it had been displaced northward to off Point Pinos.

Numerous plumes were observed during this period at many locations along the coast within the field of view. Other predominant locations were Point Conception, Monterey Bay, San Francisco, and Eureka. On 11 NOV, a plume-like feature began to develop off Point Sur. It apparently reached a maximum seaward extent of at least 60 km as observed on 20 NOV. By 27 NOV, it showed signs of dissipation. By 28 NOV, it had become indistinct. An apparent time scale "life cycle" of 17 days was, thus, indicated.

Another distinct plume started to develop by 28 NOV, and it reached its maximum size by 6 DEC. This particular plume was also the only one observed to advect northward at 4 cm sec^{-1} (30 km in 8 days). It apparently merged with a pre-existing plume off Monterey Bay.

In FNOC's SST Analysis for 26 NOV 79 (Fig. 52), a southward distortion of the isotherms was apparent near the coast with a cold pocket of 15°C water extending from Point Sur to the Channel Islands. There was no evidence of the upwelling related feature or of the cold coastal band. The analyzed SST off Point Sur during the cruise was 15°C.

b. Summary of Atmospheric Conditions

NMC 500 mb and SL charts were reviewed from 13 NOV to 14 DEC 79. The predominant feature at 500 mb was a cold core low in the Gulf of Alaska throughout the period. Numerous large wave systems passed through the area of interest with a time scale of approximately 8 days. There were also numerous short wave features. Oakland winds were westerly with speeds from 25 to 80 knots. In particular, during the cruise from 28 to 29 NOV 79, the Central California coast was initially dominated by a strong ridge parallel to the coastline extending from a weak high off Baja California into British Columbia. An enclosed high pressure system eventually developed from this ridge in the north and weak zonal flow over the area of interest resulted.

The SL charts indicated a great deal of variability in the weather systems affecting the central coast. There were numerous frontal passages from 16 until 26 NOV when a cold front propagating from the NW became stationary at Monterey Bay. A weak ridge dominated the area from 26 to 30 NOV and resulted in northerly geostrophic winds. The

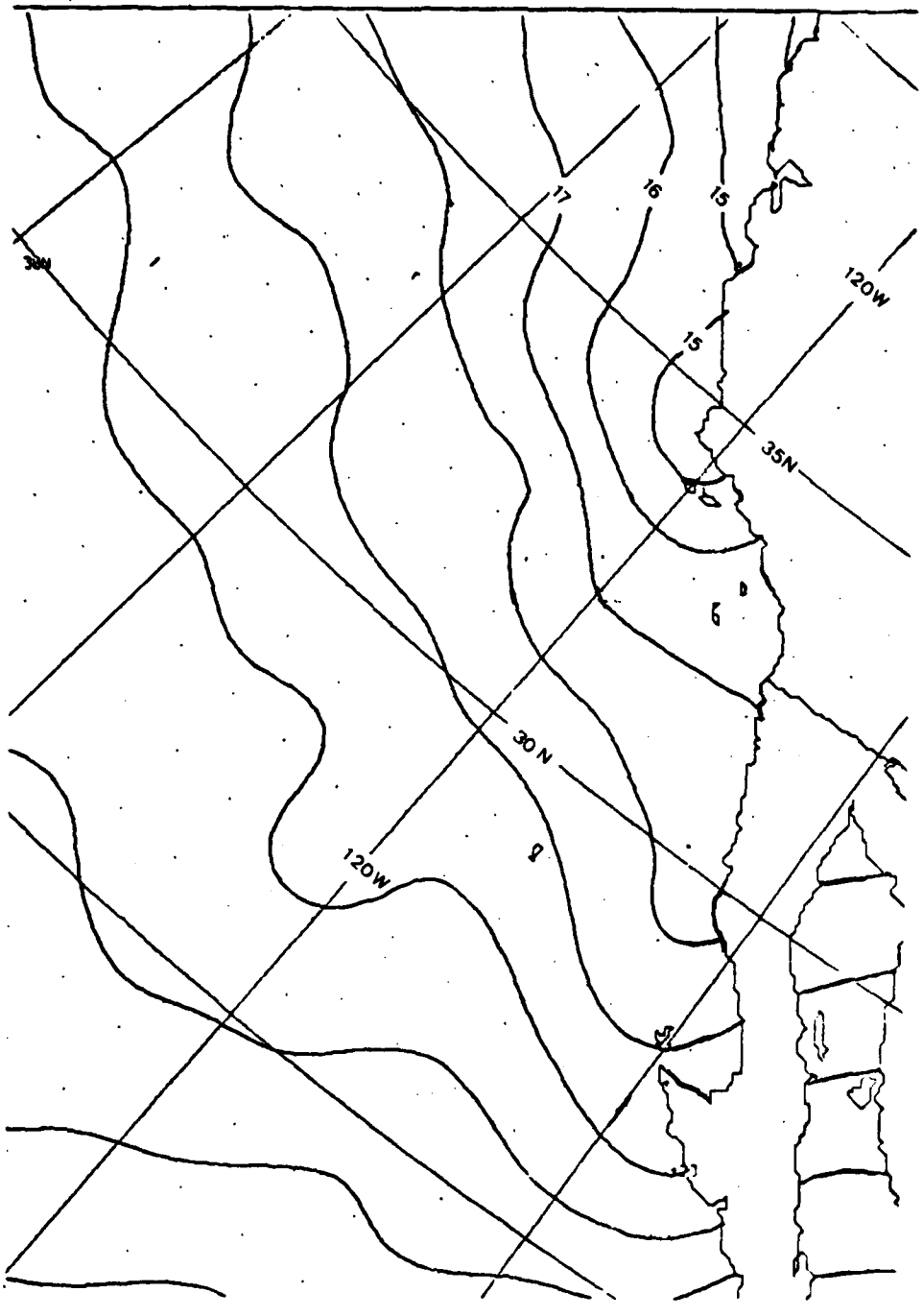

Fig. 52. FNOC SST Analysis for 26 NOV 79.

simultaneous development of a high offshore and a high over the Rockies as well as troughs to the north and south led to weak and variable winds in a col over the Central California coast which lasted from 30 NOV until 2 DEC. Another frontal passage occurred on 5 DEC, and a thermal trough started to develop from a low pressure system off Baja California NW along the coast. Geostrophic winds were northerly during this period. Frontal passages also occurred on 10 and 13 DEC. On 14 DEC, a ridge extended from a high pressure system located offshore through the area of interest. During the days of the cruise, basic meridional flow predominated due to the offshore low and a high over Eastern Washington. This system started to dissipate on 29 NOV due to the strengthening of a high pressure system off Baja California and an approaching cold front at 00Z 29 NOV (Fig. 53).

The SL pressure analysis at 36 N 122 W from FNOC varied between 1010 and 1020 mb from 22 NOV to 7 DEC. The SL pressure fluctuations had a period of six days. On the days of the cruise, there was a weak ridge, and the SL pressure was about 1026 mb.

The analyzed wind stress magnitude at 36 N 122 W was small (< 0.5 dynes cm^{-2}) from 22 NOV through 5 DEC. Ekman transport was light and variable as was the upwelling index. Open ocean upwelling vertical velocity was variable with downwelling (0.5×10^{-3} cm sec^{-1}) from 22 to 27 NOV,

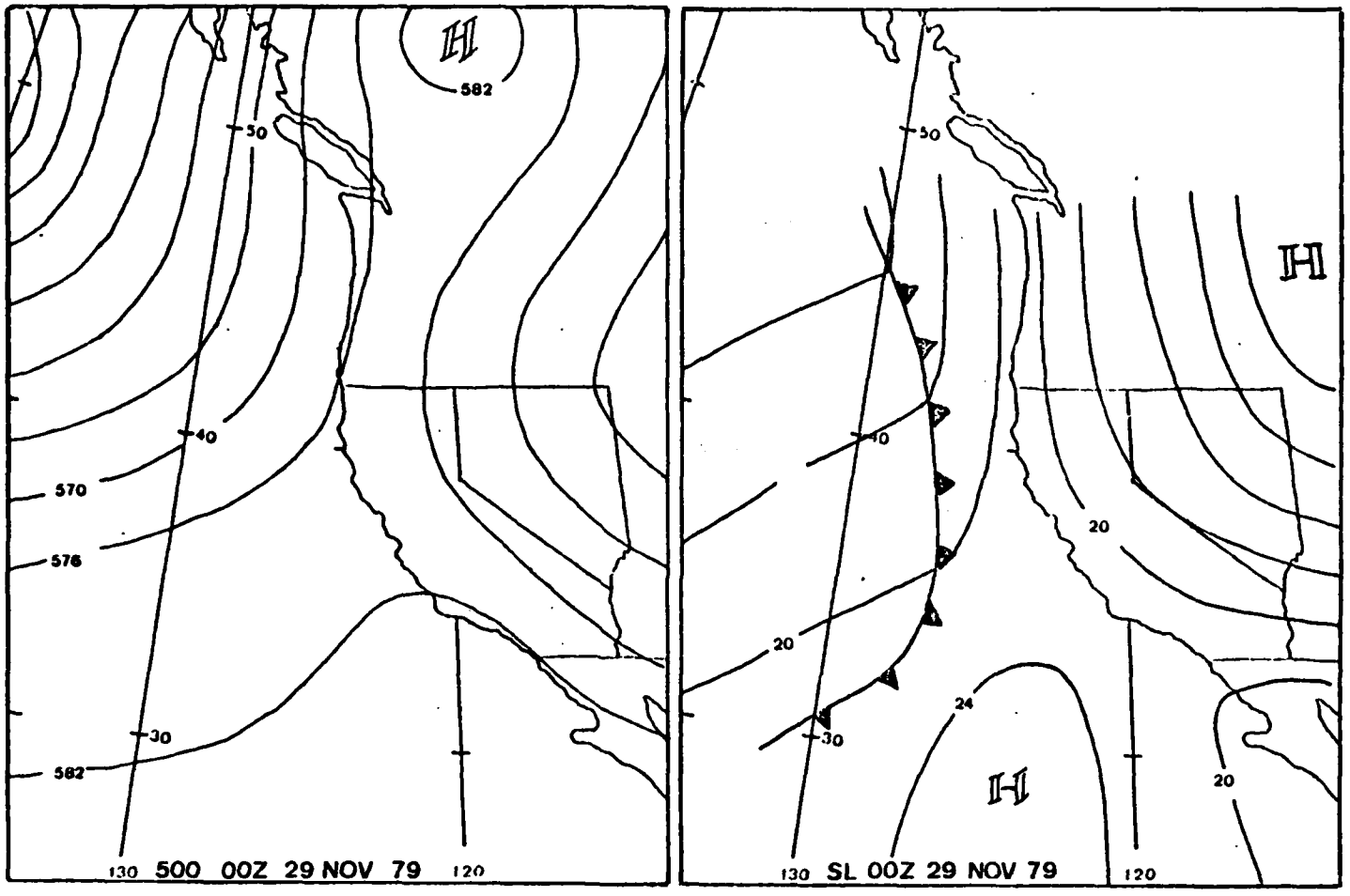

Fig. 53. 500 mb and SL analyses for 29 NOV 79.

minor upwelling of the same magnitude on 28 NOV, and negligible fluctuating values until 5 DEC (Fig. 54).

Partly cloudy conditions persisted during the entire cruise except for complete overcast 1300 to 1430, 29 NOV. Visibility was unlimited. The swell was NW, one meter. The pressure was steady at 1025.3 mb. The R/V ACANIA's winds were generally NW varying from 2 to 6 m sec^{-1}.

Reports from Points Pinos, Sur, and Piedras Blancas were reviewed for the cruise period. During the cruise the ship was greater than 40 km from Points Pinos and Piedras Blancas. Point Pinos winds were initially ENE 3 to 5 m sec^{-1}, then variable. Point Sur winds were ENE 1 to 2 m sec^{-1} shifting to NNW 3 to 6 m sec^{-1}. Point Sur also recorded clear conditions except for overcast conditions 0400 to 0700 and 1900 to 2200 29 NOV. Point Piedras Blancas were variable, shifting to NW 3 to 5 m sec^{-1}, then back to variable conditions.

Point Sur winds had an alongshore component from the NE recorded from 1300 29 NOV through the remainder of the cruise. Initially, winds were offshore from 0100 (1700 local) 29 NOV to 1000 (0200 local) 29 NOV, onshore at 1000 and 1300 29 NOV, and offshore for the remainder of the cruise. Ship winds had a continuous alongshore component from the NE at 1 to 5 m sec^{-1}. Both ship and station show onshore/offshore in phase correlation except when the ship was more than 30 km from Point Sur.

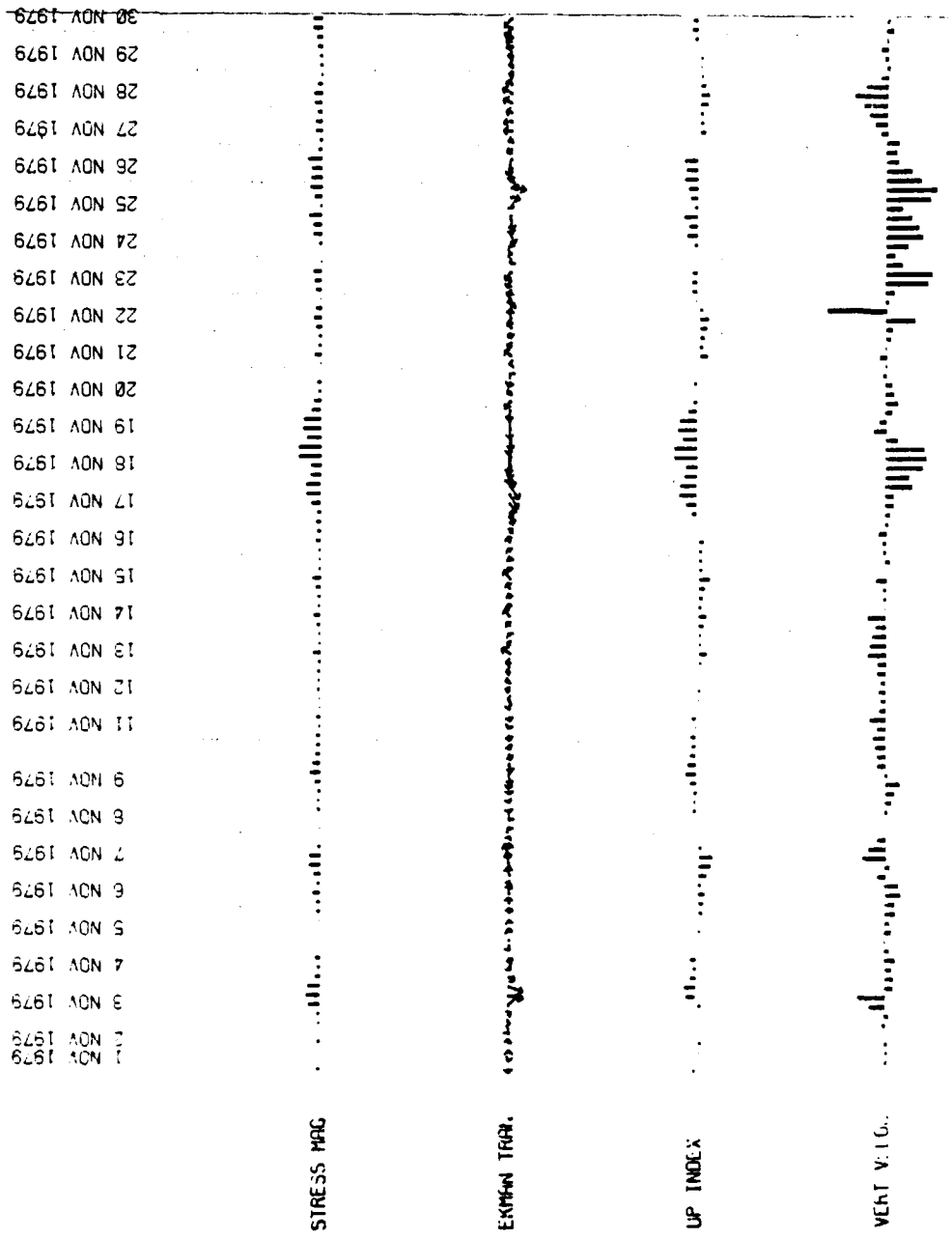

Fig. 54. Stress magnitude, Ekman transport, Upwelling Indices and Vertical Velocity for NOV and DEC 79.

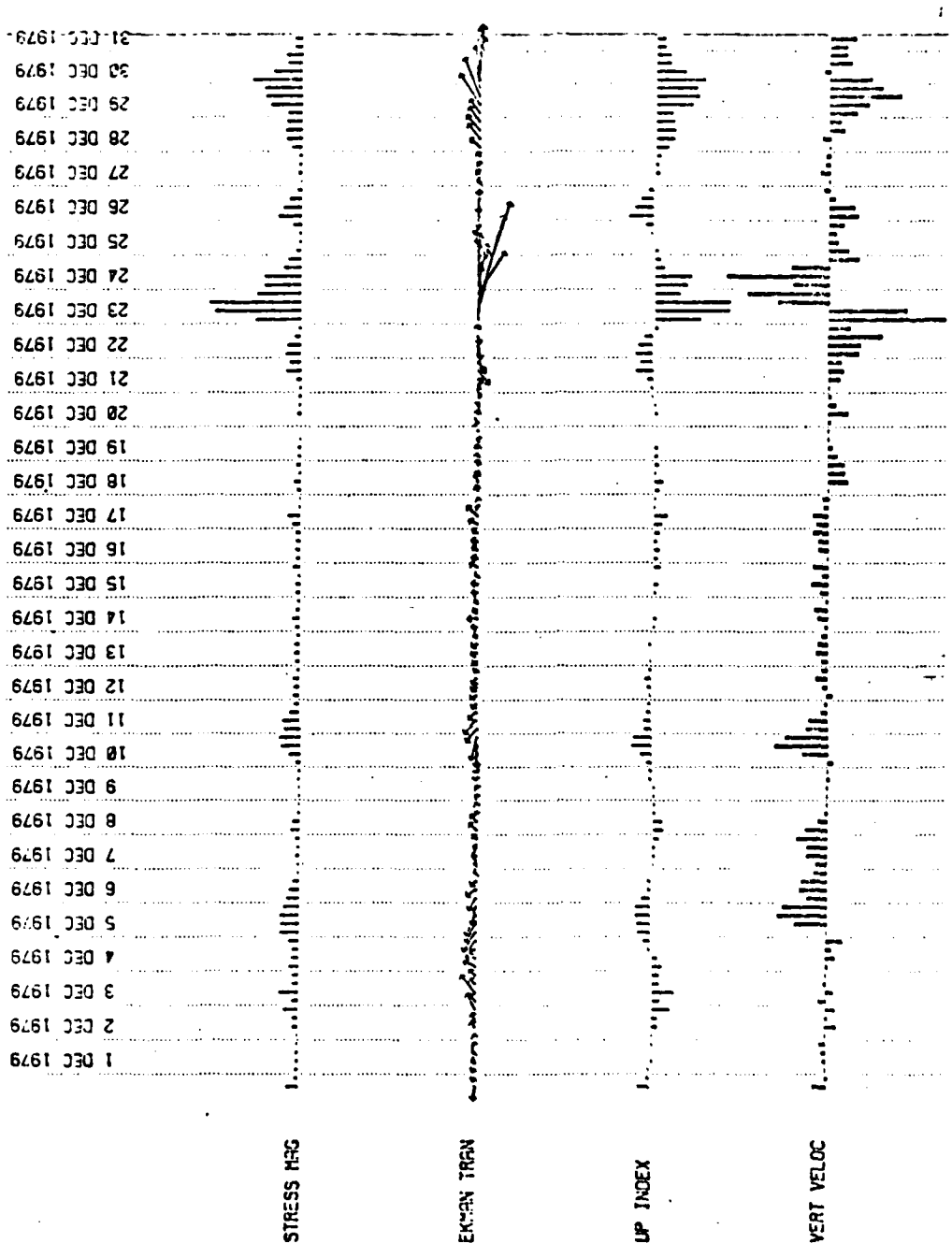

Fig. 54. (Continued)

c. Thermal Structure

The vertical cross sections (Fig. 55-59) are more difficult to analyze than those in the previous cases due to the limited number of XBT drops and the numerous course changes required in the execution of the square and ladder search. A general observation is that there is no strong thermocline as observed previously, nor any severe deepening of isotherm at isolated spots.

Leg 1 passed through the shallow, colder coastal water off Point Sur from 0015 to 0115 on a SSE course. A course change was made at 0255 towards shore in order to sample colder coastal water. Another course change to the NW parallel to the shore was made at 0455. There was a thermocline from 25 to 60 m with considerable stratification at the end of the transit, but no rise in deeper isotherms.

Leg 2 includes the square search pattern commencing at 0526 after detection of cold coastal water and continuing through the transit. Numerous penetrations of the cold water were made. The slope of the isotherms varied from 2.1 m/km to 7 m/km. The thermocline weakened and, from 0715 to 0755, the isotherms (9.5 to 12°C) below the colder surface water deepened towards the coast. The deep isotherms did not rise.

The square search pattern continued until 1035 on Leg 3. At this time, the course was changed to the NW, then W in order to intercept a surface front detected on a

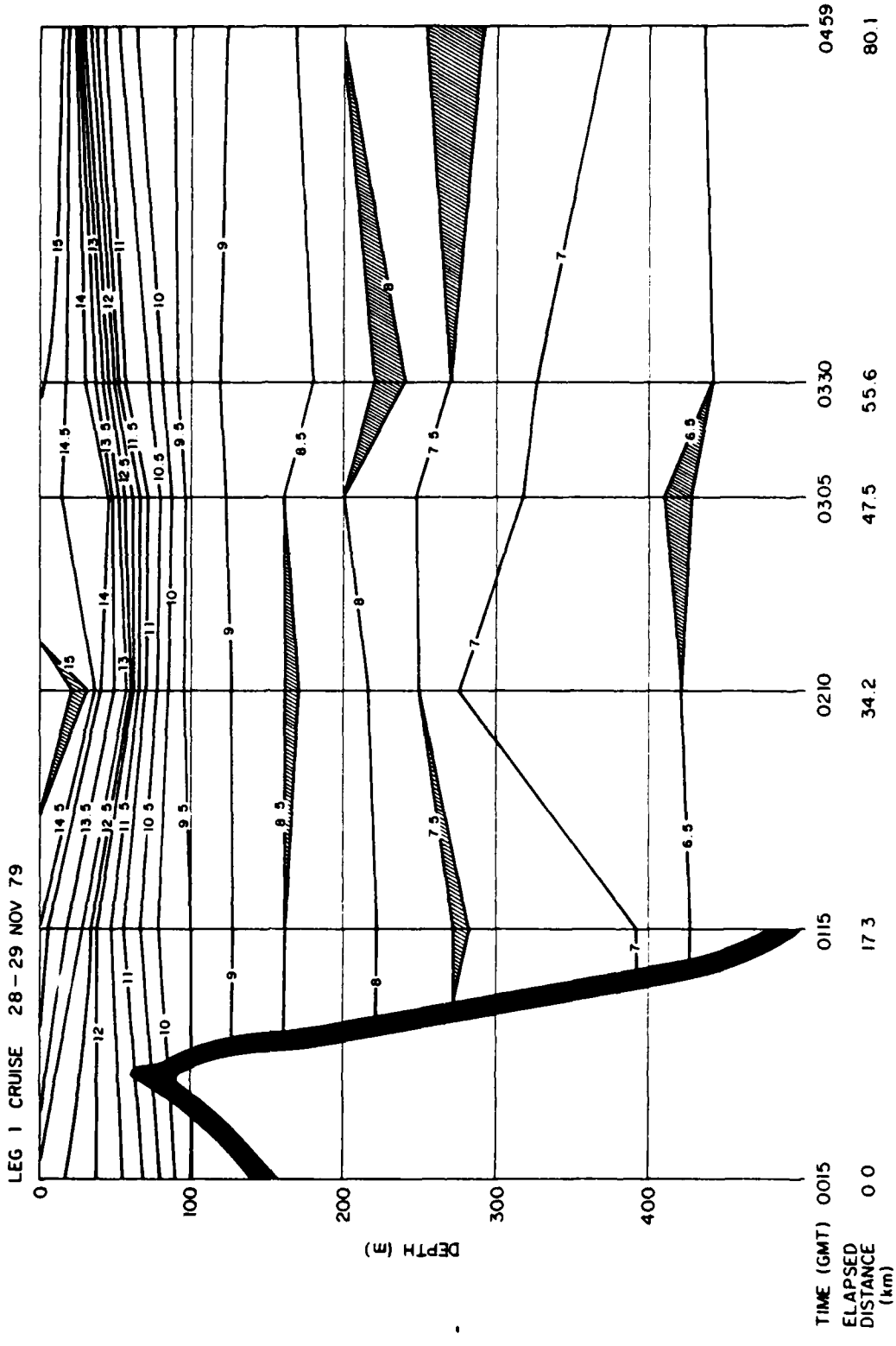

Fig. 55. Leg 1 0015 to 0459 29 NOV 79.

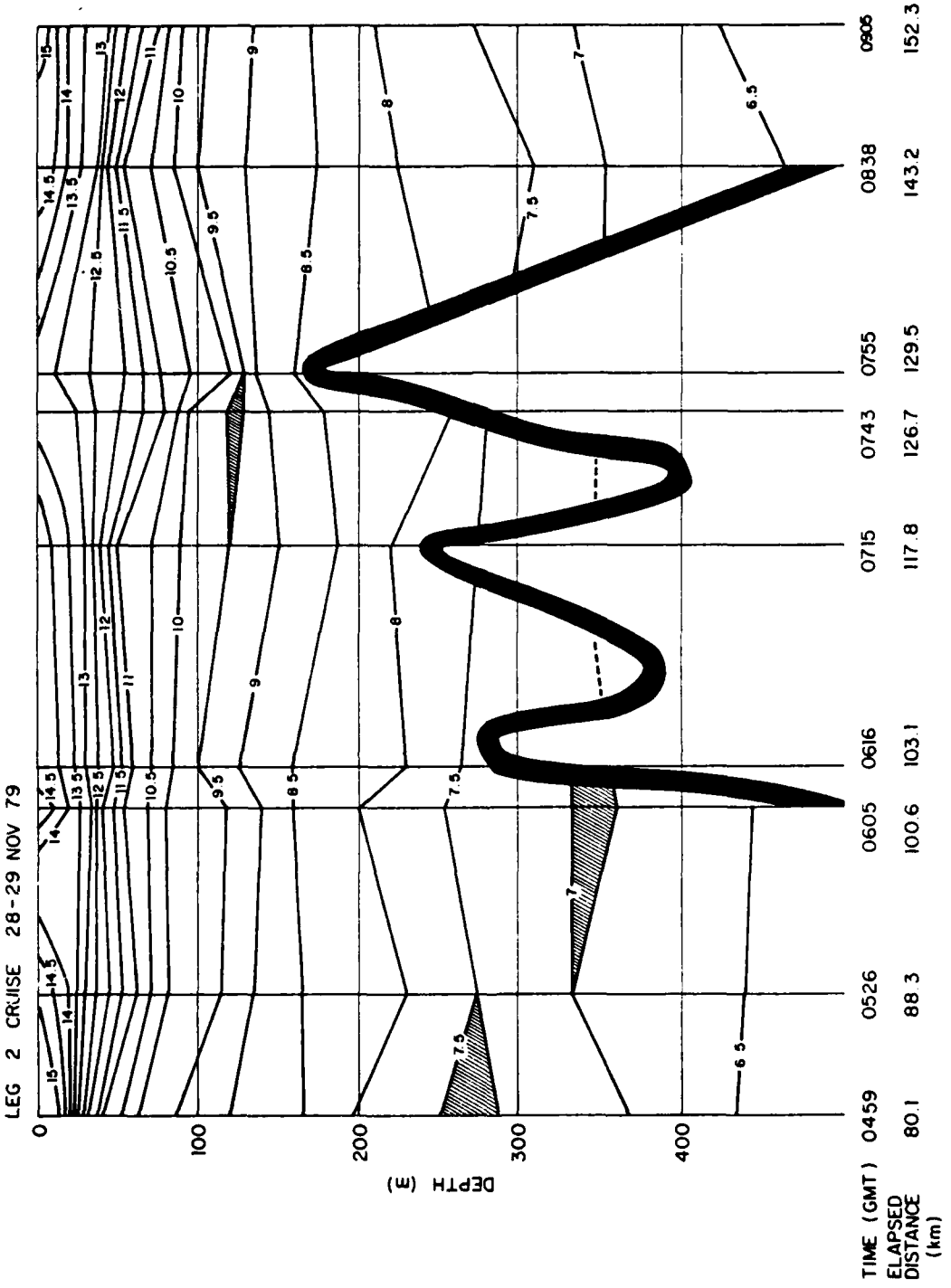

Fig. 56. Leg 2 0459 to 0905 29 NOV 79.

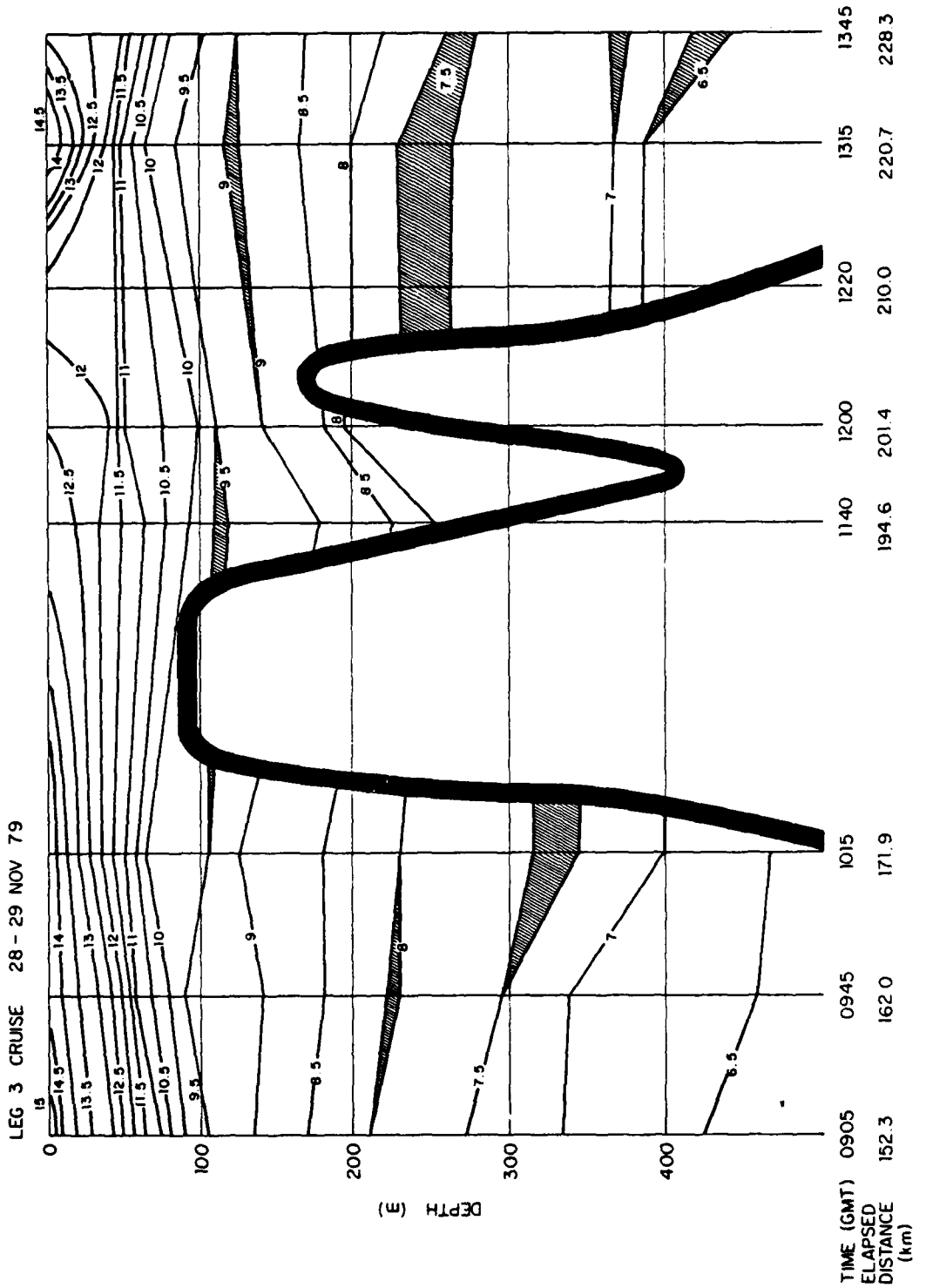

Fig. 57. Leg 3 0905 to 1345 29 NOV 79.

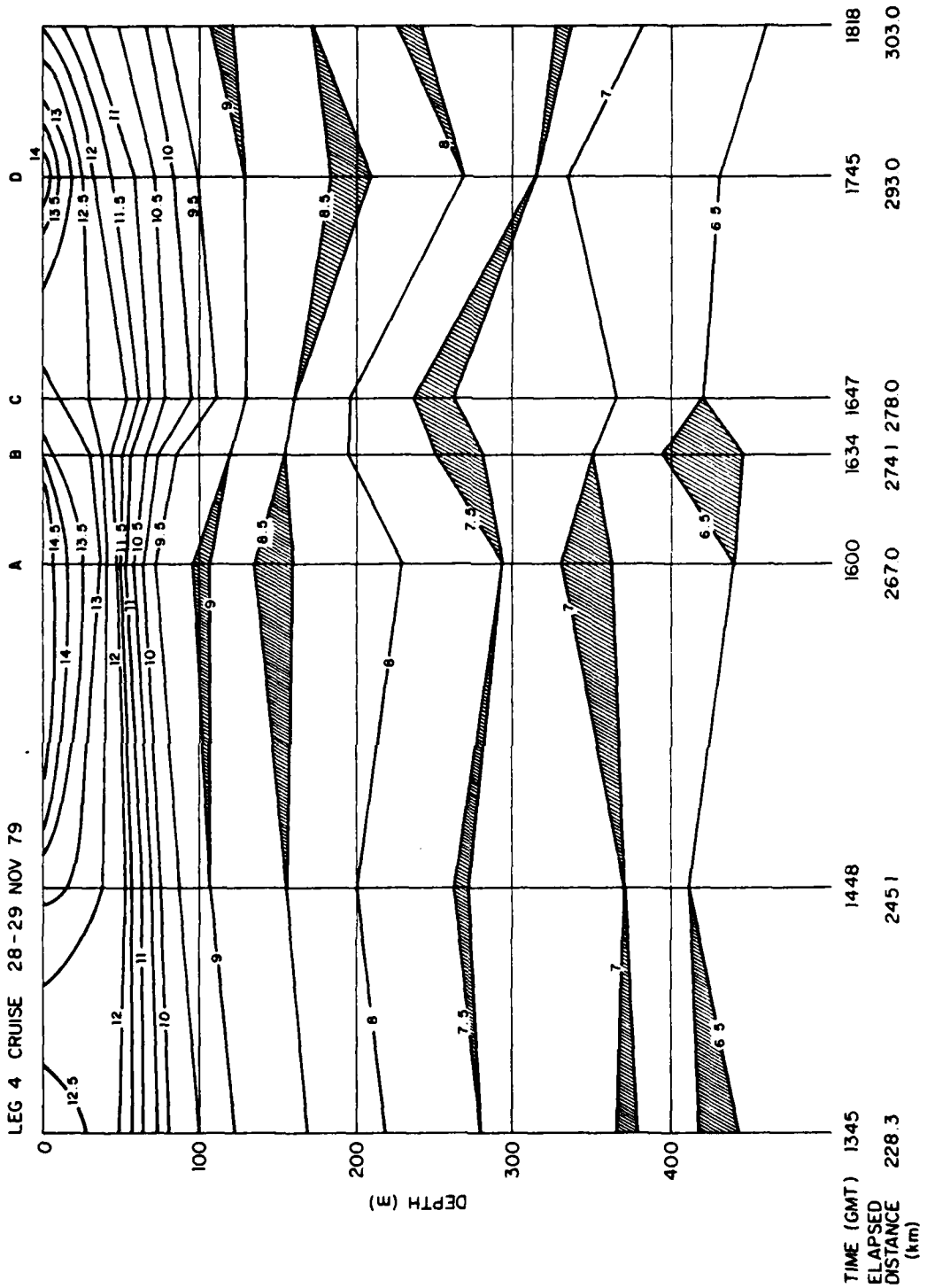

Fig. 58. Leg 4 1345 to 1818 29 NOV 79.

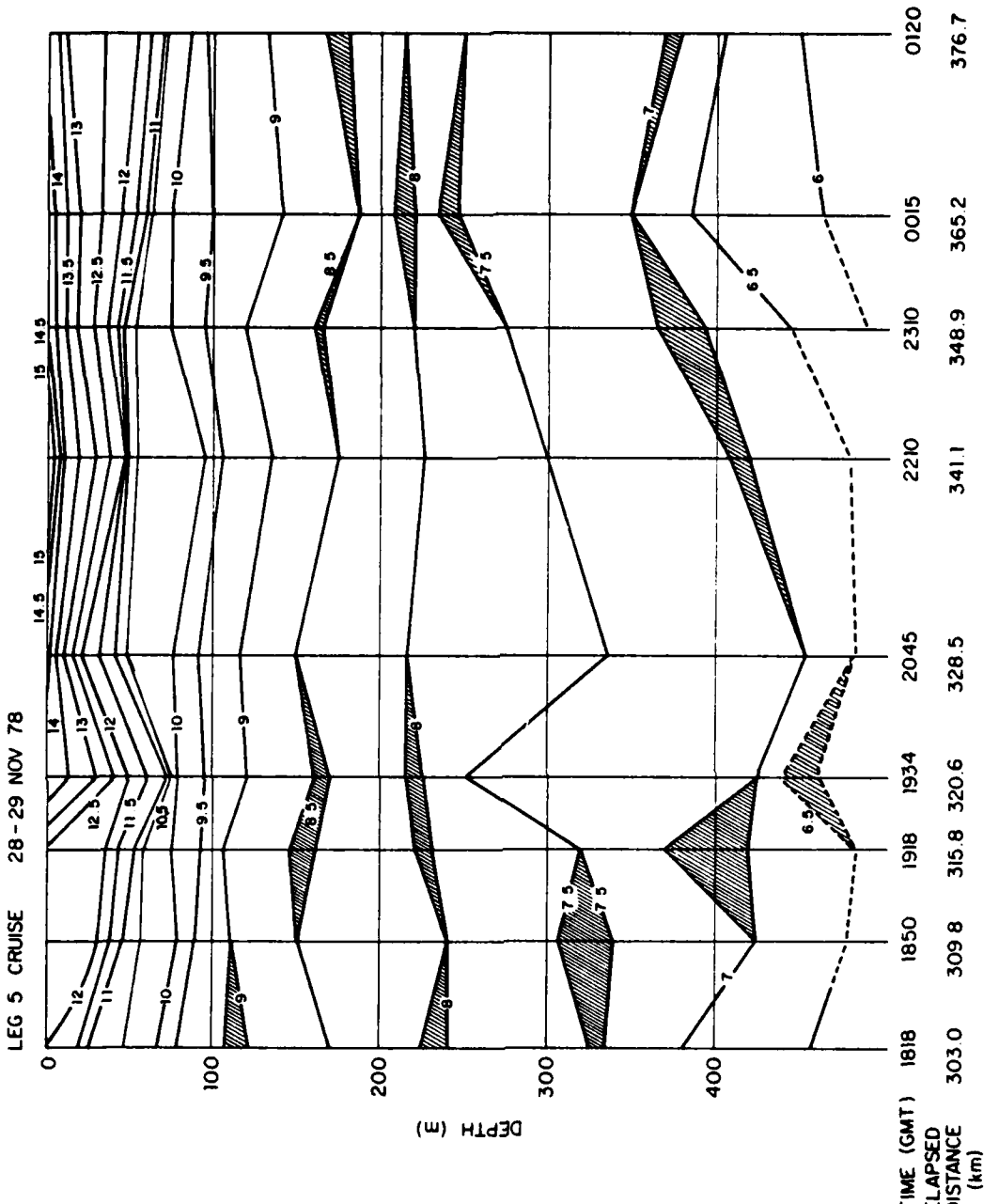

Fig. 59. Let 5 1818 29 NOV to 0120 30 NOV 79.

cruise the day before. The isotherms above 100 m rose throughout the transit, particularly when passing through the surface "cold spot" from 1200 to 1315 on a southerly course. Slopes on the north side were 9 m/km and on the south side 5.5 m/km. Surface dimensions were 7 km, subsurface (40 m) 20 km. Deepening to the north of the 10.5 and 10°C isotherms below the feature was consistent with previous cases. There was no rise in deep isotherms. A course change was made to the north at 1315 to commence a ladder search progressing westward in order to map the surface feature.

Leg 4 continued the ladder search, intercepting the cold feature from 1345 to 1448 and from 1600 to 1745. On the last intercept, the isotherms (9° to 12°C) distinctly deepened (30 m) below the feature observed earlier. Another square search pattern commenced at 1745 resulting in a complex appearing structure. At about 50 m, the thermocline intensified away from the "cold spots" (Fig. 60).

Leg 5 includes numerous course changes made while conducting STD casts. As in previous legs, the thermocline was stronger away from the "cold spots", and there was no rise in deeper isotherms.

The SST (Fig. 61) showed the developing cold surface feature detected in satellite imagery. The feature was plume-like in shape with an axis aligned SW along the cape off Point Sur, 20 km to the north of the Sur Canyon. The

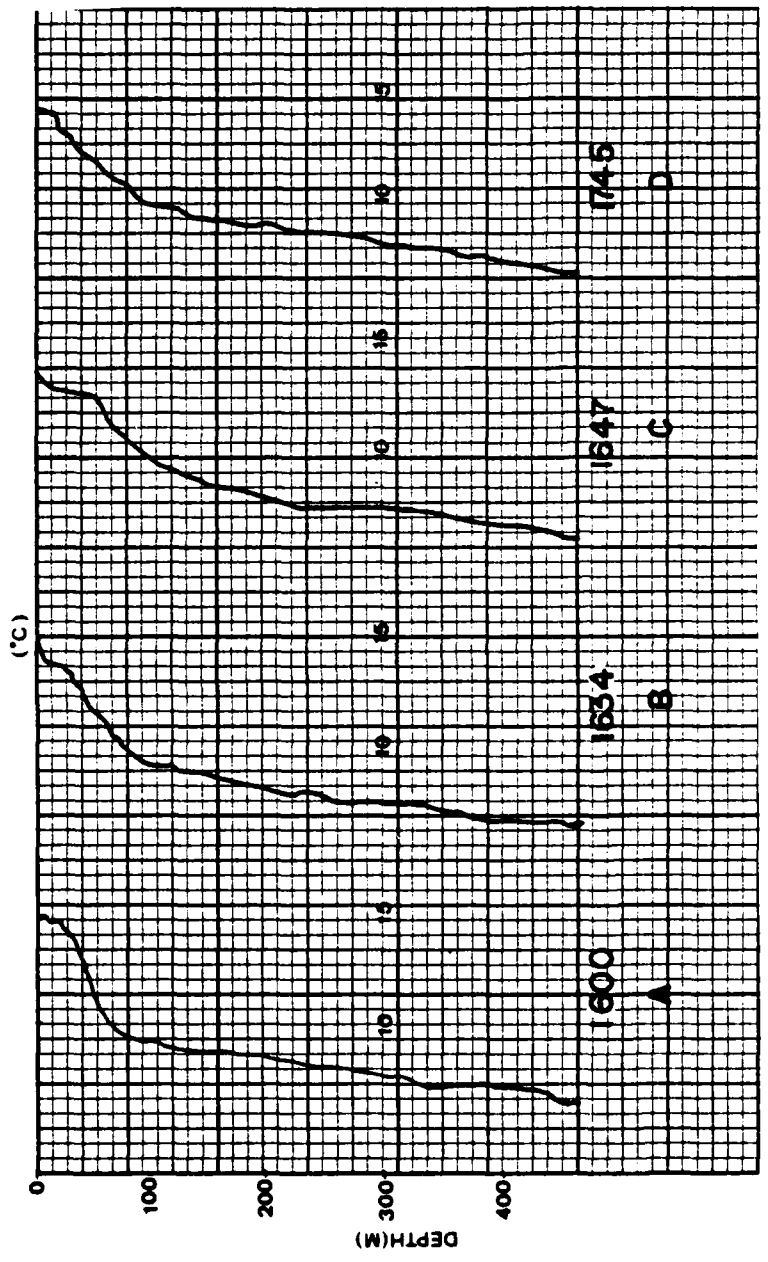

Fig. 60. Selected XBT traces from leg 4

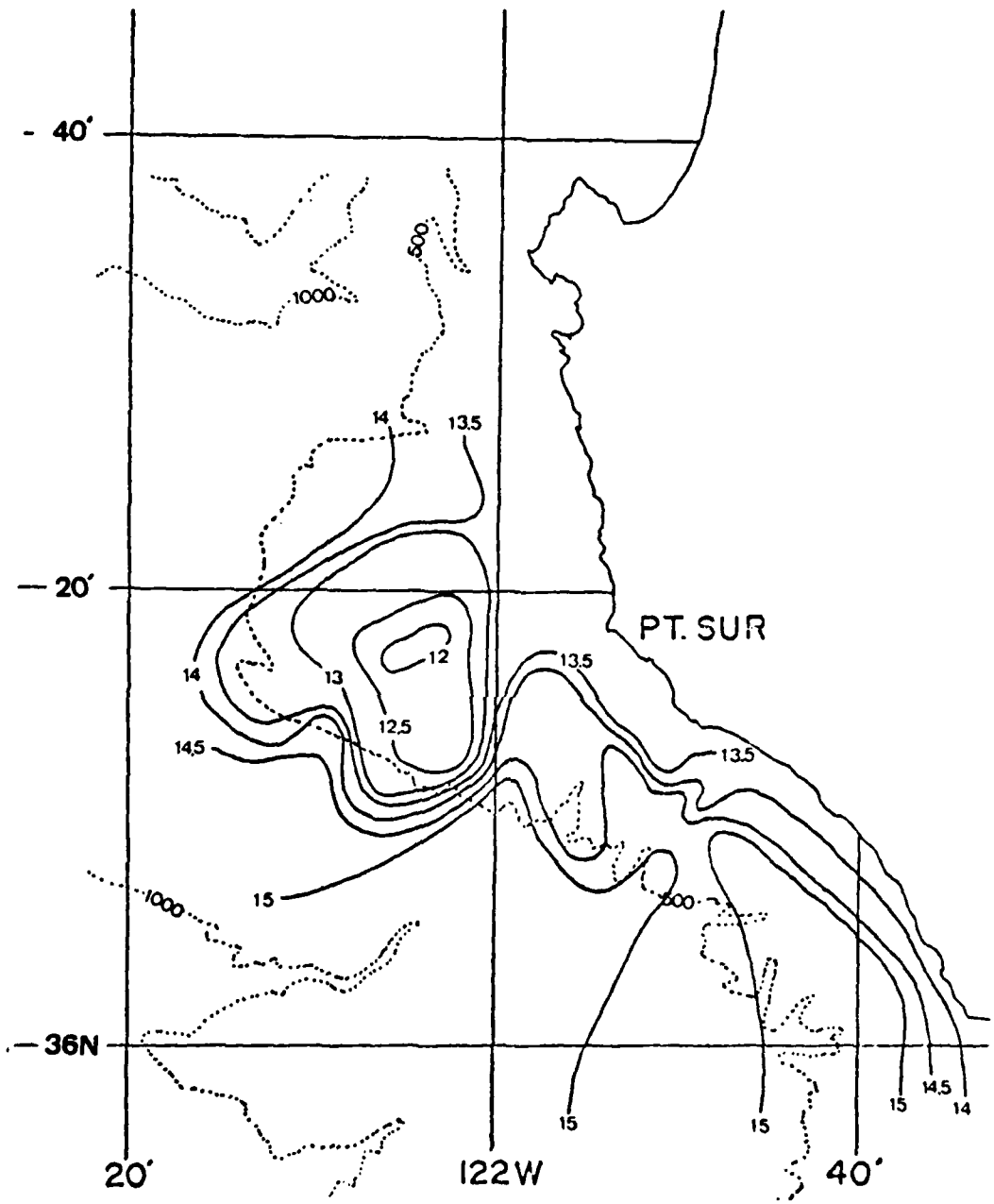

Fig. 61. SST (°C), 28 to 29 NOV 79.

surface "cold spot" enclosed within the 12°C isotherm was elliptical and 18 km^2 in area. Gradients of 2.5°C/3 km existed to the SE and 1°C/km to the SW. Gradients associated with the coastal water were 1°C/2 km.

The patterns of MLD (Fig. 62) resemble those of the SST, with the shallowest depths at the cold feature and shoreward and the maximum depths, 15 and 20 m, due north and south. Isopleths of MLD tended to parallel the surface isotherms.

The 25 m temperature field (Fig. 63) had the same basic pattern as the SST but with weaker gradients. The gradient to the south was approximately 0.25°C/km. The "cold spot" was offset to the south by about 2.5 km.

The feature was still distinguishable at 50 m (Fig. 64) as a cold tongue oriented WSW of Point Sur, with the coldest water enclosed within the 10.5° isotherm below the feature at 25 m. Also evident were several warm spots, one 5 km south of the cold tongue, the other nearshore at the end of a warm intrusion. Maximum gradients (0.8°C/km) were associated with these features; those associated with the cold tongue were 0.7°C/km.

The temperature fields at 100 to 400 m did not have patterns related to topography. The 100 and 200 m temperature fields (Figs. 65 and 66) had a cold tongue extending from Point Sur oriented in the same manner as the temperature field at shallow depths. The maximum gradients

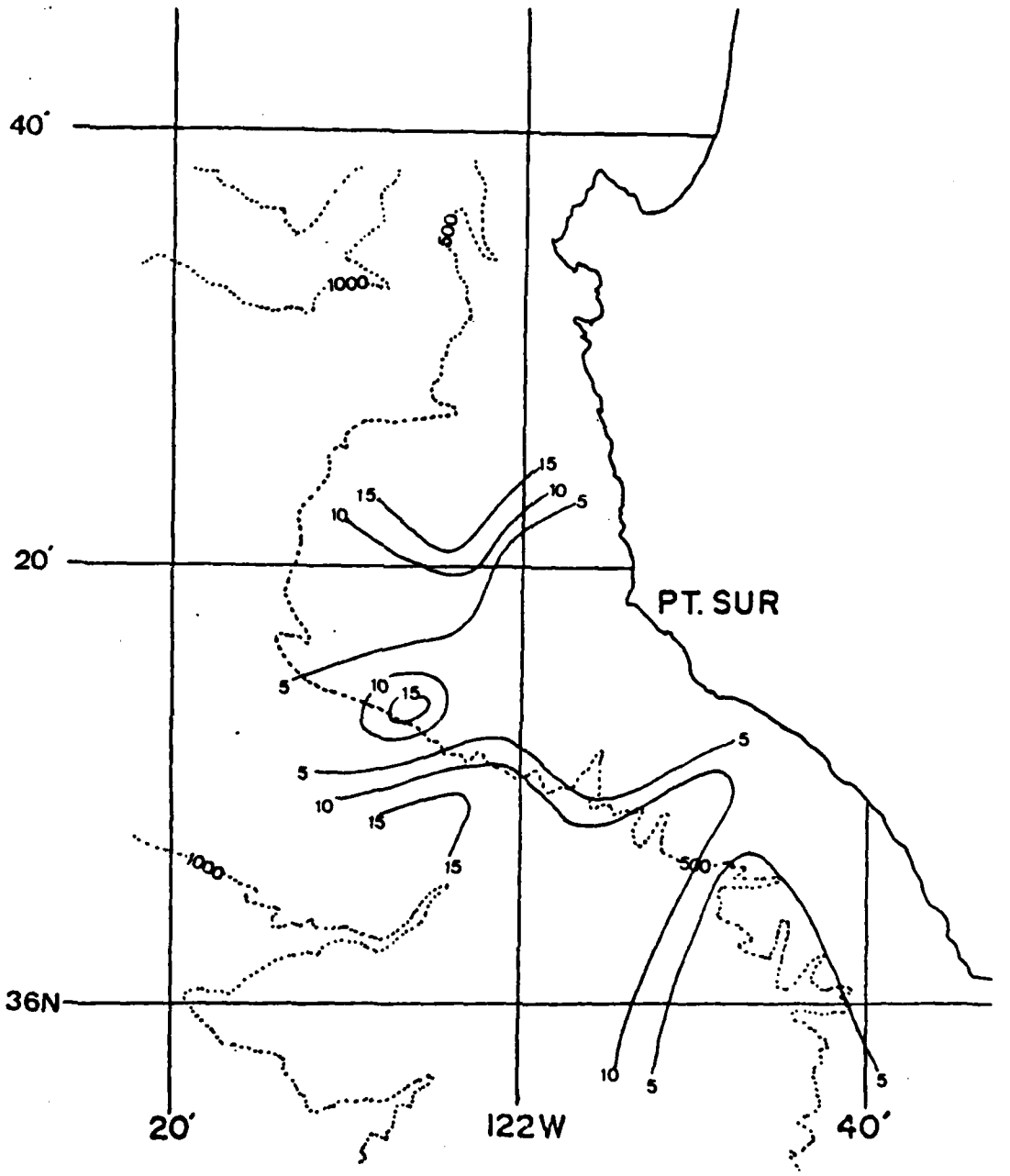

Fig. 62. MLD (m), 28 to 29 NOV 79.

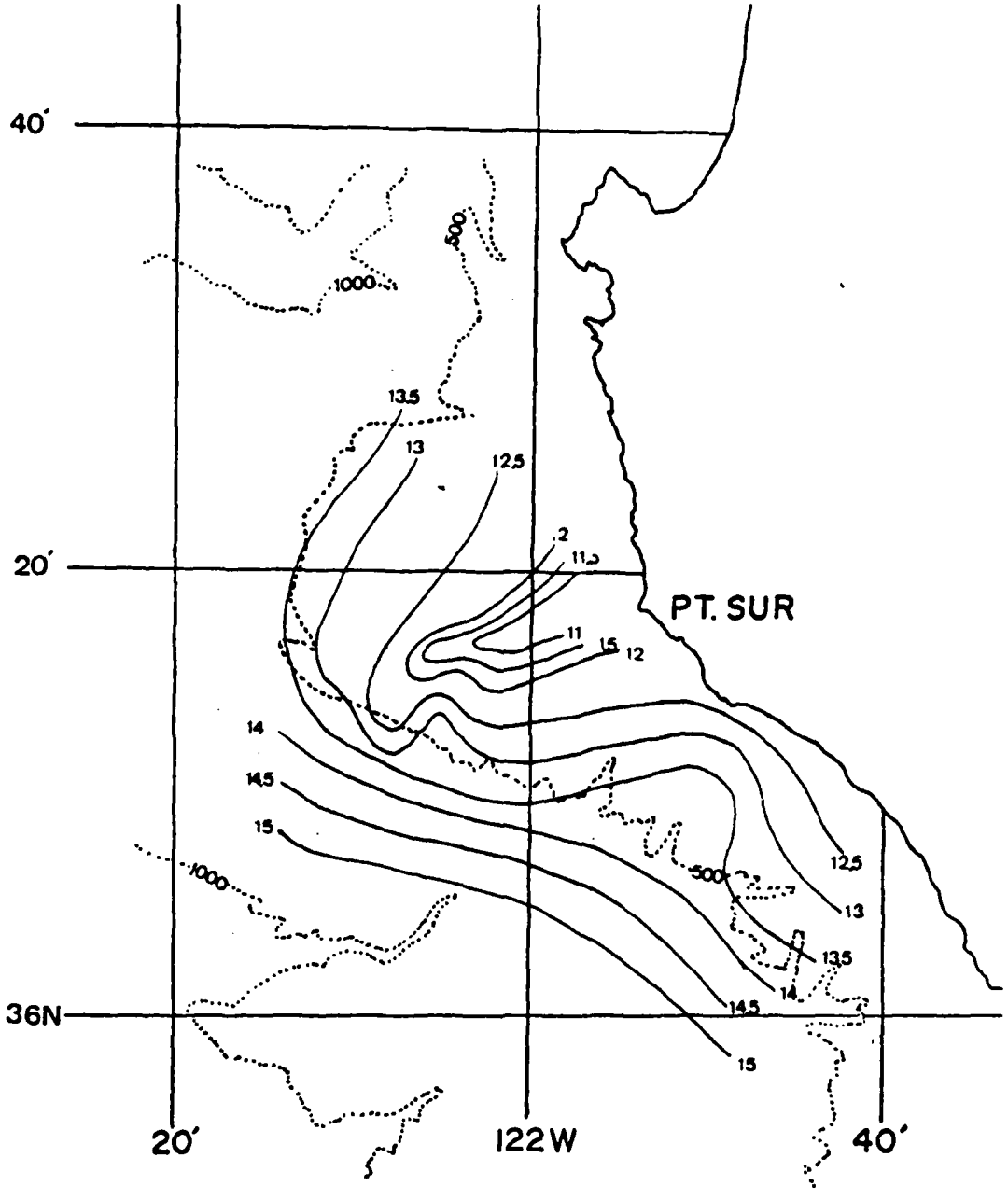

Fig. 63. 25 m temperature field (°C), 28 to 29 NOV 79.

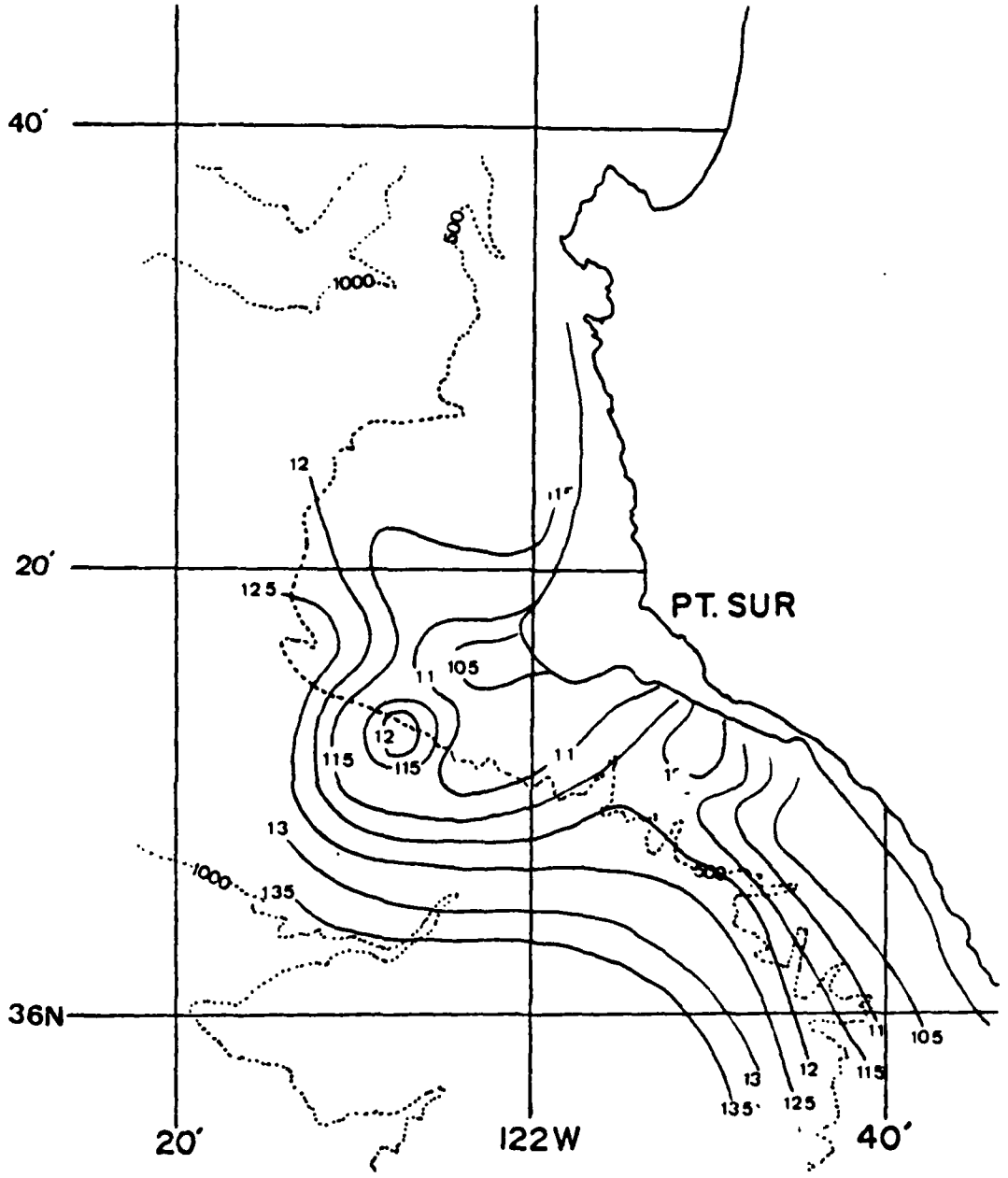

Fig. 64. 50 m temperature field (°C), 28 to 29 NOV 79.

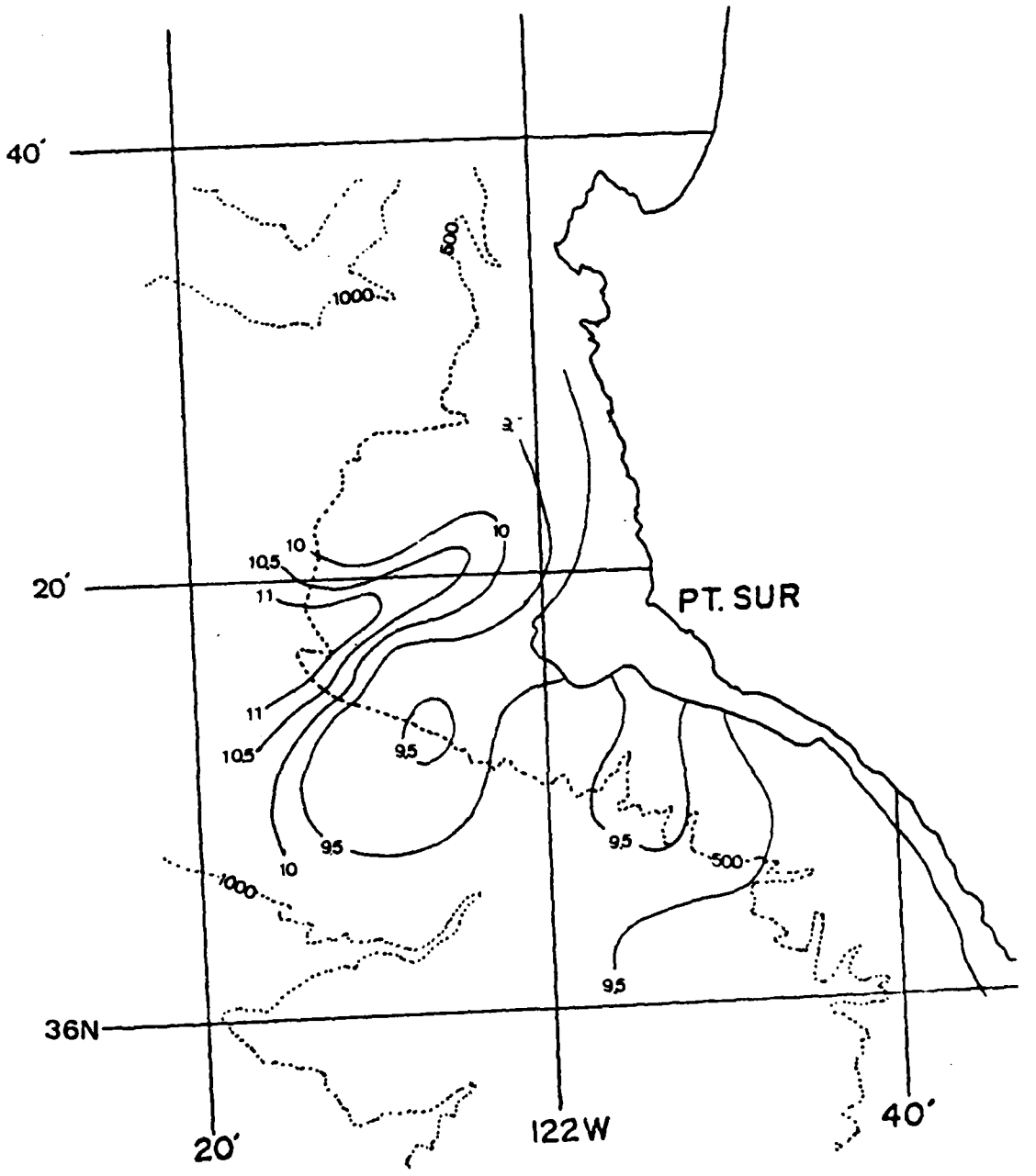

Fig. 65. 100 m temperature field (°C), 28 to 29 NOV 79.

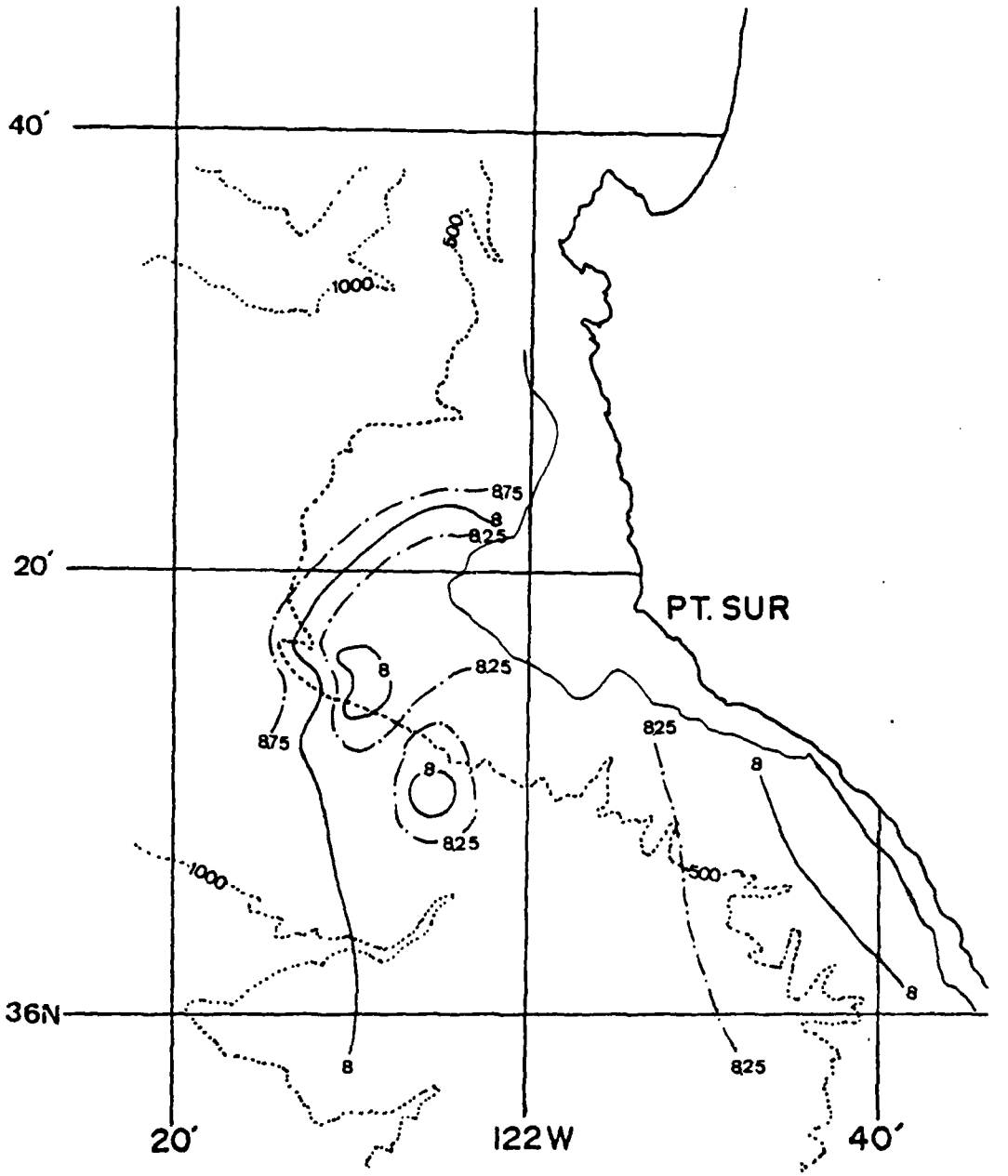

Fig. 66. 200 m temperature field (°C), 28 to 29 NOV 79.

at 100 and 200 m were 0.6°C/km and 0.8°C/km, respectively, and, they were associated with the front between the cold tongue and a warm intrusion to the north.

Both the 300 m and 400 m temperature fields (Figs. 67 and 68) had warm features below the cold shallow features. There was little other structure. The maximum gradients at 300 and 400 m were 0.1°C/km in the southeast and southwest corners, respectively.

The thickness field between the 12 and 8°C isotherms (Fig. 69) had thickness maxima in many areas, particularly in pockets adjacent to the continental shelf. There were also thicker areas to the north and southwest along the axis of the feature.

The depth of the 12°C isothermal surface (Fig. 70) closely resembles the SST pattern with shallow values at the "cold spot". The greatest depths are south and west, with a depth pocket near the coast.

The final information extracted is a time series of profiles from a set of XBT's dropped within a kilometer of each other. As in the previous cases, temporal changes in the depths of isotherms greatly exceeded the spatial slopes previously discussed. Based on the r.m.s. depth change of 17.3 m from 1000 to 2210, vertical velocities were of the order of 4×10^{-2} cm/s.

Adequate bucket temperatures were taken to evaluate them versus 2m thermistor temperatures. A 5-point running

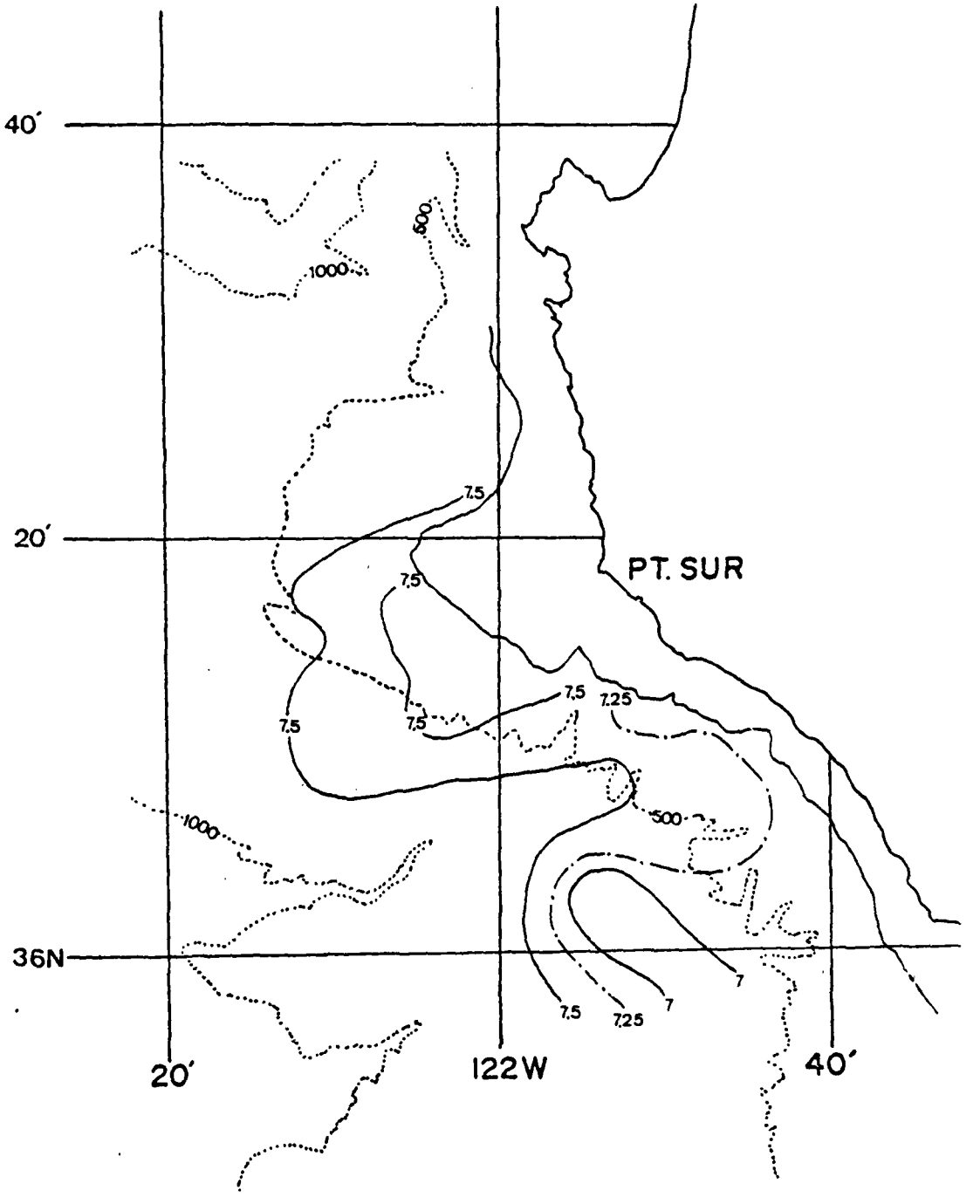

Fig. 67. 300 m temperature field (°C), 28 to 29 NOV 79.

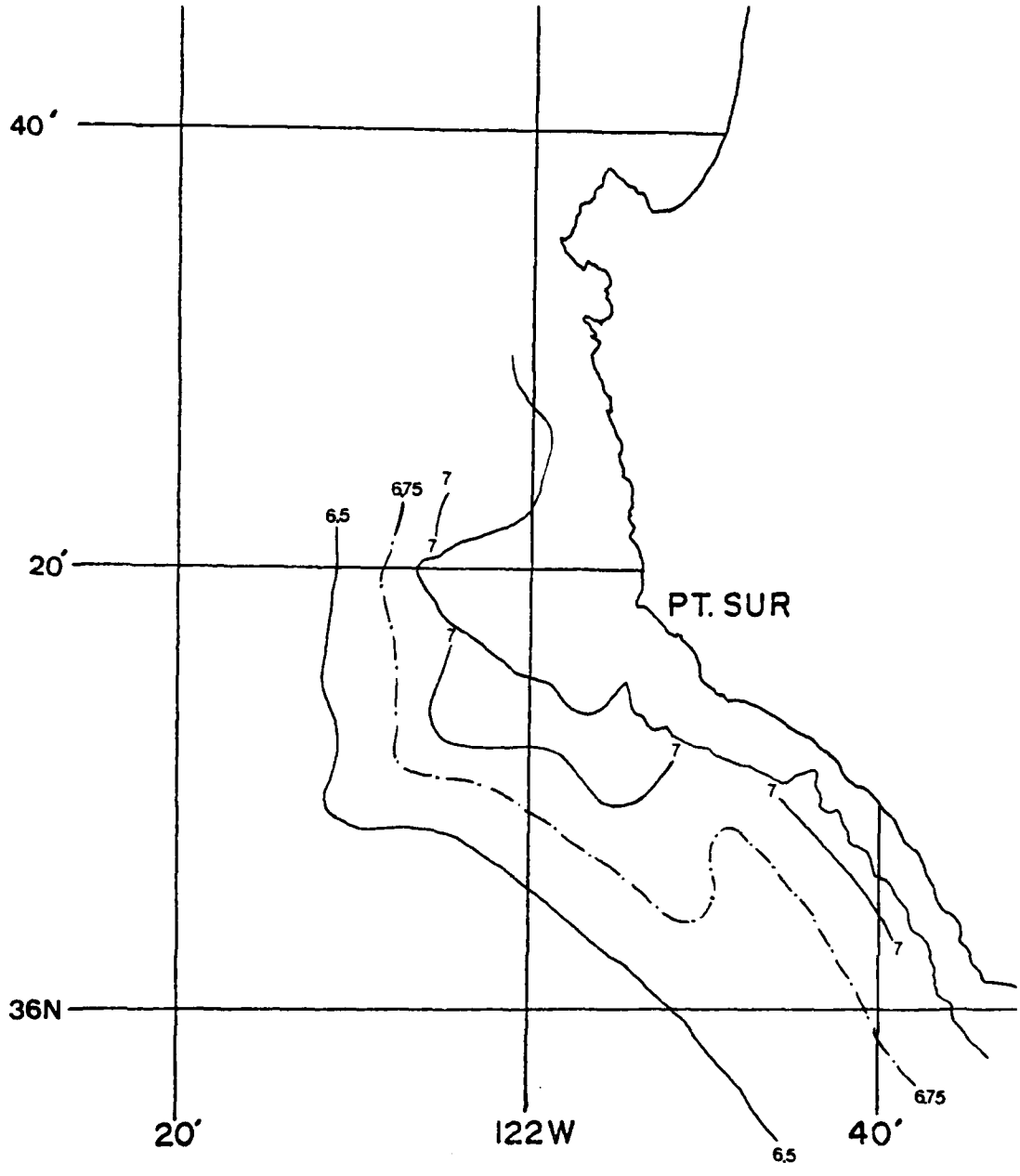

Fig. 68. 400 m temperature field (°C), 28 to 29 NOV 79.

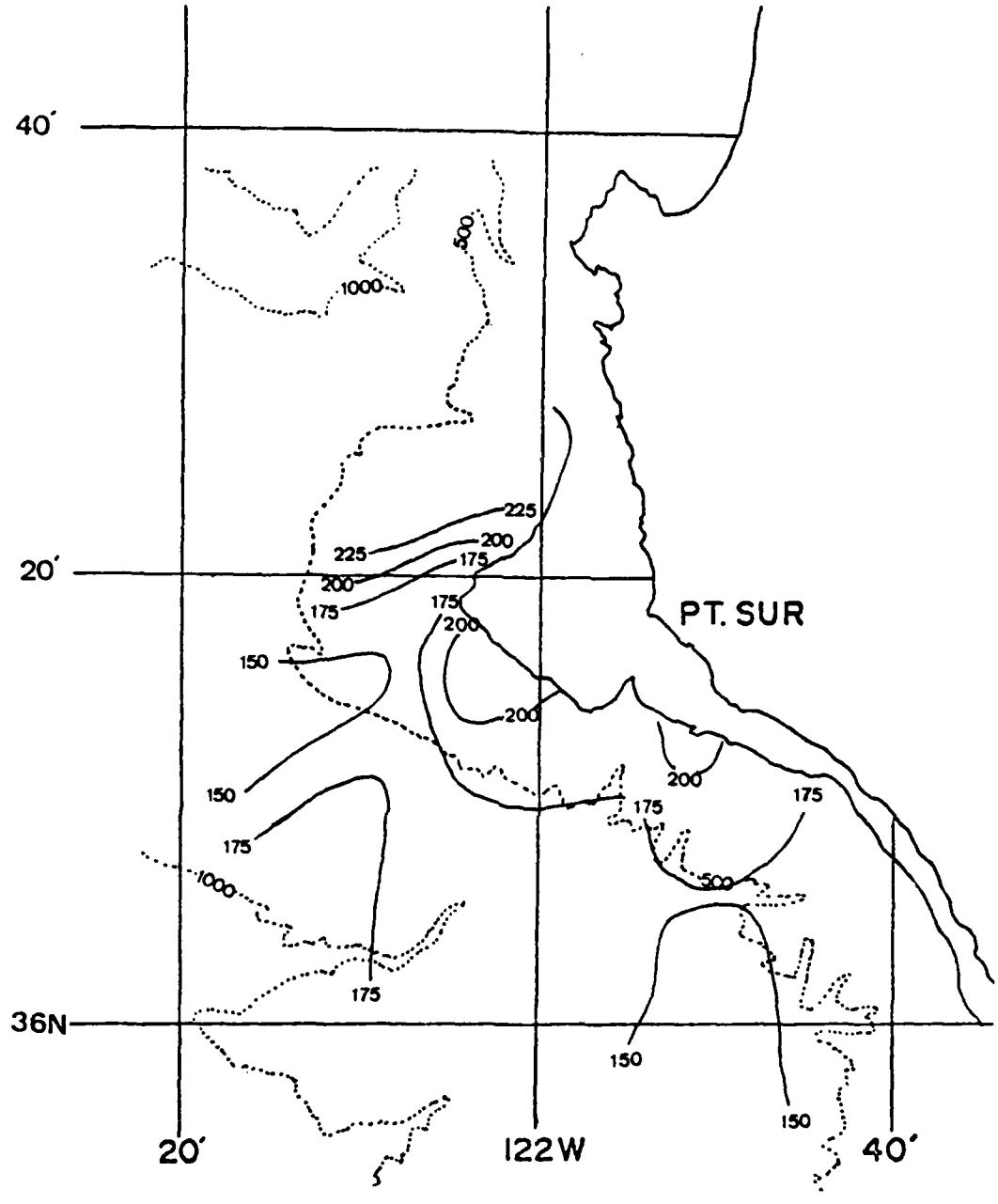

Fig. 69. Thickness (m) between 12 and 8°C isothermal surfaces, 28 to 29 NOV 79.

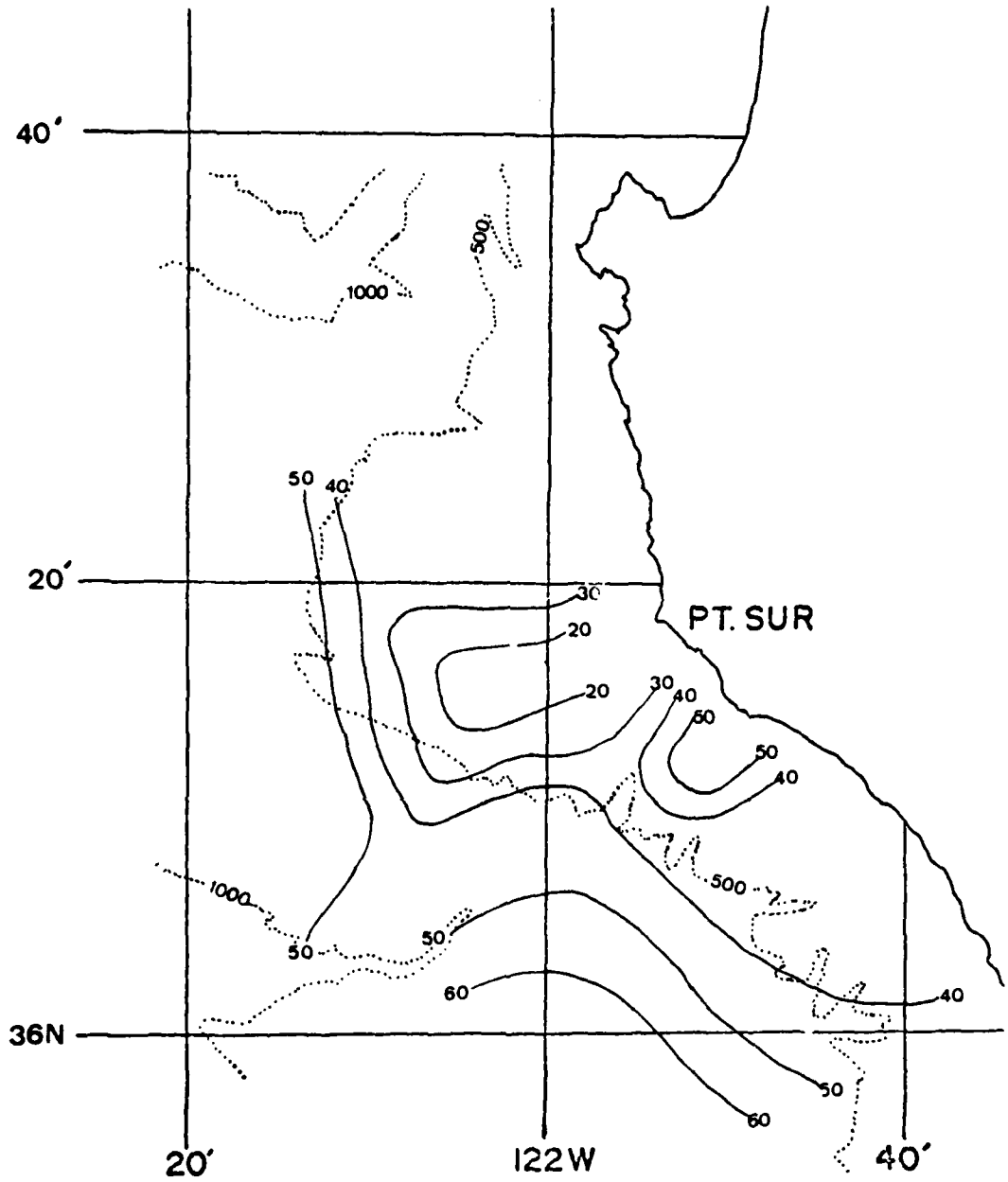

Fig. 70. Depth (m) of the 12°C isothermal surface, 28 to 29 NOV 79.

mean was used to smooth the raw data. Individual differences ranged from -.07° to +.95°C. Differences increased during the cruise, particularly during the day.

d. Surface Salinity and Sigma-t Fields

At each XBT cast, salinity samples were taken from the ship injection port (2 m). The high surface salinity (Fig. 71) (> 33.6$^{o}/_{oo}$) inshore generally paralleled the coast and protruded SW along the axis of the cold feature. There were low salinity areas offshore. There was a high salinity (> 33.5 $^{o}/_{oo}$) area to the south of the feature. In this area, surface isohalines are orthogonal to SST, offshore they are parallel. This is indicative of a density front nearshore caused by colder sea surface temperatures.

Surface values of σ_t were computed from the SST and surface salinity data (Fig. 72). High values were near shore, protruding SW along the axis of the plume. The pattern of isopycnals resembled the pattern of isotherms in the SST plot (Fig. 61). The high gradients of temperature and density are coincident.

From the T-S diagram for surface values (Fig. 73), the salinity band was narrow and centered near 33.45 $^{o}/_{oo}$. Water within the feature had the lowest temperatures. An extreme sample at 34.02 $^{o}/_{oo}$ and 15.2°C was acquired nearshore in the southeast corner of the area of interest.

e. STD and Geostrophic Data

STD cast data and geostrophic calculations between stations 2 and 4, 2 and 7, 4 and 6 and 7 and 6 are presented

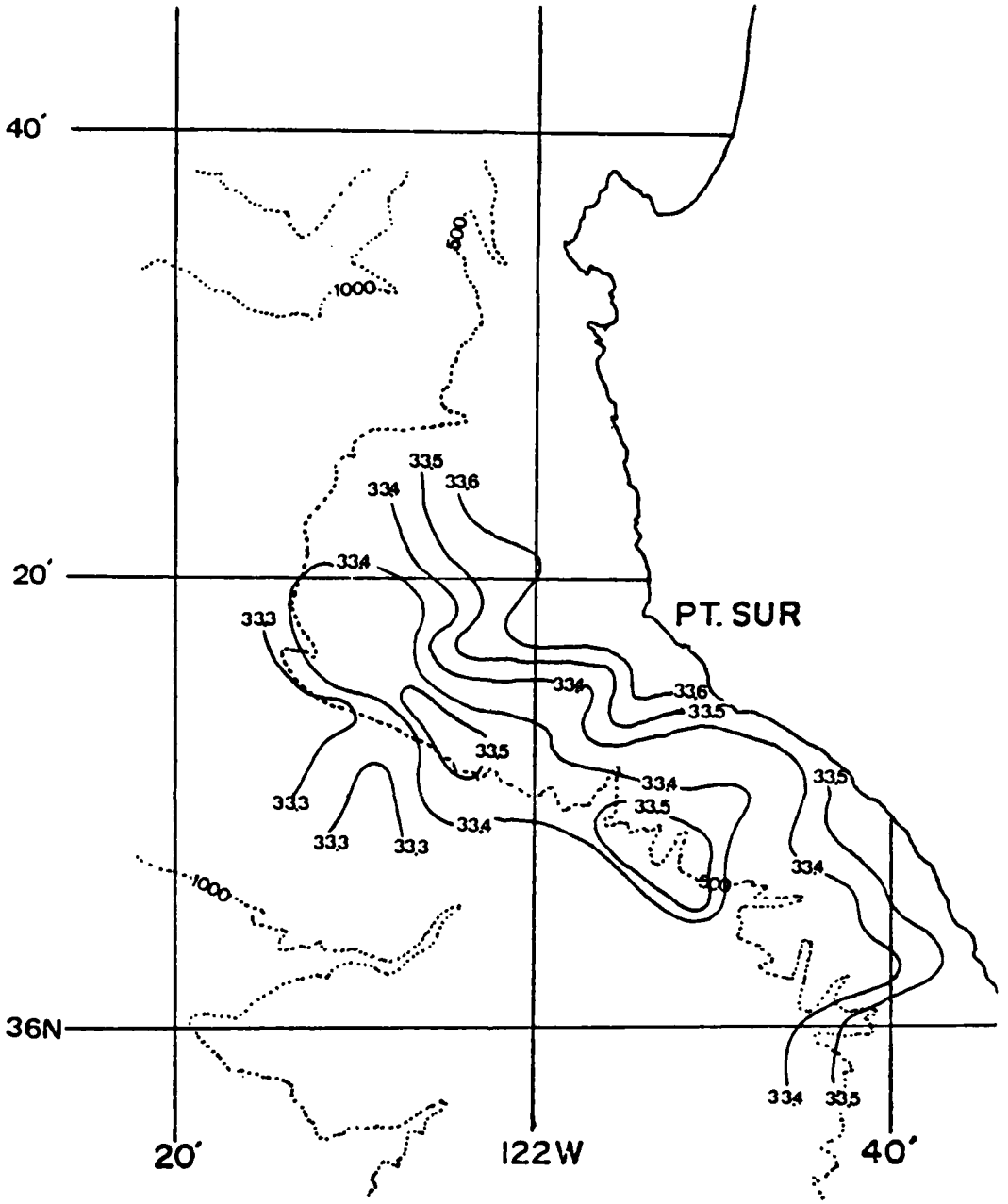

Fig. 71. Surface Salinity ($^{o}/_{oo}$), 28 to 29 NOV 79.

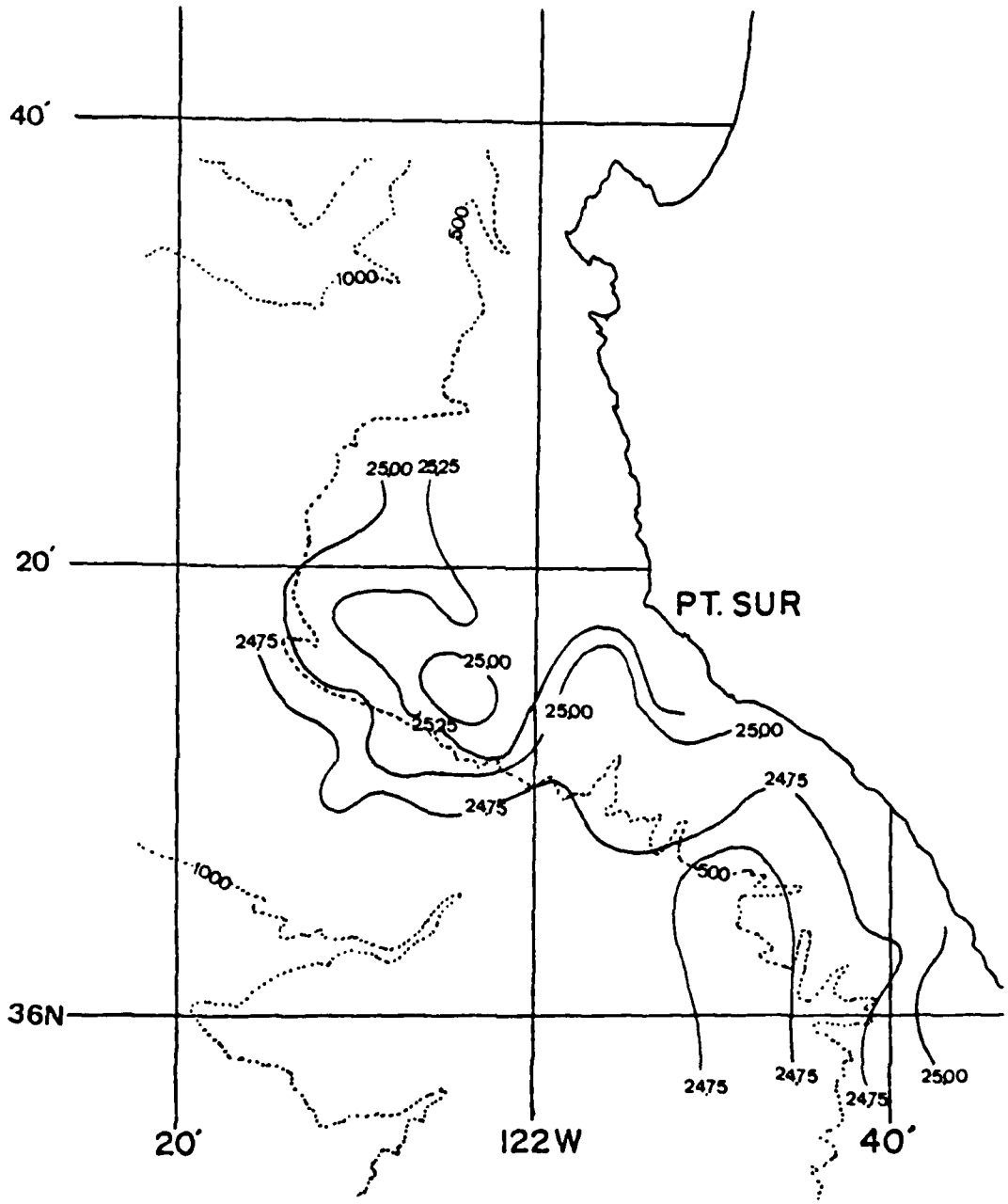

Fig. 72. Surface Sigma-t (σ_t), 28 to 29 NOV 79.

in Appendix D. Based on an isotach analysis at 75 m (Fig. 74), there was a distinct velocity maximum to the northwest and a velocity minima nearshore and at the maximum seaward extent of the cold plume-like feature.

The vertical profile (Fig. 75) of the alongshore components of the geostrophic velocity at the southern part of the area (normal to stations 2 and 4) and at the northern part of the area (normal to stations 6 and 7) showed northward flow (with respect to the reference level at 400 m). Velocity maxima were observed at the surface (12 cm sec^{-1}) and at 160 m (14 cm sec^{-1}) for the southern stations and at 60 m (41 cm sec^{-1}) for the northern stations. There was significant vertical shear near the reference level.

The vertical profiles of the cross shelf components (Fig. 76) of the geostrophic velocity at the nearshore part of the area (normal to stations 2 and 7) and at the offshore part of the area (normal to stations 4 and 6) show an offshore geostrophic component from the surface to 150 m, with a maximum of 9 cm sec^{-1} at 50 m. Weaker onshore flow was from 150 m to 300 m with a maximum of 2 cm sec^{-1} at 200 m at the nearshore stations. Onshore flow was from the surface to 400 m at the offshore stations with maxima of 18 cm sec^{-1} at the surface and 19 cm sec^{-1} at 70 m.

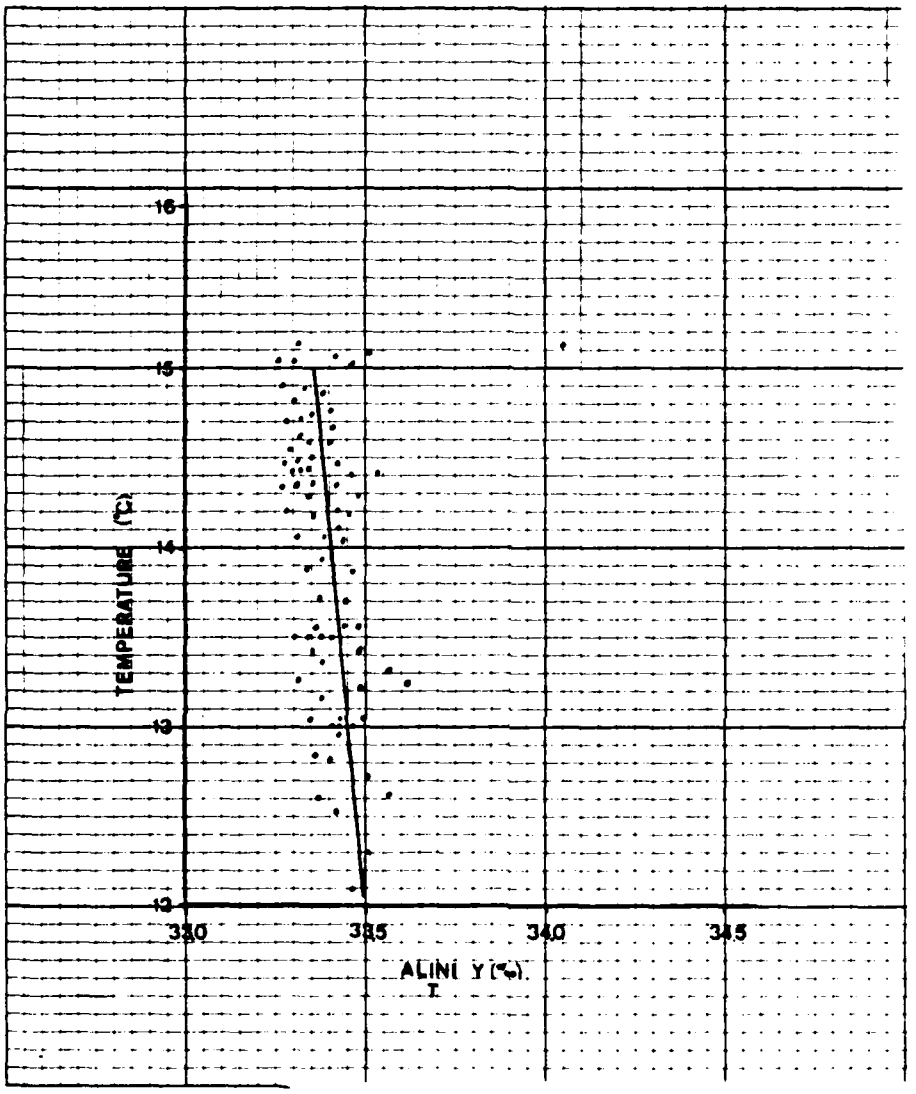

Fig. 73. Surface T-S diagram, 28 to 29 NOV 79.

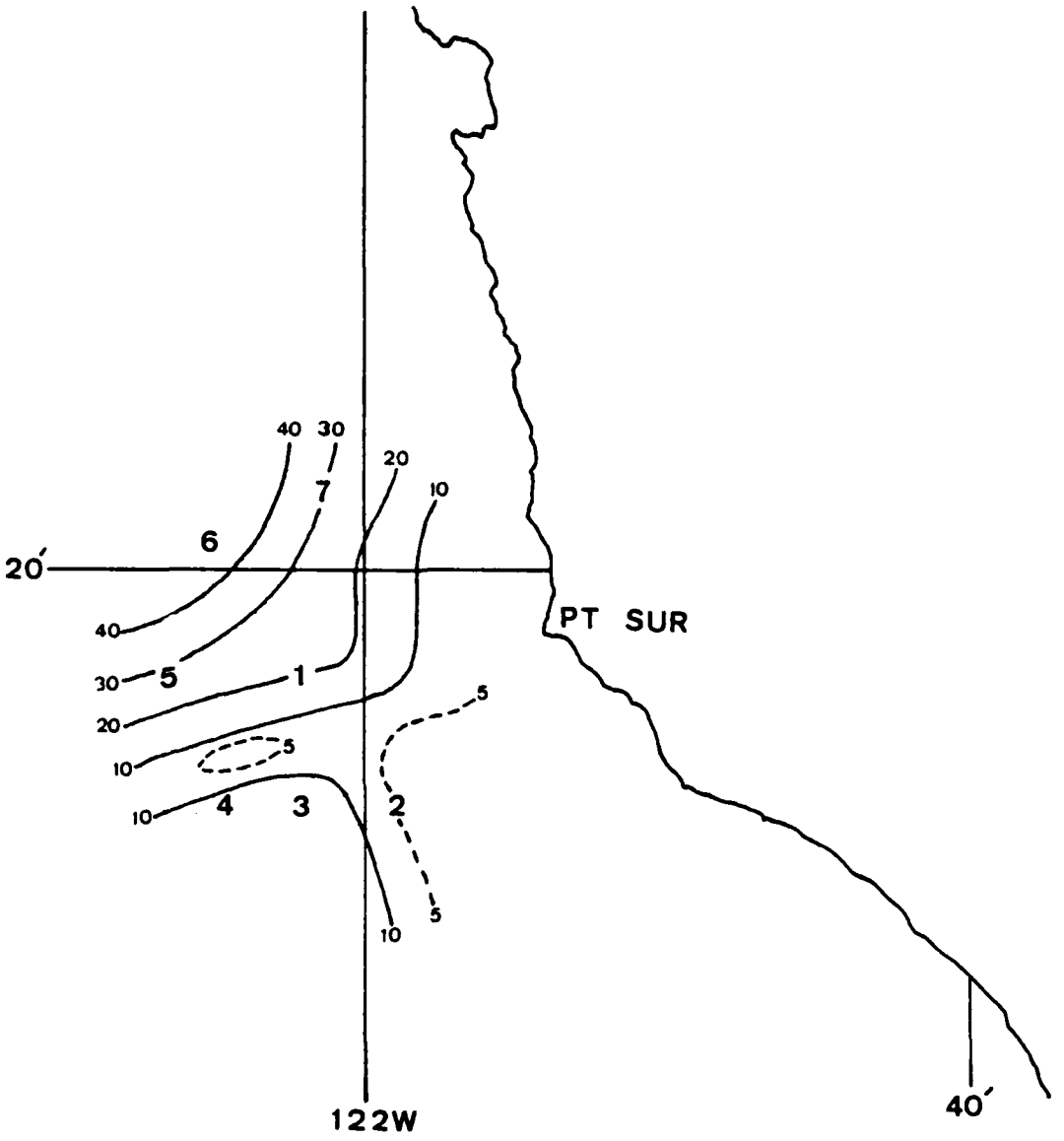

Fig. 74. Isotachs of geostrophic velocity (cm-sec^{-1}) at 75 m (in the thermocline). STD stations at labelled 1 through 7. The reference level is 400 m.

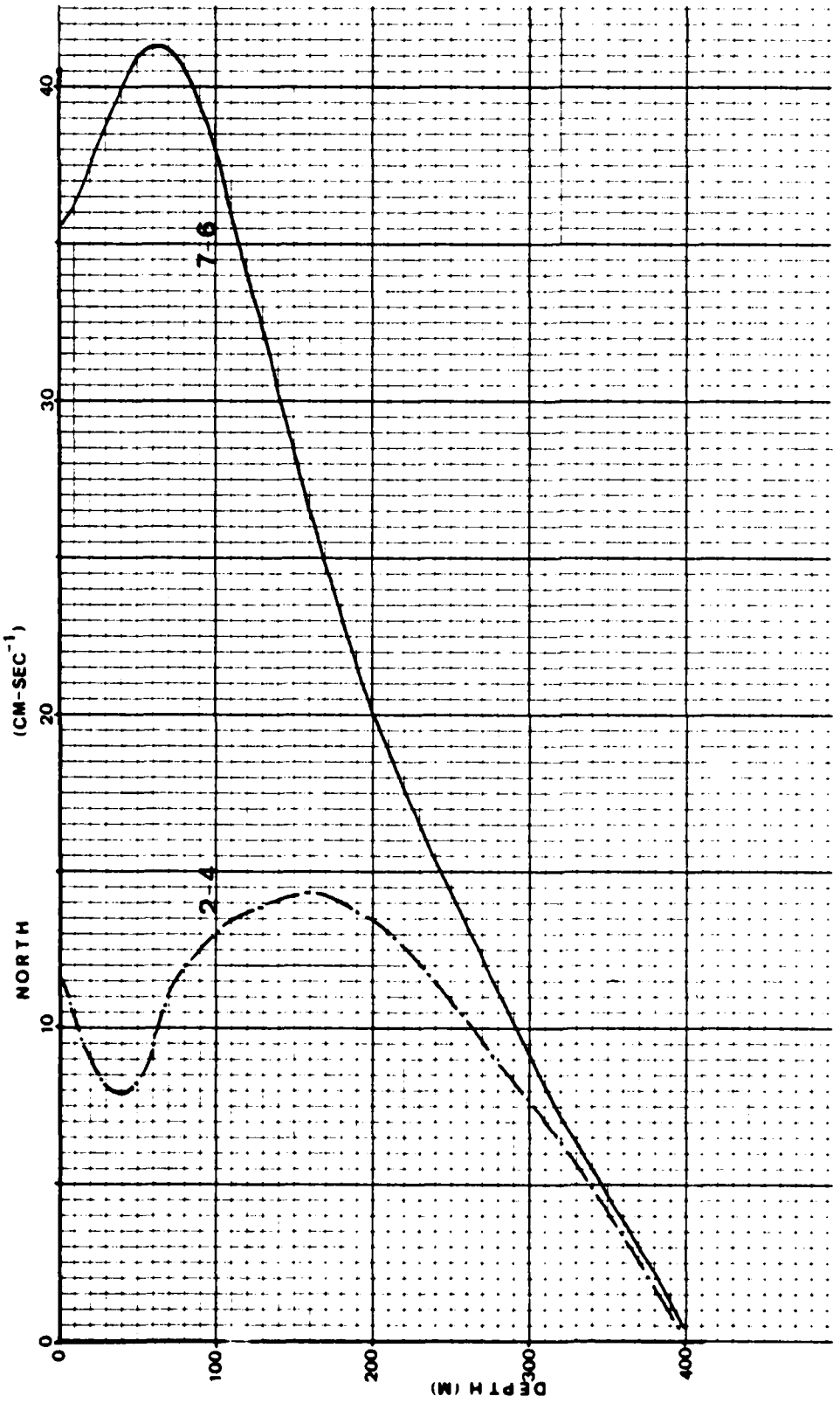

Fig. 75. Alongshore geostrophic velocities normal to stations 2 and 4 and normal to stations 6 and 7 versus depth.

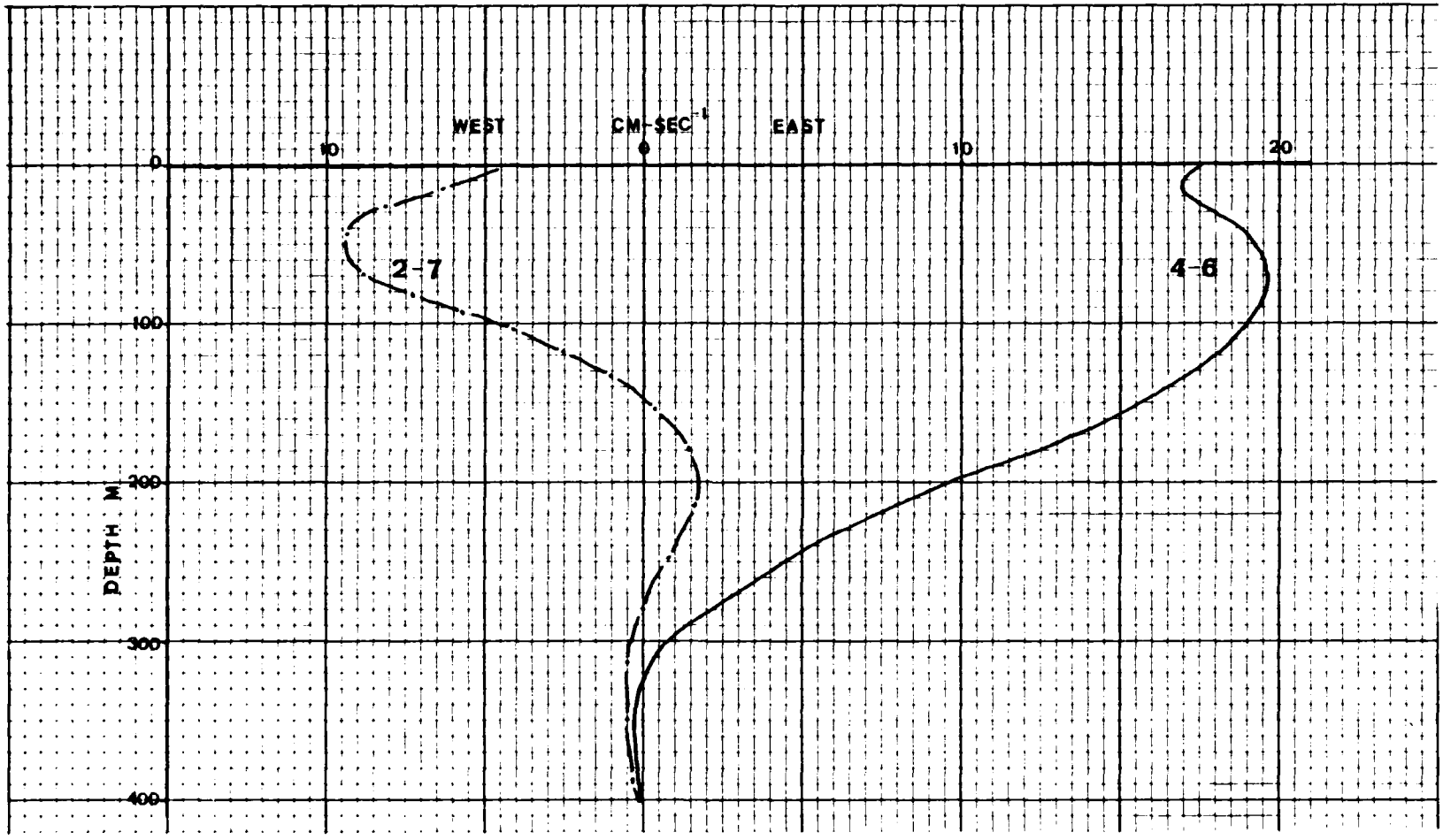

Fig. 76. Cross shelf geostrophic velocities normal to stations 2 and 7 and normal to stations 4 and 6 versus depth.

III. DISCUSSION

A. SUMMARY OF OBSERVATIONS

In all three cases, shipboard measurements confirmed the existence, magnitude and orientation of the surface thermal (cool) features detected by satellite IR imagery. Positioning of the center of the cool features by satellite analysis was accurate to within 10 km. In addition, prevalent subsurface structure common to all three cases was documented with XBT data.

The typical surface expression of the feature was an elliptically shaped cold "spot" with major axis oriented southwest from Point Sur. Approaching the cold spot, isotherms in the mixed layer sloped upwards 2 m/km to 5 m/km. Below 40 m, isotherms near the top of the thermocline increased in depth with a slope of 1 m/km to a maximum depth directly below the center of the surface feature. Hence, there was "lens" of homogeneous water below the feature. The thermocline, otherwise at a depth of 20 to 60 m, dissipated within the feature.

Geostrophic winds for all three cases were northerly, i.e., favorable to coastal upwelling. Shipboard wind measurements were also northerly (NNW). Coastal station winds were more variable. A sea breeze situation was evident only in one case at Point Piedras Blancas. Frontal passages occurred in all cases within two or three days of the cruises. The

predominant time scale for SL pressure fluctuations was about 5 days. No small scale expression, i.e., debris line, was noted on the sea surface.

In Case I, from 29 APR to 1 MAY 79, the cold plume-like feature was positioned between the Sur and Lucia Canyons. The feature was detectable to a depth of 50 m. A warm intrusion below was observable to 400 m. Based on satellite IR imagery, the feature had a life cycle of 19 days. No alongshore advection was noted.

In Case II, from 26 to 28 SEP 79, there was a cold "spot" within a plume-like feature above the Lucia Canyon, and there was a strong SST gradient (1.3°C/km) normal to the coast at Point Sur. The primary (plume-like) feature was discernable to 25 m with a warm feature at 50 m and below. A large (36 km^2) cold spot detected by satellite was not confirmed by shipboard data along the coase. Based on satellite IR imagery, the feature had a life cycle of 8 days. No alongshore advection was observed.

In Case III, from 28 to 29 NOV 79, there was a small cold plume-like feature located over the shelf off Point Sur. The cold feature was observed to a depth of 50 m with complex structure below. Based on satellite IR imagery, it had a life cycle of 17 days, and it advected to the north during calm wind conditions.

In addition, salinity measurements revealed a high salinity (> 33.6 $^{o}/_{oo}$) area coincident with the cold plume-like feature. Near the feature, isotherms and isohalines

were orthogonal implying the existence of a front which is not density-compensated. The structure of the surface σ_t field was almost identical to that of the SST field.

As far as can be determined from the limited STD casts (presented in Appendix D), the cold plume-like feature was statically stable, though in some of the casts (3, 5 and 6 near the southwestern edge of the feature) stratification in the upper 50 m is weak. It was not a buoyant plume because it was denser than adjacent year surface waters. Geostrophic calculations from the surface to 400 m show the northward flow expected due to the Davidson current. The selection of 400 m as a reference level was appropriate for the cross shelf calculations, but a deeper value was apparently required for alongshore calculations due to the large apparent shear observed between 300 and 400 m. Table II is a summary of observations.

B. FORCING

Cold plume-like features commonly form southwest of Point Sur. The interaction of coastal upwelling with the submarine canyon and cape topography is the presumed primary reason for their formation in the location. Other mechanisms which may play a role could include wind stress curl, baroclinic instability of the Undercurrent, and continental shelf or coastally trapped waves generated by remote wind stress events; e.g., storms off Baja California.

TABLE II

SUMMARY OF OBSERVATIONS

CASE	I	II	III
DATE	29 APR-1 MAY	26-28 SEP	28-29 NOV
SUNRISE	0510	0550	0648
SUNSET	1845	1750	1648
WEATHER	PCLDY	Overcast	PCLDY
WIND STRESS (10^{-3} cm sec^{-1})	0.1	1.0	0.5
SATELLITE OBSERVATIONS OF FEATURES			
DATE	29 APR	26 SEP	28 NOV
ADVECTION	No	No	Yes (North 4 km/day)
LIFE CYCLE (Days)	19	8	17
SST(°C)	12.5	13.7	N.A.
FNOC SST(°C)	12.0	15.5	15.0
SST injection (coldest) (°C)	9.0	15.0	12.0
LOCATION	BETWEEN CANYONS	LUCIA CANYON	ALONG CAPE
DEPTH OF THERMOCLINE (m)	20 to 50	20 to 40	25 to 60
SURFACE GRADIENTS (°C/km)	1.0	0.4	0.8
DEPTH DISCERNABLE (m)	50	25	50

TABLE II (Cont'd)

INTERNAL WAVE

VERTICAL VELOCITY (10^{-2} cm sec^{-1})

	6			5			4	
TIDES (GMT)								
DATE	29	39	01	26	27	28	28	29
HIGH	0707	0753	0839	0907	1016	1135	1326	0711
LOW	1335	1422	1513	1405	1458	1610	1929	1411
HIGH	2055	2152	2254	2039	2127	2225	0136	2027
LOW	0041	0248	0343	0315	0404	0513		0251

There were other influences at work as evidenced by a large cold plume-like feature extending 200 km seaward in early August 1979, limited observations of which are presented in Appendix C. Features this large possibly involve planetary long waves [Anderson and Gill, 1975], and entrainment by large eddies in the California current may be their cause.

The feature in Case III propagated northward during the calm winds of early December 1979. Northward propgating Kelvin or coastally-trapped waves could be responsible for this advection during the relaxation phase as predicted by Suginohara (1974) and Peffley (1976). However, the observed phase speed was of the order of 10 cm sec^{-1} which is much less than 50 to 100 cm sec^{-1} expected by simple theory. The difference could be due to:

(1) interaction of the perturbation with the mean flow which could result in a reduced propagation, speed, or

(2) inadequate coverage by satellite imagery, resulting in inaccurate estimation of the commencement or termination of northward propagation.

Pure advection by the mean flow is a possibility because the rate of propagation was of the same order of magnitude as the northward geostrophic, and this was a season of strong northward flow by the Davidson Current and wind conditions were calm. However, this is the only case where a feature was observed to move north or south.

Baroclinic instabilities of the mean flow could lead to formation of eddies as predicted by Mysak (1979) and described by Soluri (1971), Brown (1974) and Hickey (1979). An anticyclonic eddy located north of a cyclonic eddy can result in the offshore entrainment of cold water upwelled at the coast, resulting in a mushroom-shaped feature. Many such features have appeared in satellite IR imagery (cf. the image of 19 APR 1979).

Commonly observed is the superpositioning of a cold plume-like feature upon an older pre-existing cool plume-like feature [Conrad, 1980]. Such features seen in satellite imagery could result from the following scenario: equatorward wind event initiates the upwelling; the cold surface "spot" migrates to the shelf break [Barton, et al., 1977]; the wind event stops; relaxation of the perturbation, dissipation, and mixing result in cool surface water which is still distinguishable in satellite imagery; and another wind event renews the cycle before the earlier disturbance entirely vanishes from view.

C. PREFERRED LOCATION

The observed location of the plume-like features is consistent with background theory. Principally, the area on the south side of Point Sur is a preferred location for coastal upwelling [Arthur, 1965]. Secondarily, the effects of the Sur and Lucia Canyons are to enhance upwelling along the canyons axes nearshore and to the south of the canyons [Killworth, 1978].

D. SCALES

According to Yoshida (1955), upwelling occurs in a cross-shelf band whose width is determined by the baroclinic Rossby radius of deformation (δ) as calculated from the following approximation:

$$\delta \simeq \sqrt{\Delta\sigma_t g/\rho_o h}/f \qquad (3)$$

where $\Delta\sigma_t$ is the difference between upper layer and lower layer density anomalies (σ_t) in a two layer system, h is the thickness (cm) of the upper layer (assuming the upper layer is much thinner than the lower layer), g is the gravitational acceleration, ρ_o is the mean density, and f is the Coriolis parameter.

Using observed values from the STD casts of Case III ($\Delta\sigma_t$ = 2 g cm^{-3}, h = 2×10^4 cm, g $\simeq$ 1000 cm sec^{-2}, $\rho_o \simeq$ 1 g cm^{-3}, f = 8.5×10^{-5} sec^{-1}), δ = 20 km, a value greater than the width of the continental shelf (ca. 5 km) in this area. Climatological data over the Davidson Seamount result in δ = 30 km, which is large enought to affect the westernmost portions of the area of interest. In other words, baroclinic disturbances trapped over the Davidson Seamount could interact with the coastal upwelling center(s) over the Sur and Lucia canyons.

Orders of magnitude of scales are listed in Table III in comparison to thsoe calculated or observed off Oregon.

TABLE III

A comparison of scales of upwelling features observed by Curtin (1979) off Newport, Oregon and those observed off Point Sur in 1979

Scale	Oregon	Point Sur
Time (sec)	10^5 to 10^6	10^6
Alongshelf (km)	10^2	10^1
Cross shelf (km)	10^1	10^1
Depth (m)	10^1	10^1
Frontal Zone Width (km)	10^0	10^0

Variability is produced by shelf bathymetry, coastline irregularity and wind fluctuations [Curtin, 1979], conclusions which were reached earlier. The time scale ("life cycle") is defined as the time from initial to final observation of the feature in satellite IR imagery.

E. STRUCTURE

1. Thermal Structure

Temperatures on the level surfaces were the principle indicators of the distribution of water mass used (densities on level surfaces were not used due to the lack of salinity data for Cases I and II and to insufficient data density for Case III salinity). Temperature variations on a level surface are due to vertical displacement by internal waves as well as upwelling, mixing and horizontal advection. Surface anomalies may be used as indicators of upwelling, but similar effects are caused by wind mixing or radiative effects. Persistence of a feature lends credence to the upwelling interpretation [Shepard, 1970].

Of interest in the upper 100 m is the shoaling of isotherms (detected as a cold surface feature) which is accompanied by the deepening of isotherms below, i.e., the thickness between two isothermal surfaces increases at the cold spot. This "lens" was observed on every transit which passed through the feature. Its width at its axial depth (50 m) was approximately 20 km. The feature tilted with depth,

from the surface enclosed "cold spot" to a cold tongue at 50 m. In Case III, this tilt was to the south with a slope of 10 m/km.

Deeper than 100 m, there is a distinct thermal structure the study of which is beyond the present scope. Of interest, however, are the following properties: in some cases, isotherms parallel isobaths indicating conservation of potential vorticity; horizontal temperature gradients usually reverse sign between 200 and 300 m; and large vertical perturbations seem likely to be due to internal waves.

Anomalously warm water was noted at different levels in different cases. In the SST field of Case II, such an anomaly existed and is referred to as a "nearshore warm anomaly" [Wang and Mooers, 1976]. It is believed to be the result of surface warming and mixing during the relaxation period. All cases had other warm anomalies with vertical thickness scales of the order of 100 m.

2. Thickness Field

The importance of the isothermal layer thickness field is that areas of relative thickness maxima indicate regions where horizontal convergence or mixing has occurred. Horizontal convergence implies a stretching of the water column, which results in an increase in the relative vorticity of the parcel, i.e., increased cyclonic circulation. According to the conservation of potential vorticity principle for a homogeneous fluid:

Potential Vorticity = $(f + \xi r)/D$ is conserved,

where:

f is the planetary vorticity,

ξr is the relative vorticity, and

D is the depth.

For a density stratified fluid, with $-g\Delta p/\rho_o$ constant between iscpycnals,

$$\text{Potential Vorticity} \simeq (f + \xi r)/\Delta Z \qquad (4)$$

where:

ΔZ is the thickness of an isopycnal layer.

In the present study, ΔZ was taken as the thickness of an isothermal layer to a good approximation. In all cases, an axis of thickness maxima is distinguishable oriented southwest from the Point Sur area through the "cold spot". The thickness maxima axis parallels the Sur and Lucia canyons.

3. Thermal Wind Balance

The "thermal wind" balance is $\partial V/\partial Z = -g/fp_o \; \partial p/\partial T \; \partial T/\partial x$. From the present study, $\partial T/\partial x$ was available. In the upper 50 m, it was typically between 0.5 and 1.0 °C/km across frontal zones. A horizontal temperature gradient of 1°C/km is necessary

to provide a "thermal wind" equal to the velocity shear produced by a surface wind stress of 1 dyne/cm^2 [Blumsack, 1972]. Thus, the temperature gradients at 50 m and above created a "thermal wind" of the same magnitude as the vertical (Ekman) shear attributable to the prevailing wind stress.

At depth, the temperature gradients were much smaller and occasionally reversed sign at about 200 m. This implies no vertical shear, i.e., a subsurface velocity maximum occurred at the level of "thermal wind" reversal. Such reversals have been previously observed in the area of interest and involve the superpositioning of cold cyclonic features over warm anticyclonic features.

F. INTERNAL WAVES

The area off Point Sur and south is an area of known internal wave activity and as such, the temperature variation on a level surface must include effects of vertical motion produced by internal waves [Wickham, 1975]. Numerous investigations into temperature variations on continental shelves have demonstrated the role of large amplitude internal waves. The intensity of the temperature differences depends on several factors, the most important being the tide, topography and stratification [Miller, 1965]. Internal gravity waves have periods less than the inertial period, but greater than the Brunt-Varasala frequency.

Estimates of the vertical velocities involved with these disturbances are of the order of 5×10^{-2} cm/s an order of

magnitude greater than typical upwelling vertical velocities. Internal waves distort the temperature field, but, on short transects, the effects are negligible. The dramatic rise in isotherms, e.g., the rise during Case II of the 7.5 to 9.5°C isotherms from about 300 to 200 m, observed on various transits suggests motions consistent with tidal forced internal waves.

G. SEA BREEZE

The sea breeze phenomenon may only be an important factor where terrain allows it to occur, i.e., through river valleys. The potential sea breeze appears to be impeded in the Point Sur area due to the high (1 km) coastal mountains which block the lower level sea breeze. In addition, frontal passages occurred within two or three days of all cruises. They may have masked the effect or prevented the inshore formation of the requisite small scale thermal low during the day.

IV. SUMMARY

A. CONCLUSIONS

A simplified view of the dynamics occurring off Point Sur has been taken in order to identify scales and structures of the cold plume-like features for further use in chemical mesoscale nutrient analysis and interpretation of acoustic implications. The coastal water response observed by satellite was typical of that observed along the entire coast from Point Conception north to Point Mendocino.

It is obvious that the study of this area involves complicated interactions between dynamic forces on many scales and it must be remembered that upwelling is not an isolated phenomenon. The interaction of upwelling flows with the mean flow, bottom topography, mean flow instabilities and eddies off Point Sur are not well known. Mixed layer dynamics interact with upwelling dynamics as well. Occasionally, the cold feature off Point Sur is masked from detection by satellite IR imagery due to surface heating.

Nutrient measurements are important in monitoring these features. A feature masked from IR sensors may still maintain nutrient levels and ratios unique to the feature. Information about the source of the upwelled water, and the length of time it has been on the surface, may also be deduced from nutrient analysis.

Of interest is whether or not subsurface structure can be inferred from limited information such as a single satellite image. The variability of the thermal structure, particularly below 100 m, is sufficiently complex that inferences from a surface "snapshot" are presently difficult. Limited inferences about the structure can be made by using the information on the "lens", typical slopes and gradients, and other scales discussed earlier.

It is apparent from the acoustic analysis (Appendix A) that cold plume-like features or "cold spots" detected by satellite IR imagery should be included in temperature fields used to generate acoustic forecasts. Information for ASW oriented missions can be updated through judicious use of satellite IR imagery, inferences on subsurface structure, and a limited number of airborne XBT's. Typical information available to mission planning, i.e., FNOC SST analysis, smooth out mesoscale features (in the Point Sur area) which would be evident in satellite imagery. Even a single AXBT dropped in the center of a cold feature would beneficially update the SST and the sonic layer depth.

The necessity of using a satellite IR image to aid in drawing SST isotherms from limited in situ measurements cannot be determined from a limited number of cases. However, factors to be considered are: (1) synopticity (i.e., the time it took to sample the area in situ),

(2) spatial resolution, (3) the age of the satellite mage, (4) subsequent advection, (5) processes which alter SST (e.g., solar radiation and wind mixing), and (6) variations in the atmospheric moisture content.

B. FURTHER RECOMMENDATIONS

Future research is recommended in the following areas:

(1) determination of correlation scales for temperature variations at various depths,

(2) estimation of e-folding growth and decay time scales,

(3) analysis of the error between satellite SST, bucket temperatures, and 2 m temperature with and without moisture correction of the satellite SST,

(4) analysis of the effects of internal waves and continental shelf waves upon upwelling dynamics off Point Sur, and

(5) verification of the changes in propagation loss caused by the cold plume-like feature.

APPENDIX A: ACOUSTIC IMPLICATIONS

The presence of a wedge of cold water in the upper oceanic layers (which is not restricted to coastal waters) affects many factors of acoustic relevance. For example, it affects transmission loss as discussed below. The passive sonar equation is:

$$SL - PL - (NL - DI) = DT$$

where SL is the source level in dB, PL is the propagation loss in dB, NL is the noise level in dB, DI is the directivity index in dB, and DT is the detection threshold in dB [Coppens and Sanders, 1977]. For mission planning, the passive sonar equation is rearranged into two parts, the figure of merit (FOM) where

$$FOM = SL - (NL - DI) - DT$$

and the propagation loss (PL). There is a 50% probability of detection of the source by the receiving system at the range where the FOM and PL curves intersect. The shortest range usually associated with detection by direct path propagation is termed the median detection range (MDR)

and it is used to calculate sonobuoy spacing and to select sonobuoy array patterns.

The cold wedge changes the ocean thermohaline structure in the upper layer from its climatological structure. The sea surface temperature (SST) is cooled and the sonic layer depth shoals. These properties, together with the thermal structure, determine the transmission path taken by the acoustical energy and therefore affect TL. In addition, increased biological activity common to such oceanic features as the cold wedge can be expected to increase ambient noise level.

To assess whether or not the presence of the cold wedge made sufficiently significant changes in acoustic transmission to affect mission planning, the Parabolic Equation (PE) model was run for two cases, a climatological case for standardization and an altered case with a cold wedge feature incorporated. The PE model, which is a research model, solves the standard wave equation and produces a PL versus range curve. It allows for the input of multiple sound velocity profiles (SVP) and variable depth and bottom properties which influence the result either through refraction or bottom attenuation versus grazing angle curves. The model uses the small angle approximation which restricts energy from the source to a small cone. The beam angle is restricted to approximately ±30° though practical use is ±10°. It is also

limited to frequencies less than 350 Hz as are all non ray-tracing models [Bourke, 1979,].

The model domain was centered at 36°05'N, 122°05'W, the typical center of the observed features. The alongshore propagation path was parallel to the coast, NW to SE, over a distance of 40 nm. The across shelf propagation path was normal to the coast, SW to NE, over a distance of 30 nm. The climatological thermal structure was obtained from the Integrated Command Acoustic Prediction System (ICAPS) climatological data bank for the Northern Pacific in the month of MAY. ICAPS was also used to calculate SVP's from actual XBT's obtained during the 29 APR to 1 MAY 79 cruise. Seven were entered alongshore and six offshore to construct the thermal structure of the cold wedge. Data below 400 m was merged with the deep climatology used on the standard run. Climatological salinities were used with negligible induced errors expected since observed salinity values in the area varied from climatological values by a maximum of 0.25 ‰ above 200 m and by a maximum of 0.04 ‰ below 200 m, and since the partial of sound velocity with respect to salinity is small, i.e. 1.3 m s^{-1} ppt^{-1} [Coppens and Sanders, 1977]. Realistic water depths were entered. (See Figs. 77 and 78 and Tables IV, V, VI for model characteristics.)

Forty-eight runs were made for comparison. NW and SE alongshore, and onshore-offshore normal runs were made for both cases with source depths of 60 and 300 feet, receiver depths of 60, 90 and 300 feet, and frequencies of 50, 100 and 300 Hz.

A beamwidth of 10° was chosen for all runs in order to standardize comparisons. This beamwidth worked for all runs in a minimum of computer time while problems involving time allocations were encountered during some runs using a beamwidth of 15°. For the one successful run with a greater beamwidth, the computer time required, exclusive of the plotter, was 15 min. 50 sec. while the smaller beamwidth required 3 min. 47 sec. The basic shape of the two sets of curves is the same but the PL curves for a 15° beamwidth are the least variable for all depths (Fig. 79). Differences are attributable to different bottom interactions and transmission paths.

In addition, a few runs were made with a different "loss versus grazing angle" curve. The differences in the PL curves between these runs and the standard runs are negligible. No difference was noted less than 20 nm and only one to two dB difference from 20 to 40 nm (Fig. 80).

The runs for the two cases were then reviewed to determine the optimum receiver depth and the typical detection ranges to be expected. The differences between

"PL climatology" and "PL wedge" were then calculated within the typical detection range for the receiver depth of interest.

The calculations are broken down into the following categories: onshore propagation (Figs. 81 through 83); offshore propagation, (Figs. 84 through 86); NW alongshore propagation (Fig. 87); and SE alongshore propagation (not included in figures). Items for comparison are: the MDR obtained from an arbitrary FOM of 85 dB, the receiver depth with the least PL between the source and the MDR and the behavior of the PL curve in the region between 8 and 30 nm. These items will be used to compare the climatological and cold water wedge runs for each case in order to assess the effect of the wedge on mission planning.

The onshore propagation climatological runs result in PL curves which are distinctive due to the sharp increase in PL to 120 dB within 2 nm of the source and to a maximum of approximately 160 dB at 8 nm. From 12 to 14 nm the PL decreases to approximately 85 dB. From this point to the end of the run at 30 nm, there is a great deal of variability in the PL curves and a distinct separation of PL for different receiver depths. The MDR for all frequencies and receiver depths is between 1.5 and 2.0 nm, with the 300 foot receiver depth being the most effective.

The effect of the cold wedge is to decrease the slope of the PL curve within 2 to 3 nm. This is best seen in the deep source low frequency runs (Fig. 82). In most runs, the relative advantage of the 300 foot receiver is increased. The MDR for the deep source increased approximately 50% for all frequencies while for the shallow source, it did not change.

From 12 to 30 nm, the effect of the cold wedge was to generally alter the shape of the PL curve and decrease some of the large variations for certain receiver depths. A good example of this is the deep target high frequency run at 21 nm (Fig. 83). Here, the PL for the shallow receivers decreased from 140 dB for the climatology run to 105 dB for the wedge run.

Other notable changes in particular runs are: (1) the decrease in PL of 15 to 30 dB from 12 to 30 nm in the shallow target, high frequency run (Fig. 82), and (2) the down range shift of the PL minimum from 11 nm in the climatology case to 13 nm in the wedge case for the deep target low frequency run (Fig. 81).

The offshore propagation climatological runs result in PL curves with shapes similar to those of the onshore cases but without the broad area of high PL between 2 and 8 nm. The PL increases to 105 to 120 dB within 2 nm of the source, and then it immediately decreases to 70 to 80 dB at 6 to 8 nm. From 8 to 30 nm, the PL curve

for the deep receiver is significantly less than the PL curves for the shallow receivers. The MDR for all frequencies and receiver depths is between 1.5 and 2.0 nm with the 300 foot receiver being the most effective.

The effect of the cold wedge is to decrease the slope of the PL curve within 2 to 3 nm of the source and to decrease its maximum magnitude, especially for the deep receiver (Fig. 84). The MDR increase was negligible for the shallow source and shallow receivers, i.e., at the 60 and 90 foot depths (Fig. 85), and between 50% and 100% for the other runs (Figs. 84 and 86).

From 6 to 30 nm, the effect of the cold water wedge was minor with one exception. The PL curves for the deep source, high frequency run decreased on the order of 20 dB for the shallow receivers and decreased between 5 and 10 dB for the deep receiver (Fig. 86).

The alongshore (NW propagation) climatological runs result in features similar to but not as dramatic as the onshore or offshore propagation cases. The PL curves increase to 105 to 120 dB within 2 to 3 nm of the source and then decrease to 75 dB at 6 to 8 nm. From 8 to 40 nm, there is a great deal of variability in the PL with a general decreasing trend attributed to geometric attenuation. There is no distinct advantage of any receiver depth. The MDR for all frequencies and receiver depths is between 1.0 and 2.0 nm, with the 300 foot receiver

being the most effective. It was negligibly advantageous for the shallow target run at 100 Hz (Fig. 87).

The effect of the cold wedge is to decrease the slope of the PL curve within 2 to 3 nm in some cases and to decrease its maximum magnitude, particularly for the 300 foot receiver (Fig. 88). There was a slight change of 5 dB in the shallow target, 50 Hz case for the 300 foot receiver (Fig. 89) and negligible changes for other cases. The MDR improved only slightly for two cases, both with the deep source for 100 and 300 Hz (Fig. 88). From 60 to 40 nm, the effect was to only alter the variability of the PL curves by shifting the ranges at which the deviations occurred. These same effects are observed in the alongshore SE propagation case.

To better observe the difference between the cases, the difference between the respective propagation losses for the 300 foot receiver on the onshore and offshore runs within 15 nm of the source was evaluated. The selection of the 300 foot receiver for this calculation was dictated by the general advantage demonstrated over the shallow receiver depths, and the selection of the particular cases reflects the fact that negligible changes occurred in the alongshore runs.

For all cases, the wedge does have an effect upon propagation loss (Figs. 90 and 91). In particular, there is improvement between 2 and 4 nm which is negligible for

low frequency and a shallow source and quite large, i.e., 35 dB, for a deep source at all frequencies. In addition, there is a second area of change between 12 and 14 nm which can be classified as either an increase in variability as shown by the 300 foot source depth for all frequencies in the onshore case or as a reduction in PL as shown by all the offshore cases.

The impact of the cold water wedge on propagation loss is principally noted with cases involving a deep source, high frequency, and deep receiver, in particular the 300 foot receiver with the cross shelf runs. Generally, the least effect was noted with cases involving a shallow source, low frequency, and shallow receiver depth. The alongshore runs were not affected as much as the cross shelf runs. In all cases, the propagation loss change could lead to changes in observed signal excess at the receiving system.

In many cases, the MDR increased about 25 to 50%. If the cold wedge situation could be anticipated, this increase in MDR could be incorporated in mission planning. If not, the result would be an increased probability of detection.

The reason for the observed change may be due to the change in the radius of curvature of the acoustic transmission path induced by the thermal structure change.

This affects PL and causes different bottom loss. The variation in mixed layer depth affects transmission paths across the layer between source and receiver [Coppens and Sanders, 1977].

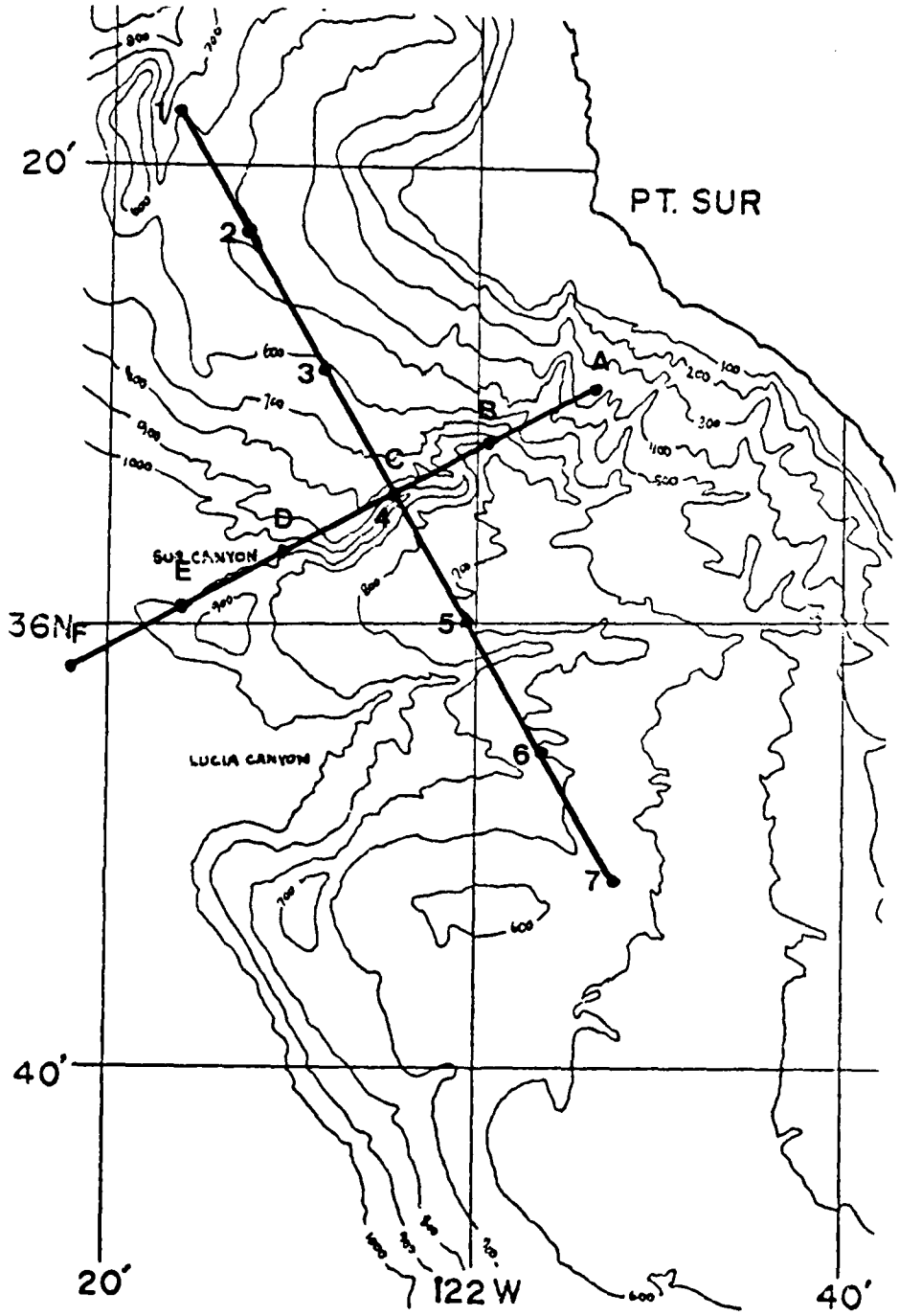

Fig. 77. Model and topography orientation showing SVP positions.

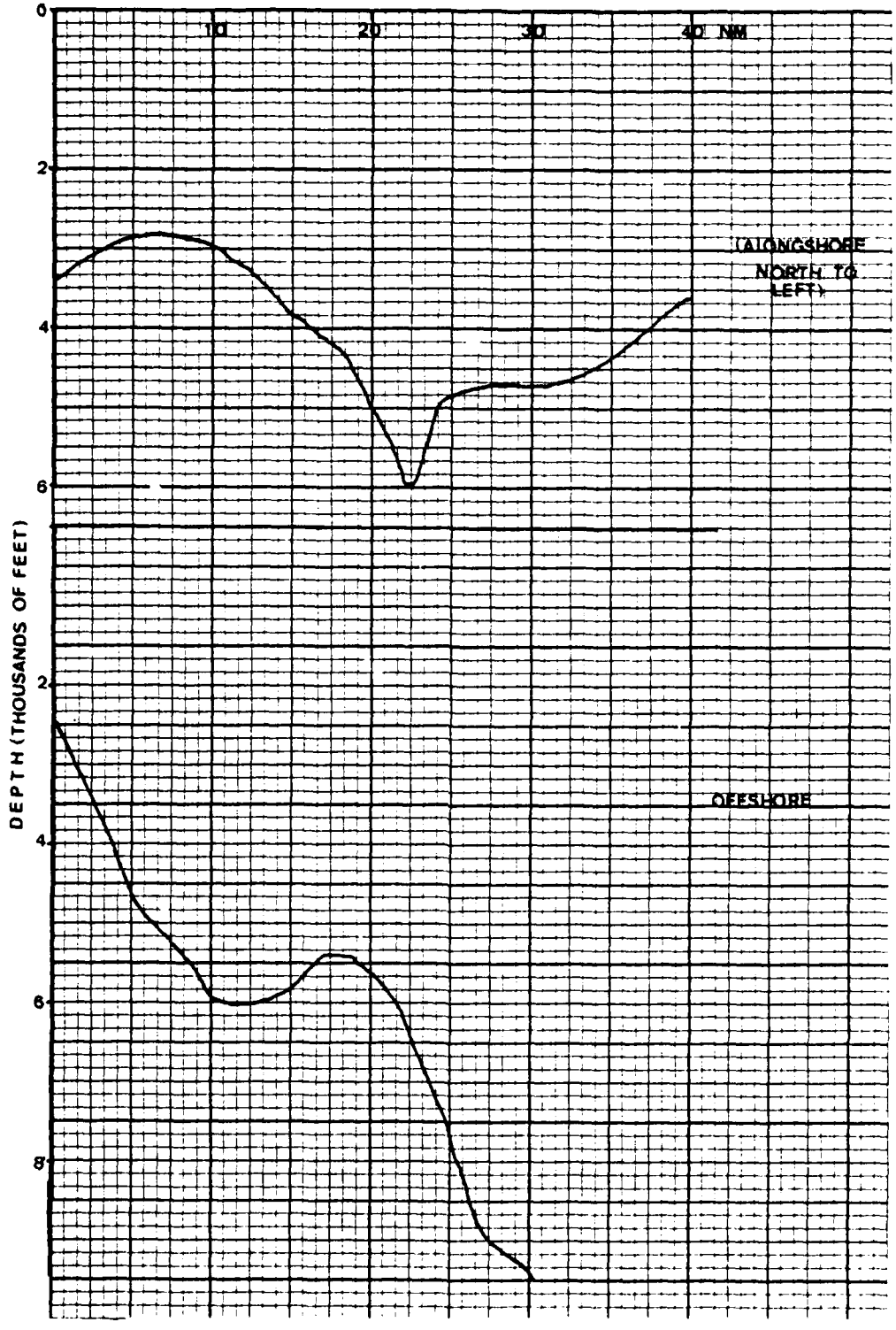

Fig. 78. Graph showing alongshore and offshore bathymetry entered into PE Model.

Table IV. Table showing SVP climatological data.

Profile at range = 0.0 nm

DEPTH (M)	SOUND SPEED (M/S)
0.	1504.
10.	1503.
20.	1502.
30.	1501.
50.	1498.
75.	1494.
100.	1491.
125.	1489.
150.	1488.
200.	1486.
300.	1484.
400.	1483.
500.	1482.
600.	1481.
800.	1481.
1000.	1482.
1200.	1483.
1500.	1486.
2000.	1491.
2500.	1499.
3000.	1507.

le V. Table showing SVP alongshore data.

file 1

TH (M)	SOUND SPEED (M/S)
0.	1500.
5.	1491.
0.	1488.
0.	1485.
0.	1483.
0.	1482.
0.	1481.
0.	1481.
0.	1480.
0.	1480.
0.	1481.
0.	1483.
0.	1486.

Profile 3

SOUND SPEED (M/S)
1488.
1489.
1486.
1484.
1483.
1481.
1481.
1480.
1480.
1480.
1481.
1483.
1486.

file 2

TH (M)	SOUND SPEED (M/S)
0.	1495.
5.	1490.
0.	1487.
0.	1485.
0.	1483.
0.	1482.
0.	1481.
0.	1480.
0.	1480.
0.	1480.
0.	1481.
0.	1483.
0.	1486.

Profile 4

SOUND SPEED (M/S)
1487.
1487.
1485.
1484.
1482.
1481.
1480.
1479.
1479.
1480.
1481.
1483.
1486.

AD-A092 632 NAVAL POSTGRADUATE SCHOOL MONTEREY CA F/G 8/10
SUBSURFACE DYNAMICAL PROPERTIES OF VARIABLE FEATURES SEEN IN SA--ETC(U)
JUN 80 J E JOHNSON

UNCLASSIFIED NL

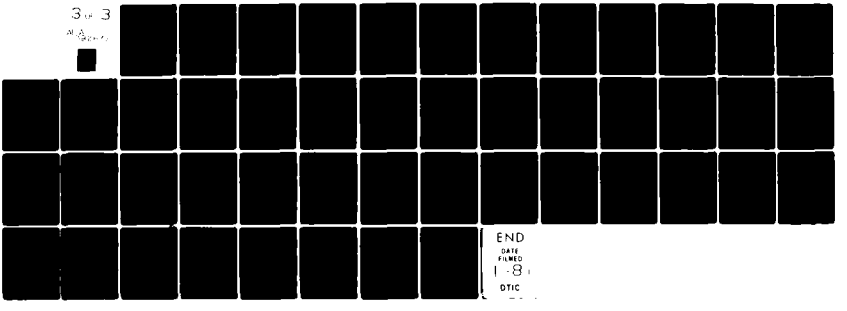

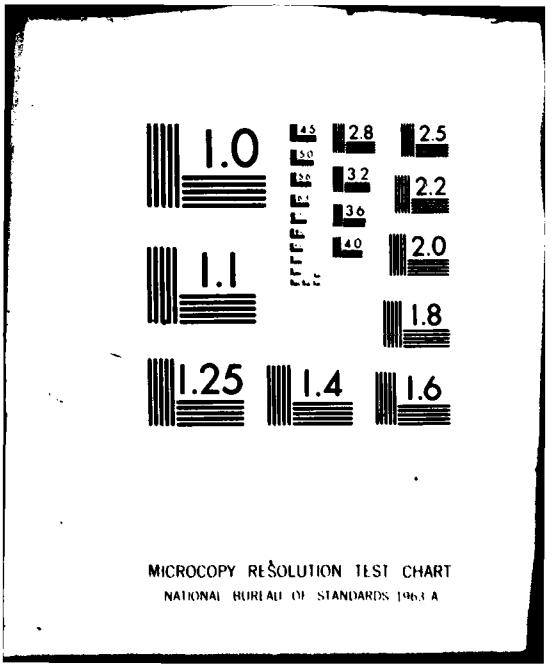
1.0
1.1
1.25
1.4
1.6
1.8
2.0
2.2
2.5
2.8
3.2
3.6
4.0
4.5
5.0
MICROCOPY RESOLUTION TEST CHART
NATIONAL BUREAU OF STANDARDS 1963 A

Table V. (continued)

Profile 5

DEPTH (M)	SOUND SPEED (M/S)
0.	1488.
25.	1489.
50.	1486.
100.	1484.
200.	1483.
300.	1481.
400.	1481.
500.	1480.
600.	1480.
800.	1480.
1000.	1481.
1200.	1483.
1500.	1486.

Profile 6

DEPTH (M)	
0.	1495.
25.	1489.
50.	1487.
100.	1485.
200.	1483.
300.	1482.
400.	1481.
500.	1480.
600.	1480.
800.	1480.
1000.	1481.
1200.	1483.
1500.	1486.

Profile 7

SOUND SPEED (M/S)
1500.
1491.
1488.
1485.
1483.
1482.
1481.
1481.
1480.
1480.
1481.
1483.
1486.

Table VI. Table showing SVP offshore data

Profile A		Profile C
DEPTH (M)	SOUND SPEED (M/S)	SOUND SPEED (M/S)
0.	1500.	1488.
25.	1491.	1489.
50.	1488.	1486.
100.	1485.	1484.
200.	1483.	1483.
300.	1482.	1481.
400.	1481.	1481.
500.	1481.	1480.
600.	1480.	1480.
800.	1480.	1480.
1000.	1481.	1481.
1200.	1483.	1483.
1500.	1486.	1486.
2000.	1491.	1491.
2500.	1499.	1499.
3000.	1507.	1507.

Profile B		Profile D
DEPTH (M)	SOUND SPEED (M/S)	SOUND SPEED (M/S)
0.	1495.	1487.
25.	1489.	1487.
50.	1487.	1485.
100.	1485.	1484.
200.	1483.	1482.
300.	1482.	1481.
400.	1481.	1480.
500.	1480.	1479.
600.	1480.	1479.
800.	1480.	1480.
1000.	1481.	1481.
1200.	1483.	1483.
1500.	1486.	1486.
2000.	1491.	1491.
2500.	1499.	1499.
3000.	1507.	1507.

Table VI. (continued)

Profile E		Profile F
DEPTH (M)	SOUND SPEED (M/S)	SOUND SPEED (M/S)
0.	1486.	1484.
25.	1486.	1484.
50.	1483.	1483.
100.	1482.	1480.
200.	1482.	1480.
300.	1480.	1479.
400.	1480.	1480.
500.	1479.	1479.
600.	1479.	1479.
800.	1480.	1480.
1000.	1481.	1481.
1200.	1483.	1483.
1500.	1486.	1486.
2000.	1491.	1491.
2500.	1499.	1499.
3000.	1507.	1507.

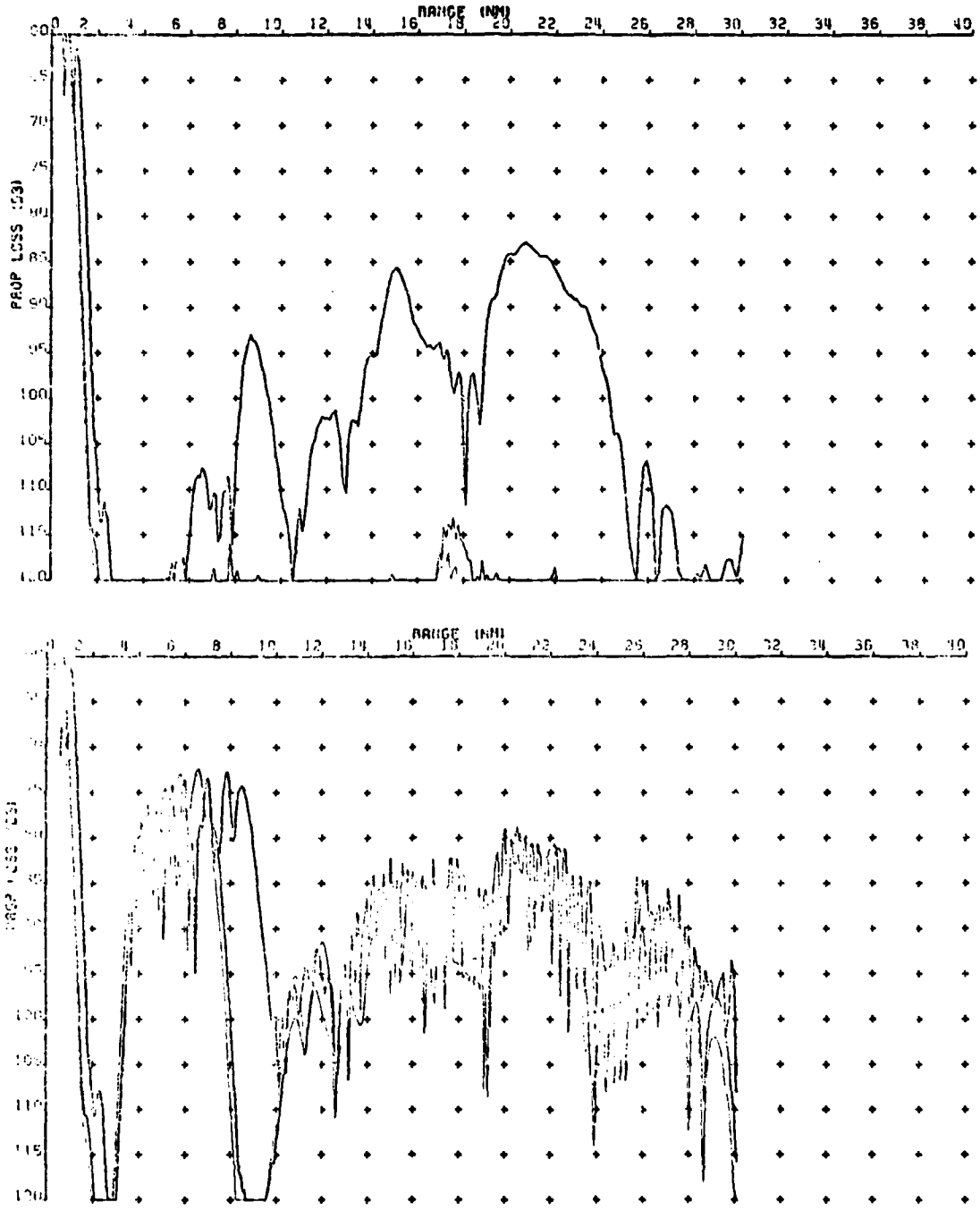

Fig. 79. PL profile showing 300 foot source at 300 Hz using 10 degree beamwidth (top) and 15 degree beamwidth (bottom). Light line indicates PL curve for 50 foot receiver, dark line indicates PL curve for 300 foot receiver.

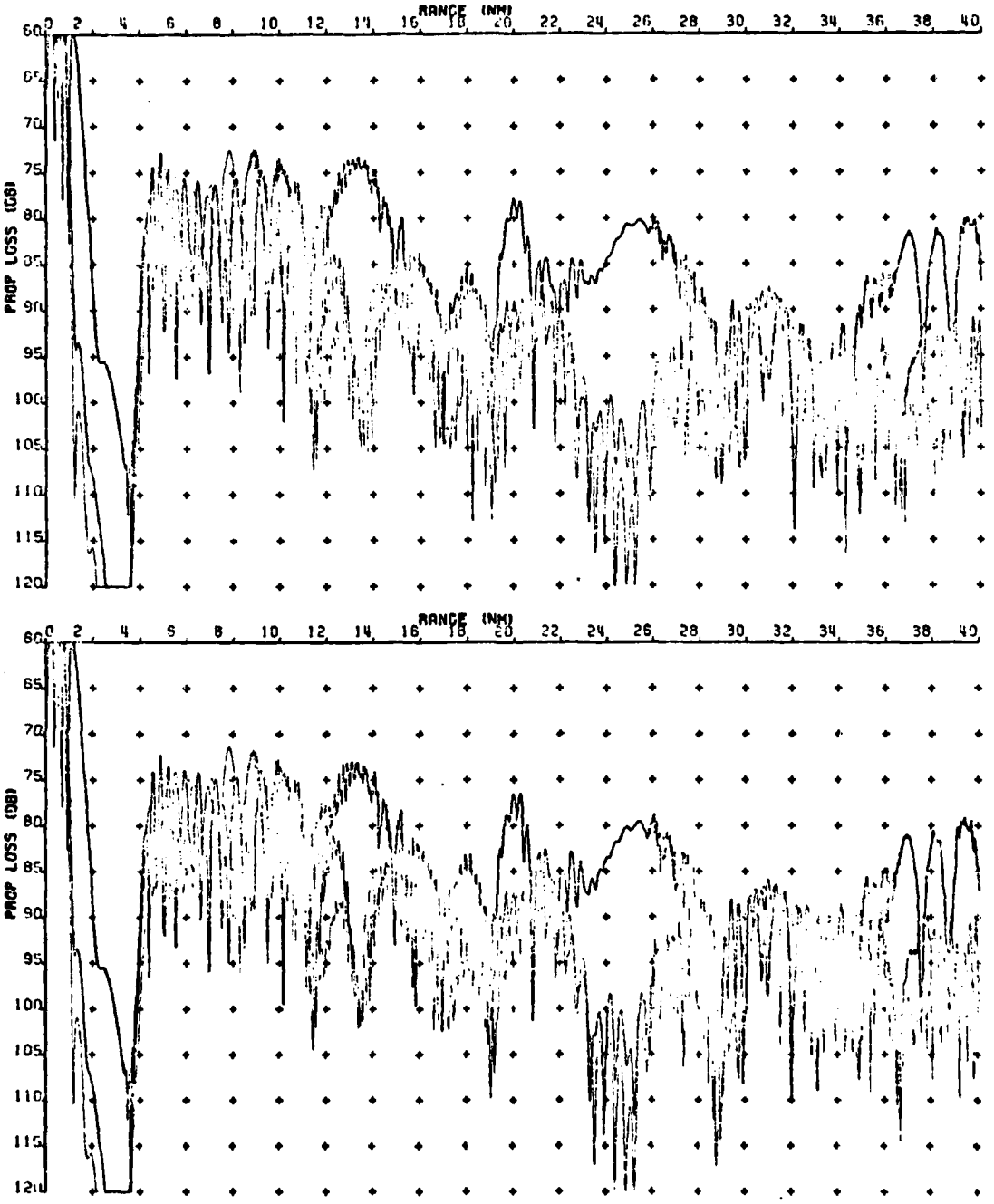

Fig. 80. PL profile showing 300 foot source at 300 Hz using different "loss (dB) versus grazing angle" curves.

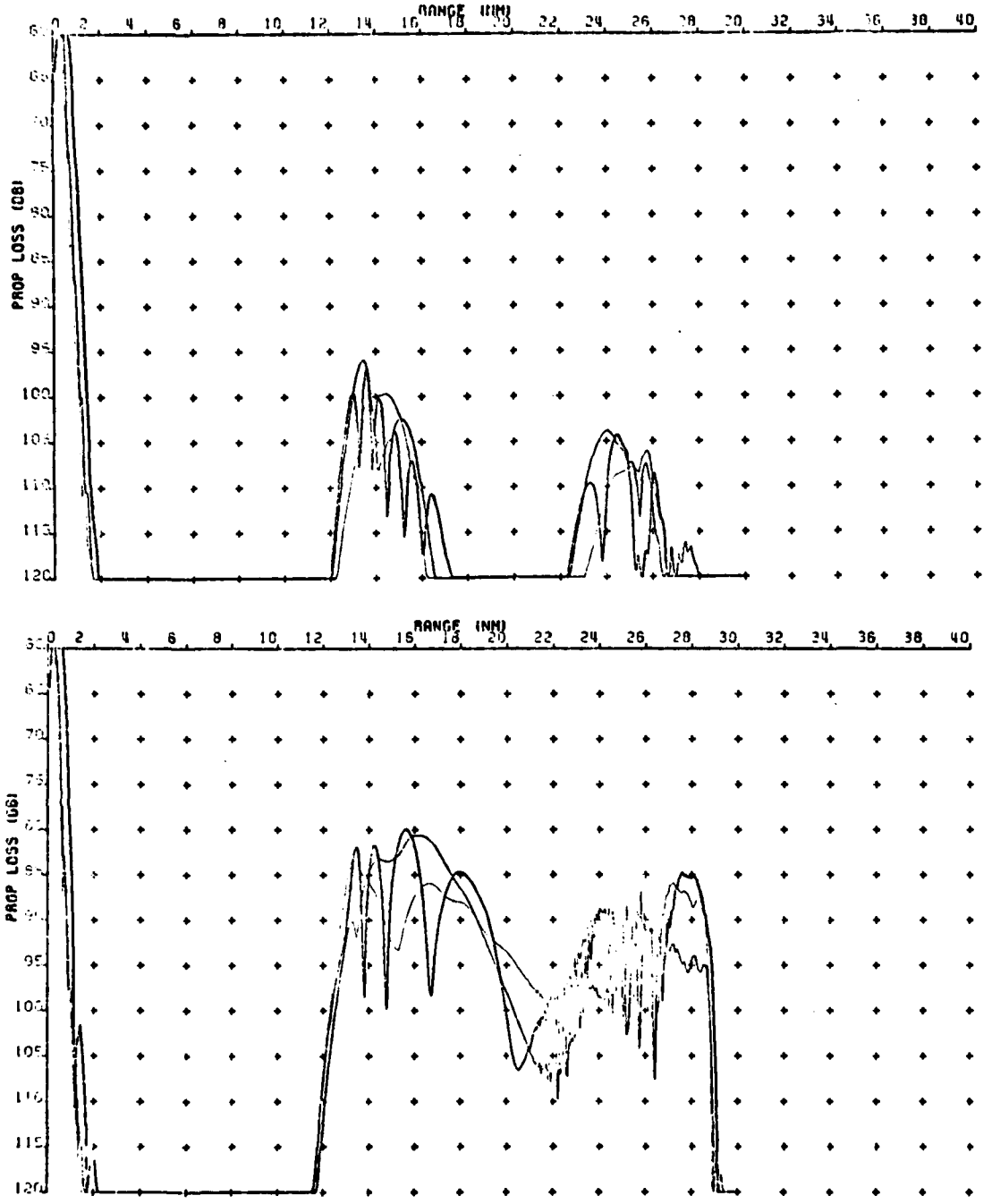

Fig. 81. PL profile showing onshore propagation of 60 foot source at 300 Hz with climatological run (top) and cold wedge run (bottom).

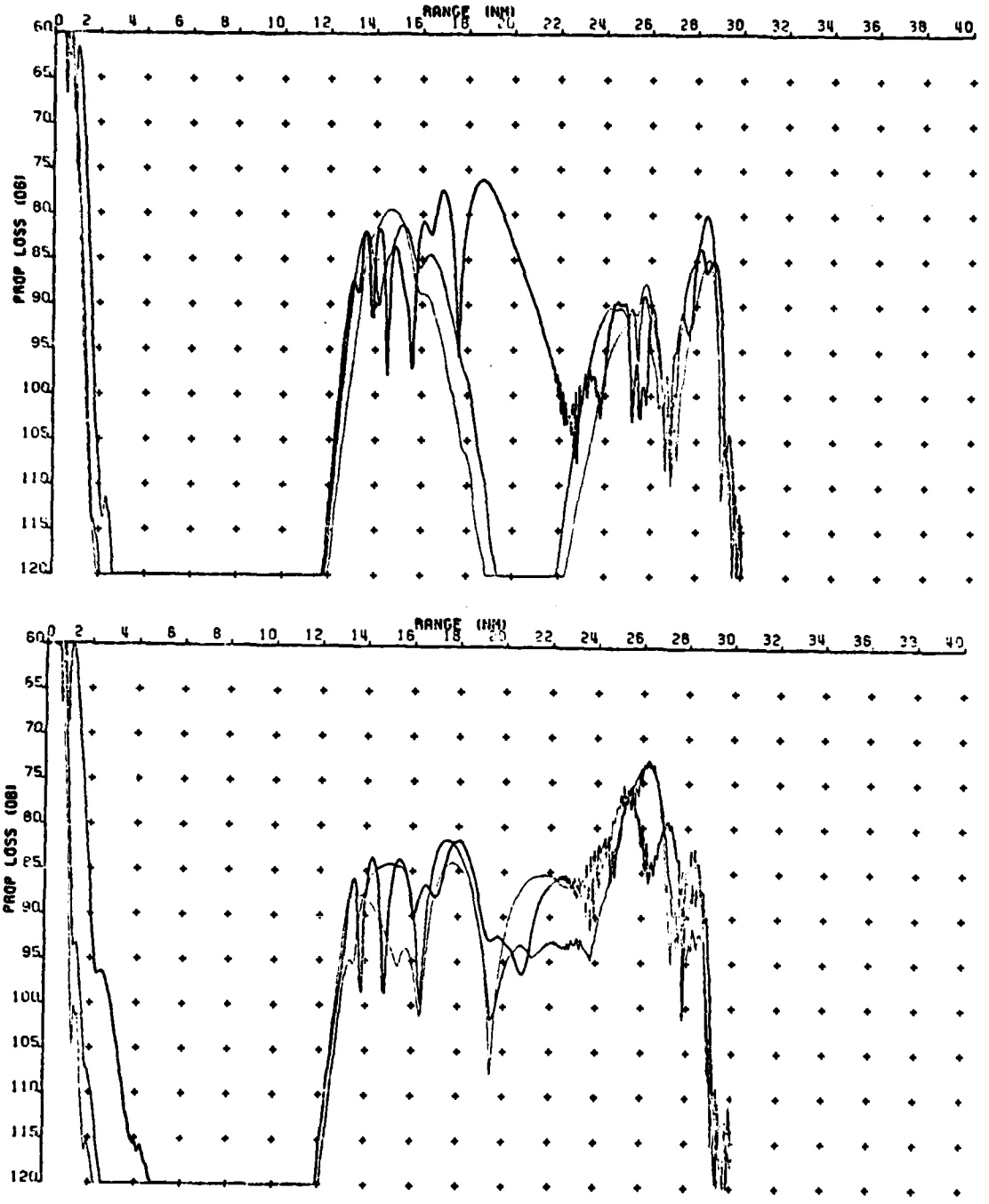

Fig. 82. Same profile as in Fig. 81 except 300 foot source at 50 Hz.

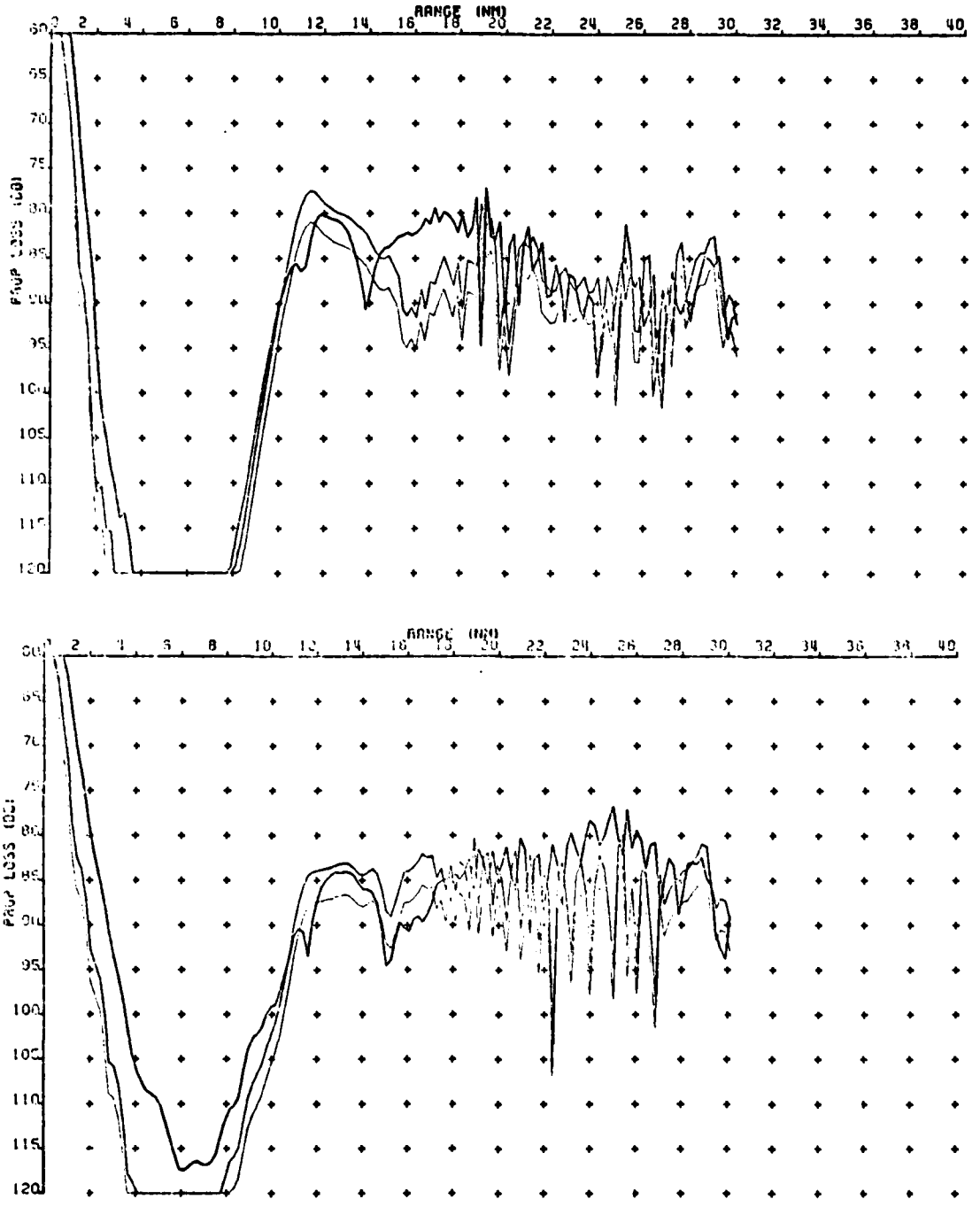

Fig. 83. Same profile as in Fig. 81 except 300 foot source at 300 Hz.

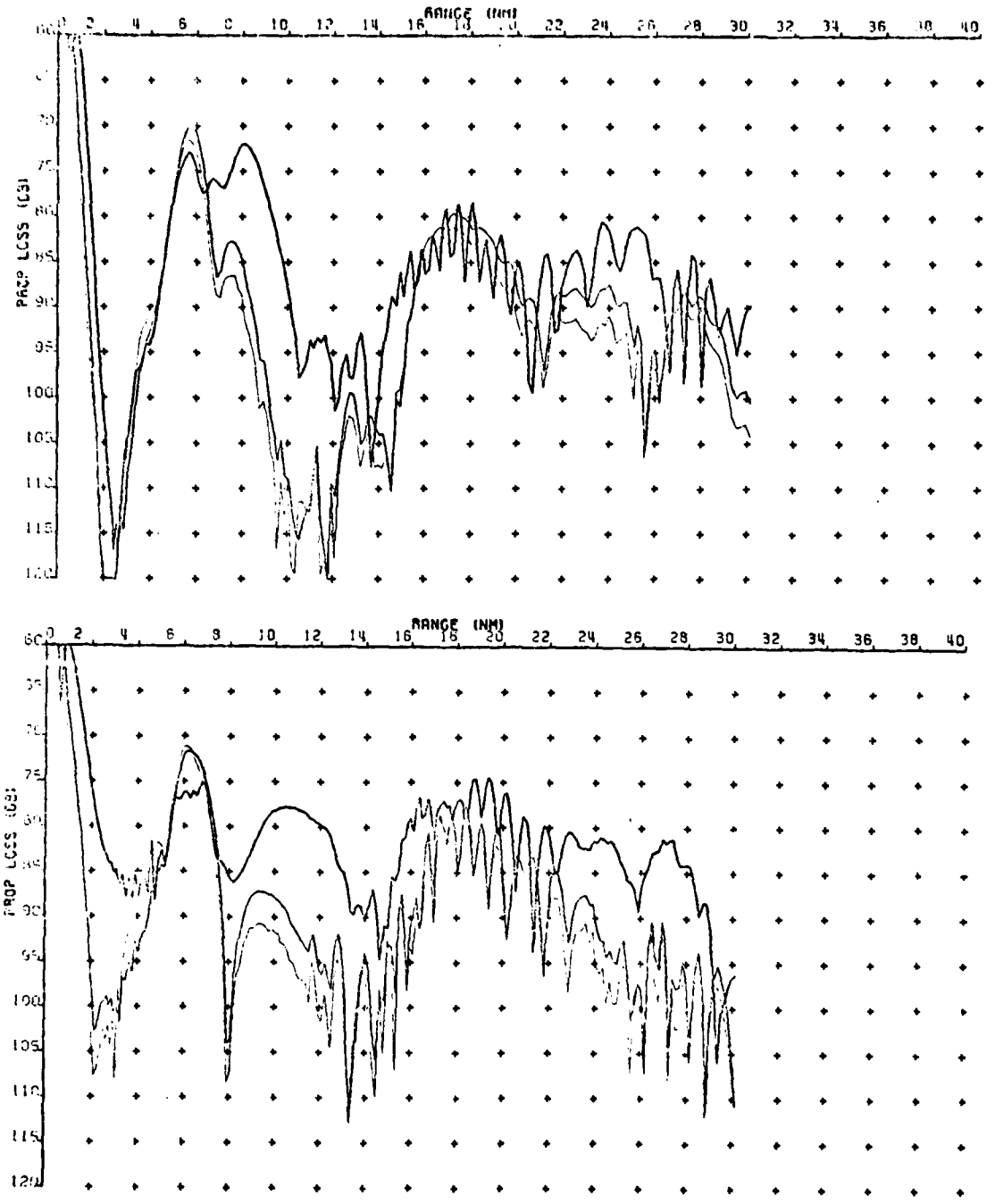

Fig. 84. PL profile showing offshore propagation of 300 foot source at 100 Hz, Climatological run (top) and cold wedge run (bottom).

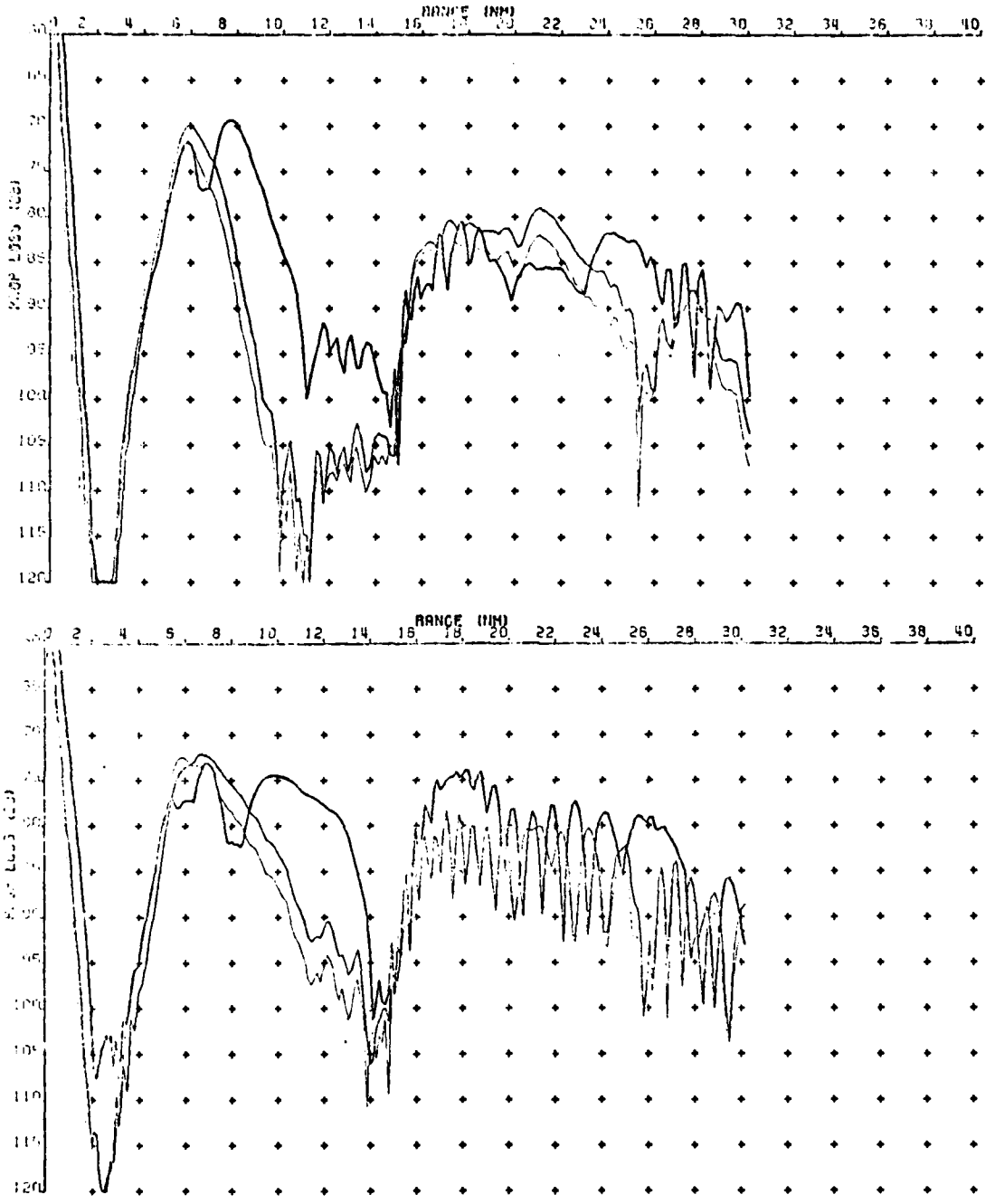

Fig. 85. Same profile as in Fig. 84 except 60 foot source at 100 Hz.

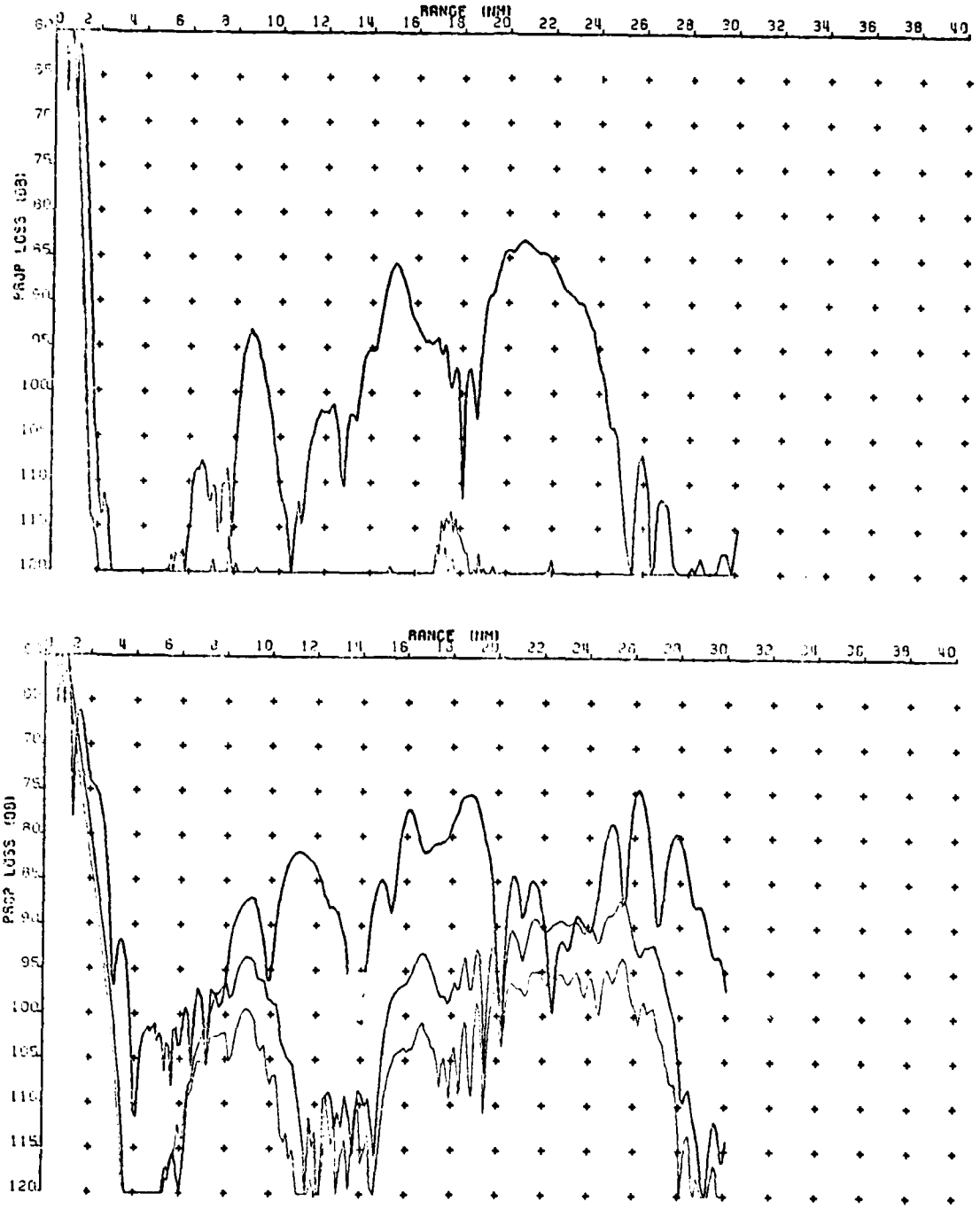

Fig. 86. Same profile as in Fig. 84 except 300 foot source at 300 Hz.

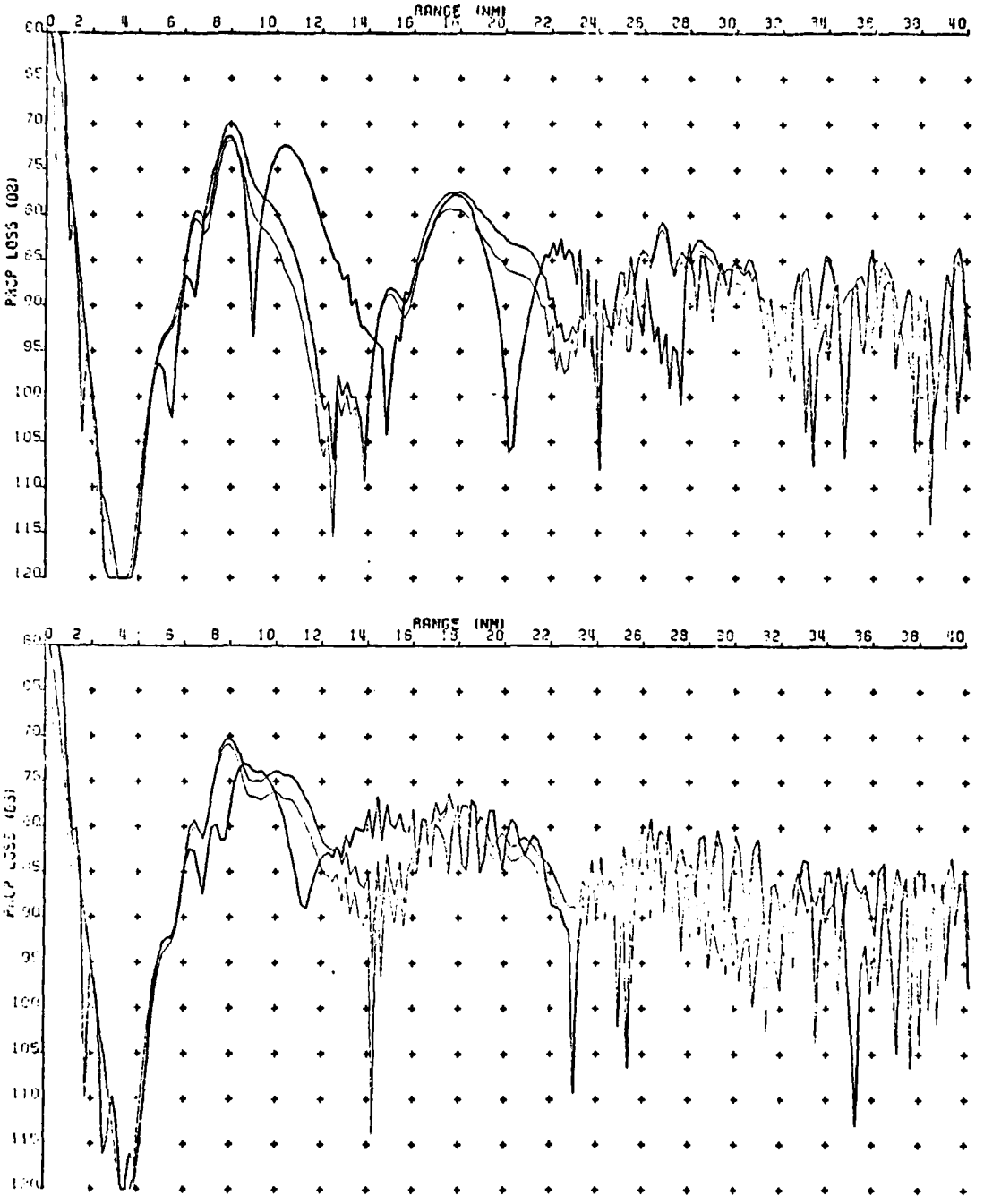

Fig. 87. PL profile showing NW alongshore propagation of 60 foot source at 100 Hz with climatological run (top) and cold wedge run (bottom).

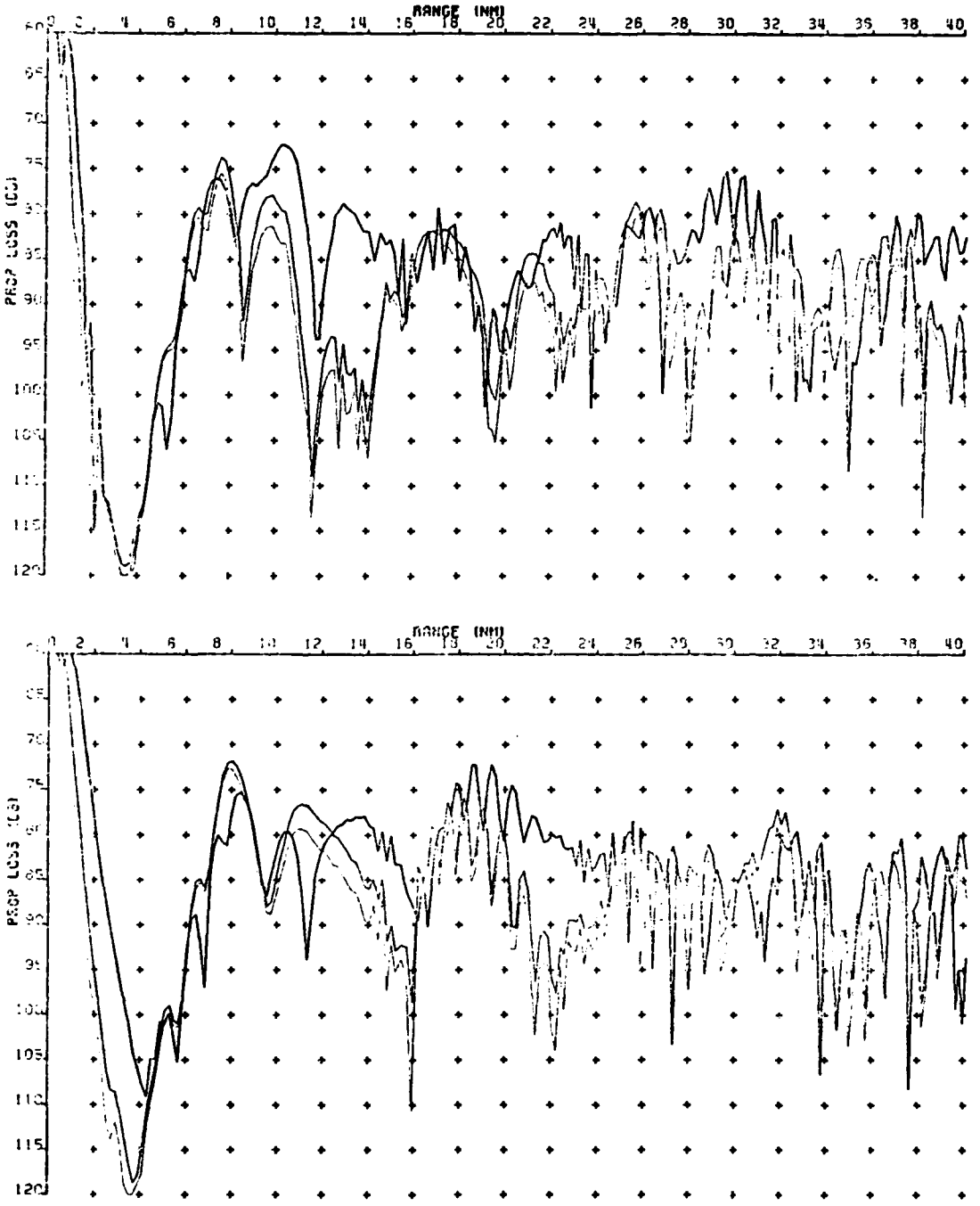

Fig. 88. Same profile as in Fig. 87 except 300 foot source at 100 Hz.

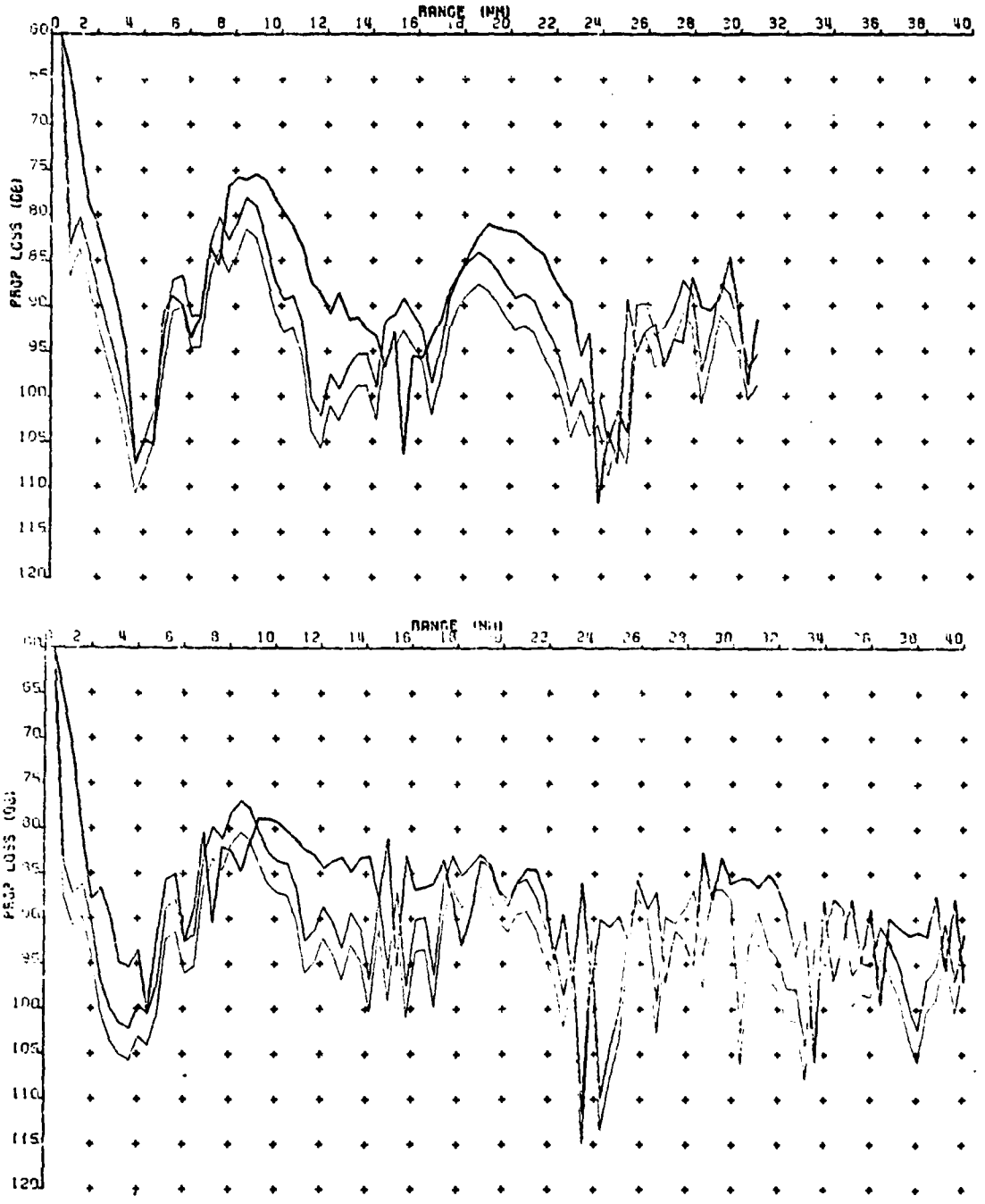

Fig. 89. Same profile as in Fig. 87 except 60 foot source at 50 Hz.

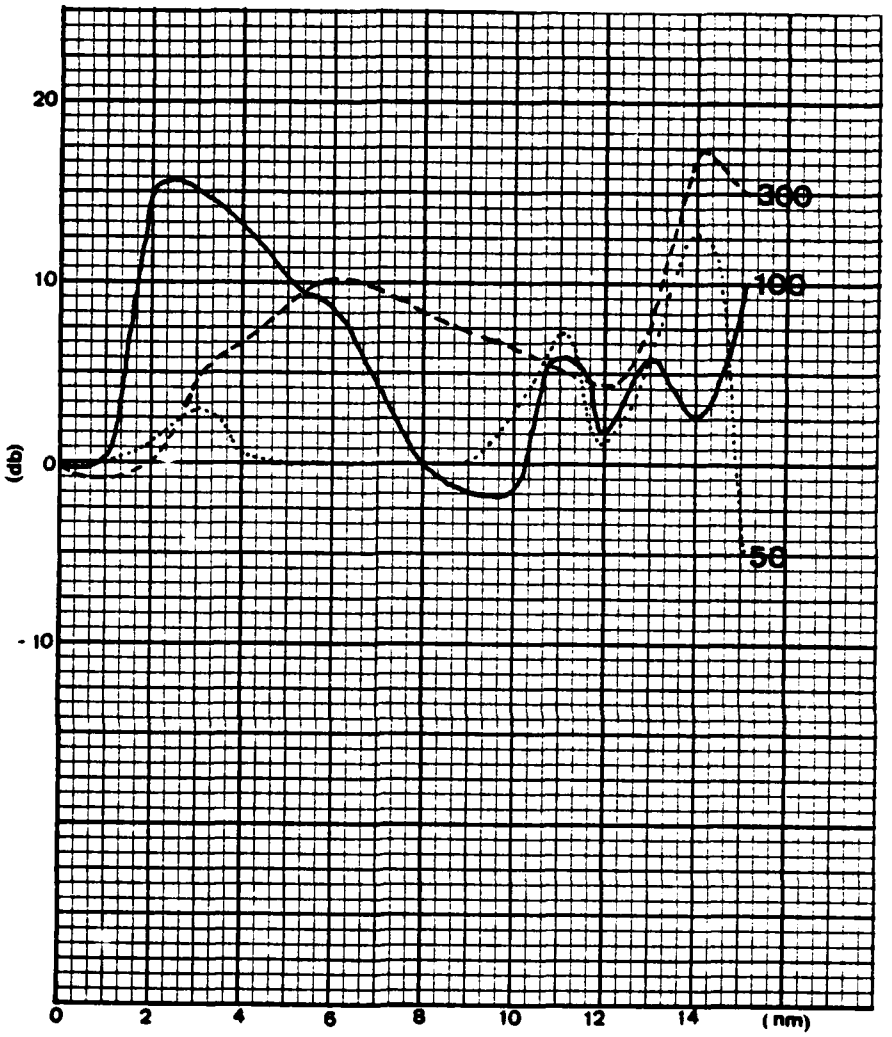

Fig. 90. Graph showing the difference between climatological PL and cold wedge PL in the onshore propagation 60 foot source run with 50 Hz (dotted), 100 Hz (solid), 300 Hz (dashed).

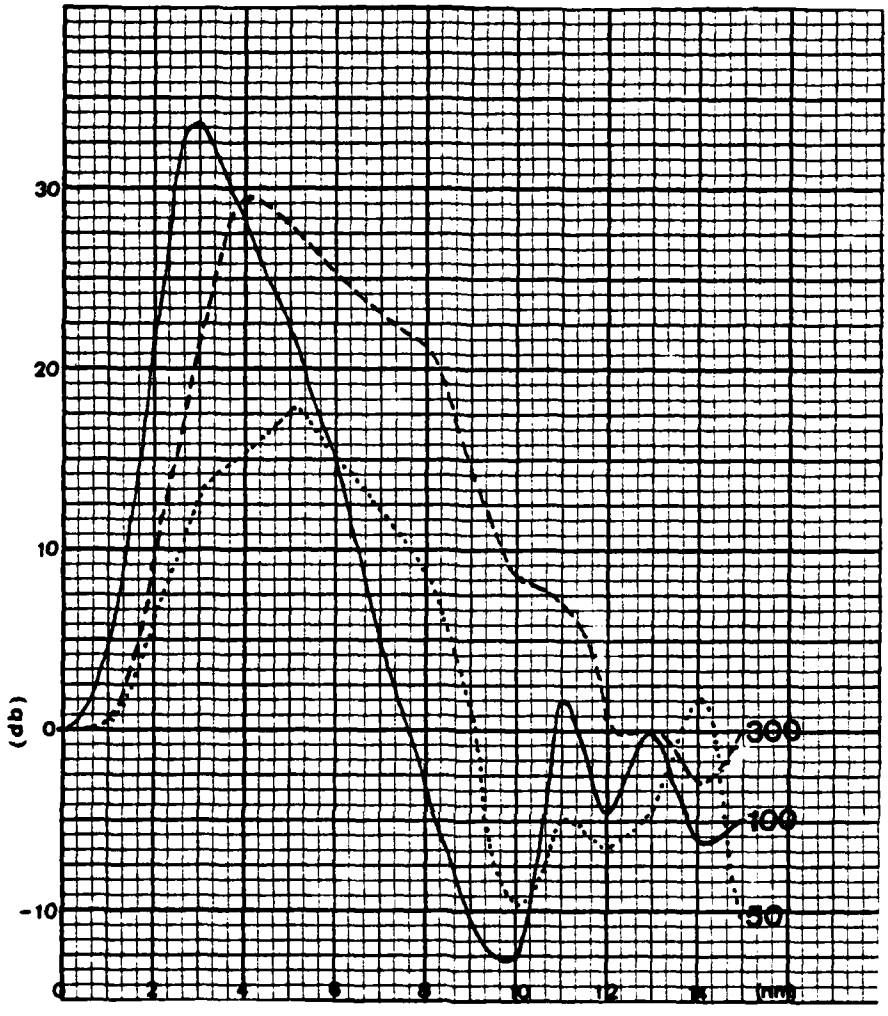

Fig. 91. Same graph as in Fig. 90 except 300 foot source.

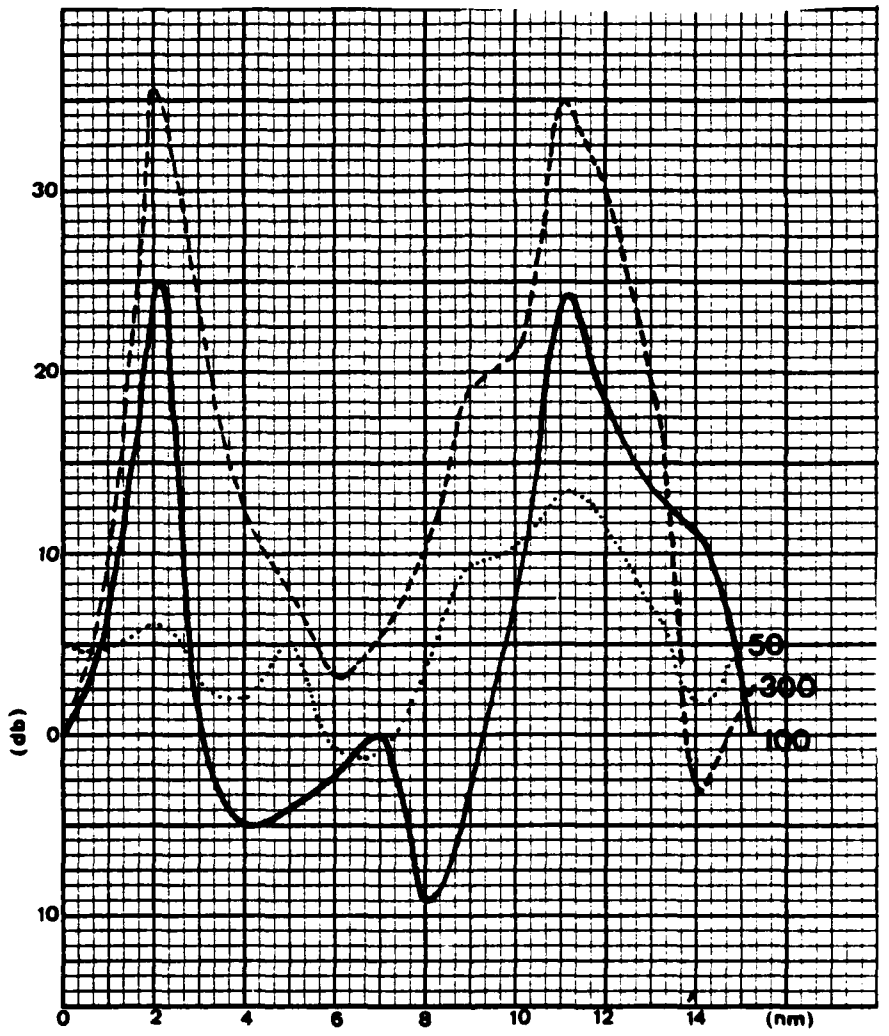

Fig. 92. Graph showing the difference between climatological PL and cold wedge PL in the offshore propagation 60 foot source run with 50 Hz (dotted), 100 Hz (solid), 300 Hz (dashed). For clarity, 5 dB has been added to the 50 Hz curve.

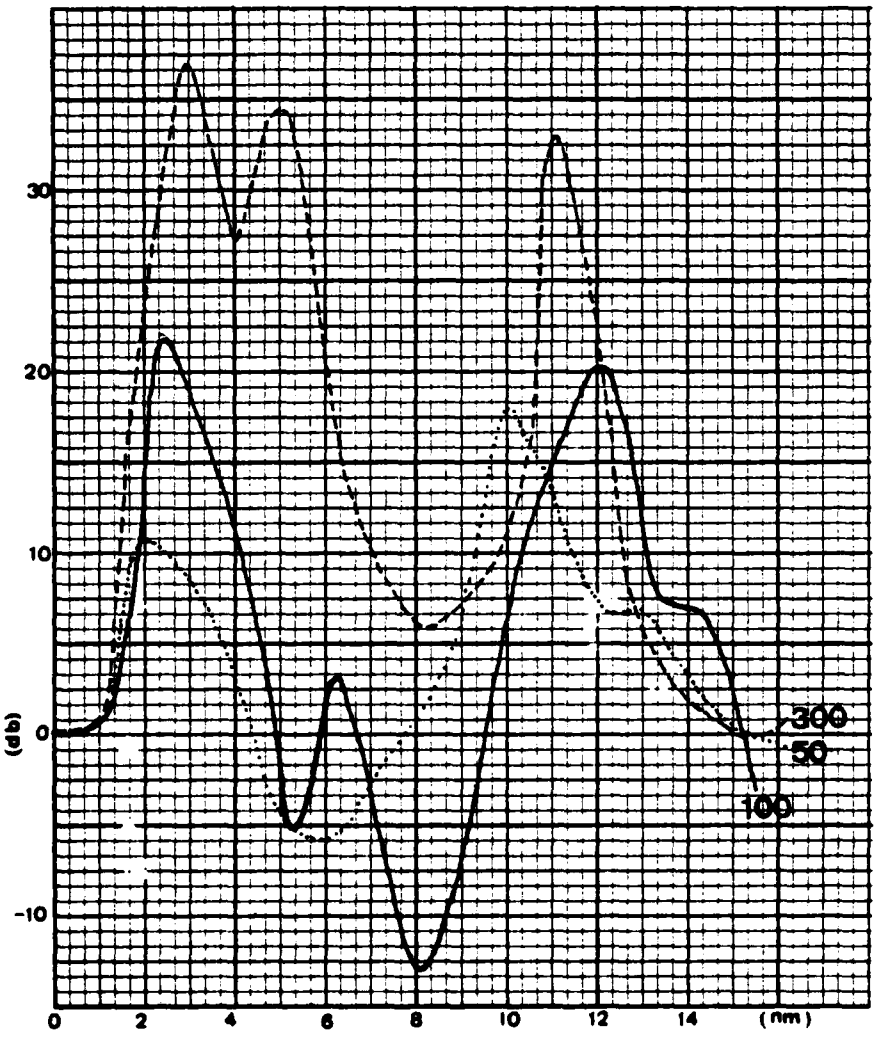

Fig. 93. Same graph as in Fig. 92 except 300 foot source.

APPENDIX B: SUMMARY OF SATELLITE IR IMAGERY

Imagery analysis was a tedious process impeded by a lack of facilities near the Naval Postgraduate School capable of processing AVHRR TIROS-N or NOAA-6 channel 4 imagery. The procedure was to review hard copy pictures of the area of interest (Table VIII) within one or two weeks of the cruise dates. From these pictures, cloud free images were selected to undergo additional analysis such as measurement of the feature in each image and changes observed in the same feature between images. A nine track 1600 bit per inch, one to one blocked tape of the image on the cruise date was then procured from the National Environmental Satellite Service in Redwood City. It was processed by the U-2 Support Group at The NASA Ames Research Laboratory located at NAS Moffett Field, California. The image was then geometrically corrected and gridded by use of a zoom transfer scope at Redwood City.

One analysis is included here (Fig. 94). It is from a channel 4 (IR) image taken of the area of interest on orbit 4915 at 22:55:45 on 26 SEP 79. This figure displays sea surface temperatures recorded at the satellite sensor without correction for the moisture field. In situ measurements were taken within 12 to 24 hours

of the image (Fig. 40). A comparison of the two fields was made by taking the root mean square of the difference between in situ measurements and satellite measurements at gridpoints spaced 2 km apart between 36 and 36 20 N and 122 and 122 20 W along the cruise track. The mean square difference was 0.91°C, which seems acceptably small considering the stated accuracies of the sensors.

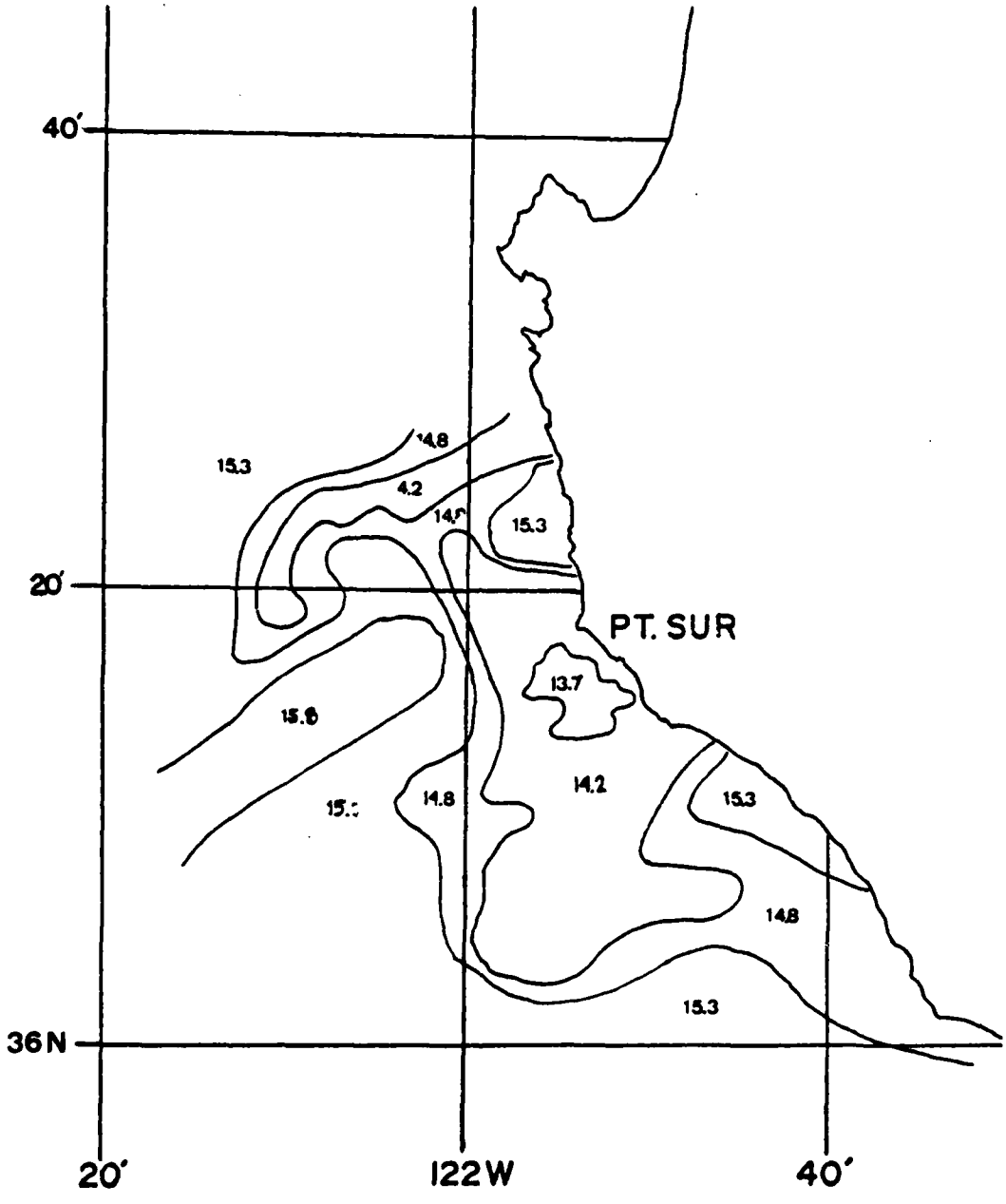

Fig. 94. Uncorrected satellite observed SST (°C) on 26 SEP 79 orbit 4915.

Table VII: Satellite images reviewed, 1979. All images are from TIROS-N unless noted otherwise.

DATE	TIME (GMT)	ORBIT	REMARKS
10 APR	100:22:27:45	2531	
17 APR	107:22:55:31	2630	
18 APR	108:22:44:31	2644	
19 APR	109:22:33:30	2658	
29 APR	119:22:30:01	2799	
6 MAY	126:22:57:10	2898	
5 AUG	217:12:17:00	4175	
8 AUG	220:23:12:00	4224	
11 AUG	223:22:40:15	4266	
16 AUG	228:23:28:00	4337	
9 SEP	252:22:34:00	4675	
10 SEP	253:22:24:37	4680	
15 SEP	258:11:47:15	4753	
15 SEP	258:23:12:00	4760	
16 SEP	259:23:01:25	4774	
18 SEP	261:22:40:05	4805	
19 SEP	262:22:29:25	4816	
20 SEP	263:03:22:55	1201	NOAA 6
24 SEP	267:23:16:55	4886	
25 SEP	268:23:06:55	4901	
26 SEP	269:22:55:45	4915	
28 SEP	271:22:34:00	4943	

DATE	TIME (GMT)	ORBIT	REMARKS
29 SEP	272:03:30:45	1329	NOAA 6
2 OCT	275:16:22:00	1379	NOAA 6
14 OCT	287:23:04:15	5169	
16 OCT	290:22:32:05	5211	
9 NOV	313:23:26:45	5536	
11 NOV	315:23:05:00	5564	
19 NOV	323:23:18:00	5677	
20 NOV	324:03:10:00	2068	NOAA 6
23 NOV	327:22:34:55	5733	
27 NOV	331:12:08:15	5783	
28 NOV	332:16:00:03	2819	NOAA 6
29 NOV	333:23:10:15	5818	
6 DEC	340:12:09:29	5910	
6 DEC	340:23:34:30	5917	
7 DEC	341:03:46:30	2310	NOAA 6
9 DEC	343:03:03:30	2338	NOAA 6
11 DEC	345:11:16:00	5980	
11 DEC	345:22:37:00	5987	
12 DEC	346:15:57:45	2388	NOAA 6
12 DEC	346:22:28:25	6001	
13 DEC	347:15:35:50	2402	NOAA 6
13 DEC	347:22:15:00	6015	
14 DEC	348:02:55:00	2409	NOAA 6

APPENDIX C: CRUISE 7-9 AUG 79 DATA

The cruise from 7 to 9 AUG 79 investigated and verified the existence of a large cold plume-like anomaly extending approximately 250 km SW from Point Sur. The ship transited along the axis of the plume, penetrated the front at the seaward limit and returned along the same axis. Limited data were collated (Figs. 96 and 97).

From 5 AUG to 16 AUG 79, four TIROS-N orbits were reviewed. Cloud contamination due to low level stratus and fog was severe. The predominant feature was an elongated plume off Point Sur which was typical of many plumes along the entire coast within the field of view. For example, there were plumes off Eureka, California and San Francisco Bay. Their size, characteristics and orientation were similar to those of the plumes off Point Sur.

On 5 AUG, 0517 local time, low level stratus obscured much of the area. A large cold plume extended from Point Sur along 240° T, 200 km. Towards the seaward end, it had a slight northward anticyclonic curvature. The coastal band of cold water was not uniform in width or intensity due to the numerous plumes present.

Three days later, at 1612 local time, the plume had apparently shifted south to a bearing of 230° T off

Point Sur and it had extended seaward to 250 km. Coastal fog prohibited measurement of features within 30 km of the coast.

Seaward extension of the plume was apparent in the image of 11 AUG, 1540 local time. The plume had shifted back to a bearing of 240° T from Point Sur and extended seaward in excess of 300 km. Local fog persisted.

Finally, on 16 AUG, 1628 local time, the feature had dissipated into a band of colder coastal water 100 km wide.

One plume-like feature off Point Sur dominated these images. Generally, it extended WSW, 250 km. Rapid seaward growth was observed over the six-day period from 5 to 11 AUG, of the order of 15 km increase in offshore extent per day. The apparent dissipation between 11 and 16 AUG was of the order of 40 km decrease in offshore extent per day. No advection was observed.

NMC 500 mb and SL charts were reviewed from 24 JULY to 23 AUG 79. The predominant large scale features at 500 mb during this period were numerous enclosed circulation centers which propagated zonally through the area at varying rates. Numerous short waves were superimposed upon the basic flow. In particular, over the cruise period from 7 to 9 AUG, the 500 mb pattern shifted from

a broad trough extending from an enclosed low off Vancouver, B.C. on 5 AUG to a weak ridge extending NW parllel to the coast from a weak high pressure system over Southern Nevada. Oakland winds were light and backed from the SW to the SE.

The SL pressure was dominated by a strong thermal trough over the Central California area which occasionally evolved into enclosed low pressure systems. Geostrophic winds were generally northerly. There were no frontal passages through the area of interest until 19 AUG. In particular, during the cruise, the low in Northern Baja California remained stationary in position and constant in strength, while the weak offshore high was quite variable as it extended southward from 45 N 130 W. Geostrophic flow was consistently northerly.

A low overcast throughout 7 AUG cleared by 0100, 8 AUG. Clear conditions existed until the return leg of the cruise when the ship reentered the area of stratus cover at 0400 9 AUG. Visibility was good, i.e., 15 km, throughout the cruise. Winds were initially WNW at 4 m s^{-1} on 7 AUG and shifted to NNW at 10 m s^{-1} on 8 AUG and remained strong through 9 AUG. Swells were northwesterly 1 to 2 m throughout the period. The surface pressure increased from 1017.3 mb on 7 AUG to 1020.7 mb on 8 AUG, it then decreased to 1019.3 mb on the return leg 9 AUG.

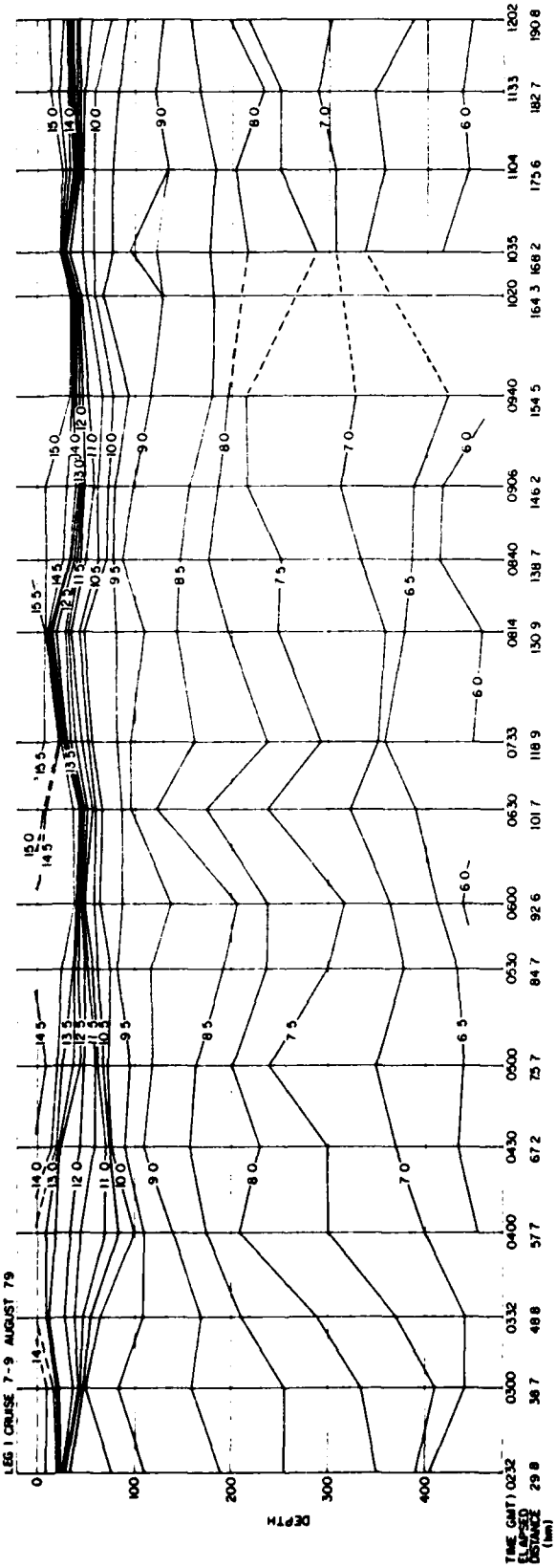

Fig. 95. Leg 1 0232 to 1202, 7 to 9 AUG 79

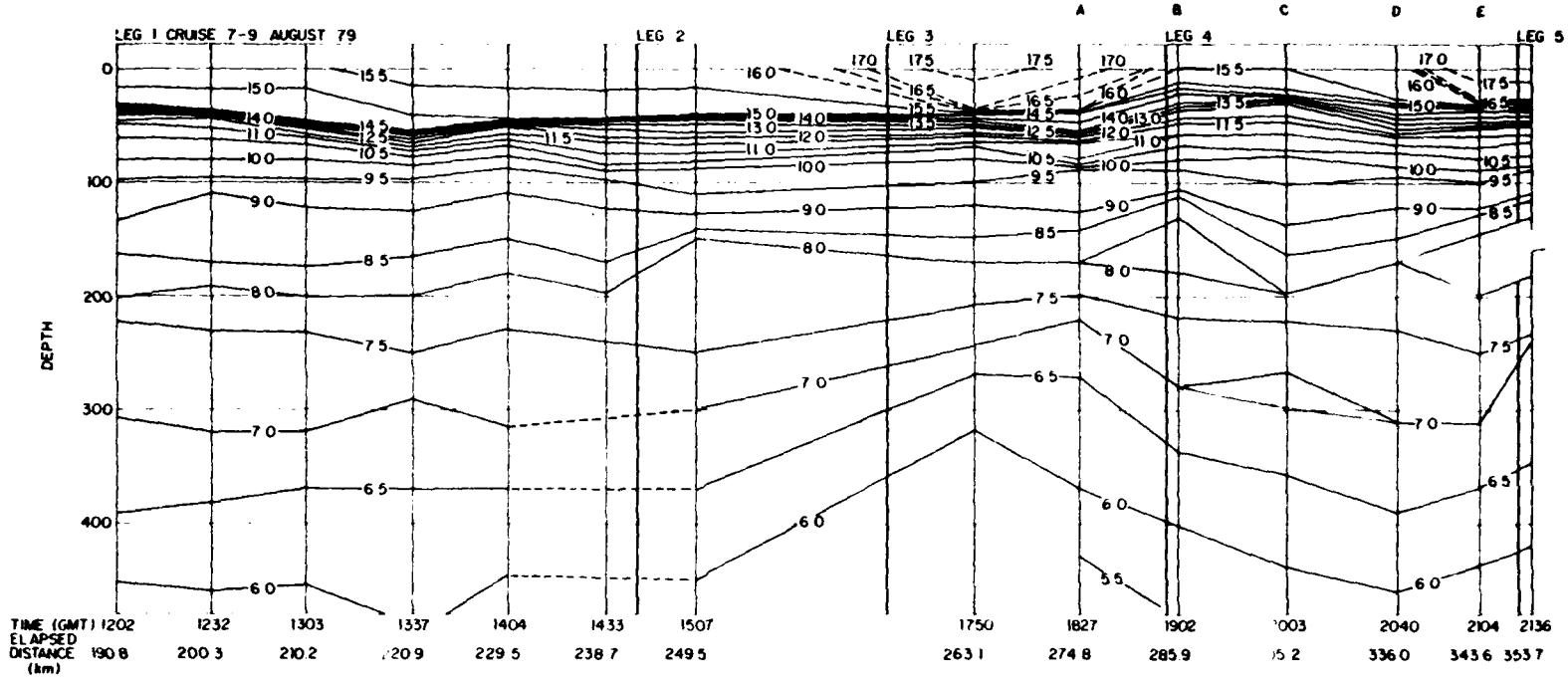

Fig. 96. Leg 1 1202 to 2136, 7 to 9 AUG 79.

STATION STATION 1 10 LATITUDE = 36 15.8N LONGITUDE = 122 4.8W DATE 29NOV79 2035

***** OBSERVED VALUES *****

DEPTH	TEMPERATURE	SALINITY	SIGMA-T	OXYGEN	IDENTIFICATION
2.0	14.00	33.359	24.940	0.0	
25.0	12.21	33.423	25.327	0.0	
50.0	10.20	33.531	25.752	0.0	
100.0	9.42	33.746	26.089	0.0	
200.0	8.14	34.024	26.516	0.0	
300.0	7.73	34.051	26.621	0.0	
400.0	7.46	34.158	26.712	0.0	

* INDICATES ADJUSTED VALUE

***** INTERPOLATED VALUES *****

DEPTH	TEMPERATURE	SALINITY	SIGMA-T	SND VEL	SPEC VOL	SPEC V ANOM	MEAN SVA	DELTA D	DYNAMIC HEIGHT	OXYGEN
0.	14.00	33.359	24.940	1503.41	0.9757	0.003024			0.0	0.0
							0.002962	0.029621		
10.	13.43	33.379	25.014	1501.53	0.9755	0.002900			0.02962	0.0
							0.002821	0.028206		
20.	12.69	33.438	25.242	1496.05	0.9753	0.002742			0.05783	0.0
							0.002655	0.026550		
30.	11.86	33.444	25.427	1496.24	0.9751	0.002568			0.08438	0.0
							0.002396	0.047922		
50.	10.20	33.531	25.752	1490.44	0.9746	0.002224			0.13230	0.0
							0.002135	0.053483		
75.	9.62	33.640	25.975	1488.77	0.9744	0.002055			0.18578	0.0
							0.002033	0.050086		
100.	9.43	33.746	26.089	1488.59	0.9741	0.001952			0.23587	0.0
							0.001843	0.052158		
150.	8.73	33.907	26.326	1486.53	0.9737	0.001734			0.32803	0.0
							0.001648	0.082357		
200.	8.14	34.024	26.516	1485.59	0.9733	0.001561			0.41042	0.0
							0.001534	0.076678		
250.	7.89	34.072	26.582	1485.48	0.9730	0.001506			0.48710	0.0
							0.001491	0.074542		
300.	7.73	34.051	26.621	1485.69	0.9728	0.001476			0.56164	0.0
							0.001440	0.143564		
400.	7.46	34.158	26.712	1486.35	0.9722	0.001404			0.70563	0.0

STATION STATION 2 10 LATITUDE = 36 11.40 LONGITUDE = 121 58.16 DATE 29NOV79 22 5

***** OBSERVED VALUES *****

DEPTH	TEMPERATURE	SALINITY	SIGMA-T	OXYGEN	IDENTIFICATION
2.0	14.70	33.366	24.758	0.0	
25.0	13.17	33.473	25.159	0.0	
50.0	10.99	33.478	25.613	0.0	
100.0	9.80	33.731	26.016	0.0	
175.0	8.28	33.987	26.458	0.0	
292.0	7.51	34.097	26.657	0.0	
395.0	7.06	34.164	26.782	0.0	
400.0	6.93	34.170	26.756	0.0	EXTRAPOLATED DATA POINT

* INDICATES ADJUSTED VALUE

***** INTERPOLATED VALUES *****

DEPTH	TEMPERATURE	SALINITY	SIGMA-T	SND VEL	SPEC VOL	SPEC V ANOM	MEAN SVA	DELTA D	DYNAMIC HEIGHT	OXYGEN
0.	14.70	33.366	24.758	1505.52	0.9758	0.003160			0.0	0.0
							0.003095	0.030944		
10.	14.19	33.407	24.937	1504.33	0.9756	0.003030			0.030944	0.0
							0.002949	0.029488		
20.	13.52	33.451	25.110	1502.13	0.9754	0.002868			0.060431	0.0
							0.002786	0.027855		
30.	12.72	33.472	25.286	1499.41	0.9752	0.002703			0.088286	0.0
							0.002549	0.025478		
50.	10.99	33.478	25.613	1493.25	0.9748	0.002355			0.133764	0.0
							0.002290	0.022896		
75.	10.21	33.594	25.835	1490.58	0.9745	0.002184			0.156591	0.0
							0.002103	0.021032		
100.	9.80	33.731	26.016	1489.99	0.9742	0.002021			0.245708	0.0
							0.001877	0.018764		
150.	8.75	33.912	26.328	1486.58	0.9737	0.001733			0.334293	0.0
							0.001646	0.016465		
200.	8.06	34.021	26.518	1485.24	0.9733	0.001558			0.425200	0.0
							0.001516	0.015161		
250.	7.70	34.072	26.610	1484.74	0.9730	0.001478			0.501122	0.0
							0.001457	0.014572		
300.	7.49	34.101	26.664	1484.75	0.9727	0.001435			0.573956	0.0
							0.001378	0.013785		
400.	6.93	34.170	26.756	1484.25	0.9722	0.001321			0.711744	0.0

STATION STATION 3 10 LATITUDE = 36 12.1N LONGITUDE = 122 3.1W DATE 29NOV79 2305

***** OBSERVED VALUES *****

DEPTH	TEMPERATURE	SALINITY	SIGMA-T	OXYGEN	IDENTIFICATION
2.0	13.15	33.506	25.227	0.0	
25.0	12.69	33.483	25.300	0.0	
50.0	10.85	33.463	25.642	0.0	
100.0	9.34	33.827	26.166	0.0	
180.0	8.30	34.009	26.472	0.0	
280.0	7.47	34.021	26.633	0.0	
360.0	7.12	34.111	26.723	0.0	
400.0	6.94	34.160	26.787	0.0	EXTRAPOLATED DATA POINT

* INDICATES ADJUSTED VALUE

***** INTERPOLATED VALUES *****

DEPTH	TEMPERATURE	SALINITY	SIGMA-T	SND VEL	SPEC VOL	SPEC V ANOM	MEAN SVA	DELTA D	DYNAMIC HEIGHT	OXYGEN
0.	13.15	33.506	25.227	1500.53	0.9754	0.002751			0.0	0.0
							0.002747	0.027469		
10.	13.06	33.497	25.238	1500.24	0.9753	0.002743			0.02747	0.0
							0.002727	0.027272		
20.	12.84	33.487	25.273	1499.71	0.9753	0.002712			0.05474	0.0
							0.002670	0.026697		
30.	12.34	33.479	25.365	1498.03	0.9751	0.002628			0.08144	0.0
							0.002497	0.024950		
50.	10.85	33.483	25.642	1492.83	0.9748	0.002367			0.13139	0.0
							0.002236	0.022358		
75.	9.95	33.643	25.923	1491.03	0.9744	0.002105			0.18730	0.0
							0.001991	0.019916		
100.	9.34	33.827	26.166	1488.35	0.9741	0.001878			0.23708	0.0
							0.001778	0.017778		
150.	8.61	33.964	26.365	1486.52	0.9736	0.001674			0.32566	0.0
							0.001622	0.016220		
200.	8.11	34.015	26.505	1485.44	0.9733	0.001571			0.40658	0.0
							0.001542	0.015419		
250.	7.69	34.022	26.573	1484.60	0.9730	0.001514			0.48419	0.0
							0.001488	0.014880		
300.	7.37	34.041	26.633	1484.21	0.9728	0.001463			0.55851	0.0
							0.001396	0.139597		
400.	6.94	34.160	26.787	1484.28	0.9722	0.001329			0.69611	0.0

STATION STATION 4 10 LATITUDE = 36 11.6N LONGITUDE = 122 8.0W DATE 30NOV79 0005

***** OBSERVED VALUES *****

DEPTH	TEMPERATURE	SALINITY	SIGMA-T	OXYGEN	IDENTIFICATION
2.0	13.55	33.365	25.027	C.0	
25.0	12.72	33.489	25.257	0.0	
50.0	11.99	33.523	25.465	C.0	
100.0	9.62	33.614	25.954	C.0	
200.0	7.26	33.569	26.592	0.0	
300.0	6.86	34.076	26.732	C.0	
400.0	6.54	34.272	26.929	C.0	

* INDICATES ADJUSTED VALUE

***** INTERPOLATED VALUES *****

DEPTH	TEMPERATURE	SALINITY	SIGMA-T	SND VEL	SPEC VOL	SPEC V ANOM	MEAN SVA	DELTA D	DYNAMIC HEIGHT	OXYGEN
0.	13.55	33.365	25.027	1501.80	0.9756	0.002932			C.C	C.0
							0.002887	0.028871		
10.	13.26	33.413	25.134	1501.56	0.9754	0.002843			0.02887	0.0
							0.002791	0.027907		
20.	12.90	33.466	25.245	1499.91	0.9753	0.002739			0.05678	0.0
							0.002695	0.026947		
30.	12.59	33.458	25.332	1498.55	0.9752	0.002659			0.08377	0.0
							0.002598	0.025996		
50.	11.99	33.523	25.465	1497.12	0.9750	0.002537			0.13572	C.0
							0.002422	0.060555		
75.	10.82	33.565	25.711	1493.23	0.9746	0.002307			C.19628	0.0
							0.002193	0.054829		
100.	9.62	33.614	25.954	1489.15	0.9743	0.002079			0.25111	0.0
							0.001912	0.095565		
150.	8.23	33.752	26.313	1484.79	0.9737	0.001745			0.34665	0.0
							0.001615	0.040727		
200.	7.26	33.569	26.592	1482.02	0.9732	0.001485			0.42742	C.0
							0.001447	0.072332		
250.	6.97	34.029	26.679	1481.78	0.9729	0.001409			0.49575	0.0
							0.001387	0.069365		
300.	6.86	34.076	26.732	1482.20	0.9727	0.001366			0.56911	0.0
							0.001279	0.127876		
400.	6.54	34.272	26.929	1482.82	0.9720	0.001192			0.69699	0.0

STATION STATION 5 LATITUDE = 36 16.6N LONGITUDE = 122 10.0W DATE 30NOV79 0135

***** OBSERVED VALUES *****

DEPTH	TEMPERATURE	SALINITY	SIGMA-T	OXYGEN	IDENTIFICATION
2.0	12.90	33.427	25.215	0.0	
25.0	12.58	33.547	25.371	0.0	
50.0	10.64	33.587	25.760	0.0	
100.0	9.28	33.751	26.117	0.0	
180.0	8.37	34.007	26.469	0.0	
295.0	7.28	34.121	26.709	0.0	
400.0	6.81	34.227	26.857	0.0	

* INDICATES ADJUSTED VALUE

***** INTERPOLATED VALUES *****

DEPTH	TEMPERATURE	SALINITY	SIGMA-T	SND VEL	SPEC VOL	SPEC V ANOM	MEAN SVA	DELTA D	DYNAMIC HEIGHT	OXYGEN
0.	12.90	33.427	25.215	1499.52	0.9754	0.002762			0.0	0.0
							0.002743	0.027433		
10.	12.87	33.473	25.257	1499.63	0.9753	0.002725			0.02743	0.0
							0.002692	0.026922		
20.	12.71	33.524	25.328	1499.27	0.9752	0.002660			0.05435	0.0
							0.002604	0.026035		
30.	12.21	33.557	25.449	1497.66	0.9751	0.002548			0.08039	0.0
							0.002491	0.024908		
50.	10.64	33.587	25.760	1492.17	0.9747	0.002255			0.12942	0.0
							0.002160	0.021591		
75.	9.79	33.664	25.965	1489.47	0.9744	0.002064			0.16241	0.0
							0.001994	0.019955		
100.	9.28	33.751	26.117	1488.02	0.9741	0.001924			0.18227	0.0
							0.001819	0.018197		
150.	8.65	33.917	26.347	1486.59	0.9737	0.001714			0.21324	0.0
							0.001639	0.016394		
200.	8.16	34.034	26.513	1485.67	0.9733	0.001564			0.24520	0.0
							0.001513	0.015061		
250.	7.67	34.088	26.627	1484.64	0.9730	0.001462			0.48086	0.0
							0.001423	0.071126		
300.	7.25	34.126	26.717	1483.84	0.9727	0.001383			0.55199	0.0
							0.001323	0.132263		
400.	6.81	34.227	26.857	1483.65	0.9721	0.001262			0.68425	0.0

STATION STATION 6 10 LATITUDE = 36 19.0N LONGITUDE = 122 13.0W DATE 30NOV79 0155

***** OBSERVED VALUES *****

DEPTH	TEMPERATURE	SALINITY	SIGMA-T	OXYGEN	IDENTIFICATION
2.0	13.50	33.461	25.122	0.0	
25.0	13.20	33.425	25.154	0.0	
50.0	12.21	33.552	25.446	0.0	
100.0	9.74	33.676	25.983	0.0	
172.0	7.65	34.202	26.650	0.0	
296.0	7.42	34.249	26.790	0.0	
400.0	6.93	34.296	26.855	0.0	

* INDICATES ADJUSTED VALUE

***** INTERPOLATED VALUES *****

DEPTH	TEMPERATURE	SALINITY	SIGMA-T	SND VEL	SPEC VOL	SPEC V ANOM	MEAN SVA	DELTA D	DYNAMIC HEIGHT	OXYGEN
0.	13.50	33.461	25.122	1501.74	0.9755	0.002852			0.0	0.0
							0.002854	0.028536	0.02854	
10.	13.43	33.440	25.120	1501.62	0.9755	0.002855				0.0
							0.002848	0.028484	0.05702	
20.	13.29	33.427	25.137	1501.26	0.9754	0.002842				0.0
							0.002810	0.028100	0.08512	
33.	13.02	33.447	25.206	1500.49	0.9753	0.002779				0.0
							0.002667	0.053338	0.13846	
50.	12.21	33.552	25.446	1497.97	0.9750	0.002555				0.0
							0.002426	0.048641	0.18510	
75.	10.96	33.613	25.723	1493.83	0.9746	0.002296				0.0
							0.002174	0.054349	0.23945	
100.	9.74	33.676	25.983	1489.69	0.9742	0.002052				0.0
							0.001813	0.090653	0.32410	
151.	8.32	34.043	26.454	1485.46	0.9735	0.001574				0.0
							0.001455	0.072747	0.41685	
200.	7.65	34.244	26.752	1483.95	0.9731	0.001336				0.0
							0.001314	0.065705	0.48255	
250.	7.45	34.273	26.805	1483.55	0.9728	0.001252				0.0
							0.001302	0.065065	0.54764	
300.	7.40	34.251	26.754	1484.60	0.9726	0.001311				0.0
							0.001269	0.126522	0.67456	
400.	6.93	34.296	26.855	1484.42	0.9721	0.001227				0.0

STATION STATION 7 LATITUDE = 36 21.9N LONGITUDE = 122 3.7W DATE 30NOV79 0325

***** OBSERVED VALUES *****

DEPTH	TEMPERATURE	SALINITY	SIGMA-T	OXYGEN	IDENTIFICATION
2.0	13.60	33.657	25.252	0.0	
25.0	12.51	33.505	25.355	0.0	
50.0	11.63	33.500	25.514	0.0	
100.0	10.34	33.509	25.751	0.0	
185.0	7.58	34.009	26.520	0.0	
300.0	7.44	34.116	26.682	0.0	
400.0	6.90	34.132	26.771	0.0	

* INDICATES ADJUSTED VALUE

***** INTERPOLATED VALUES *****

DEPTH	TEMPERATURE	SALINITY	SIGMA-T	SND VEL	SPEC VOL	SPEC V ANOM	MEAN SVA	DELTA D	DYNAMIC HEIGHT	OXYGEN
0.	13.60	33.657	25.252	1502.34	0.9754	0.002727			0.0	0.0
							0.002712	0.027120		
10.	13.21	33.598	25.287	1501.01	0.9753	0.002697			0.02712	0.0
							0.002677	0.026773		
20.	12.74	33.535	25.331	1499.38	0.9752	0.002657			0.05389	0.0
							0.002632	0.026320		
30.	12.32	33.503	25.366	1497.95	0.9751	0.002607			0.08021	0.0
							0.002548	0.025483		
50.	11.63	33.500	25.514	1495.76	0.9749	0.002490			0.13116	0.0
							0.002436	0.060905		
75.	10.96	33.494	25.631	1493.67	0.9747	0.002383			0.19208	0.0
							0.002328	0.058159		
100.	10.34	33.509	25.751	1491.76	0.9745	0.002273			0.25028	0.0
							0.002058	0.102907		
150.	8.89	33.753	26.211	1487.39	0.9738	0.001843			0.35319	0.0
							0.001681	0.084026		
200.	7.85	34.037	26.561	1484.47	0.9733	0.001518			0.43721	0.0
							0.001477	0.073852		
250.	7.55	34.100	26.654	1484.18	0.9730	0.001436			0.51107	0.0
							0.001426	0.071320		
300.	7.44	34.116	26.682	1484.57	0.9727	0.001417			0.58239	0.0
							0.001381	0.138018		
400.	6.90	34.132	26.771	1484.68	0.9722	0.001345			0.72045	0.0

STATION STATION 2 10 LATITUDE 36 11.4N LONGITUDE 121 58.1W DATE 29NC579 22.5
TO STATION 4 10 LATITUDE 36 11.4N LONGITUDE 122 8.0W DATE 30NC579 0005

MEAN LATITUDE = 36.19
DISTANCE = 14.87 KILOMETERS

DEPTH M.	DYN HT STA A	DYN HT STA B	DIFF HT A-B	REL VEL CM/SEC	ABS VEL CM/SEC	ABS VOL TRANSPORT *
0.	0.0	0.0	0.0	0.0	11.52	
						0.01593
10.	0.03095	0.02887	0.00207	-1.62	9.90	
						0.01381
20.	0.06043	0.05678	0.00366	-2.86	8.67	
						0.01238
30.	0.08829	0.08377	0.00452	-3.53	7.99	
						0.02489
50.	0.13927	0.13572	0.00355	-2.77	8.75	
						0.03735
75.	0.19651	0.19628	0.00023	-0.18	11.34	
						0.04544
100.	0.24908	0.25111	-0.00203	1.58	13.11	
						0.10248
150.	0.34293	0.34669	-0.00376	2.94	14.68	
						0.10303
200.	0.42520	0.42742	-0.00221	1.73	13.25	
						0.08811
250.	0.50112	0.49575	0.00137	-1.07	11.45	
						0.06761
300.	0.57396	0.56911	0.00484	-3.78	7.74	
						0.05755
400.	0.71174	0.69699	0.01475	-11.52	0.0	

* VALUES IN THIS COLUMN REPRESENT TRANSPORTS IN LAYER INCREMENTS

TOTAL VOLUME TRANSPORT IS COMPUTED BY SUMMING INCREMENTAL TRANSPORTS ABOVE LEVEL OF NO MOTION
TOTAL TRANSPORT PERPENDICULAR TO THE PLANE OF THE STATIONS IS 0.569 SVERDRUPS RELATIVE TO 400. METERS

STATION:STATION 2 IS LATITUDE 36 11.4N LONGITUDE 121 58.1W DATE 28NOV79 22.5
VS.STATION 4 IS LATITUDE 36 21.0N LONGITUDE 122 3.7W DATE 30NOV79 0.25

MEAN LATITUDE = 36.28
DISTANCE = 21.15 KILOMETERS

DEPTH M.	DYN HT STA A	DYN HT STA B	DIFF HT A-B	REL VEL CM/SEC	ABS VEL CM/SEC	ABS VOL TRANSPORT *
0.	0.0	0.0	0.0	0.0	-4.77	
						-0.01232
10.	0.03095	0.02712	0.00383	-2.10	-6.87	
						-0.01611
20.	0.06043	0.05385	0.00654	-3.58	-8.36	
						-0.01857
30.	0.08829	0.08021	0.00808	-4.43	-9.20	
						-0.03894
50.	0.13927	0.13118	0.00809	-4.43	-9.21	
						-0.04338
75.	0.19651	0.19208	0.00442	-2.42	-7.20	
						-0.02992
100.	0.24908	0.25028	-0.00120	0.66	-4.12	
						-0.01728
150.	0.34293	0.35319	-0.01026	5.62	0.85	
						0.01405
200.	0.42520	0.43721	-0.01201	6.58	1.81	
						0.01312
250.	0.50112	0.51107	-0.00994	5.45	0.67	
						0.00274
300.	0.57356	0.58235	-0.00843	4.62	-0.16	
						-0.00164
400.	0.71174	0.72045	-0.00871	4.77	0.0	

* VALUES IN THIS COLUMN REPRESENT TRANSPORTS IN LAYER INCREMENTS

TOTAL VOLUME TRANSPORT IS COMPUTED BY SUMMING INCREMENTAL TRANSPORTS ABOVE LEVEL OF NO MOTION:
TOTAL TRANSPORT PERPENDICULAR TO THE PLANE OF THE STATIONS IS -0.148 SVERDRUPS RELATIVE TO 400. METERS

STATION STATION 4 10 LATITUDE 36 11.5N LONGITUDE 122 8.0W DATE 30NOV79 0005
TO STATION 6 10 LATITUDE 36 19.7N LONGITUDE 122 13.0W DATE 30NOV79 0155

MEAN LATITUDE = 36.26
DISTANCE = 15.12 KILOMETERS

DEPTH M.	DYN HT STA A	DYN HT STA B	DIFF HT A-B	REL VEL CM/SEC	ABS VEL CM/SEC	ABS VOL TRANSPORT *
0.	0.0	0.0	0.0	0.0	17.21	
						0.02582
10.	0.02687	0.02654	0.00034	-0.26	16.95	
						0.02556
20.	0.05678	0.05702	-0.00024	0.19	17.39	
						0.02694
30.	0.08377	0.08512	-0.00136	1.04	18.25	
						0.05677
50.	0.13572	0.13846	-0.00274	2.11	19.31	
						0.07309
75.	0.19628	0.19910	-0.00282	2.17	19.37	
						0.17252
100.	0.25111	0.25345	-0.00234	1.80	19.00	
						0.12934
150.	0.34669	0.34410	0.00259	-1.99	15.22	
						0.09190
200.	0.42742	0.41685	0.01057	-8.11	9.10	
						0.04956
250.	0.49575	0.48255	0.01319	-13.19	4.01	
						0.01794
300.	0.56511	0.54764	0.02147	-16.47	0.73	
						0.00553
400.	0.69695	0.67456	0.02243	-17.21	0.0	

* VALUES IN THIS COLUMN REPRESENT TRANSPORTS IN LAYER INCREMENTS

TOTAL VOLUME TRANSPORT IS COMPUTED BY SUMMING INCREMENTAL TRANSPORTS ABOVE LEVEL OF NO MOTION
TOTAL TRANSPORT PERPENDICULAR TO THE PLANE OF THE STATIONS IS 0.575 SVERDRUPS RELATIVE TO 400. METERS

STATION:STATION 7 10 LATITUDE 36 21.9N LONGITUDE 122 3.7W DATE 30NOV79 0325
TO:STATION 6 10 LATITUDE 36 14.0N LONGITUDE 122 13.0W DATE 30NOV79 0155

MEAN LATITUDE = 36.34
DISTANCE = 14.91 KILOMETERS

DEPTH M.	DYN HT STA A	DYN HT STA B	DIFF HT A-B	REL VEL CM/SEC	ABS VEL CM/SEC	ABS VOL TRANSPORT *
0.	0.0	0.0	0.0	0.0	35.62	
10.	0.02712	0.02854	-0.00142	1.10	36.72	0.05393
20.	0.05385	0.05702	-0.00313	2.43	38.04	0.05574
30.	0.08021	0.08512	-0.00491	3.81	39.43	0.05777
50.	0.13118	0.13846	-0.00728	5.65	41.27	0.12034
75.	0.19208	0.19910	-0.00702	5.45	41.07	0.15348
100.	0.25028	0.25345	-0.00317	2.46	38.08	0.14753
150.	0.35319	0.34410	0.00909	-7.05	28.57	0.24846
200.	0.43721	0.41665	0.02056	-15.81	19.81	0.18036
250.	0.51101	0.48255	0.02851	-22.13	13.49	0.12416
300.	0.58239	0.54764	0.03475	-26.97	8.65	0.08254
400.	0.72045	0.67456	0.04589	-35.62	0.0	0.06451

* VALUES IN THIS COLUMN REPRESENT TRANSPORTS IN LAYER INCREMENTS

TOTAL VOLUME TRANSPORT IS COMPUTED BY SUMMING INCREMENTAL TRANSPORTS ABOVE LEVEL OF NO MOTION:
TOTAL TRANSPORT PERPENDICULAR TO THE PLANE OF THE STATIONS IS 1.289 SVERDRUPS RELATIVE TO 400. METERS

BIBLIOGRAPHY

Allen, J.S. 1973. Upwelling and coastal jets in a continuously stratified ocean. J. Phys. Oceanogr., 3(3): 245-257.

Allen, J.S. 1976. Continental shelf waves and alongshore variations in bottom topography and coastline. J. Phys. Oceangr., 6(6): 864-878.

Anderson, D.L.T. and P.D. Killworth, 1977. Spin Up of a Stratified Ocean with Topography. Deep Sea Research 24(5): 709-732.

Anderson, D.L.T. and A.E. Gill 1975. Spin up of a Stratified Ocean with Applications to Upwelling, Deep Sea Research 22(9): 583-596.

Bakun, A. 1973. Coastal Upwelling Indices, West Coast of North America, 1946-1971. NOAA Tech. Rep. NMFS SSRF-671, 103 pp.

Bakun, A., D.R. Mclain and F.V. Mayo. 1974. Notes: The mean annual cycle of coastal upwelling off western North America as observed from surface measurements. U.S. Fish. Bull., 72(3): 843-844.

Bakun, A., and C.S. Nelson. 1977. Climatology of upwelling related processes off Baja California. CalCOFI Rep., 19: 107-127.

Barton, E.D., A. Huyer and R. Smith, 1977. Temporal Variation observed in the Hydrographic Regime near Cabo Caorveiro in the Northwest African Upwelling Region, February to April 1974. Deep Sea Research 24(1): 7-23.

Beland, C.L. 1971. Sea-surface and related subsurface temperature anomalies at several positions in the North-east Pacific Ocean. Master's Thesis (B358), Naval Post-graduate School, Monterey, California, 144 pp.

Bernstein, R.L., L. Breaker and R. Whritner. 1977. California Current eddy formation: ship, air and satellite results. Science, 195: 353-359.

Blumbert, R.E. 1975. Mesoscale spatial and temporal variations of water mass characteristics in the California Current region of Monterey Bay 1973-1974. Master's Thesis (B583), Naval Postgraduate School, Monterey, California, 140 pp.

Blumsack, S.L. 1972. The Transverse Circulation near a Coast. J. Phys. Oceanogr., 2(1): 34-40.

Bourke, R.H. 1979. Introduction to the P.E. Model. Unpublished Notes, Naval Postgraduate School, Monterey, California.

Breaker, L. 1978. Quantitative Measurements of Sea Surface Temperature at Several Locations Using the NOAA-3 Very High Resolution Radiometer. NOAA TECH. MEMO. NESS 98, 28 pp.

Breaker, L. 1979. Proposal: A synoptic Study of coastal Upwelling "Plumes" in the California Current System. Ph.D. Proposal; Naval Postgraduate School, Monterey, California.

Brink, R.H. and J.S. Allen 1978. On the Effect of Bottom Friction on Barotropic Motion over the Continental Shelf. J. Phys. Oceanogr. 8(10): 919-922.

Brink, R.H. and J.C. Van Leer 1980. Physical and Biological Structure of Upwelling Plume off Peru at 15°S, paper presented at IDOE International Symposium on Coastal Upwelling, Los Angeles, California, 4 February 1980.

Brown, R.L. 1974. Geostrophic circulation off the coast of Central California. Master's Thesis, Naval Postgraduate School, Monterey, California.

Camp, N.T. and R.L. Elsberry 1978. Oceanic Thermal Response to Strong Atmospheric Forcing II: The Role of One Dimensional Processes. J. Phys. Oceanogr., 8: 215-224.

Coddington, K. 1979. Measurement of the California Undercurrent. Master's Thesis, Naval Postgraduate School, Monterey, California.

Cogan, J., and J. Willand 1976. Measurement of Sea Surface Temperature by the NOAA-2 Satellite. Journal of App. Met., Vol. 15, 173-180.

Conrad, J. 1980. Relationship Between Sea Surface Temperature and Nutrients in Satellite Detected Oceanic Frontier. Master's Thesis, Naval Postgraduate School, Monterey, California.

Coppens, A.B. and J.V. Sanders 1977. Acoustics. Unpublished Notes, Naval Postgraduate School, Monterey, California.

Curtin, T.B. 1979. Physical Dynamics of the Coastal Upwelling Frontal Zone off Oregon. Doctoral Dissertation, University of Miami, Coral Gables, Florida.

Cutchin, D.L. and R.L. Smith 1973. Continental Shelf Waves: Low Frequency Variations in Sea Level and Currents over the Oregon Continental Shelf J. Phys. Oceanogr., 3: 73-82.

Elliott, D.L. and J.J. O'Brien 1977. Observational Studies of the Marine Boundary Layer Over an Upwelling Region, Monthly Weather Review 105(1): 86-98.

Elsberry, R.L. and N.T. Camp 1978. Ocean Thermal Response to Strong Atmospheric Forcing I. Characteristics of Forcing Events J. Phys. Oceanogr. Vol 8: 206-214.

Elsberry, R.L. and P.C. Gallacher. One Dimensional Model Predictions of Ocean Thermal Anomalies during Fall 1976. Naval Postgraduate School TR 63-79-003.

Elsberry, R.L. and S.D. Raney 1978. Sea Surface Temperature Response to Variations in Atmospheric Wind Forcing. J. of Phys. Oceanogr., 8: 881-887.

Elsberry, R.L. and R.W. Garwood 1978. Sea Surface Temperature Anomaly Generation in Relation to Atmospheric Storms. Bulletin American Meteorological Society. 59(7): 780-784.

Emery, E.J. and L.A. Mysak 1979. Dynamic Interpretation of Satellite Sensed Thermal Features off Vancouver Island. J. Phys. Oceanogr., Preprint, 20 September 1979.

Emery, W.J. and A. O'Brien. 1978. Inferring salinity from temperature at depth for dynamic height computations in the North Pacific. Atmosphere-Ocean, 16(4): 348-366.

Endoh, M., C.N.K. Mooers and W.R. Johnson 1980. A Coastal Upwelling Circulation Model with Eddy Viscosity Dependency upon Richardson Number. Preprint IDOE International Upwelling Symposium. February 1980.

Fett, R., and W. Mitchell 1977. Navy tactical applications guide. Volume 1 Techniques and applications of image analysis. NAVENVPREDRSCHFAC Applications Rpt. 77-03, Naval Environmental Prediction Research Facility, Monterey, California.

Garvine, R.W. 1979. An Integral Hydrodynamic Model of Upper Ocean Frontal Dynamics I. J. Phys. Oceanogr., 9(1): 1-36.

Gerst, A.L. 1969. Correlation of sea-surface temperature with cloud patterns off the West Coast of North American during the upwelling season. Master's Thesis (G333), Naval Postgraduate School, Monterey, California.

Gill, A.E. and A.J. Clarke 1974. Wind Induced Upwelling Coastal Currents and Sea Level Changes. Deep Sea Research 21(5): 325-345.

Greer, R.E. 1975. Mesoscale components of the geostrophic flow and its temporal and spatial variability in the California Current off Monterey Bay in 1973-1974. Master's Thesis (G756), Naval Postgraduate School, Monterey, California, 177 pp.

Hastrup, O.F. and Oleson. O.V. 1974. Sound Propagation in Shallow Water. Vol II: Unclassified Papers, Saclant, ASW Research Center Conference Proceedings No. 14.

Henrickson, David E. 1976. An Evaluation of a Computer Simulation Model of Plankton Dynamics in Monterey Bay, Master's Thesis, Naval Postgraduate School, Monterey, California, 93 pp.

Hickey, Barbara M. 1979. The California Current System - Hypotheses and Facts. Department of Oceanography, University of Washington, Seattle, Washington.

Holly, R.W. 1968. Temperature and density structure of water along the California Coast. Master's Thesis (H688), Naval Postgraduate School, Monterey, CAlifornia, 127 pp.

Holloway, Greg 1978. A Spectral Theory of Nonlinear Barotropic Motion Above Irregular Topography J. Phys. Oceanogr. 8: 414-427.

Howton, H.M. 1972. A study of time variability of surface currents at a point in Monterey Bay. Master's Thesis (H8265), Naval Postgraduate School, Monterey, Calfornia.

Hurlburt, H.E. 1974. The Influence of Coastline Geometry and Bottom Topography on the Eastern Ocean Circulation. CUEA Technical Report 21, 103 pp.

Johnson, W.F. 1977. Upper Ocean Thermal Structure Forecast Evaluation of a Model using Synoptic Data. Master's Thesis, Naval Postgraduate School, Monterey, California.

Kidwell, Katherine B. NOAA Polar Orbiter Data (TIROS-N) Users Guide Preliminary Version April 1979. National Climatic Center Satellite Data Services, Washington, D.C.

Lammers, L.L. 1971. A Study of Mean Monthly Thermal Conditions and Inferred Currents in Monterey Bay. Master's Thesis, Naval Postgraduate School, Monterey, California.

Lazanoff, S.M. 1971. An Evaluation of a Numerical Water Elevation and Tidal Prediction Model Applied to Monterey Bay. Master's Thesis, Naval Postgraduate School, Monterey, California.

Legeckis, R. 1978. A Survey of Worldwide Sea Surface Temperature Fronts Detected by Environmental Satellite. J. Geophys. Res. 83(C9) pp. 4501-4523.

Leipper, D.F. 1955. Sea Temperature Variations Associated with Tidal Currents in Stratified Shallow Water over an Irregular Bottom. J. Mar. Res., 14(3): 234-252.

Maul, G.A. and M. Sidran 1973. Atmospheric Effects on Ocean Surface Temperature Sensing from the NOAA Satellite Scanning Radiometer, J. Geophys. Res., 78(12): 1909.

McNider, R.T. and J.J. O'Brien 1973. A Multilayer Transient Model of Coastal Upwelling. J. Phys. Oceanogr. 3(7) p. 258.

McClelland, J.J. 1972. An Oceanographic Investigation of Thermal Changes in Monterey Bay California, SEPT 1971-JAN 1972. Master's Thesis, Naval Postgraduate School, Monterey, California.

Mickelson, M.J. 1978. Solar Radiation in Peru During Joint 2: A Guide for Modelers. CUEA TR 43.

Miller, R.H. 1965. Short-period temperature oscillations in the vicinity of Monterey Bay. Master's Thesis (M5884), Naval Postgraduate School, Monterey, California.

Molnar, D.L. 1972. California Undercurrent Reconnaissance Between Monterey and Santa Barbara, Master's Thesis, Naval Postgraduate School, Monterey, California.

Mooers, C.N.K., C.A. Collins and R.L. Smith 1976. The Dynamic Structure of the Frontal Zone in the Coastal Upwelling Region off Oregon. J. Phys. Oceanogr., 6(1): 3-21.

Mooers, C.N.K. et al., 1979. Summertime Synoptic Varrability of the Middle Atlantic Shelf Water/Slope Water Front, J. Geophys. Res. 84(C8): 4837-4854.

Muraki, H. 1974. Poleward Shift of the Coastal Upwelling Region off the California Coast. J. Oceanogr. Soc. Jap., 30(2): 49-53.

Mysak, L.A. 1967. Response of Sea Surface to Low Frequency Long Wavelength Plane Wave Pressure Distribution, J. Mar. Res. 25(3): 205-227.

Mysak, L.A. 1967. On the Theory of Continental Shelf Waves. J. Mar. Res. 25(3): 205-227.

Mysak, L.A. 1977. On the Stability of the California Undercurrent off Vancouver Island. J. of Phys. Oceanogr. 7(11): 904-917.

Nelson, C.S. 1976. Wind stress and wind stress curl over the California Current. Master's Thesis, Naval Postgraduate School, Monterey, California.

Nestor, D.A. 1979. A Study of the Relationship Between Oceanic Chemical Mesoscale and Sea Surface Temperature as Detected by Satellite IR Imagery. Master's Thesis, Naval Postgraduate School, Monterey, California.

Pavlova, Y.V. 1966. Seasonal Variations of the California Current. Oceanology. 6: 806-814.

Pedlosky, J. 1978. An Inertial Model of Steady Coastal Upwelling. J. Phys. Oceanogr., 8(1): 171-177.

Peffley, M.B. and J.J. O'Brien 1976. A Three Dimensional Simulation of Coastal Upwelling off Oregon. J. Phys. Oceanogr., 6(2): 164-180.

Pirie, D.M. 1973. California Coast Nearshore Processes Study. ERTS A Experiment Number 088. Goddard Space Flight Center, Greenbelt, Maryland.

Pirie, D.M., M.. Murphy and J.R. Edmisten 1975. California Nearshore Currents. Shore and Beach, 43(2): 23-34.

Platz, B.W. 1975. A comparison of Satellite Images Capable of Detecting Ocean Surface Features. Master's Thesis (P614), Naval Postgraduate School, Monterey, California.

Reid, J.L., Roden, G.I., and Wylie, J.G. 1958. Studies of the California Current System, Contribution From the Scripps Institution of Oceanography. Progress report - California Cooperative Oceanic Fisheries Investigation, July 1, 1956 - January 1, 1958.

Roden, G.I. and D.F. Pakausky 1977. Estimates of Rates of Fronto-genesis and Frontolysis in the North Pacific Ocean Using Satellite and Surface Meteorological Data from January 1977. J. Geophys. Res. 83(C9): 4545-4551.

Shepard, A.B. 1970. A comparison of oceanic parameters during upwelling off the central coast of California. Master's Thesis (S4427), Naval Postgraduate School, Monterey, California.

Simpson, J.G. and R.D. Pingress, Oceanic Fronts in Coastal Processes: Proceedings of a Workshop held at the Marine Sciences Research Center May 25-27, 1977, pp. 29-42, Springer-Verlag, 1978.

Skogsberg, T. 1936. Hydrography of Monterey Bay, California Thermal Conditions, 1929-1933, Transactions of the American Philosophical Society of Philadelphia, New Series, 29, 1936.

Smith, R.L. 1968. Upwelling. Oceanic Marine Biology Annual Review 1968 6: 11-46.

Soluri, E.A. 1971. A Comparison of Oceanic Parameters During the Oceanic Period off the Central Coast of California, Master's Thesis, Naval Postgraduate School, Monterey, California.

Stieglitz, R., and others 1979. Incorporation of an Ocean Bottom into The Parabolic Equation (PE) Algorithm. Science Application, Incorporated SAI-79-S78-WA. pp. 2-15.

Sturr, H.D. 1969. Continental Shelf Waves over a Continental Slope. Master's Thesis, Naval Postgraduate School, Monterey, California.

Suginohara, N. 1974. Onset of Coastal Upwelling in a Two Layered Ocean by Wind Stress with Alongshore Variation. J. Oceanogr. Soc. Jap., 30(1): 23-33.

Tang, C. 1975. Baroclinic Instability of Stratified Shear Flows in the Ocean and Atmosphere, J. Geophys, Res. 80(9): 1168-1175.

Thompson, J.D. 1974. The Coastal Upwelling Cycle on a Beta Plane, Technical Report, Florida State University, Tallahassee, Florida.

Tont, S.A. 1975. The Effect of Upwelling on Solar Irradiance Near the Coast of Southern California. J. Geophys. Res. 80: 5031-5034.

Traganza, E.D., D.A. Nestor and A.K. McDonald 1979. Satellite Observation of a Nutrient Upwelling off the Coast of California. Preprint submitted to J. Geophys. Res.

Traganza, E.D. 1979. Chemical Mesoscale. Unpublished Notes, Naval Postgraduate School, Monterey, California

Traganza, E.D. 1979. The Use of Temperature and Color in Satellite Detection of Ocean Fronts and Mesoscale Eddies for ASW Applications. Naval Postgraduate School Tech Report NPS-68-79-008.

Walsh, J.J. 1974. Spin up of the Baja California Upwelling Ecosystem. Limnology and Oceanography 19(4): 553-572.

Wang, D.P. 1976. Coastal Water Response to the Variable Wind Theory and Coastal Upwelling Experiment. Tech. Rep. TR76-2. University of Miami, Miami, Florida, 174 pp.

Wang, D.P. and C.N.K. Mooers 1976. Coastal-Trapped Waves in a Continuously Stratified Ocean. J. Phys. Oceanogr., 6(6): 853-863.

Wang, D.P. and C.N.K. Mooers 1977. Evidence for Interior Dissipation and Mixing during a Coastal Upwelling Event off Oregon, J. Mar. Res. 35(4): 697-713.

Whittemore, M.A.N. 1973. Small scale temperature fluctuations near the sea surface. Master's Thesis (W567), Naval Postgraduate School, Monterey, California.

Wickham, J.B., R.E. Greer and R.E. Blumberg 1974. Variations in the California Countercurrent off Monterey Bay, 1973-1974. Appendix III Draft, 13 pp.

Wickham, J.B. 1975. Observations of the California Countercurrent. J. Mar. Res., 33(3): 325-340.

Wooster, W.S. and J.H. Jones 1970. California Undercurrent off Northern Baja, J. Mar. Res., 28: 235-250.

Yoshida, K. and H.L. Mao 1957. A Theory of Upwelling of Large Horizontal Extent, J. Mar. Res., 16: 40-54.

INITIAL DISTRIBUTION LIST

		No. Copies
1.	Defense Technical Information Center Cameron Station Alexandria, Virginia 22314	2
2.	Library, Code 0142 Naval Postgraduate School Monterey, California 93940	2
3.	Dr. C.N.K. Mooers, Code 68Mr Department Chairman Department of Oceanography, Naval Postgraduate School Monterey, California 93940	5
4.	Dr. E.G. Traganza, Code 68Tg Department of Oceanography Naval Postgraduate School Monterey, California 93940	3
5.	LIEUTENANT J.E. Johnson Officer in Charge Naval Oceanographic Command Detachment N.A.S. Barbers Point, Hi 96862	5
6.	Mr. Larry Breaker National Oceanic and Atmospheric Administration National Environmental Satellite Service 660 Price Avenue Redwood City, California 94063	1